University of Strathclyde
Glasgow
Department of Mechanical Engineering

Applied Modelling Techniques for Welding Induced Distortions and Residual Stresses

Pierluigi Mollicone B.Eng.(Hons)

2006

Thesis Presented for
The Degree of Doctor of Philosophy

Declaration of Author's Rights

Abstract

Prediction of residual stresses and distortion induced by welding is relevant to many industries involved with the manufacture and assembly of thin plate structures. The ability to predict these unwanted effects on such structures subjected to welding processes is important to minimise costs associated with rework and other corrective actions. The main challenge is to model the complex and at times indeterminate nature of the welding process, preferably in a simple and transparent manner.

The present work dealt with the development, validation and application of advanced simulation techniques for the prediction of welding induced residual stresses and distortions. Current literature presents a wide-ranging number of approaches, which vary in complexity and purpose, but at times fail to present a clear methodology for numerical based analysis. In the current work a commercial finite element software package was used to develop thermo-elasto-plastic models suited for this application. The proposed methodology was developed by initially analysing simple set-ups, validated through the use of experimental measurement techniques for both residual stresses and distortions predictions. This provided confidence in the application of the numerical models, which were then used to investigate more complex cases of particular interest to the shipbuilding industry. This part of the project dealt with ancillary operations, namely the initial application of tack welds and restraints on the structure, for which little attention is usually given due to their apparent insignificance compared to the final welding process. Their effects are in fact substantial and were investigated by using the thermo-elasto-plastic models together with experimental trials. A better understanding of their influence was hence illustrated, providing a basis for the establishment of a best industrial practice.

Acknowledgements

I would like to express my sincere gratitude to my supervisor Prof. T.G.F. Gray for the constant guidance, encouragement and support throughout the duration of the project.

Other people I would like to mention are my second supervisor Dr. T. Comlekci, for all the contributions made throughout the project and Dr. D. Camilleri for providing support, advice and background knowledge, vital for the successful completion of the current work. Prof. J.T. Boyle, Head of the Department of Mechanical Engineering, for giving me the opportunity to contribute to research work being carried out at the University of Strathclyde.

The Engineering and Physical Research Council and BAE Systems Marine supported the project. I would like to acknowledge my main contact at BAE Systems Marine, Dr. N. MacPherson, for the support, technical advice and the provision of welding materials and Mr. E. Duncan for coordinating all the technical staff of the University involved in the project.

This is not an exhaustive list and consequently I would like to acknowledge all members of staff who directly or indirectly contributed to the project.

I am particularly grateful to my parents Antonio and Connie, for all their guidance which they have consistently given me in the past three years. Finally, I would like to make a special acknowledgement to my fiancée Francesca Gatt, for all the support and encouragement throughout my stay in Glasgow.

Contents

List of Figures

List of Tables

Nomenclature

Latin Symbols

a	Thermal diffusivity
$\tilde{a}$	Strain gauge calibration coefficient
A	Area
A_1	Area over which residual stress for phase 1 acts
A_2	Area over which residual stress for phase 2 acts
A_z	Sampling area
$\bar{A}$	Strain gauge calibration coefficient
b	Weld width
$b_{0...23}$	Coefficients for statistical based welding simulation
$\bar{b}$	Strain gauge calibration coefficient
$\bar{B}$	Strain gauge calibration coefficient
c	Specific heat
C	Constant describing type of air flow for convection heat transfer
C_0	Heat flux constant for the Gaussian distribution heat input model
d	Thickness

$[D]$	Stiffness matrix
$[D]_{th}$	Thermal conductivity matrix
E	Young's Modulus
f_A	Area 1 fraction
F_B	Restraint force of the bar in the spring-bar model
F_S	Restraint force of the spring in the spring-bar model
F_{st}	Driving parameter for statistical based welding simulation
g	Acceleration due to gravity
Gr	Grashof number
h	Convection film coefficient
h_r	Film coefficient due to radiation
H	Enthalpy
I	Current
k	Thermal conductivity
k_{air}	Thermal conductivity of air
k_w	Weld geometric parameter
k_{xx}	Thermal conductivity coefficient in the x direction
k_{yy}	Thermal conductivity coefficient in the y direction
k_{zz}	Thermal conductivity coefficient in the z direction
K_0	Bessel function of first kind, zero order

l	Length
$\{L\}$	Partial difference operator
L	Typical dimension for convection heat transfer computation
m	Constant describing type of air flow for convection heat transfer
N_{st}	Driving parameter for statistical based welding simulation
Nu	Nusselt number
$\bar{p}$	Residual strain component
$\bar{P}$	Residual strain component
Pr	Prandtl number
q	Heat flux
$\bar{q}$	Residual strain component
q_0	Heat flux constant for the Gaussian distribution heat input model
q_{rad}	Heat transfer due to radiation
$\ddot{q}$	Heat generation rate per unit volume
Q	Total heat input
$\bar{Q}$	Residual strain component
r	Radial position
r_a	Hole radius
$\bar{r}$	Welding radius
s	Weld penetration

t	Time
$\bar{t}$	Residual strain component
t_0	Weld thickness
T	Temperature
$\bar{T}$	Residual strain component
T_0	Room temperature
T_f	Film temperature
T_{inf}	Ambient temperature
T_{ref}	Reference temperature
T_s	Starting temperature for weld contraction
T_w	Wall temperature
v	Heat source speed
$\{v\}$	Vector operator
V	Voltage
x	Coordinate in the longitudinal direction
y	Coordinate in the transverse direction
z	Coordinate in the through-thickness direction

Greek Symbols

α	Coefficient of thermal expansion

α_{in}	Instantaneous coefficient of thermal expansion
β	Volume coefficient of expansion
ϵ	Strain
$\{\epsilon\}$	Strain matrix
ϵ_e	Elastic strain
$\{\epsilon_e\}$	Elastic strain matrix
ϵ_{g1}	Strain measured from gauge 1
ϵ_{g2}	Strain measured from gauge 2
ϵ_{g3}	Strain measured from gauge 3
ϵ_p	Plastic strain
$\{\epsilon_p\}$	Plastic strain matrix
ϵ_r	Emissivity
ϵ_{th}	Thermal strain
$\{\epsilon_{th}\}$	Thermal strain matrix
ϵ_{tot}	Total strain
θ	Transverse angular deformation
λ	Thermal conductivity
ν	Viscosity
ξ	Distance traveled in the longitudinal direction
ρ	Density

σ Stress

$\{\sigma\}$ Stress matrix

σ_1 Principal Stress

$\langle\sigma_{1,II}\rangle$ Phase 1 related residual stress component

σ_2 Principal Stress

$\langle\sigma_{2,II}\rangle$ Phase 2 related residual stress component

σ_3 Principal Stress

σ_{max} Maximum stress

σ_{min} Minimum stress

σ_{sb} Stefan-Boltzmann constant

σ_x Stress in the x coordinate

σ_y Stress in the y coordinate

$\bar{\sigma_y}$ Uniaxial yield strength

σ_z Stress in the z coordinate

$\sigma_{z,II}$ Type II residual stress in the z direction

τ Temperature

τ_{max} Maximum shear stress

τ_{xy} Shear stress

υ Poisson's ratio

ϕ Angular position of the strain gauges

η Welding efficiency

Chapter 1

Introduction

1.1 Background

Welding is the most widely used process amongst common metal joining techniques. Key features are the potentially high integrity of the mechanical bond formed and the economic benefits for industrial production that come as a result of speed and versatility. Gas metal arc welding (GMAW), in particular, is a standard in industries such as shipbuilding and automotive. Notwithstanding its wide-spread use, there are still many challenges related to this type of joining technique. Most engineering problems arise from the basic requirement that the heat source must raise the material temperature to melting point. This scenario, coupled with the complex response of the materials commonly used, generates adverse mechanical and metallurgical effects that compromise the quality of the final result.

The current work deals with certain of the unwanted aspects induced by welding, namely, distortion and residual stress. Particular emphasis is placed on simple but important structural configurations, mainly encountered in the shipbuilding industry. Both distortion and residual stress are unwanted effects caused by the high temperature gradients imposed on the structure during the welding process. They lead to problems of misalignment, induced buckling, stress induced cracking etc., together with disadvantages caused by set-backs and downtime during production and assembly that come as a result of the waste in resources

needed for re-work and corrective actions. Although several mitigation techniques are available, these rely on an understanding of the mechanisms driving welding induced distortions and residual stresses, and are still not entirely developed to a point where the effects can be completely removed at the fabrication stage. As numerical analysis becomes more widely used in the design stage, it is of particular interest to develop tools for the investigation of these unwanted effects, especially if they can be used in the early stages of the design process.

The rapid increase in computer power experienced over the past few decades has made it possible to apply numerical methods to a large range of problems. The complex nature of the welding process however, together with its extensive range of applications, make it difficult to find a clear methodology that can readily be applied to cases of industrial relevance. Analysis of welding induced effects is not trivial or straightforward, due to the number of physical phenomena involved and the large variations in material response that come as a result of the wide range of loadings present. The different aspects involved in GMAW range from electromagnetic arc physics, to others related to the thermal, metallurgical and structural response of the materials. The main challenge hence lies in adopting a simulation technique that is appropriate to the welding induced effect under investigation and that can be used as a tool at an early design or fabrication stage. Furthermore, the complex nature of welding analysis means that there are still many scenarios that have not received particular or any attention in literature, leading to a deficiency in the understanding of the effects that certain fabrication procedures have on welding induced distortions.

1.2 Scope of Work

The main contribution of the present work to this field of research therefore comprised of:

- The development of simulation methodologies for the prediction of welding induced distortion and residual stress
- The application of these simulations to industrial cases to which little or no attention has been previously given

A basic requirement is a relatively simple approach, capable of providing valid predictions for distortion and residual stress. Experimental measurements are an essential part of the development of such models. These are carried out, not only to validate the numerical results, but to understand which aspects of the simulation deserve particular attention in view of the relevant welding induced effects. Distortion measurements for the chosen configurations are hence required, together with tests carried out to extract the various material properties that are critical in achieving useful predictions. Residual stress measurements are also very beneficial as they provide further insight into the strengths and weaknesses of the numerical models.

Finite element models were developed using commercial general purpose software. Extensive scripting facilities give full control on the the type of analysis and algorithms used, and there is no need to develop the already well established thermal and structural solution methods embodied in the software. The algorithms developed had to have the potential to be applied to a wide range of scenarios, in a transparent manner, while providing reliable predictions. It was evident from the start of the project that successful analysis of welding processes requires many simplifications and assumptions. Nevertheless, all transient and residual aspects of distortion and residual stress have to be included. In practice, the outcome of these welding induced effects depends on a large number of

factors, meaning that simple weld configurations had to be considered to develop the numerical models.

The objective for the initial phase of the project was to investigate different modelling approaches in order to establish the best methodology for the cases of interest. The main challenges and practical limits relate to the extent to which simulations can be used to provide useful results. The difficulties lie in the lack of comprehensive material property data (which are in most cases difficult and expensive to obtain by means of experiments) together with the customisation required when using a general purpose finite element software for this type of analysis. Nevertheless, a number of strategies are investigated to determine the best approach, keeping in mind that the computational effort had to be kept within reasonable limits since it was required to create a methodology that could be used to investigate cases of industrial relevance.

Following the successful development of the numerical models, simulations were carried out to investigate scenarios of industrial relevance. Case studies for fabrication procedures that influence the outcome of distortions and residual stresses were considered. This part dealt with the investigation of the common fabrication operations of tack welding and restraining, and their effects on simple welded assemblies. These procedures have not received much attention to date and there is consequently a lack of clear understanding with regard to effects on induced distortions, and concerning the best procedures to be adopted in the fabrication stages. Tack welding procedures can be analysed in terms of the sequence in which they are laid. Restraining the structure during welding can be simulated in order to understand what effects are induced by the adoption of this technique. The application and use of the models developed in the early stages is hence demonstrated. These investigations were carried out in conjunction with experimental trials in order to strengthen the level of confidence in the numerical results. The simulations provide a useful means to extend the work to cases which would otherwise be expensive to investigate by means of experimental trials only.

1.3 Structure of Thesis

The thesis structure follows the chronological order of the different phases comprising the current project. A literature review identifies the current state of the art and trends in welding residual stress and distortion simulation, showing the large amount of literature available, together with the range of approaches and case studies that previous authors have investigated. The thermal and structural parts of the analyses were separated, as this is the approach adopted in most cases, owing to the weak coupling of the two phenomena and the considerable reduction in computational time when adopting such an approach. When considering the thermal aspect of the simulation, those methodologies relevant for subsequent structural analysis of distortions and residual stresses were considered. The review hence shows many different considerations, assumptions and techniques that can lead to a temperature field prediction suitable for the structural analysis that follows.

The structural analysis review finds an even large scope for classification, even when considering models purely dedicated to distortion prediction, with only a secondary emphasis on residual stresses. The most convenient classification was that of simplified vs. complex methods. The former aim at predicting distortions in the most computationally efficient manner, often lacking information on aspects such as the transient phase and induced stresses. The complex methods are often very specific to the case studies investigated, requiring more information on the specific process and various material parameters. Other interesting aspects of relevant literature are presented, namely, those dealing with alternative simulation techniques (such as artificial neural networks) and investigation of numerical techniques of particular interest for welding simulation.

Based on this review, a need for a modelling technique that could capture transient effects of distortion and residual stress in a relatively simple manner was identified. Chapter 3 presents all theoretical considerations necessary for an understanding of the developed numerical models whilst Chapter 4 illustrates

the work carried out in developing and validating such models. Two simple butt welding and fillet welding configurations were considered. Reference distortion experimental data was employed and results also compared to one of the simplified techniques in the literature, in order to better understand the level of complexity of the models and their advantages and limitations.

Having validated the models against distortion measurements, residual stress measurements were also made to provide further insight. Hole drilling measurements were carried out and are presented in Chapter 5, together with an illustration of the theory underlying the calculations used to extract the required values. Comparisons with predicted values were useful in understanding the level of complexity that the chosen modelling technique embodies. This added another level of confidence on the numerical models, and hence their applicability to this class of industrial scenarios.

The next part of the project dealt with the investigation of key fabrication operations, namely the initial application of tack welds and restraints on the structure, which have a perceived insignificance compared to the final welding process. Their effects are in fact substantial and were investigated by using the thermo-elasto-plastic models together with experimental trials. The investigation proved useful in achieving a better understanding of their influence, providing a basis for the establishment of a best industrial practice.

Chapter 2

State of the Art in Welding Residual Stress and Distortion Simulation, Literature Review

2.1 Introduction

There is extensive literature reporting research work on computer aided welding simulation. The application of computational techniques in the field of welding technology has been an active area of research since the early development of numerical methods. Owing to the range of welding processes and the different physical phenomena involved, there are several fields of application depending on which aspect of the welding process has to be predicted. This review focuses on the state of the art in modelling welding processes for the prediction of induced residual stresses and distortion. The application of the modelling techniques developed throughout the thesis focuses on Gas Metal Arc Welding processes, but work carried out on other types of welding processes is still relevant from a simulation point of view, as many modelling techniques are relevant to a range of welding processes.

The first step in welding simulation is the correct determination of the temperature fields. This can be achieved through purely analytical or computational methods and usually always requires some form of experimental calibration due to the many unknown factors involved.

Computation of the other physical phenomena (structural, metallurgical, fluid dynamics etc) is then required. This poses many obstacles to the successful use of numerical simulation techniques. The increase in the required computational effort and the difficulty in determining temperature dependant material properties are only two of the main obstacles encountered when trying to include all physical aspects in the simulation. The latter aspect was particularly important in early studies when computational power was considerably limited, but is still relevant today as it is still not computationally feasible to carry out complex welding analyses on extremely large structures. For this reason one important approach is to carefully consider which parts of the welding process can be simplified and/or un-coupled and which assumptions are valid in order to successfully predict residual stresses and distortion. This has led to a considerable amount of research work on the development of simplified methods. These methods have the attractive feature of greatly reducing the computational effort, thus expanding the possible range of application for the size and combination of structure types.

Another possible approach is to include *all* aspects of the welding process, starting from thermal formulations and considering all possible coupling effects between thermal, structural and metallurgical aspects. It is still however necessary to include certain assumptions and simplifications in order to carry out an analysis since it is not possible to simulate all aspects of the welding process with purely numerical techniques.

Because of the latter restriction another possibility is to move away from the more classical deterministic approach and use completely different modelling techniques, such as statistical methods or artificial neural networks. The appealing feature of such approaches is that any number of factors can be included in the simulation, the main downfall being that such an approach requires careful training of the intelligent system and hence it is not possible to carry out predictions *a priori*. This is not particularly useful when new and unknown set-ups need to be investigated.

Work on welding simulation can be further subdivided according to which physical domain is being investigated. Hence some of the literature focuses purely on specific aspects such as detailed prediction of the formation of the weld pool. Such analyses do not always yield residual stress and distortion results directly but are nevertheless important, as the thermal aspect of the welding process is undoubtedly the driving force for distortion and stresses.

Finally another relevant field of research is the investigation and development of numerical techniques which are particularly relevant to welding simulations such as adaptive meshing, element formulations etc.

2.2 Thermal Simulations

It has been recognised early in the study of welding induced residual stresses and distortion that the high temperature gradients generated during welding provide the driving force for the development of residual stresses and distortions. It is therefore fundamental to be able to simulate the thermal response due to welding of the structure under investigation.

Earlier studies focussed on analytical solutions of the thermal conduction equation (2.1) for a moving heat source [2.1]:

$$\frac{\partial^2 T}{\partial x^2} + \frac{\partial^2 T}{\partial y^2} + \frac{\partial^2 T}{\partial z^2} = 2\lambda \frac{\partial^2 T}{\partial t^2} \tag{2.1}$$

Where T is the temperature, x, y and z are the coordinates in the longitudinal, transverse and through-thickness directions respectively, t is the time and λ is the thermal conductivity.

Rosenthal et al [2.2] considered linear, two and three dimensional solutions for this heat flow problem. Results for two and three dimensional temperature distributions are given in equations (2.2) and (2.3) respectively:

$$T - T_0 = \frac{q}{2\pi\lambda dv} \exp\left(\frac{v\xi}{2a}\right) K_0\left(\frac{vr}{2a}\right) \tag{2.2}$$

$$T - T_0 = \frac{q}{2\pi\lambda rv} \exp\left(\frac{-v\xi}{2a}\right) \exp\left(\frac{-vr}{2a}\right) \tag{2.3}$$

Where K_0 is the Bessel function of first kind, zero order, d is the thickness of the plate, t is time, T_0 is the room temperature and r is defined as:

$$r = \sqrt{\xi^2 + y^2 + z^2} \tag{2.4}$$

The above formulations take into account the heat flowing into the plate q and the thermal diffusivity a. The term ξ is defined as:

$$\xi = x - vt \tag{2.5}$$

Where v is the heat source speed. This is a simple transformation required to keep the coordinate system fixed on the plate relative to the moving heat source.

The following assumptions are taken in order to obtain these solutions:

- The plate under investigation in assumed to be infinite
- A quasi stationary solution is assumed
- Properties are taken to be constant with temperature

A temperature plot obtained using these equations for typical Gas Metal Arc Welding (GMAW) welding conditions is given in Figure 2.1. Equations (2.2) and (2.3) are chosen depending on the thickness of the plate relative to the actual

weld. The three dimensional solution must be used if the plate is thick enough to allow heat transfer in the direction of the thickness. On the other hand if the thickness of the plate is relatively small the problem can be approximated by a two dimensional heat flow pattern.

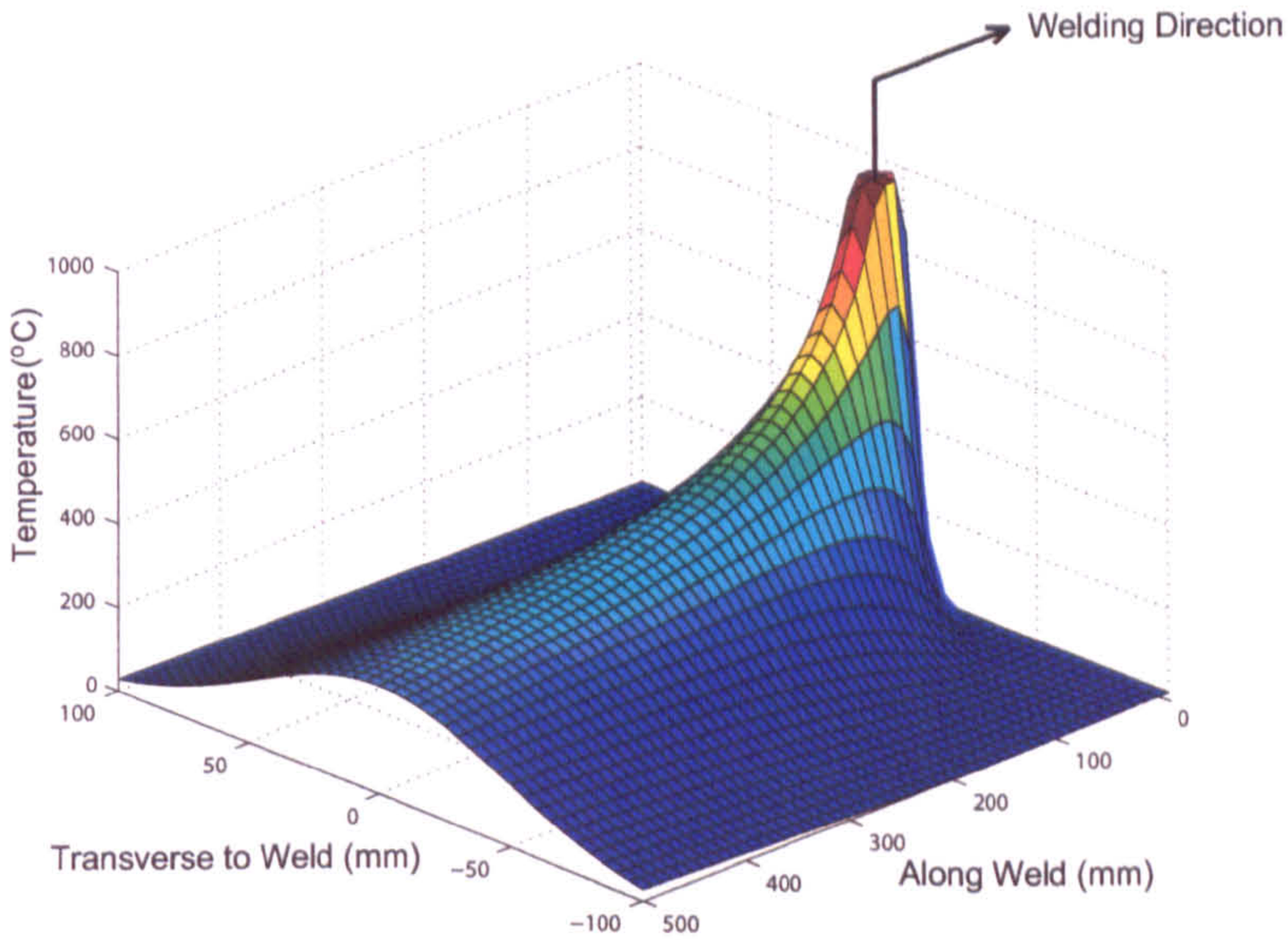

Figure 2.1: Analytical solution for the temperature distribution using typical GMAW steel parameters

Lindgren [2.3] investigated the effects of using thermal analytical solutions when comparing the results with previous work [2.4] in which thermal finite element analyses were used and found that analytical solutions could be used if the residual stresses were of interest. However, these fail to give a good thermal simulation if the weld gap is to be computed from the subsequent structural elasto-plastic analysis.

Friedman [2.5] in an early paper highlights the advantages of using numerical techniques over analytical solution for the thermal part of the simulation. He states that it is required to account for phenomena such as temperature dependant material properties, phase changes, through-thickness temperature variations, irregular weldment geometries, non-uniform distribution of energy from the heat source, and deposition of filler material, amongst others.

The development of computer based numerical methods led to a wider use

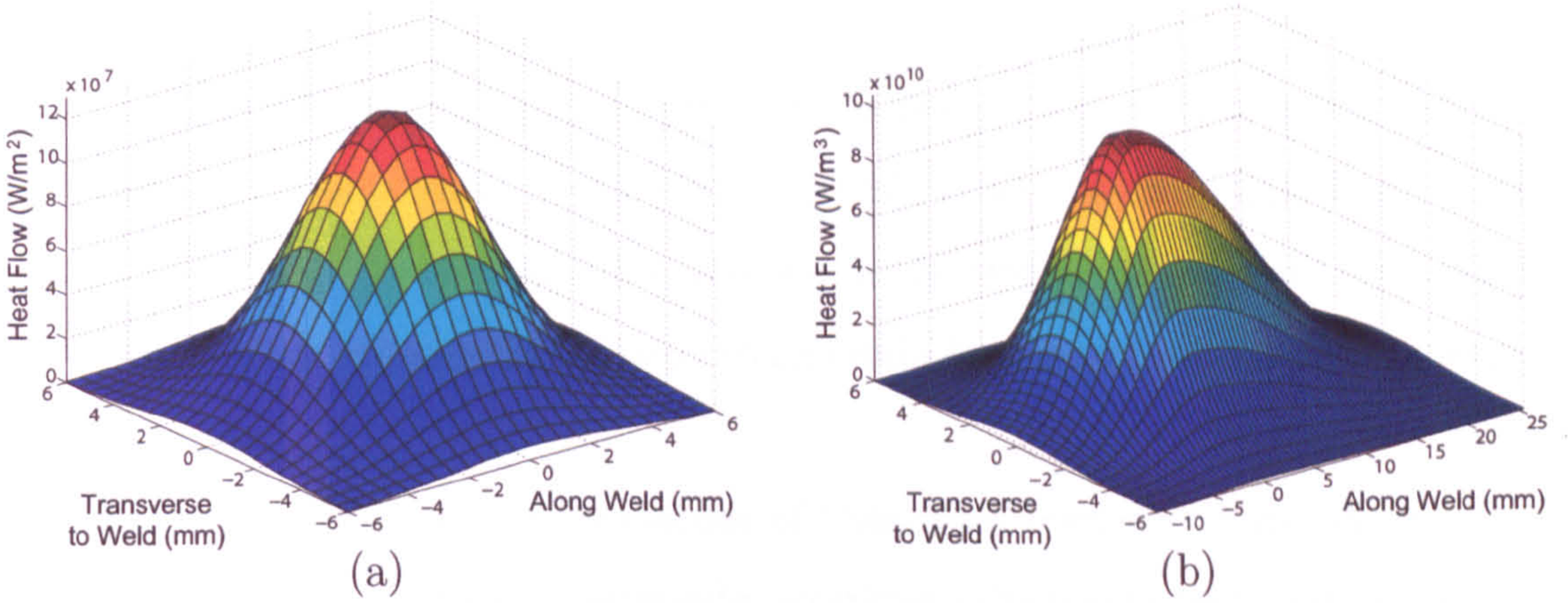

Figure 2.2: Heat input distribution using: (a) Circular Gaussian distribution and (b) Double ellipsoid model (using typical parameters as in Figure 2.1)

of numerical methods for thermal analysis. Goldak et al [2.6] presents a review of the different possible computational approaches. Three groups are identified depending on the region of interest: the weld pool, the area near the weld pool, or the area far away from the weld pool and hence the whole welded structure. Similarly to the analytical solutions presented by Rosenthal, the analysis of the thermal response of the whole structure is of most relevance for welding induced residual stresses and distortion simulation.

The latter fact and the adoption of a cut-off temperature technique (discussed later in chapter 3) led to the adoption of heat generation distributions applied as loads in numerical analyses. Friedman [2.5] used a Gaussian circular heat input distribution (shown in Figure 2.2(a)) for his work, which was also adopted by Camilleri et al [2.7] and validated against experimental studies that made use of thermocouple and infrared measurement techniques [2.8].

Goldak et al [2.9] also proposed a general heat source model consisting of a double ellipsoid (Figure 2.2(b)). This is widely used by many researchers since it is relatively straightforward to implement in numerical codes.

Combined heat source models are often also used. Wahab et al [2.10] used a split heat source model consisting of the Goldak double ellipsoidal distribution in conjunction with a spherical distribution. They applied this modelling technique

to two-dimensional (normal to the welding direction) and a three dimensional heat flow models. The predicted weld pool shapes were verified experimentally for various cooling times. Bachorsky et al [2.11] also used a split heat source model consisting of a Gaussian distribution at the surface to simulate arc heating and a cylindrical volume heat source to simulate heat input of molten droplets of the electrode.

Chai et al [2.12] investigated the use of a modified heat source model to reduce the number of transient steps required to complete the simulation, thus increasing the computational efficiency in order to simulate welding of large structures. The authors recognised the limitation in the use of welding simulation for practical residual stress and distortion control and identified ways in which researchers often tried to simplify the approach. Notwithstanding this they conclude that three-dimensional thermo-elastic-plastic simulations are often required to obtain meaningful results and hence concentrated their efforts on simplifying the thermal analysis. To this end they proposed two computationally efficient heat source models:

- Prolonged Gaussian distribution: this is an extruded form of the traditional Gaussian distribution. It requires a modified acting time to ensure that the heat input is equal to the originally chosen model (Gaussian distribution in this case). This method, though computationally efficient, requires modification for different cases (e.g. fillet welding) and sub-routines to be developed.

- Prolonged point heat source model: a simplification of the above. The Gaussian distribution is assumed to be concentrated at a number of nodes and act simultaneously for the same heating time of the prolonged Gaussian model.

Verification was done by simulating a bead on plate with the two proposed heat source models against a base-line simulation in which the standard Gaussian

disc heat distribution was used. The number (and hence the size) of segments used for the prolonged models was also varied to give a total of five cases. Low discretisation levels were purposely considered by using very few segments in order to investigate the poorest possible precision levels. The least number of segments to be used is three as that can represent the beginning, quasi-steady and final conditions of the welding process. In-house code was used and the longitudinal curvature forming on one side of the plate was taken as the representative measure of distortion. Results showed similar distortion magnitudes, but a variation in the distribution. The models with more than one segment yielded an unsymmetric pattern, due to transient effects. The coarse meshes gave a reasonably good prediction. As can be intuitively expected, an increase in the number of segments yielded better predictions, at the expense of computational time. It was concluded that the prolonged heat source model can be used for stress and distortion prediction. However the authors mention that there are some differences in the heat source models that could be hidden by the fact that shell elements were used. Therefore it is still advisable to validate the applicability of shell elements for each specific case.

The above models all aimed at bypassing the complex part involving the weld pool formation. This is convenient and is advisable when the thermal analysis will be used as an input to the structural simulation in order to obtain a global structural response. However there are also many researchers who have focussed on detailed simulation of the weld pool. Zhao et al [2.13] dealt with the simulation of dynamic changes of the weld pool as welding parameters are changed during the actual welding process. They were able to predict the weld pool shape and use their model to investigate the effects of step changes in welding current and welding speed.

2.3 Structural Simulations

2.3.1 Simplified Models

Reduction in computational time has always been a priority in welding simulation. This has led to the development of simplified methods which allowed for the reduction in computational effort in order to extend the applicability of the relevant simulations.

A possible first step in the simplifying the simulation is to recognise the weak coupling between the thermal and structural behaviour, a technique which is extensively used by many researchers (e.g. [2.14], [2.15], [2.16], [2.17]) and is shown schematically in Figure 2.3. Lindgren [2.18] illustrates the effect that de-coupling has on the simulation process. Jiang [2.19] carried out a study in which coupled and un-coupled models are compared as regards to their capability of predicting residual stresses and distortion. It was found that using un-coupled fields element greatly reduced the computational time without any loss of accuracy in the prediction of residual stresses. This means that a sequentially coupled approach can be adopted in which the thermal analysis is first carried out and is then used as an input load for the structural analysis.

Figure 2.3: Simulation flow for cases of (a) Coupled vs. (b) Uncoupled thermal-structural welding physical phenomena. Adapted from [2.18]

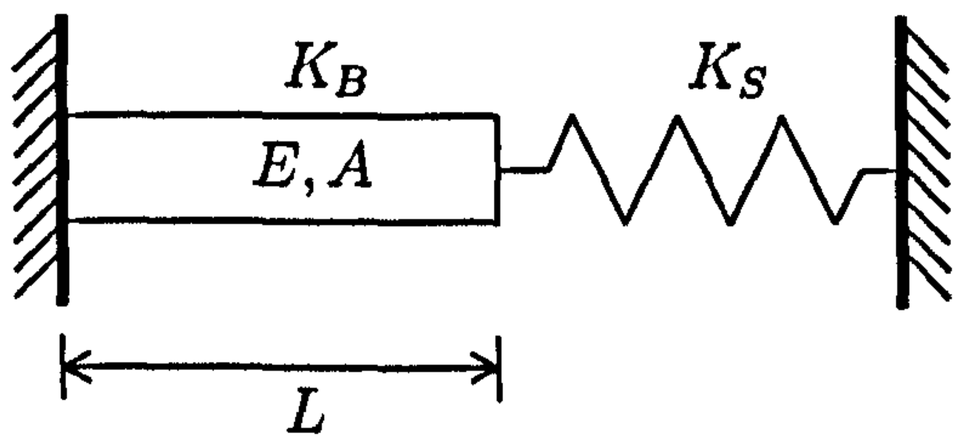

Figure 2.4: Spring bar model

This simplification however still leaves the complex elasto-plastic structural part to be solved. This can also be reduced to a simpler analysis by looking at the evolution of stresses and strains during the welding process and noticing certain features that can lead to the safe adoption of simplifying assumptions.

A very simple and rudimentary strategy was proposed by Bachorsky et al [2.11], named the Shrinkage Volume Approach. This reduces the complex transient elasto-plastic analysis into a single elastic finite element analysis in which elements associated with the weld pool are given a contraction strain of $(-\alpha\Delta T)$. By assigning initial nodal temperatures to the weld metal elements, the heating part of the thermal cycle is essentially ignored reducing the problem to a steady-state approach. This assumption also causes the stress history during heating to be ignored meaning that the magnitude of the predicted residual stress field in a given analysis cannot be accurate. A drawback of this method is the fact that the results depend heavily on the assumed weld pool shape obtained from the thermal simulation. Discrepancies between predicted and experimental values were noted for some of the models, which the authors attributed to bad prediction of weld pool shape. In order to obtain good distortion predictions macro graphs were used to obtain real weld pool shapes.

Jang et al [2.20] developed a simplified method called the Inherent Strain Approach. This is based on a spring-bar model schematically shown in Figure 2.4. The spring models the weld pool whilst the bar represents the surrounding (and hence restraining) material.

The following relations can be formulated for the system:

$$\varepsilon = \varepsilon_{th} + \varepsilon_e + \varepsilon_p \tag{2.6}$$

$$\sigma = E\varepsilon_e \tag{2.7}$$

$$F_B = F_S \tag{2.8}$$

The above relations are used to determine the amount of residual plastic strain as a function of degree of restraint. In this context the degree of restraint is the level of resistance against thermal deformation of the welding region. The amount of plastic strain is determined for each case and used to formulate equivalent loads (longitudinal and transverse forces and moments) to be applied to the structure by means of an elastic finite element analysis.

Another simplified technique is presented by Deo et al [2.21] (already presented in earlier work [2.22]). The authors recognise how early models provided good prediction for residual stresses even if most of the modelling techniques were two dimensional. However, for set-ups which yield out-of-plane distortion, two dimensional models may prove to be inadequate. The authors illustrate how de-coupled, two-dimensional welding simulations can be carried out in conjunction with three-dimensional buckling analyses on structures where movement is restricted by fixtures or tacking. For fully clamped structures the buckling effects would be noticeable once the clamps are removed. Based on this understanding the author uses a simplified approach in which a two-dimensional welding simulation is performed followed by a three-dimensional buckling analysis.

This approach is analogous to the work by Jang [2.20] et al using the inherent strain method, with the advantage that the applied stress/strain field comes from a two-dimensional analysis rather than an empirical determination based on the temperature field and the spring-bar model. Hence a two-dimensional de-coupled sequential thermo-mechanical analysis is first performed. This is an elasto-plastic

analysis carried out in a quasi-static Lagrangian frame subdivided in several small static steps. Generalised plane strain conditions were assumed, which imply linear variation of the longitudinal strain. The resulting plastic strains are then applied as equivalent loads in a three-dimensional eigenvalue analysis. A constant negative thermal load is applied at the weld region to introduce the effect of welding in the three-dimensional structure. The authors further simplify the analysis by assuming the same material model for the weld and parent material, based on previous work that which showed that a 20% difference in yield strength of the electrode material causes only a 3% change in residual stress. Finally, the longitudinal residual stress obtained from the two-dimensional elasto-plastic analysis is compared with the buckling critical stress to determine if the structure will indeed buckle. Eigenvalue analyses were used for determining the buckling stress (an incremental large deformation analysis could have been performed instead but would have been more computationally intensive). The models were verified experimentally and an in-house FE-code was used. The method was successful in predicting whether the plates buckled or not and recommendations could be made regarding the influence of geometric parameters on buckling.

Camilleri et al [2.23], [2.24] proposed another simplified approach aimed at reducing the computational time. Similarly to all simulation procedures described so far (in this section) the thermal part is performed first with a thermal analysis. The approach for the structural part is based on the early ideas of N. Okerblom [2.25]. The approach comprises two algorithms, namely the 'Thermal Contraction Strain (TCS)' algorithm for computing the angular deformation and the 'Mismatched Thermal Strain (MTS)' for determining the longitudinal contraction. The algorithms are based on key characteristics of the thermal transients generated by the fast-moving, intense heat sources: the temperature gradient on the approach side of the thermal source is steep, as the forward heat flow rate is relatively small, and for similar reasons, the temperature profile transverse to the weld is steep, whereas the gradient in the trailing region where cooling takes place

is relatively shallow. Okerblom was the first to draw attention to these features and argued that the thermo-mechanical processes might therefore be modelled by considering a transverse plane strain slice, which would be passed through the quasi-stationary temperature field in the direction of welding.

In the case of the angular deformation (TCS) algorithm, the assumption is that the transverse angular deformation is dictated predominantly by contraction across the weld fusion zone, which typically varies in transverse width across the thickness. The starting temperature assumed for this process should correspond to a level at which the material begins to develop some strength (which can be safely assumed to be 1000°C). Similarly to the 'shrinkage volume' approach used in [2.11] (and by other authors presenting simplified models), the TCS algorithm neglects the heating phase and assumes that an arbitrarily defined zone contracts. However the authors show how the notion of transverse contraction can be extended to express the transverse angular deformation θ in terms of the relative depth of penetration of the weld $\frac{s}{t_0}$ and the relative width of the fusion zone on the surface $\frac{b}{t_0}$ by using the following relation:

$$\theta = \frac{s}{t_0}\frac{b}{t_0}\alpha T_s \left[3(1-k_w^2) - 2\frac{s}{t_0}(1-k_w^3)\right] \tag{2.9}$$

Where k_w is a geometric parameter dependent on the shape of the fusion zone (parallel, triangular, or parabolic).

The notion of contraction is developed in a different manner for strains in the longitudinal direction (MTS algorithm). In this case the longitudinal contraction forces are derived from the thermal strain mismatches developed during the cooling phase of the welding process. A plane strain slice can be imagined to pass through the transient temperature field which in turn progressively spreads outwards. An important consequence of this is that the development of longitudinal stress is driven mainly by the envelope of maximum temperatures reached across the slice, shown in Figure 2.5 for typical welding parameters. Although

these temperatures are reached at different times in practice, there are always mismatches at each transverse location and therefore the assumption is that it is not necessary to take account of the time offset in attaining the respective maxima. It is however worth noting that in this approach the contraction forces are determined by the full temperature field and not, as in the shrinkage volume approach by the behaviour of a defined region.

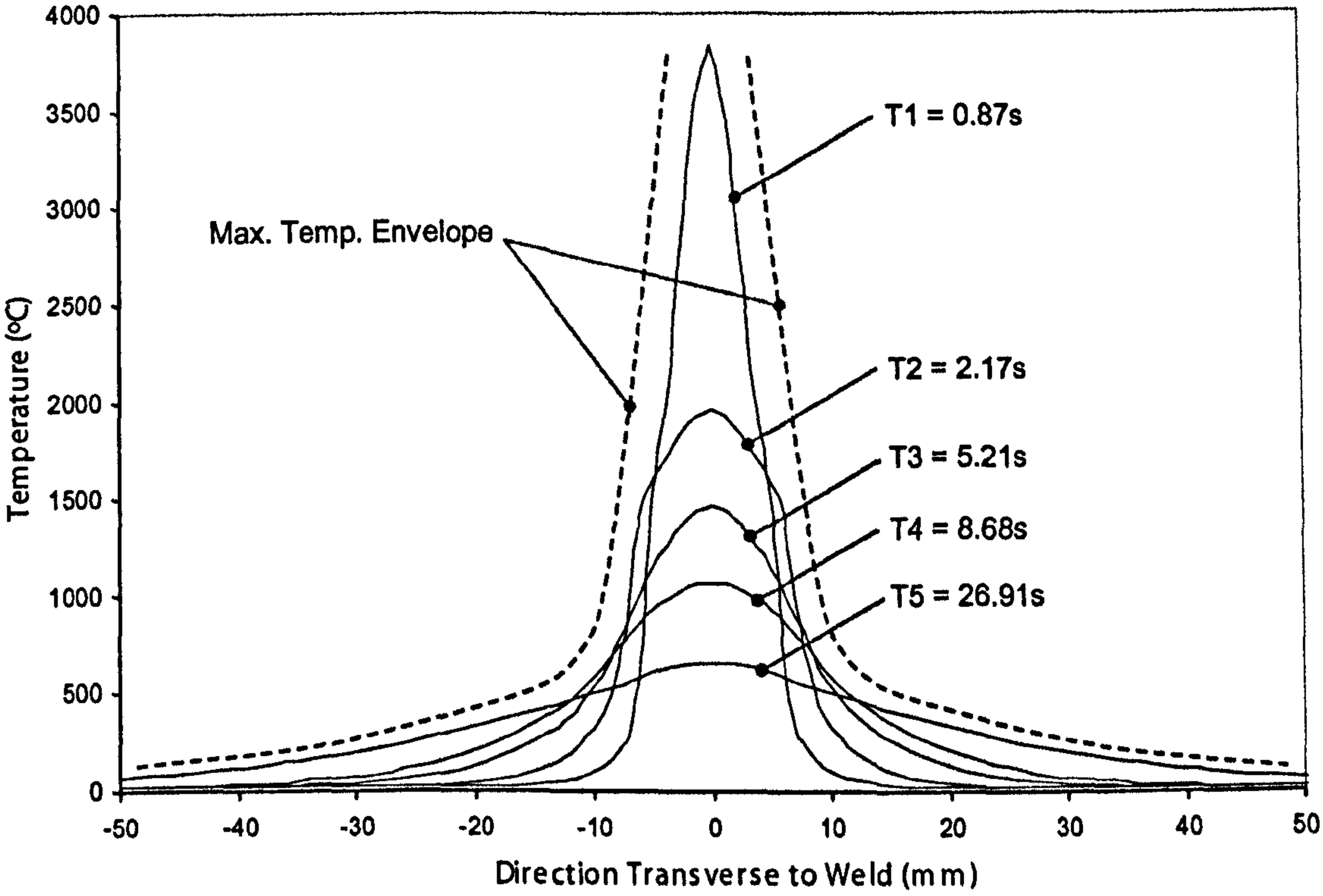

Figure 2.5: Envelope of maximum temperatures reached across a slice normal to the welding direction

The longitudinal stress aspect is the most difficult to analyse in principle, due to the complexities of material behaviour mentioned earlier. However, substantial simplifications are admissible due to the fact that the longitudinal stress levels in central regions of the weld where the complex behaviour takes place are limited by the final yield strength. The authors also show that the typical profile of maximum transverse temperatures is inversely proportional to the distance from the centre line of the weld, approximately, and this leads to a weak dependence on the actual yield strength value, leaving the expansivity as the major driving force.

The expansivity and yield characteristics in an elastic-perfectly plastic model for steel are such that a relatively small temperature difference (120°C) causes yielding in a typical case. Hence the mechanics of contraction force development are driven primarily by the cooling phase of the cycle within a relatively low temperature range (e.g. less than 300°C for steel) within which the material properties are likely to be fairly constant. The resulting MTS algorithm is implemented within a three-dimensional, elastic, finite-element formulation by applying a 'load' profile corresponding to an artificial temperature reduction at points across the width of the plane strain slice. In the central region, defined by thermal strain levels which exceed twice yield strain, yield magnitude tensile strain levels are applied. No loads are applied in the other regions which remain elastic, defined by thermal strain levels less than yield strain (ε_Y). In the zones between the fully plastic and elastic regions, loads corresponding to ($\alpha T_M - \varepsilon_Y$) are applied, where T_M is the maximum temperature reached at the location. These algorithms were applied, in the studies reported earlier [2.26] , to a 3D elastic model of a 6 mm thickness, half-metre square test geometry (two 0.25 m wide by 0.5 m long plates butt welded along the 0.5 m edges). Comparison between these results and the average experimental deformation was good although it should be noted that the complete results are sensitive to the temperature-dependant properties assumed. These algorithms, however, proved to be a good basis to develop further simplified methods for different cases such as single [2.27] and multiply stiffened [2.28] plate structures.

Finally, another simplifying approach is presented by Ueda et al [2.29] , this time with regards to multi-pass welding. The authors recognise how overlapping weld passes successively relieve stresses at temperatures higher than phase transformation temperatures. The multi-pass welding process is hence simplified in the simulation by missing out the simulation of individual passes, reducing the mesh density.

It is essential to be aware of the deficiencies that are commonly present in

most simplifying approaches in order to make correct use of them and obtain meaningful results. The following are usually true for most simplifying welding simulation approaches:

- The transient evolution of stresses is normally bypassed, leading to weak prediction of residual stresses
- The effect of high temperature material properties is usually ignored or approximated in a particular temperature range and this choice usually affects the results to some degree
- The initial shape of the structure under investigation has an important effect on the final result
- Transient aspects such as intermediate buckling cannot be predicted

Notwithstanding this, the above deficiencies do not pose a limit for the use of such simplified simulation techniques in several industrial applications. They are in fact, particularly useful when:

- A relatively large structure has to be analysed
- Parametric studies have to be carried out
- Some of the expected distortion modes are validated through experiments and distortion of similar set-ups needs to be investigated

Much research effort is therefore still being put into the use of simplified simulation techniques, usually verified and validated through experimental investigations and/or the use of more complex modelling techniques.

2.3.2 Complex Models

More complex models, that aim at including some or most of the aspects on the elastic-plastic phase are usually adopted if the following aspects need to be investigated:

- The effects of temperature dependant material properties
- Effects of phase changes
- Plastic response of the material
- Transient aspect

Transient elasto-plastic analysis carries a penalty in terms of computational time. The other drawback is usually the lack of information on material properties for the full range of temperatures to which the welded structure is subjected. Nonetheless, a great deal of literature is available on complex finite element analysis of welding induced residual stresses and distortion. It is important to notice that in most cases the thermal part of the analysis is still de-coupled, on the same basis as described in the previous section for the simplified models. The approach is sometimes referred to as 'sequentially coupled', but does not imply the use of coupled field elements. Some authors (such as [2.30]), however, still prefer to resort to fully coupled analyses in which thermal and structural fields are solved simultaneously, at the expense of computational time.

Friedman [2.5] was amongst the first to illustrate the use of numerical techniques for the analysis of the complex elasto-plastic parts of the welding process, despite the fact that his work was done when computer limitations placed a considerable restriction for developing full models. Again the author highlights the low thermo-elastic coupling coefficient which makes it possible to use the uncoupled thermal-structural approach. Friedman gives a detailed description of dynamic stress development during welding, and the effect of plane strain assumption. An important result is the demonstration of how the residual stresses in the plastic regions exceed the room temperature yield strength because of material strain hardening. The brief initial compressive yielding produces an expansion of the yield surface followed, during cool-down, by yielding in tension at a stress level higher than the monotonic yield strength.

Murthy et al [2.31] also present numerical techniques for the solution of the elasto-plastic phase of the simulation. They also carry out a de-coupled thermal analysis to be subsequently input in the structural analysis. The authors highlight the restriction in running three-dimensional models because of the computational effort required. The accuracy of the two-dimensional model increases as the welding speed increases since temperature gradients in the longitudinal direction become negligible. The authors mention Goldak's three-dimensional double ellipsoid heat source model and then present a simpler, easier to converge, trapezoidal model (ramp up - constant - ramp down). The authors reference work demonstrating that the time independent thermo-elasto-plastic formulations are sufficient as opposed to the thermo-elasto-visco-plastic models. Creep must be included however when analysing stress relief conditions of post welding heat treatments. The authors show how the material dilation produced as a result of solid phase transformations during cooling induce microscopic plastic flows that are similar to the thermally induced strains. These are found to cause a reduction in the peak longitudinal tensile stress and are limited to the weld zone and part of the heat affected zone. They can be evaluated either by:

- Reducing the thermal expansion coefficient over the transformation temperature range
- Computing the dilatations proportional to the quantities of various phases formed

The first method is more convenient for implementation in commercial software, but the second gives more accurate predictions of changes occurring during the transformation.

On the other hand the microscopic plastic flows that occur during metallurgical transformations (transformation plasticity) are modelled by either:

- Reducing the yield strength of the material over the temperature range for which the transformation is occurring

- Including an additional plastic strain which is related to the progress of transformation and also the instantaneous deviatoric stress state

The first method is more suitable for commercial codes, but the second case gives better results with user generated codes. Also, it is highlighted how the effects of phase transformations may be neglected unless:

- They occur at very low temperatures
- They are comparable to the thermal contraction strains
- There is a rapid cooling of the weld pool

Berglund et al [2.32] investigated the prediction capabilities of two-dimensional and three-dimensional shell elements by comparing the result with equivalent three-dimensional solid element analyses. For each type of model they investigated three cases of clamping ranging from a fully clamped model to one loosely fixed at one end. With the exception of the transverse deformation of the fully clamped case, the two dimensional plane strain models proved inadequate to predict the out-of plane deformation. Residual stresses were also predicted correctly for all models with the exception of the longitudinal stress of the two-dimensional plane strain model which exhibits the characteristic profile shifted upwards (greater residual tensile stress).

Nasstrom et al [2.33] also investigated the effects of introducing shell elements in order to reduce the number of degrees of freedom. They created models with a combination of solid and shell elements together with models containing purely either or type of elements. An un-coupled, sequential thermal-structural approach was used with the use of a welding efficiency in order to relate the heat input in the model to the actual energy being provided by the welding power source. Similarly to previous authors, thermal analyses were carried out in a two-dimensional fashion based on the fact that the greatest thermal gradients are found in the direction transverse to the weld. An in-house finite element code was used to carry

out the thermal and the elasto-plastic analyses, without phase change modelling, as the material under investigation experiences no solid state transformations.

The authors carried out another interesting investigation with regards to modelling techniques by varying the cut-off temperature from 900°C to 1200°C. This turned out to yield only a small change (5%) in the predicted maximum residual stress. As regards the solid vs. shell element investigation, the results showed that for the longitudinal stresses, the results from the combined model approached the solid model residual stress field whilst the shell model gave erroneous results especially in the region close to the weld. This is in contrast to Berglund et al [2.32] who found three dimensional shell elements to be adequate. This might be attributed to the differences in case studies and shows how there often are many uncertainties and unknowns as to the correct modelling technique to be adopted.

The authors identified one source or error as being the lack of temperature variation through thickness for the shell element model. For transverse residual stresses, differences between solid and combined model were even greater and might have been caused by the adopted solid to shell transformation. Another source of error was the restriction of movement in the shell's normal direction for nodes connecting the solid and shell elements. The possibility to adopt shell elements in a commercial general purpose finite element package is also illustrated in [2.34] together with the programming/scripting methods that must be adopted in order to implement various welding modelling strategies and techniques.

Borjesson et al [2.35] tried to include several material modelling aspects for multi-pass welding simulation, especially focussing on the temperature dependency of the properties. They used a mixture rule in order to resolve the problem of modelling different properties for the different phases. This technique was also used by other researchers (e.g. [2.36]) and consists of computing properties at a macro level according to volume ratios of the respective phases present in the material. The increased complexity of the material model did not lead to a great improvement in correlation with experimental data, and this was attributed to

the limitation of the material data available for the different phases.

Zhu et al [2.37] investigated the implications of increasing the complexity of the material model for aluminium (stating the investigation could be extended to steel) by comparing three models in which the properties were taken as:

- Constant (room temperature values)
- Averaged over the temperature range and history
- Fully dependant on temperature

Again an un-coupled thermal-structural approach was used with a Gaussian heat distribution input and a cut-off temperature technique which was taken to be two thirds of the melting temperature. An in-house (user developed) code was used in which dummy elements were used to simulate multi pass welding. This is analogous to the element birth and death technique, sometimes referred to as element activation/de-activation. The temperature dependency of material properties was investigated for both thermal and structural analyses. In the former analysis the authors considered a number of models by varying the combination of density, specific heat and thermal conductivity each one of these properties in turn being taken as constant, averaged or completely temperature dependant. The case in which all properties were set to be temperature dependant was taken as the reference analysis. The following conclusions were reached from the thermal analyses results:

- Density can be taken as room temperature value
- Specific heat can also be taken as room temperature value
- For thermal conductivity:
  - Room temperature values resulted in an overestimate of temperature, by less than 10%

  - Averaged value gave a very close match

- When all three properties were set to room temperature values, the results were very close to the case where the conductivity was given a room temperature value and other properties were made temperature dependant. For this case the results were within 10% of the base-line simulation and also close to experimental data

The same study was performed to investigate the dependency on structural material properties. The authors illustrated the elasto-plastic constitutive equations show that the Young's modulus, yield stress and thermal expansion coefficient are the driving factors for deformation modelling. Poisson's ratio and plastic hardening were not included as varying factors and were kept constant. Again authors used a combination for the type of temperature dependence to be used. The heat input models were also varied to see the effect that the thermal properties temperature dependence has on the final structural analysis, leading to a larger number of cases. Similarly to the thermal investigation, the case for which all properties (for both the thermal and structural analyses) were taken to be temperature dependant was taken as the reference analysis. Keeping the same mechanical properties but varying the thermal input material properties led to the following conclusions:

- If averaged conductivity is used, values agree well, except in regions very close to weld line

- For all thermal properties taken at room temperature values, the maximum error was found to be less than 10%

Hence the authors conclude that the variation in thermal properties has no effect on the subsequent structural analysis.

For cases in which same thermal input was used the following observations were made:

- If room temperature Young's modulus values are used, results matched well
- If average Young's modulus values are used, results deviated considerably
- If room temperature yield stress is used, the residual stress and deformation were incorrect
- If averaged yield stress is used, results were in the correct mode but of incorrect magnitude
- In the case of the thermal coefficient of expansion, both the room temperature and averaged value cases agreed very well with reference and test data

The discrepancy in the cases where a constant yield stress was used led the authors to formulate a piece-wise function to model the variation of yield stress with temperature. This proved to be a good approximation.

Bergheau et al [2.36] investigated the effects of modelling visco-plastic material behaviour by comparing results obtained from analyses with plastic and visco-plastic material formulations. Their work stems from an interest in welding induced residual stress prediction for the nuclear industry and the control of distortion in automotive welding applications. The authors highlight the scarcity of literature presenting simulations that have accounted for visco-plastic effects. These are often neglected because the welding processes under investigation are usually too short in duration to account for creep effects. However their experimental work consisted of a set-up (schematically shown in Figure 2.6) specifically designed to maximise the influence of the material behaviour in the heat affected zone (HAZ), where viscous effects can take place. It also provided a simple geometry which is easy to simulate with an axisymmetric model. The following measurements were taken for experimental verification:

- Thermocouples for an *a priori* determination of the unknown thermal boundary conditions (this is similar to the method used to determine welding

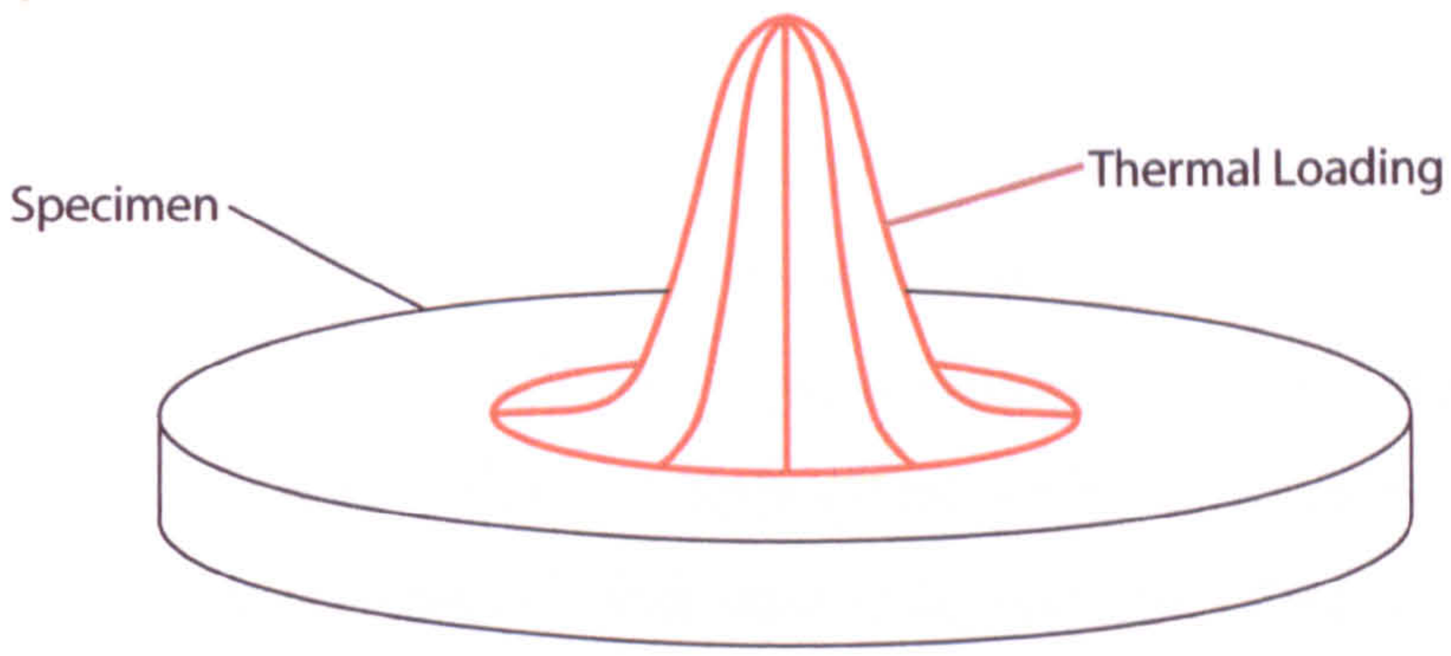

Figure 2.6: Schematic representation of set-up used in [2.36]

efficiency in the present work)

- Inductive sensors to measure transient displacements
- X-Ray diffraction measurements for final residual stresses
- Strain measurements using the "numerical image correlation" technique to check for axisymmetry
- Metallurgical macro-graphs

The experimental error on measured stresses was thought to be of the order of 50MPa. In their simulations the thermal and metallurgical computations were fully coupled. Heating arising from plastic (or visco-plastic) dissipation and the influence of stresses and transformation kinetics were disregarded. This essentially meant that the thermo-metallurgical calculation was de-coupled from the mechanical one.

Enthalpy was used in the thermal analysis to avoid numerical problems caused by sharp changes of conductivity with temperature. The overall specific heat vs. temperature variation was determined experimentally from a small sample. It was not fed in the model directly but instead used to calculate properties of different phases so that metallurgical aspects could be fully included. This essentially led to a custom made heat input distribution. The use of such an advanced material model however required extensive efforts for the determination of the actual

properties. This is evident by the extent of the referenced data which was used in order to carry out the metallurgical calculations. The volumetric fractions of each material model were determined with "first-order evolution equations" (this is a similar approach to that used in [2.35]) from parameters obtained experimentally from free dilatometry tests. This, in conjunction with the Koistinen-Marburger martensitic transformation model, was used to extend modelling up to the HAZ. Transformation plasticity is hence fully accounted for whilst other mechanisms involving metallurgical to mechanical changes were proved to be negligible for this class of material.

The viscous effects were introduced by allowing a variation of yield stress with strain rate. Isotropic hardening was used and was set to zero for newly formed phases. The remaining material data were determined experimentally with a focus on plastic vs. visco-plastic effects. The low strain rate data (no visco-plastic effects) was taken so that the strain rate was roughly equal to the experimental cooling part. This obviously meant that the purely plastic (no viscous effects) models did not pick up the high strain rate effects that occur in the heating part of the welding cycle. An important consideration made by the authors was that the purely plastic models could only be made to fit precisely either the heating or the cooling part of the process. This relates to the present work in which purely plastic models were used, with an emphasis on the cooling part of the thermal cycle since this is the driving part for the formation of residual stresses and distortion. The authors determined visco-plastic material properties experimentally. Extrapolation of the data to higher temperatures was validated by means of comparison with independent tests. Finally, the analysis was carried out with the inclusion of large displacements in a Lagrangian numerical framework.

The results showed an accurate thermal history prediction which even exhibits perturbations caused by phase changes. HAZ predictions of temperature matched with experimental data. The transient distortion prediction however did not compare as well. The main form of distortion occurred early in the plastic-

model simulation with the residual distortion being over-predicted by a factor of two. The discrepancy was greatly reduced in the visco-plastic-model simulation. Residual strains were well predicted for both models, with a slight over prediction of the maximum radial and tangential strain for the plastic model. The maximum residual stresses were found on the periphery of the HAZ. Within the HAZ the stresses decrease because of the expansion caused by the bainitic and martensitic transformations and the transformation plasticity. Good correlation with plastic and visco-plastic models was achieved. Both calculations predicted the location and magnitude of peak values. On average, the visco-plastic models predicted stresses slightly better. Hence the author concludes that the effects of visco-plasticity were marginal on residual stress prediction.

Abid et al [2.38], [2.39] omitted the complicated metallurgical transformations when modelling pipe-flange joint welds. They carried out sequential un-coupled thermal-structural simulations with material model complexity limited to the inclusion of non-linear, temperature-dependant thermal and structural properties. Nevertheless this method proved to be adequate in the prediction of welding induced flange distortion. Residual stresses could also be extracted from these models that were also used to investigate the effects of tack weld positions on the flange. It is worth noting that the tacks were considered by assuming them as existing material prior to the simulation of the full weld, i.e. no simulation as regards to the tack welding process was included. The element birth and death technique was used for simulating metal deposition in the joint V-groove. The thermal simulations were carried out in a similar manner to the models referenced earlier, with the addition of a "scalar multiplier" for the thermal input model. This additional feature is analogous to the welding efficiency: i.e. a parameter whose initial value is chosen arbitrarily and is then re-adjusted iteratively to achieve a good match to the weld pool shape. Whilst the welding efficiency is a single parameter representing the ratio of total net heat input in the model to the heat provided by the welding equipment (power = current × voltage)

the "scalar multiplier" used by the authors varied with axial and radial distance from the weld and outer surface respectively. This allowed for a relatively simple heat input model (the authors use a volumetric heat input model) that still gave detailed weld pool and HAZ predictions.

It has been shown how most researchers employ an element birth and death technique in order to simulate weld metal deposition. This simulation technique is based on multiplying those terms in the stiffness matrix that represent the de-activated elements by a very low factor (multiplying by zero is not permitted to avoid numerical problems). This is done to remove the effects the welded elements have on the structure until they are deposited/activated. Fanous et al [2.40] compared this technique with a slightly different re-activation technique based on gap elements. The activation of the elements was based on an arbitrarily set spacing between the gap element and the base plate, which is changed as the elements became reactivated. Results showed a good match with the standard element birth and death technique and a reduction in computational time.

Tsirkas et al [2.41] attempted to partially apply the complex thermo-elastic-plastic treatment at an industrial scale by applying a "local-global" approach, first presented by Michaleris et al [2.22], to laser welding of large shipbuilding sub-assemblies. Laser-welding processes are attractive as they provide a smaller heat input and hence a smaller susceptibility to distortion. Trial-and error approaches have proved to be problematic in the prediction of distortion and control techniques based on numerical simulations are therefore required. Many laser welding models concentrated on small specimens where the heat affected zone area is comparable to the work-piece. Although these are fundamental for the understanding of the process, global models are required in order to predict residual distortion correctly. The authors highlight how it would not be feasible to create a model with enough refinement at the HAZ to include both local and global effects, hence the adoption of the "local-global" approach. A number of authors have previously dealt with the simulation of the localised effects of laser welding (key-hole)

and the application of various heat source models. As a general rule they have all approximated the shape of the key-hole to simple geometrical models. In this work however, the software Physica was used to determine the fused zone. The author references various research work for the complex elasto-plastic approaches for welding simulation but highlight the fact that in many cases not all the parameters influencing the welding process are taken into account. In an attempt to include all possible factors the commercial package Sysweld was used. Many aspects of the package are however similar to the approaches presented earlier such as the use of a Gaussian heat distribution (based on the key-hole model) with an elasto-plastic analysis that includes the effects of temperature-dependence and metallurgical transformations. The case study consisted of a stiffened panel, with particular emphasis on the fillet welds and on their sequence of welding. Although parameters vary during the actual process because of adaptive process control, they were kept constant in the numerical models. The following is the procedure required for the adoption of the local-global approach:

1. Evaluate key-hole size with a multi-physics simulation package (Physica)

2. Build the local model (thermo-elasto-plastic: a number of iterations were required at times)

3. Build the global model

A detailed analysis for the formation of the key-hole was carried out. This involved detailed and iterative algorithms specific to the laser welding process. Two major steps were involved:

1. Determining the shape of the keyhole with respect to the process parameters and the actual work-piece

2. Creating a suitable mesh according to the shape of the keyhole and applying the relevant boundary conditions (evaporation temperature) to then solve using Physica, and deduce the extent of the liquid region

For the T-joint configuration a special algorithm was used to determine the heat distribution which was then used to carry out three sequentially un-coupled thermo-elasto-plastic models to cater for the different sequences found in the global model. Kinematic hardening with phase-transformation computations were included. Convective and radiation heat losses were included in the model by means of user-subroutines. A key assumption for this approach was that the formation of local strains was dependant on the area very close to the weld line only. Hence the justification for carrying out the thermo-elasto-plastic analyses for the local parts only.

After the complete welding process was simulated with the thermo-elastic-plastic models, the stress field (σ) could be expressed locally in terms of the Elastic Young's modulus (E), the total stress field ε_{tot} and the plastic strains ε_P as:

$$\sigma = E\left(\varepsilon_{tot} - \varepsilon_P\right) \tag{2.10}$$

Thus the residual stress for the whole structure could be computed by carrying out an elastic simulation and applying ε_P as initial strains. This was done by linking the local model to the global model which was made up of shell elements. Even though the authors mention that the development of strains in the local models depended solely on localised structural evolutions, they then state that the boundary conditions of the local thermo-elasto-plastic models must be selected carefully to match the global model. This leaves some uncertainty as to the adoption of this approach for a wider range of applications.

Experiments were carried out for the two different sequences of welding. However, the initial deformations due to tack welds and supports were not included. The exact boundary conditions were not recorded during the experiments so that the plates were assumed to be lying flat on the ground in the computational model. Dead weight has an important effect on sub-assemblies of this size and

was included in the simulations. The computed reaction forces showed that the assembly effectively rested on points at specific locations on the ground, meaning that the positions of the supports have an important effect. From the experimental investigations it was evident how the differences in distortion for the two sequences depended mainly on the global geometry of the structure. The computational models compared well to one of the sequences only. The authors believe this was due to the effects of the supporting pins, for which further investigations must be carried out. The computational time achieved was however within an acceptable industry time-frame.

A full thermo-elasto-plastic model was carried out by Boitout et al [2.42], [2.43] using the commercial package Sysweld. The authors recognise how the welding process is based on the interrelated phenomena of electromagnetism, heat transfer, metallurgical transformations and structural evolutions. However, for continuous seam welding, the thermal, microstructural and mechanical parts need only be considered. Electromagnetic effects are relevant in spot welding and induction hardening whilst diffusion effects are relevant in case hardening, nitration or carbonitriding. For the thermal simulations, non-linear, temperature-dependant and phase-dependant properties were used, together with the inclusion of latent heat effects. Convection and radiation boundary conditions were also modelled in a non-linear fashion.

The authors explain how there are essentially two possible types of welding simulation: one to determine the molten pool shape and the other to determine stresses and distortions in the whole work-piece. If the molten shape can be predicted it can be used as an input to the thermo-mechanical simulation, but a more convenient alternative is to use analytical heat input models that depend on the type of welding. Similarly to previous referenced authors, a double ellipsoidal volumetric heat source was used. The commercial software used can also include the influence of the metallurgical phase transformations that occur during cooling. Again calculation of phase fraction formation was done in accordance to classical

metallurgical models (namely the Johnson-Mel-Avrami law) whilst the martensite transformation was calculated in accordance to the Kostinen-Marburger law. Energy transfer/retention associated with latent heat changes was accounted for through the variation in enthalpy with respect to temperature, which in turn is related to the phase transformations. The software also allows for auxiliary parameters to cater for additional chemical elements (for example excess carbon in the surface layer of carburised components).

Results for typical case studies were presented, for both residual stresses and distortion predictions. The software proved successful in modelling these cases, and proved effective in constructing a complex model, which is however built on many years of experience and knowledge focussed at generating material data and computational methods to solve the complex analyses.

The above references have shown the great diversity in complexity and approaches used when developing numerical models for welding induced residual stress and distortion simulation. Although the case studies and simulation techniques are different and the results sometimes conflict they are nevertheless useful as reference when choosing which strategy to adopt for the application to be analysed.

2.4 Artificial Neural Network Approach

It is apparent from the above references that the use of finite element simulation techniques for stresses and distortion prediction is not trivial and requires a good understanding of computational methods for both thermal and structural analyses. Moreover, many factors of the real welding process and procedures are not included or cannot easily be simulated using purely numerical techniques. This has led some researchers to adopt alternative simulation techniques, the most recent being the implementation of artificial neural networks (ANN). Lightfoot et al [2.44], [2.45], [2.46] used a commercial artificial neural network package to simulate welding induced distortions.

Artificial neural networks are electronic models that find inspiration from available knowledge of the working mechanisms of the biological brain [2.47]. The aim is to make the model learn from experience and their structure allows for an arbitrary number of inputs and outputs. The input parameters are passed through a network consisting of a number of layers whose architecture allows for all possible interactions of the driving (input) parameters, each combination being weighted by a scalar factor. The network is designed to be as general purpose as possible so that it can be used as a 'black box'. This however requires that the neural network is appropriately trained before it can make any useful predictions. The authors used a set of experiments to train and develop the neural network for the prediction of out of plane distortions. An interesting feature of this simulation technique is the ability of the software to highlight which parameters have the greatest influence on the prediction. The main conclusions drawn from their simulation work was the recognition of the great potential in applying these methods to distortion related issues. It is however also important not to simply take the outputs from the models at face value without first acquiring an understanding of the scientific developments of the process.

The main drawback of an approach based purely on neural networks is the training required by the model in order to make useful predictions. Casalino et al [2.48] attempted to overcome this deficiency by using a combination of finite element and neural networks techniques. They identified the following operational parameters affecting metal transfer during welding:

- Welding current
- Arc voltage
- Wire feed rate
- Electrode extension
- Composition of the shielding gas

- Polarity of the electrode
- Wire diameter

Artificial neural networks were used to calculate the bead geometry from the welding parameters. The bead geometry predicted from the ANN was then used together with the welding speeds as input parameters for the finite element models. Finally, fuzzy logic was used to qualitatively classify the results. The authors point out how the artificial neural network must not be over-trained to avoid the risk of the model just 'remembering' the training and losing the ability to give good predictions for other data sets. This means that even though every network could have been trained for better performance, it would have reduced its ability to generalise its knowledge for new data, which in turn decreases the validation performance. The prediction of the artificial neural network was then used as a thermal input in the finite element model by applying the molten temperature, taken as 1500°C, to the weld pool geometry (this is a simpler approach than the double ellipsoid heat input model used by most authors).

Contrary to Lightfoot et al [2.44], [2.45], [2.46], the authors did not investigate the effect of the weighting of each process variable on the final results. Their main conclusions were:

1. The artificial neural network proved adequate to predict the weld bead geometry
2. The predicted weld bead geometry proved to be a valid input for the subsequent distortion finite element simulation

Kim et al [2.49] also investigated the possible interaction between neural networks and finite element (FE) methods by developing a system that integrates a database, a finite element analyses and an ANN. The system was designed to predict optimum parameters for pipeline welding set-ups. The authors acknowledge the large number of researchers that have used experiments and welder experience

in order to obtain optimum welding parameters. Many have tried to model the relation between welding parameters and weldability, with limited success, owing to the great complexities and uncertainties the arc welding process involves. Moreover, different models exhibit great variations mainly because:

- They are based on a particular set of experiments
- They use linear regression techniques to model the data (which are in fact highly non-linear)
- They assume various simplifications

The authors give references of researchers that have tried to apply ANN techniques for similar studies and show how some of these models exhibit the advantage of not needing any simplifications. Expert systems have been developed which cater for:

- Welding process selection
- Welding fault diagnosis
- Welding materials selection

These models are not however ideal for application to pipeline welding systems. Hence they developed a system made up of the following steps:

1. A database and a FE model: this first step dealt with obtaining the optimal welding parameters for each weld pass depending on a number of inputs such as material thickness, groove angle and on outputs such as bead geometry, mechanical and metallurgical outcomes. The FE analysis was carried out with the commercial package Sysweld and consisted of a two-dimensional model with temperature dependant material properties and a double ellipsoid heat input source. The predicted temperature and residual stress distributions were used to determine the number of passes to be employed

2. A back propagation (BP) neural network: this model predicted the welding parameters (current, voltage and speed) for each pass from the data obtained from step 1

3. A BP neural network model for welding quality: outputs for each pass number from step 2 were fed in this model to predict the bead quality, expressed as the top and back bead heights and widths

4. A corrective neural network (CNN) model: this computes a corrective coefficient based on a number of parameters (such pipe thickness, joint angle, gas flow rate, arc length etc)

The author highlights how it is not possible to train a universal neural network for all welding tasks and specific neural networks must be developed for each application. The system was implemented in a custom program which was not focussed on looking at distortions. Flux cored welding of 22mm thick pipe was carried out to verify the program experimentally. Welding parameters (including the pass number) to be used were calculated from the database and FE model. Macro-sections and tensile testing of the welds were carried out as part of the validation process.

The program was deemed adequate based on the fact that quality criteria were not violated when using the predicted parameters. All fractures on the tensile testing occurred away from the weld proving that the joint was stronger than the base metal and that the choice of welding parameters did not affect the tensile strength of the specimen. The following main conclusions were drawn:

- Integration of database, FE model and artificial neural network models can be carried out successfully

- Program was verified in producing good and strong joints

- The program can be used for avoiding bad weld design and can be extended to cover other more complex cases

Finally, another method of simulating welding induced distortion by avoiding the use of numerical analysis is to use statistical models. This approach can be thought of as analogous to the artificial neural network one, with the difference that the processing layer is made up of clearly defined mathematical formulations. Hence the method is not as much of a "black-box" as ANN is. Murugan et al [2.50] developed a statistical mathematical model to predict angular distortion of multi-pass welds from three parameters. They gave a review of researchers that used statistical methods for angular distortion prediction and investigated various parameters, amongst which:

- Shape of groove
- Degree of restraint
- Plate thickness
- Weight of the electrode consumed per unit length of weld
- Elastic pre-straining
- Welding speed

The above were chosen as independent controllable parameters that could be varied individually during the experiments. The welding speed is an important parameter but was not included as it can be derived from other parameters, on the basis that the V-groove welding volume must remain the same. A statistical method was then employed which consists of building up a design matrix that considers all possible combinations of the working ranges of each parameter. This allowed for the estimation of the linear, quadratic and two-way interactive effects of the process parameters on angular distortion by considering twenty experiments. The experiments were hence designed in terms of the design matrix and carried out randomly in order to avoid systematic errors. The design matrix also included five experimental runs in which all parameters were kept the same.

The latter still gave slight variations in angular distortion due to unknown effects (referred to as noise) and could be used to determine the amount of such effects. The angular distortion (θ) is then formulated as a second order function of the important parameters (t_{st}, N_{st}, F_{st}), in the form:

$$\begin{aligned}\theta = {} & b_0 + b_1 t_{st} + b_2 N_{st} + b_3 F_{st} \\ & + b_{11} t_{st}^2 + b_{22} N_{st}^2 + b_{33} F_{st}^2 \\ & + b_{12} t_{st} N_{st} + b_{13} t_{st} F_{st} + b_{23} N_{st} F_{st}\end{aligned} \tag{2.11}$$

A statistical software package (Quality America) was used to estimate the coefficients (b_0 to b_{23}). Insignificant coefficients were then dropped along with the respective parameters to form a new and simpler mathematical model. The adequacy of the model was then checked by the "analysis of variance techniques" and by comparing predictions with experimental data. The results then show the relationship of angular distortion with the different parameters. It was concluded that the mathematical models were useful in predicting angular distortion and identifying the important parameters.

The above referenced work shows an interesting approach for predicting welding induced distortions and/or weld quality. The main drawback being that a great deal of experimental data is usually required. Additionally, the data must be specific to the case study that is to be investigated. Owing to the latter disadvantage, an interesting trend is to integrate these methods with numerical analysis to try and compensate for the deficiencies that each approach is bound to have.

2.5 Investigations of Numerical Techniques

Specialised simulation techniques are often necessary to simulate welding processes. Since these are not commonly used for classical structural/thermal en-

gineering analysis, several authors have focussed on the investigation of such techniques in a welding simulation framework.

Qingyu et al [2.51] investigated the use of adaptive meshing techniques. These are of particular interest because of the great difference in mesh densities usually required between localised and far-field regions of the welded structure. The authors point out the computational difficulty in performing three-dimensional analyses and how adaptive meshing techniques can help in reducing the computational cost. They consider the motion of a relatively small, non-linear zone traveling on a larger elastic body. An imaginary boundary of 45 × 25 × 10 mm was considered within which the adaptive meshing technique was implemented. The analysis was transient so that elements falling within that box were subdivided in a 1:64 ratio whilst those leaving the boundary were restored to their original size. Every time the mesh was subdivided, field variables were transferred to the newly generated nodes by extrapolation. An un-coupled thermal to structural simulation was carried out in order to compare the different meshing strategies. The adaptive meshing technique provided a 71% reduction in computational time. Transient variations of temperature and distortion of specific points close to and away from the weld were chosen to compare the two different methods. Results showed agreement of temperature prediction. The adaptive meshing technique proved to be more accurate because of the finer mesh employed. The displacements in the longitudinal direction matched well whilst those in the transverse direction did not correspond very well, especially in regions close to the weld. This was attributed to the fact that the boundary of the dense and the coarse mesh for the adaptive meshing technique was made to correlate only for the displacement field whilst the stress (which is derived from the differential of the displacement field) did not follow this correlation. The differences were most apparent in the transient domain and mismatches usually decreased with the increase of time (i.e. as the analyses approach a steady-state). An interesting conclusion drawn from the transient stress results was that the stress was observed to still be changing

while the temperature tended to be stable.

Runnemalm et al [2.52] also investigated the use of adaptive meshing techniques in the context of welding simulation. They proposed a method for controlling the refinement strategy. Their work also stems from the recognition that simulation techniques must be computationally efficient to try and reduce the amount of experiments required to generate welding guidelines. The authors use an in-house code to enable welding simulation features such as un-coupled thermo-mechanical solution process, automatic mesh refinement and coarsening, quiet or inactive element technique (element birth and death), adoption of a cut-off temperature technique for the material properties, geometry-based user input for model definition, analysis of the microstructure evolution for hypo eutectoid steels and finally error indication to control the adaptive meshing, on which this work was focussed. An uncoupled thermo-elastic-plastic simulation was carried out ignoring phase change volume changes and transformation plasticity using a cut-off temperature of 1000°C. The author references other researchers who have shown that linear hexahedral elements are superior to linear tetrahedral elements in many cases. The work presented in this paper follows on re-meshing techniques investigated by Lindgren with the addition of an error measuring technique introduced to control the re-meshing process. An error term is hence required for this approach. The error term would ideally be computed by comparing finite element results with exact solutions. However the latter are not available and the comparison was instead made with a smoothed continuous function. A total summation term for all elements in the old mesh is computed and this is normalised against the smoothed function. This final value was used to determine whether re-mesh is required. Two criteria were identified for the application of the global error term:

- Equal distribution of the error term within all elements
- Equal distribution of the error density within the mesh

The element length is then related to the error term to find the optimum element size. Both structural and thermal fields were used to compute the error terms. The re-meshing process is ideally carried out automatically. However, a manual input is still required to specify a maximum and minimum element size and prevent the adaptive algorithm from creating extremely small or large elements in the newly generated mesh. Application of the analysis technique was carried out on circumferential and butt welding case studies. Temperature dependant material properties were used. Results showed that when using heat flux as the error criterion the refined mesh took an elliptical shape, different from the shape taken when using stress as the error criterion. The stress driven mesh regeneration produced considerably more elements than the heat flux driven one. This is due to the residual stress fields that remain in the component. Also, the development of the re-meshing differed for the circumferential and butt welding cases.

Other authors concerned with the investigation of numerical techniques relevant to welding simulation include Ramsay [2.53] and Comlekci et al [2.54]. The former investigated the use of integration points, element order, mesh density and reactivation algorithm (amongst his conclusions was the fact that reduced integration elements are generally preferred and that a large number of simple elements are easier to use as opposed to fewer higher order elements) whilst the latter proposed a convenient way of quantitatively representing the out-of-plane deformations for experimental and computational investigations.

2.6 Conclusions

The above review illustrates the current practices and trends for the simulation of welding induced residual stresses and distortion. This is of course a large field of research that is constantly evolving and producing new and interesting data. Some authors (e.g. [2.55], [2.56], [2.57]) have compiled extensive reviews on the literature the research community has to offer.

What is important to notice is that a vast range of techniques is presented, which inevitably creates uncertainty as to which method to adopt. This uncertainty poses a limit on the effective use of computational methods in industry. Lindgren et al [2.58], [2.59] address this issue and, although the authors present a very useful classification of simulation strategies, they then conclude that this is only a first step in trying to harmonise welding simulation techniques and more feedback is required to achieve this. In fact, in practical applications, the choice of simulation technique usually depends on factors such as access to material data, extent of process knowledge, available equipment and computational power (to mention a few) rather than clear and validated guidelines.

Hence, the present study sets out to develop and validate numerical methods for the prediction of residual stresses and distortions, making use of a general purpose finite element software. These methods will then be applied in the investigation of industry related problems caused by distortion and residual stresses. The analysis will have a certain level of complexity and will include transient effects and thermo-elasto-plastic computations, but will also be developed with a limit of computational effort in mind, so that comparison with experimental trials on actual welded plates is still feasible.

References

[2.1] K. Easterling. *Introduction to the Physical Metallurgy of Welding.* Butterworth Heinemann, 1993.

[2.2] D. Rosenthal. The theory of moving sources of heat and its application to metal treatments. *Transactions of the American Society of Mechanical Engineers*, 68(8):849–846, 1946.

[2.3] L. E. Lindgren. Temperature fields in simulation of butt-welding of large plates. *Communications in Applied Numerical Methods*, 2:155–164, 1986.

[2.4] M. Jonsson, L. Karlsson, and L. E. Lindgren. Deformation and stresses in butt welding of large plates. *Numerical Methods in Heat Transfer*, III:35–57, 1985.

[2.5] E. Friedman. Thermo mechanical analysis of the welding process using the finite element method. *American Society of Mechanical Engineers - Journal of Pressure Vessel Technology*, 97(3):206–213, 1975.

[2.6] J. Goldak and M. Bibby. Computational thermal analysis of welds: Current status and future directions. *Modeling and Control of Casting and Welding Processes*, IV:153–166, 1988.

[2.7] D. Camilleri, T. Comlekci, C.K Lee, H. Tan, and T. G. F. Gray. Investigation of temperature transients during flux-cored co2/ar butt welding of cnn steel plates. In *Proc. Int. Conf. on Metal Fabrication and Welding Technology*, pages 107–116, Nottingham, UK, 2003.

[2.8] D. Camilleri, T. Comlekci, and T. G. F. Gray. Use of thermography to calibrate fusion welding procedures in virtual fabrication applications. In *Proc. of Inframation 2004 Conference*, pages 121 –131, Las Vegas, USA.

[2.9] J. A. Goldak, A. Chakravarti, and M. J. Bibby. A new finite element model for welding heat sources. *Metallurgical Transactions*, 15(B):299–305, 1984.

[2.10] M. A. Wahab, M. J. Painter, and M. H. Davies. The prediction of the temperature distribution and weld pool geometry in the gas metal arc welding process. *Journal of Materials Processing Technology*, 77:233–239, 1998.

[2.11] A. Bachorski, M. J. Painter, A. J. Smailes, and M. A. Wahab. Finite-element prediction of distortion during gas metal arc welding using the shrinkage volume approach. *Journal of Materials Processing Technology*, 92-93:405–409, 1999.

[2.12] Z. Chai, H. Zhao, and A. Lu. Efficient finite element approach for modelling of actual welded structures. *Science and Technology of Welding & Joining*, 8(3):195–204, 2003.

[2.13] P. C. Zhao, C. S. Wu, and Y. M. Zhang. Numerical simulation of the dynamic characteristics of weld pool geometry with step-changes of welding parameters. *Modelling and Simulation in Materials Science and Engineering*, 12:765780, 2004.

[2.14] S. M. Roberts, O. Hunziker, and R. C. Reed D. Dye, H. J. Stone. Nickel based super alloy welding - models for residual stress, distortion and weldability. In *Keynote Lecture at the Symposium "Recent Advances in Welding Simulation"*, London, 1999. Institution of Mechanical Engineers.

[2.15] T. L. Teng, C. P. Fung, P. H. Chang, and W. C. Yang. Analysis of residual stresses and distortions in t joint fillet welds. *International Jounral of Pressure Vessels and Piping*, 78:523–538, 2001.

[2.16] E. Olden and R. Leggat. Modelling of residual stresses at girth welds in pipes. In *Keynote Lecture at the Symposium "Recent Advances in Welding Simulation"*, London, 1999. Institution of Mechanical Engineers.

[2.17] P. Dong, J.K. Hong, and P.J. Bouchard. Analysis of residual stresses at weld repairs. *International Journal of Pressure Vessels and Piping*, 82(4):258 – 269, 2005.

[2.18] L. E. Lindgren. Finite element modeling and simulation of welding part 1: Increased complexity. *Journal of Thermal Stresses*, 24:141–192, 2001.

[2.19] W. Jiang, K. Yahiaoui, F. R. Hall, and T. Laoui. Comparison of sequentially and fully coupled genralised plane strain fe modelling of multipass welding. In *Engineering Simulation: Best Practices and Visions of the Future*, Malta, 2005. NAFEMS.

[2.20] C. D. Jang, H. S. Ryu, and C. H. Lee. Prediction and control of welding deformations in stiffened hull blocks using the inherent strain approach. In *Proceedings of the Fourteenth International Offshore and Polar Engineering Conference*. The International Society of Offshore and Polar Engineers, 2004.

[2.21] M. V. Deo, P. Michaleris, and J. Sun. Prediction of buckling distortion of welded structures. *Science and Technology of Welding & Joining*, 8(1):55–61, 2003.

[2.22] P. Michaleris and A. DeBiccari. Prediction of welding distortion. *Welding Journal (Miami, Fla)*, 76(4):172–181– –, 1997.

[2.23] D. Camilleri and T. G. F. Gray. Computationally efficient welding distortion simulation techniques. *Modelling Simul. Mater. Sci. Eng*, 13:1365–1382, 2005.

[2.24] D. Camilleri, T. Comlekci, and T. G. F. Gray. Computational prediction of out-of-plane welding distortion and experimental investigation. *J. Strain Anal. Eng. Des.*, 40:161–176, 2005.

[2.25] N. O. Okerblom. *The Calculations of Deformations of Welded Metal Structures.* Her Majesty's Stationery Office, London, 1958.

[2.26] D. Camilleri and T.G.F. Gray. Out-of plane distortion of *cmn* steel plates during flux-cored co_2/ar automatic butt welding. In *Proc. Int. Conf. on Metal Fabrication and Welding Technology*, pages 117–127, Nottingham, UK, 2003.

[2.27] D. Camilleri, T. Comlekci, and T. G. F. Gray. Thermal distortion of stiffened plate due to fillet welds - computational and experimental investigation. *J. Therm. Stresses*, 29:111–137, 2006.

[2.28] D. Camilleri, T. Comlekci, and T. G. F. Gray. Design support tool for prediction of welding distortion in multiply stiffened plate structures: Experimental and computational investigation. *J. Ship Prod.*, 21:219–234, 2005.

[2.29] Y. Ueda and K. Nakacho. Simplifying methods for analysis of transient and residual stresses and deformations due to multipass welding. *Trans. JWRI*, 11(2):95–103, 1982.

[2.30] M.A. Wahab, M.S. Alam, M.J.Painter, and P.E. Stafford. Experimental and numerical simulation of restraining forces in gas metal arc welded joints. *Welding Research - Supplement to the Welding Journal*, pages 35s–43s, February 2006.

[2.31] Y. V. L. N. Murthy, G. Venkata Raot, and P. Krishna Iyer. Numerical simulation of welding and quenching processes using transient thermal and thermo elasto plastic formulations. *Computers and Structures*, 60(1):131–154, 1996.

[2.32] D.Berglund and H.Runnemalm. Comparison of deformation pattern and residual stresses in finite element models of a tig welded stainless steel plate. In *Proc. 6th International Conference on Trends in Welding Research*, Pine Mountain, Georgia, USA, 2002.

[2.33] M. Nasstrom, L. Wikander, L. Karlsson, L. E. Lindgren, and J. Goldak. Combined solid and shell element modelling of welding. In *Proc. of IUTAM Symp. on the Mechanical Effects of Welding*, pages 10–14, Lulea, Sweden, 1991.

[2.34] Welding simulation with Abaqus. Technical report, Abaqus Technology Brief, February 2005.

[2.35] L. Borjesson and L.-E. Lindgren. Simulation of multipass welding with simultaneous computation of material properties. *Journal of Engineering Materials and Technology, Transactions of the ASME*, 123(1):106–111, 2001.

[2.36] J. M. Bergheau, Y. Vincent, J. B. Leblond, and J. F. Jullien. Viscoplastic behaviour of steels during welding. *Science and Technology of Welding & Joining*, 9(4):323–330, 2003.

[2.37] X.K. Zhu and Y.J. Chao. Effects of temperature-dependent material properties on welding simulation. *Computers and Structures*, 80(11):967 – 976, 2002.

[2.38] M. Abid, M. Siddique, and R.A. Mufti. Prediction of welding distortions and residual stresses in a pipe-flange joint using the finite element technique. *Modelling and Simulation in Materials Science and Engineering*, 13(3):455 – 470, 2005.

[2.39] M. Abid and M. Siddique. Numerical simulation to study the effect of tack welds and root gap on welding deformations and residual stresses of

a pipe-flange joint. *International Journal of Pressure Vessels and Piping*, 82(11):860 – 871, 2005.

[2.40] Ihab F.Z. Fanous, Maher Y.A. Younan, and Abdalla S. Wifi. 3d finite element modeling of the welding process using element birth and element movement techniques. *American Society of Mechanical Engineers, Pressure Vessels and Piping Division (Publication) PVP*, 442:165 – 172, 2002.

[2.41] S. A. Tsirkas, P. Papanikos, K. Pericleous, N. Strusevich, F. Boitout, and J.M. Bergheau. Evaluation of distortion in laser welded shipbuilding parts using local - global finite element approach. *Science and Technology of Welding & Joining*, 8(2):79–88, 2003.

[2.42] F. Boitout, D. Dry, P. Mourgue, H. Porzner, and Y. Gooroochurn. Transient simulation of welding processes. thermal, metallurgical and structural model - sysweld 2004. Technical report, ESI Group, 2004.

[2.43] F. Boitout, D. Dry, P. Mourgue, H. Porzner, and Y. Gooroochurn. Distortion control for large maritime and automotive structures coupling with stamping simulation - sysweld 2004. Technical report, ESI Group, 2004.

[2.44] M.P. Lightfoot, G.J. Bruce, N.A. McPherson, and K. Woods. Artificial neural networks - an aid to welding induced ship plate distortion? *Science and Technology of Welding & Joining*, 10(2):187–189, 2005.

[2.45] M.P. Lightfoot, N.A. McPherson, K. Woods, and G.J. Bruce. Artificial neural networks as an aid to welding induced ship plate distortion. *Journal of Materials Processing Technology*, 172:238–242, 2006.

[2.46] M.P. Lightfoot, G.J. Bruce, N.A. McPherson, and K. Woods. The application of artificial neural networks to weld-induced deformation in ship plate. *Welding Research - Supplement to the Welding Journal*, pages 23s–30s, February 2005.

[2.47] D. Anderson and G. McNeill. Artificial neural networks technology. Technical report, Kaman Sciences Corporation, 258 Genesse Street, Utica, New York 13502-4627, August 1992.

[2.48] G. Casalino, S.J. Hu, and W. Hou. Deformation prediction and quality evaluation of the gas metal arc welding butt weld. *Proceedings of the Institution of Mechanical Engineers, Part B: Journal of Engineering Manufacture*, 217(11):1615 – 1622, 2003.

[2.49] I.S. Kim, Y.J. Jeong, C.W. Lee, and P.K.D.V. Yarlagadda. Prediction of welding parameters for pipeline welding using an intelligent system. *International Journal of Advanced Manufacturing Technology*, 22(9-10):713 – 719, 2003.

[2.50] V. Vel Murugan and V. Gunaraj. Effects of process parameters on angular distortion of gas metal arc welded structural steel plates. *Welding Journal (Miami, Fla)*, 84(11):165–171– –, 2005.

[2.51] Shi Qingyu, Lu Anli, Zhao Haiyan, and Wu Aiping. Development and application of the adaptive mesh technique in the three-dimensional numerical simulation of the welding process. *Journal of Materials Processing Technology*, 121(2-3):167 – 172, 2002.

[2.52] H. Runnemalm and S. Hyun. Three-dimensional welding analysis using an adaptive mesh scheme. *Computer Methods in Applied Mechanics and Engineering*, 189(2):515 – 523, 2000. Adaptive mesh method;.

[2.53] A. C. Ramsay. A study of the finite elements mmeshing methods to be used in welding simulations of ship structures. In *Keynote Lecture at the Symposium "Recent Advances in Welding Simulation"*, London, 1999. Institution of Mechanical Engineers.

[2.54] T. Comlekci, D. Camilleri, and T. G. F. Gray. Finite element representation of experimental surface deformation data from fusion welded plates. In

Proc. 11th Annual Conf. of Association for Computational Mechanics in Engineering, pages 33–36, Glasgow, UK, 2003.

[2.55] Jaroslav Mackerle. Finite element analysis and simulation of welding: a bibliography (1976-1996). *Modelling and Simulation in Materials Science and Engineering*, 4(5):501 – 533, 1996.

[2.56] P. Dong. Residual stresses and distortion in welded structures - a perspective for engineering applications. *Science and Technology of Welding & Joining*, 10(4):389–398, 2005.

[2.57] A. Yaghi and A. A. Becker. State of the art review - weld simulation using finite element methods. Technical report, NAFEMS, 2005.

[2.58] L. E. Lindgren. Modelling for residual stresses and deformations due to welding. 'knowing what isnt' necessary to know'. In *Keynote at 6th Int. Seminar Numerical Analysis of Weldability*, Graz, Austria, October 2001.

[2.59] L. E. Lindgren and B. L. Josefson. Welding residual stresses and distortions simulated by the use of simplified methods. In *Symposium "Recent Advances in Welding Simulation"*, London, 1999. Institution of Mechanical Engineers.

Chapter 3

Welding Induced Residual Stresses and Distortion Simulation, Theoretical Background

3.1 Introduction

Welding processes offer a wide range of engineering challenges with respect to control and optimisation. There are also many adverse metallurgical and structural effects on a typical welded fabrication. The advantages of a fast and effective joining process are undermined by problems of induced residual stresses, distortions and susceptibility to cracking. These problems are, in general, a result of the extreme range of thermal loading to which the material is subjected, and are normally difficult to control owing to the large number of parameters affecting the quality and strength of a single joint. Furthermore, the wide range of physical phenomena involved makes analysis of the welding process complex. Nevertheless, the wide application of this process has created a large knowledge base, which is essential in tackling its detrimental effects. The current project is aimed at developing simulation techniques for the prediction of welding induced residual stresses and distortion. The importance of developing efficient and transparent simulation techniques is evident from the research work presented in the previous chapter. Computer simulation, if adequately developed and validated, can prove

to be a valuable tool for the investigation of welding induced residual stresses and distortions. The most attractive feature is the ability to investigate different scenarios, that would be too expensive or impracticable to analyse by means of experiments only.

The current chapter sets out to define the problem under investigation, together with the basic notions used in the analyses presented throughout the current work. This includes the definition of the problem and conventions used to describe the out of plane distortion, some of the theory relating to the type of finite element analysis employed in the investigations and the algorithms used to carry out the numerical investigations.

3.2 Distortion Representation

The differential nature of the thermal loading in welding, both in space and time, causes structural responses that ultimately deform the structure from its original shape. The weld metal deposition and its subsequent solidification also contribute to distort the structure. The current work focussed on thin plate structures, mainly relevant to the shipbuilding industry. For this type of structure it is convenient to consider three of the welding induced deformation components, shown in Figure 3.1 for two rectangular plates joined by a single butt weld. Longitudinal and transverse contractions also take place but cause less problems in ship production.

This classification allows for a simple quantification of the deformations induced by welding. Furthermore, experimental results are rarely as smooth or uniform as the ones shown in Figure 3.1. A smoothing procedure must hence be used in order to compare computational and experimental values. The smoothing algorithm presented by Comlekci [3.1], [3.2] was used throughout the current project. The algorithm provides a fast and convenient way of smoothing any distortion data which will inevitably contain noise. The smoothed data can then be analysed more conveniently by extracting components of out of plane, angular

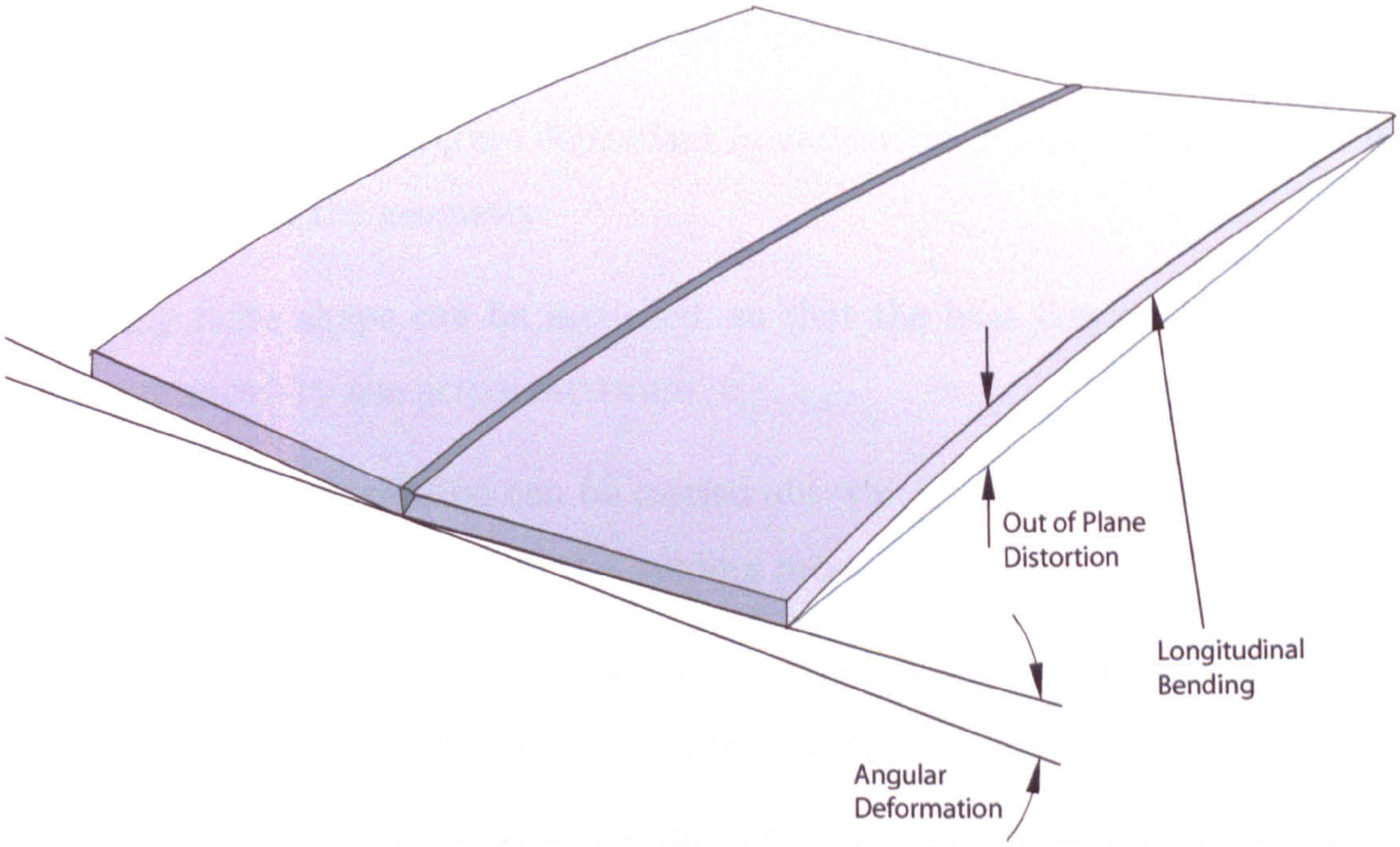

Figure 3.1: Classification of welding induced deformations

and longitudinal deformation and representing them with single root mean square values.

3.3 Thermal Analysis

3.3.1 Overview

The previous chapter described current practices and trends in welding simulation. The first step in the simulation of welding induced residual stresses and distortion is the correct determination of the temperature transients generated by the welding process. Rosenthal presented analytical solutions by considering linear, two and three dimensional solutions of the heat flow problem. Whilst these solutions offer a fast and effective way of obtaining the temperature transients, numerical simulation was still preferred for the current project. The following are the main advantages thermal simulations offer over the purely analytical approach:

- Non linear, temperature dependent material properties can easily be applied

as input to standard commercial packages

- Non linear, temperature dependant boundary conditions can be applied to any part of the geometry
- Any finite shape can be modelled, so that the heat flow can be properly influenced by the actual structure
- A transient simulation can be carried out which will include start-stop and quasi-stationary stages of the welding process
- Weld metal deposition effects can be included through the use of element birth and death techniques (discussed later)

The finite element analysis essentially still follows the basic heat flow equation (2.1). The latter is derived from the first law of thermodynamics, which applied to a differential control volume takes the form [3.3]:

$$\rho c \left(\frac{\partial T}{\partial t} + \{v\}^T + \{L\} T \right) + \{L\}^T \{q\} = \ddot{q} \tag{3.1}$$

Where $\{L\}$ and $\{v\}$ are partial and vector operators for three dimensional space, ρ and c are density and specific heat of the material, T and t are temperature and time whilst $\ddot{q}$ and q are heat generation rate per unit volume and heat flux. The heat generation rate can be input directly as a known value and will prove to be a very convenient heat input model. For the heat flux vector Fourier's Law is used to relate material conduction as follows:

$$q = -[D]_{th} \{L\} T \tag{3.2}$$

Where:

$$[D]_{th} = \begin{pmatrix} k_{xx} & 0 & 0 \\ 0 & k_{yy} & 0 \\ 0 & 0 & k_{zz} \end{pmatrix} \tag{3.3}$$

k_{xx}, k_{yy}, and k_{zz} are material conductivity coefficients in three dimensions which can be input as a function of temperature. This traditional modelling approach accounts for the heat flow of the problem. Applied to a finite element framework it allows modelling of any geometry. In the current projects Ansys *'plane 55'* and *'solid 70'* [3.3] elements were used for two and three dimensional cases respectively. In the welding simulation framework the most important aspects of the thermal models are the heat input and boundary conditions.

3.3.2 Heat Input Models

The predicted temperature field will serve as an input for the subsequent structural analysis. The main aim of the thermal analysis presented in the current work is to predict the temperature field over the entire structure. Temperature variations within the fused zone are not of primary interest since a cut-off technique will be used (discussed later). Hence the choice of heat input strategy must satisfy this criterion.

Two heat input techniques can be conveniently implemented in the commercial finite element package used here:

- Volumetric
- Surface Distribution

For the volumetric heat input methodology a value is defined for the heat generation rate $\ddot{q}$ in Equation 3.1 to a specified set of elements. This is a convenient modelling technique since the shape of the fusion zone can be usually obtained from weld run trials carried out with the same set-up. The mesh is then designed so that a particular set of elements represents the fused area. This is shown schematically in Figure 3.2 for a volumetric heat input applied at a particular load step. It can be seen that an assumption has to be made as to which elements will be considered as the fused zone. Another aspect of this assumption is the longitudinal length of the heat input volume chosen for any single load step. This

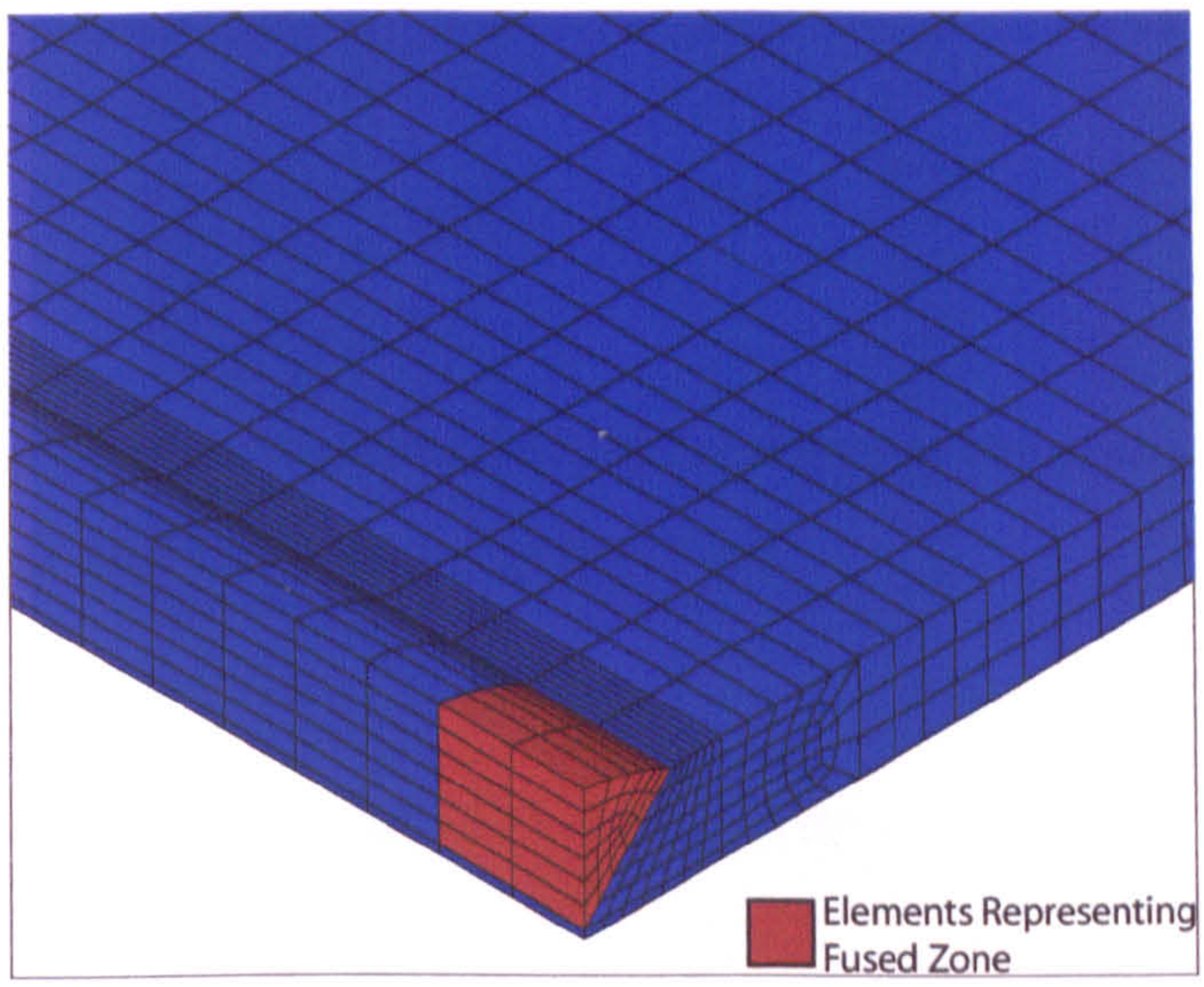

Figure 3.2: Volumetric heat input during a single time step, applied to a set of elements representing the fused zone

can be taken as being equal to the assumed radius of the welding arc, but will also depend on the discretisation level adopted for the mesh (i.e. a multiple of element length in the longitudinal direction must be made as close as possible to twice the assumed welding radius).

The second method assumes some kind of distribution, which usually includes a number of parameters that have to be adapted depending on the specific welding process. As shown in Chapter 2, two of the most commonly used are:

- Gaussian (circular)
- Double ellipsoid

These are shown schematically in Figure 3.3 (a) and (b). The Gaussian distribution is convenient as only one parameter is needed for modelling the heat input, the welding radius $\overline{r}$. Friedman [3.4] illustrated the use of this kind of distribution by presenting the formulation that had already been used in earlier work. Taking r as the radial distance form the centre of the electrode, the heat flux can be described as:

$$q(r) = q_0 e^{-C_0 r^2} \tag{3.4}$$

Where q_0 and C_0 are constants derived by defining the total heat input of the welding process Q and the welding radius $\overline{r}$ as:

$$Q = 2\pi \int_0^\infty q(r) r dr \tag{3.5}$$

$$q(\overline{r}) = 0.05 q_0 \tag{3.6}$$

Which essentially means that the total heat input provided by the weld torch Q is the the result of the integrated function, so that 95% of the heat is kept within the welding radius $\overline{r}$. Applying these criteria to Equation (3.4) yields:

$$q(r) = \frac{3Q}{\pi \overline{r}^2} \exp\left[-3\left(\frac{r}{\overline{r}}\right)^2\right] \tag{3.7}$$

The above can be implemented in the finite element code by means of user subroutines. As the transient analysis is advanced on the structure, the position of each node relative to the weld head is computed and used to evaluate r. Parameter $\overline{r}$ is assumed for the specific welding process whilst Q is computed from the welding power rating of current I and voltage V. A welding efficiency parameter η must be introduced as not all of the energy generated by the welding power source will be converted to heat flowing into the plate. Hence:

$$Q = \eta I V \tag{3.8}$$

The welding efficiency depends on many aspects of the actual welding process. These are difficult to obtain *a priori*, which means that an iterative method must be used. The maximum temperatures predicted throughout the cycle are compared to experimental data taken at specific points transverse to the weld line. If the comparison is made with data from a similar configuration, an accurate value for the welding efficiency can be obtained. It is sometimes convenient to carry out this procedure on a two-dimensional model on a plane normal to the welding direction in order to save on computational time, as the resulting welding efficiency will be similar to the one obtained by comparison with a three dimensional model. This is due to the fact that for most welding processes the resulting temperature distribution will have the largest gradients in the transverse direction and hence the assumption taken for the two-dimensional model of no heat flow in the longitudinal direction is a valid one.

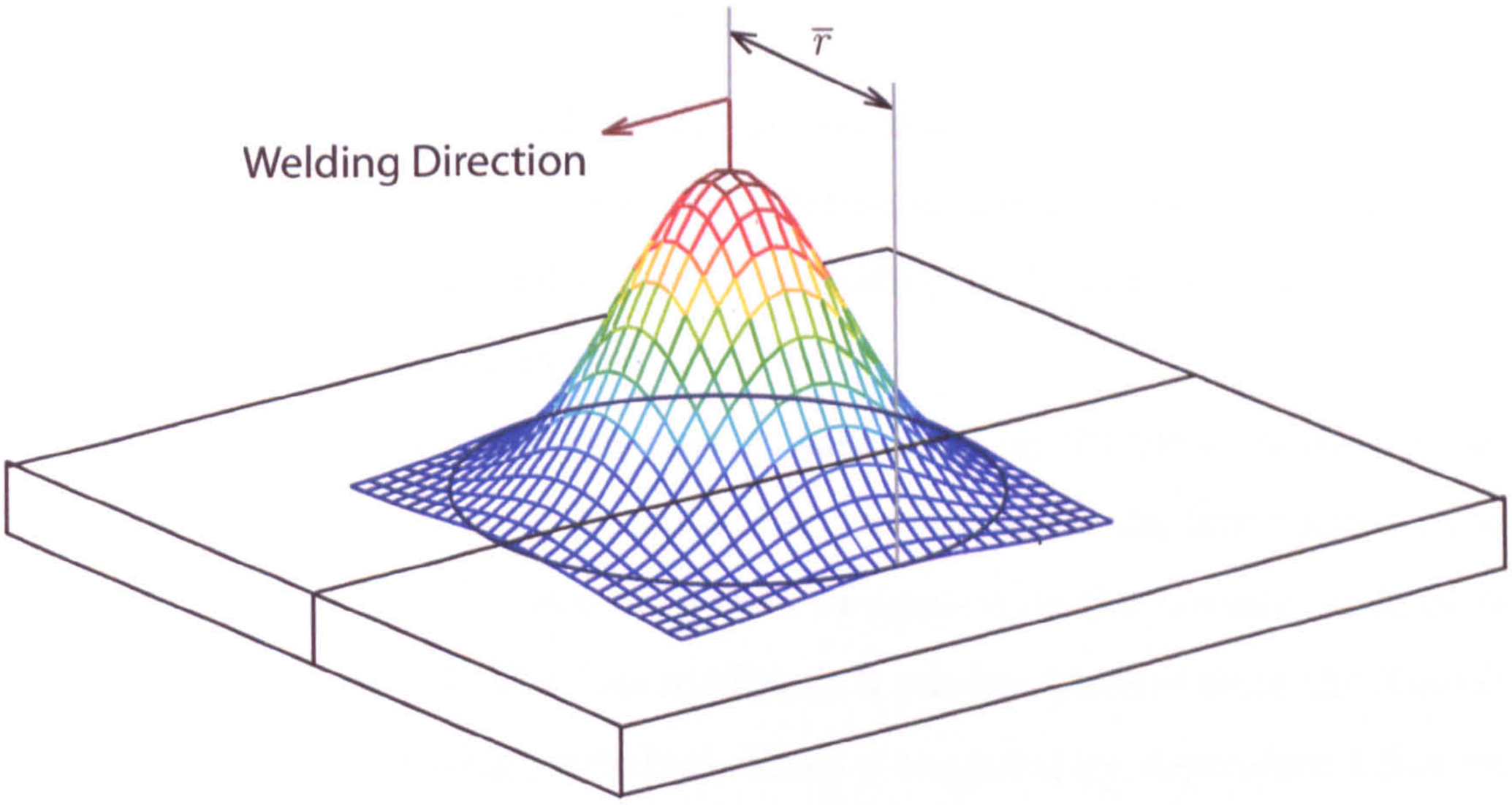

(a)

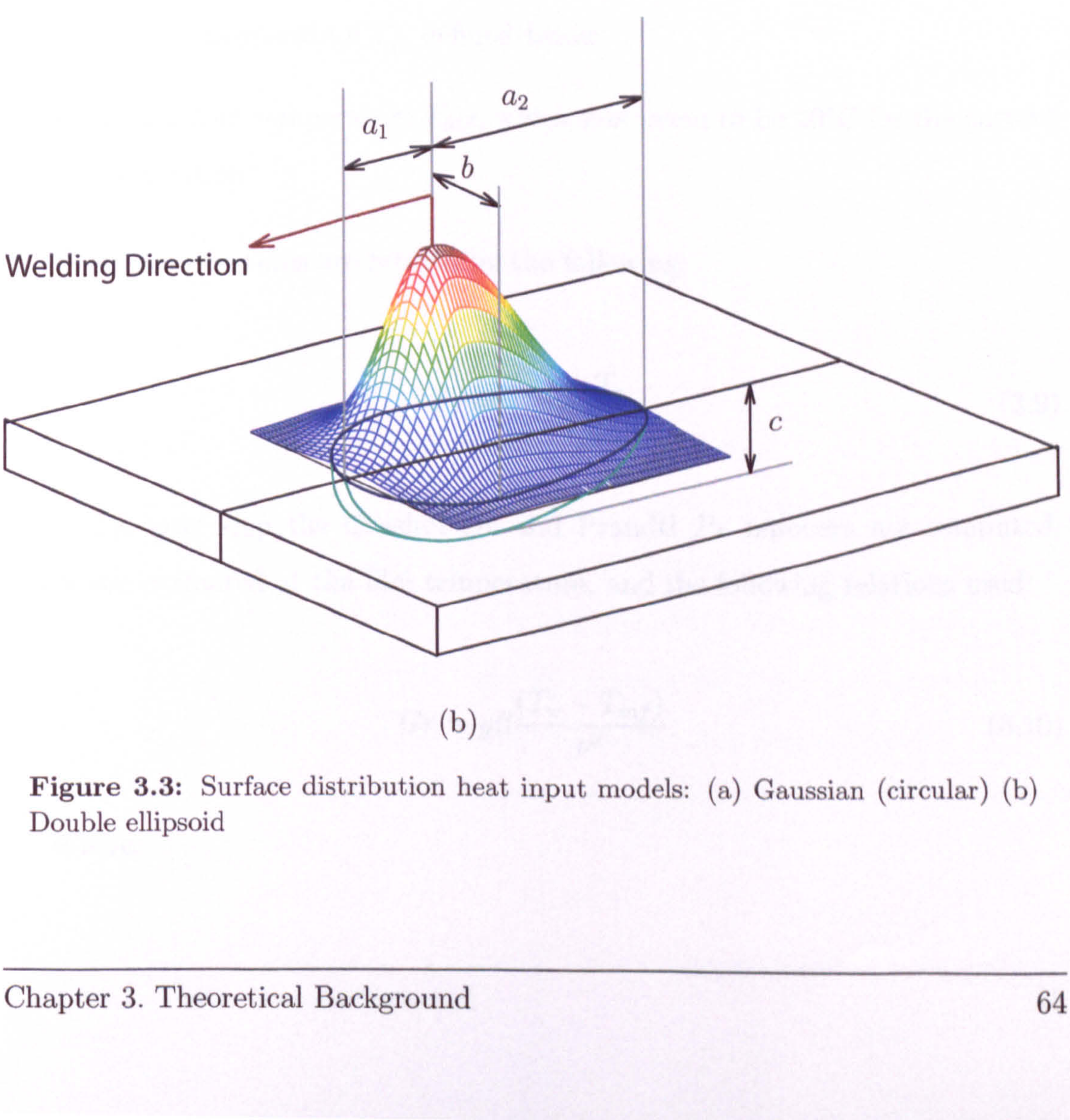

(b)

Figure 3.3: Surface distribution heat input models: (a) Gaussian (circular) (b) Double ellipsoid

3.3.3 Boundary Conditions

The next important step in setting up the thermal model is to define the boundary conditions. Conduction within the structure has been taken into account by defining the thermal conductivity in Equation (3.3) so that convection and radiation remain to be specified.

Natural convection will be assumed to take place on the plate surfaces. Classical free convection theory [3.5] can be used to determine the film coefficient as a function of temperature, which can then be applied on the relevant surfaces of the finite element model. The film coefficient h can be obtained from the Nusselt number using the following procedure. Since a temperature dependant value for h is desired, the following steps were repeated for a range of temperatures. For each case three positions must be considered to define the required temperatures:

- The wall temperature T_w, which is the temperature of the actual plate
- The film temperature T_f, defined below
- The ambient temperature T_{inf}, which was taken to be 20°C for the current investigation

These temperatures are related by the following:

$$T_f = \frac{T_{inf} + T_w}{2} \tag{3.9}$$

In the next step the Grashof Gr and Prandtl Pr numbers are computed. These are evaluated at the film temperature, and the following relations used:

$$Gr = g\beta \frac{(T_w - T_{inf})}{\nu^2} \tag{3.10}$$

Where:

- g: acceleration due to gravity
- β: the volume coefficient of expansion
- ν: viscosity

Values for the above with respect to temperatures are provided in [3.5] for air. The Prandtl Pr number is given by:

$$Pr = \frac{k}{\alpha} \tag{3.11}$$

Where:

$$\alpha = \frac{k}{\rho c} \tag{3.12}$$

ρ and c being the values of density and specific heat for air at the evaluated temperature. Again, Pr can be obtained from [3.5] for a range of temperature values. Once the Grashof and Prandtl numbers have been evaluated, the following empirical relation is used to determine the Nusselt number Nu:

$$Nu = C\,(GrPr)^m \tag{3.13}$$

The above is a well established empirical relation that provides an adequate representation of free convection for a variety of cases. Values of C and m depend on the type of air flow developed during the heat transfer, which can be quantified by the range in which the product $GrPr$ lies. Values for different flow regimes can be obtained from [3.5], which also take into consideration the spatial positioning of the plate (i.e. lower horizontal, upper horizontal or vertical surface).

Once the Nusselt number is computed, the convection film coefficient h can be evaluated using:

$$Nu = \frac{hL}{k_{air}} \tag{3.14}$$

Where L is a typical dimension, taken to be the ratio of the area of the plate to its perimeter, whilst k_{air} is the air conductivity, again evaluated at the film temperature T_f.

The film coefficient is then applied to the finite element model as a function of temperature. The software will automatically determine the correct value to apply on each element depending on the temperature for the current iteration.

Finally, radiation effects must also be included in the thermal model. Finite element package Ansys provides a number of methods to analyse radiation heat transfer problems. Amongst them are specialised elements for computing the transfer of heat between points and/or surfaces and the implementation of radiation matrices [3.3] for more complex shapes. All these methods yield a non-linear solution which would hence require an intensely iterative approach to achieve converged results. Since the radiation loss primarily occurs from the rectangular plates to the surrounding area, a simpler method is to include radiation effects in the film coefficient using the following relation which embodies the classical Stefan-Boltzmann law:

$$\begin{aligned} q_{rad} &= \sigma_{sb}\varepsilon_r \left(T_w^4 - T_{inf}^4\right) \\ &= h\left(T_s - T_{inf}\right) \end{aligned} \tag{3.15}$$

Where σ_{sb} and ε_r are the Stefan-Boltzmann constant and the emissivity respectively. Hence, the film coefficient due to radiation h_r becomes:

$$h_r = \frac{\sigma_{sb}\varepsilon_r \left(T_w^4 - T_{inf}^4\right)}{\left(T_w - T_{inf}\right)} \tag{3.16}$$

The above can then be added to the convection film coefficient to obtain a single value applied to the finite element model. This proved to be a convenient way of including convection and radiation effects in the thermal finite element model.

3.4 Structural Analysis

3.4.1 Overview

The term structural analysis is here used to refer to the elastic-plastic phase of the welding simulation. As shown in Chapter 2, the thermal and structural parts of the analyses can be un-coupled without significant loss of accuracy. This is an advantage from the computational point of view, as there is no need to use coupled-field elements, which would otherwise require a considerable larger computational effort.

It is usually convenient to use the same mesh for both models, as this allows a direct transfer of the thermal loads between the two models. Scripting capability within the software package Ansys allows the implementing of mapping processes that could be used to adopt different meshes for the thermal and structural analyses. This would however require a considerable amount of coding and could lead to problems as regards to the accuracy of the loads applied. A mapping process from a two dimensional thermal history to a three dimensional model was investigated in the initial stages of the project. Results from the the two dimensional thermal analysis are similar to the ones of the three dimensional model, which however require more time to solve. As mentioned previously this is due to the nature of the temperature profiles associated with most welding processes and materials. The procedure consisted in loading the temperature profiles obtained from the two dimensional analysis into the three dimensional model. The chosen time intervals for the two dimensional model had to be equivalent to the longitudinal spacing of elements in the three dimensional model. This procedure turned out to be cumbersome and as it required lots of scripting to implement the

mapping process and to resolve any differences the meshes might have, however small these might be. The saving in computational time was not considerable, so that it was more feasible to use identical meshes for the thermal and structural analyses.

Detailed discussion of the finite element formulations for structural analysis is beyond the scope of this text. It is sufficient to say that the finite element approach essentially discretises the problem so that the problem can be modelled in terms of a series of simultaneous equations, each containing all the required degrees of freedom. Un-coupling the thermal and structural parts of the welding simulation leaves only displacement degrees of freedom to be solved, which then yield strains and stresses through the following standard relation for stresses $\{\sigma\}$ and strains $\{\varepsilon\}$:

$$\{\sigma\} = [D]\{\varepsilon\} \tag{3.17}$$

Where $[D]$ is the stiffness matrix and embodies the material model as regards stress / strain response and Poisson's ratio. $\{\varepsilon\}$ is the strain and is made up of a number of components, depending on the complexity level of the material model. For the elasto-plastic part of the simulation, strain rate independent non-linearities were included in the simulation, which led to the following components of strain:

$$\{\varepsilon\} = \{\varepsilon_e\} + \{\varepsilon_{th}\} + \{\varepsilon_p\} \tag{3.18}$$

Where:

- $\{\varepsilon_e\}$: elastic strain
- $\{\varepsilon_{th}\}$: thermal strain

- $\{\varepsilon_p\}$: plastic strain

The elastic strains are derived from the elastic Young's Modulus through standard elastic structural analysis, whilst development of plastic strains is more complex and depends on the the type of material model employed.

3.4.2 Material Models

The plastic part of the material response could not be neglected as the temperature differences encountered in regions close to the weld are high enough to induce yielding in the material. Rate independent plasticity was employed for the elasto-plastic simulations, as this was deemed sufficient in order to capture the plastic effects induced by the Gas Metal Arc Welding process. Furthermore, this material model only required quasi static testing data to extract the required parameters.

The model uses a Von Mises yield criterion, which is best suited for this class of material, and relates the uniaxial yield strength $\bar{\sigma_y}$ to the three principal stresses σ_1, σ_2 and σ_3 through the following:

$$\bar{\sigma_y} = \sqrt{\frac{1}{2}\left[(\sigma_1 - \sigma_2)^2 + (\sigma_2 - \sigma_3)^2 + (\sigma_3 - \sigma_1)^2\right]} \tag{3.19}$$

More conveniently expressed in terms of the coordinates stresses σ_x, σ_y,σ_z and shear stresses σ_{xy}, σ_{yz} and σ_{xz} as:

$$\bar{\sigma_y} = \sqrt{\frac{1}{2}\left[(\sigma_x - \sigma_y)^2 + (\sigma_y - \sigma_z)^2 + (\sigma_z - \sigma_x)^2 + 6\left(\sigma_{xy}^2 + \sigma_{yz}^2 + \sigma_{xz}^2\right)\right]} \tag{3.20}$$

The above equations describe the yield surfaces, within which the state of the material is deemed to be elastic. As the material stress-strain state reaches the surface boundary, the finite element code adjusts the stiffness matrix in order to follow strain hardening effects. It is evident that a non-linear iterative process is

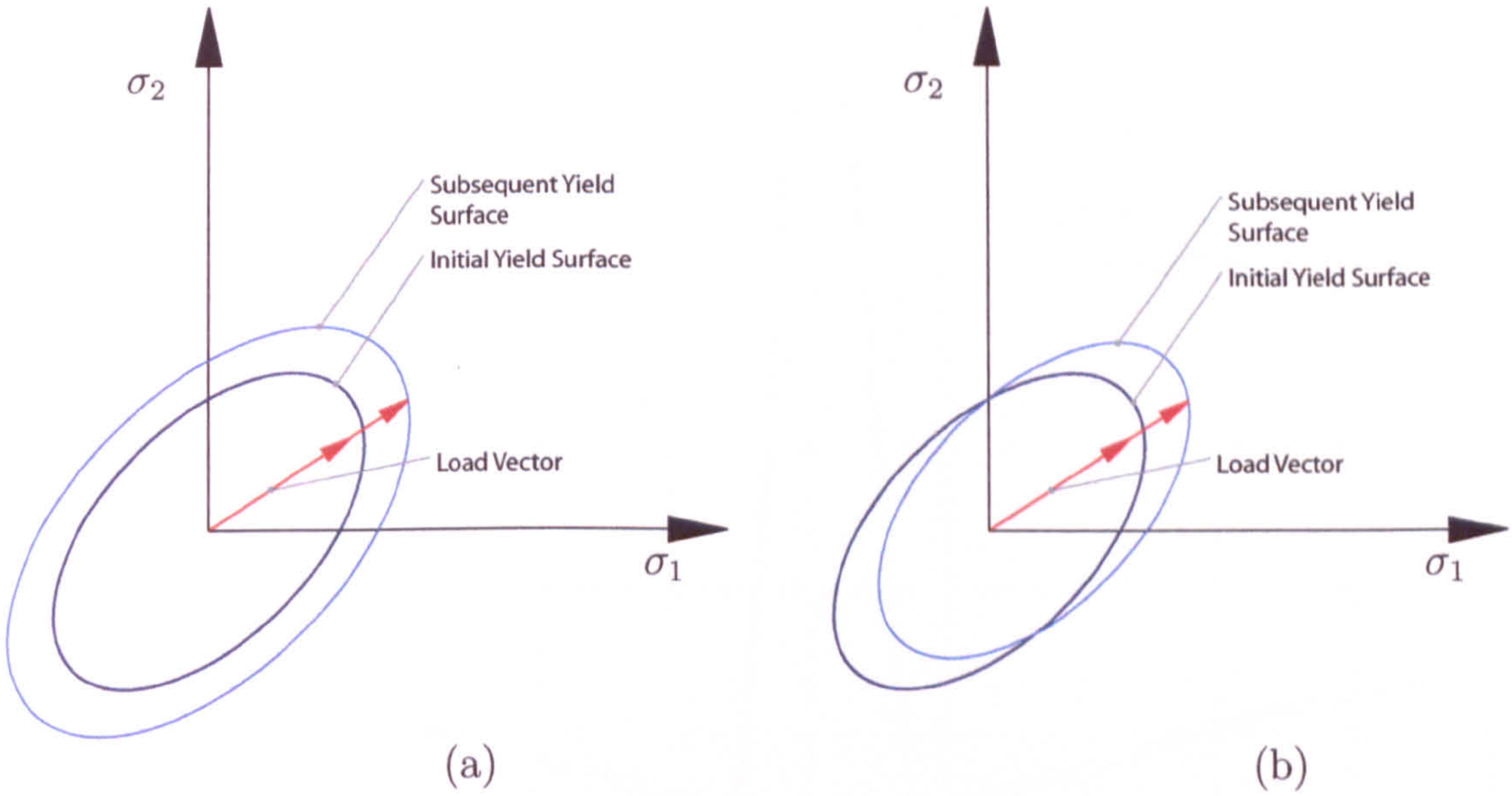

Figure 3.4: (a) Isotropic and (b) Kinematic hardening rule for a two dimensional load case. Adapted from [3.3]

required in order to adjust the stiffness matrix once the material yield point is reached.

As the material is pushed beyond the yield point the yield surface expands in a direction normal to the surface. Alternative hardening rules were used in the elasto-plastic models: isotropic and kinematic. The isotropic hardening rule assumes a uniform expansion of the yield surface in all directions, hence keeping the centre of such surface unchanged. The kinematic model instead assumes a constant yield surface that moves in the direction of the stress vector. This is shown schematically in Figure 3.4.

It was found that the two hardening rules yielded similar results, with the exception of regions very close to the weld line that exceed the material yield stress. An example is shown in figure 3.5 where the residual longitudinal stress is plotted for simulations using bilinear isotropic and bilinear kinematic hardening rules applied to the material model. Bilinear representation was preferred over multi-linear one as it is the simplest and hence most computationally efficient, whilst it still provides a very good representation of the material response as found through uniaxial tensile testing.

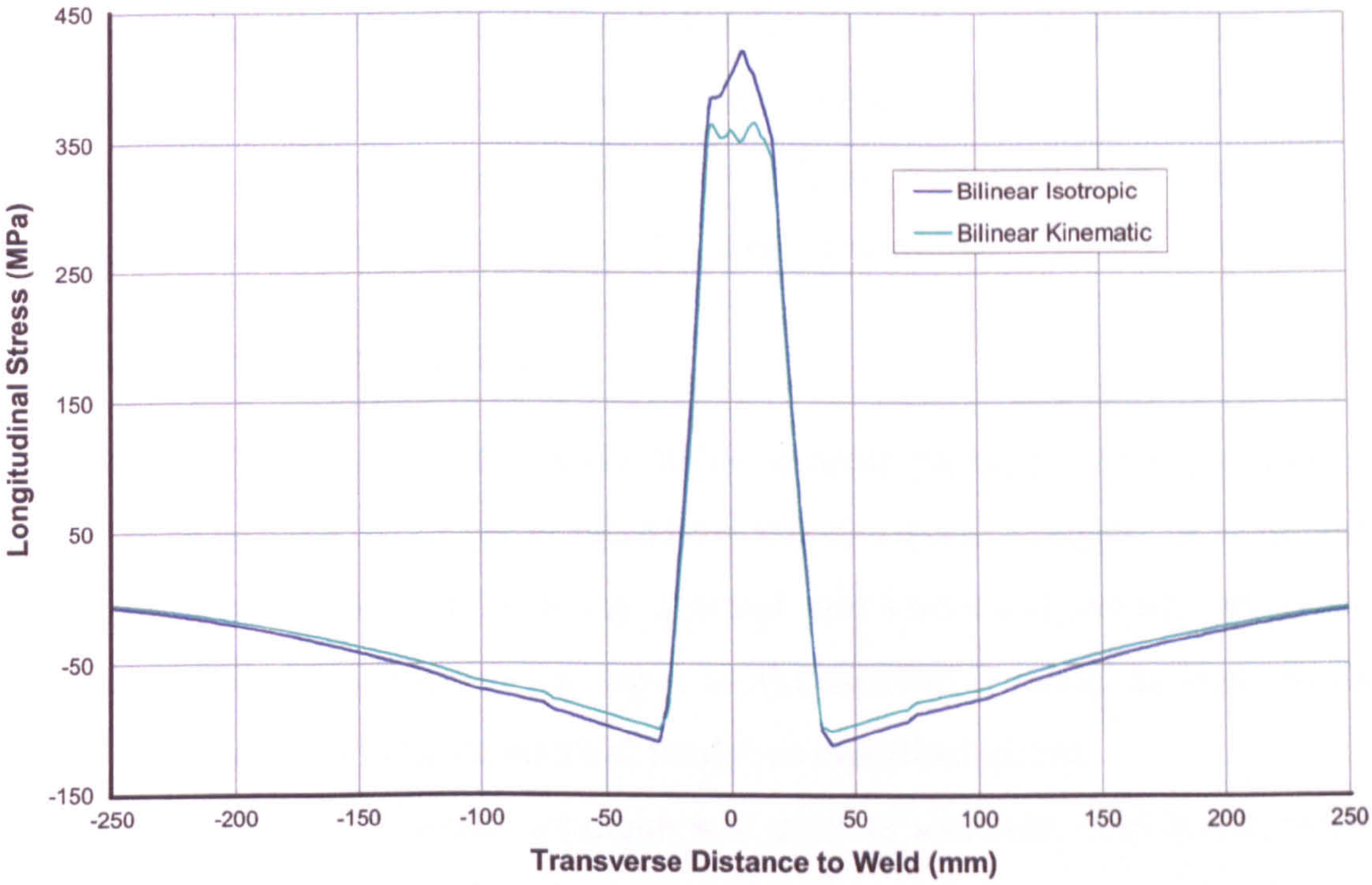

Figure 3.5: Comparison of fillet weld longitudinal residual stresses using bilinear isotropic and bilinear kinematic hardening rules

The loads applied in the structural model are the temperatures obtained from the thermal analysis. These are applied as body loads and are used to compute the thermal strains $\{\varepsilon_{th}\}$ according to the following:

$$\varepsilon_{th} = \int_{T_{ref}}^{T} \alpha_{in}(T) dT \tag{3.21}$$

Where $\alpha_{in}(T)$ is the instantaneous coefficient of thermal expansion, as a function of temperature. This was extracted directly from dilatometry tests, described in Chapter 5, for the required temperature range. T_{ref} is the reference temperature for the computation of the thermal strains. This needs to be set to room temperature (taken to be 20°C throughout this study) for material that does not reach the melting temperature throughout the simulation. For the fusion zone the reference temperature T_{ref} will instead be set to the the material's melting temperature following the algorithm presented in the following section. This is

done on the notion that the material that has been fused (melted) must have any strains re-set to zero as the newly formed metal starts to solidify. This implies that thermal strains for the fused zone will be computed from the melting temperature, taken to be 1493°C for this class of material.

3.4.3 Implementation

The scripting facility present in the finite element package Ansys provided a means of creating a tailor made model for the structural analysis. A transient approach was adopted for both the thermal and structural models, with the thermal temperature distribution input to the structural model as body loads which are then used in the numerical model as described above.

Element birth and death technique was used to simulate weld metal deposition. Elements associated with the metal to be deposited are present in the model but are deactivated at the start of the analysis. As the temperature field is loaded along the plate the elements representing material deposited by the weld are reactivated. When an element is deactivated its contribution to the stiffness matrix is effectively removed as the relevant coefficients are multiplied by an extremely low scalar factor. This is then set to 1 upon activation of the element so that it can be included again in the structural analysis.

For the preliminary studies, element activation was based solely on the shape of the weld-preparation area. This greatly simplifies the analysis as the elements to be deactivated are known prior to the start of the simulation. This approach is however not appropriate in the following cases:

- If the fusion zone turns out to be considerably larger than the weld preparation area
- If the plates are set up so that there is no weld preparation, e.g. square edge preparation

In the first case there will be elements outside the deactivated set which in

fact are loaded beyond the melting temperature. This is an unrealistic simulation procedure and often leads to convergence problems. In the second case the weld material to be fused is initially unknown so an assumption has to be taken as to which elements will be deactivated/activated during the structural simulation.

Hence, an activation strategy based solely on the shape of the weld preparation or on an assumed weld fusion zone was deemed inappropriate. Another approach, based upon post processing of the thermal results was adopted. The algorithm is shown in Figure 3.6.

Starting from the solved thermal analysis the structural part can be divided into three sections:

1. Element De-activation

2. Heating Cycle

3. Cooling cycle

The first part is carried out prior to commencing the transient structural analysis. A cut-off temperature technique was adopted throughout this study. This is a temperature above which the material is deemed to have lost considerable strength, so that any thermal load equal to or greater in value can be set equal to the cut-off temperature value. Values of 1000°C and 1493°C were investigated in the initial stage of the project on the basis that the former is the value at which the material under investigation has lost most of its strength, whilst the latter value is the melting temperature and hence represents the material that has been fused.

The thermal model is hence first scanned to determine the maximum temperature reached throughout the weld cycle. If all nodes in the scanned element have reached the designated cut-off temperature the element is deactivated (killed), its material properties are set to weld metal / fusion zone values and the reference temperature set to the cut-off temperature in order to compute the thermal strains ε_{th} correctly, as shown previously.

Once the elements have been tagged using the above procedure, the actual structural analysis is started in a transient fashion by loading the corresponding load step from the thermal analysis. for the 'Heating Cycle' of the analysis (see Figure 3.6) numerical model is scanned for each load step to determine which nodes have reached values equal to or greater than the cut-off temperature. When this happens the corresponding element is reactivated and all of its body loads set to the cut-off temperature value. During this part of the simulation procedure care must be taken in order to ensure that any particular element is reactivated only if all of its volume has reached the cut-off temperature value. Failure to ensure such condition will almost inevitably lead to convergence problems due to the extreme range of temperature loading to which the numerical model is subjected.

This is repeated until all elements have been activated, from which point the structural analysis can be continued until the structure is cooled to room temperature.

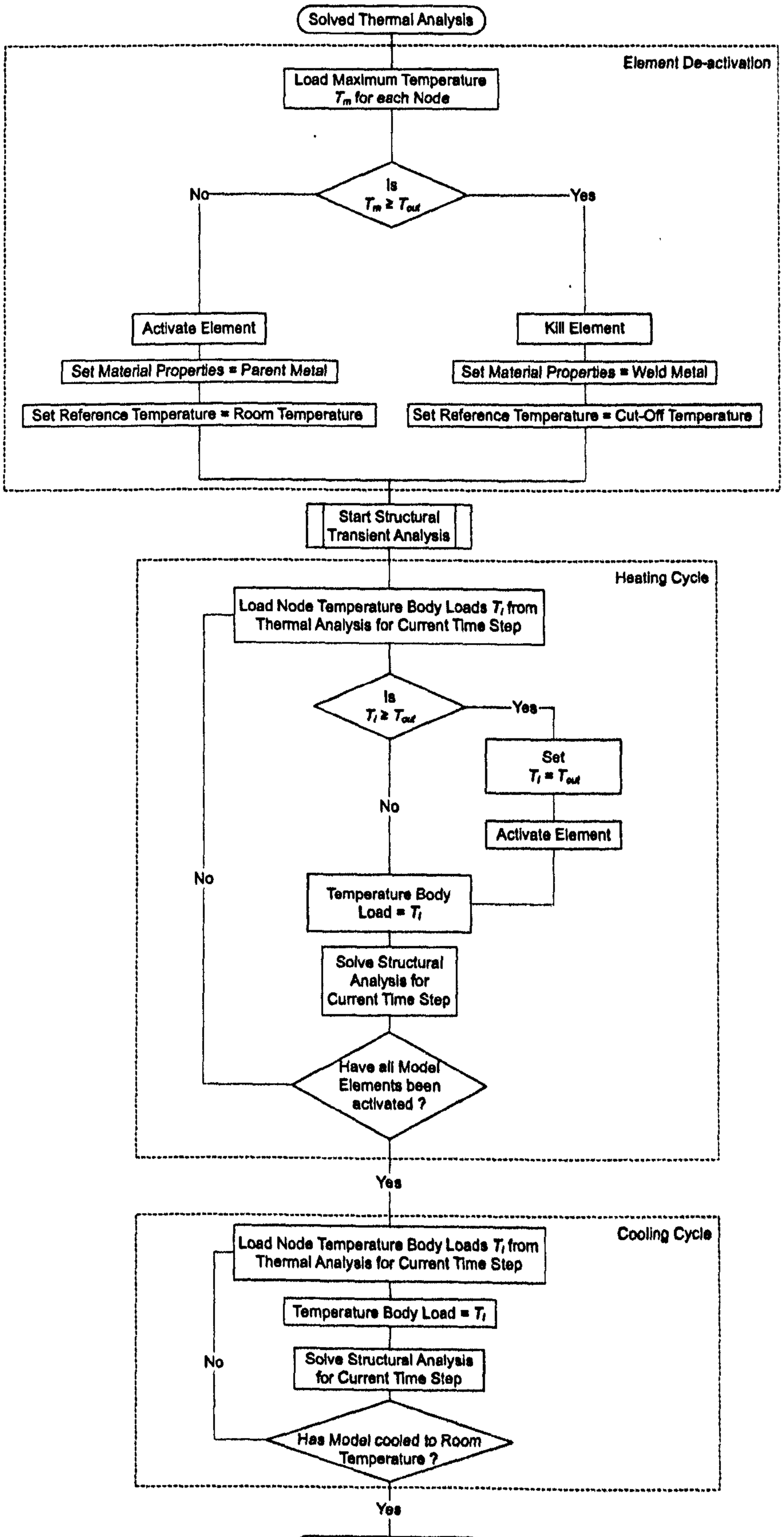

Figure 3.6: Algorithm used for the thermo-elasto-plastic analyses

References

[3.1] T. Comlekci. *Development of hybrid experimental -numerical methods for thermoelastic stress analysis.* PhD thesis, University of Strathclyde, 1995.

[3.2] T. Comlekci, D. Camilleri, and T. G. F. Gray. Finite element representation of experimental surface deformation data from fusion welded plates. In *Proc. 11th Annual Conf. of Association for Computational Mechanics in Engineering*, pages 33–36, Glasgow, UK, 2003.

[3.3] Ansys Inc. *Ansys Documentation*, release 10.0 edition.

[3.4] E. Friedman. Thermo mechanical analysis of the welding process using the finite element method. *American Society of Mechanical Engineers - Journal of Pressure Vessel Technology*, 97(3):206–213, 1975.

[3.5] J.P. Holman. *Heat Transfer.* McGraw Hill, Inc., 8th edition, 1997.

Chapter 4

Development of Thermo-Elasto-Plastic Models

4.1 Introduction

Theoretical considerations necessary for the development of the numerical models have been described in the previous chapter, together with the algorithms used for the implementation of the simulation techniques. The present chapter deals with the development and validation of the numerical models, applied to two basic case studies for butt weld and fillet weld joint configurations. Development of the thermo-elasto-plastic models for these configurations is described, together with results and comparisons with reference experimental deformation data. These simple case studies allowed for a basic understanding of the effects leading to welding induced distortions and residual stresses. Reference experimental data for the main forms of deformation allowed a comparison with predictions obtained from the transient elasto-plastic models.

Another objective for the development of the elasto plastic model is to allow comparison with other more simplified modelling techniques, developed for the purpose of predicting welding induced distortions in a computationally efficient manner [4.1]. The elasto-plastic model provides some understanding of the effects of simplifications adopted in the computationally efficient models, together with the main limitations.

Furthermore, different modelling strategies were investigated within the thermo-elasto-plastic methodology, particularly as regards to the two-dimensional models, as these present an attractively low computational effort compared to their three dimensional counterparts. Other variations in the modelling strategies included investigating different heat input strategies and structural boundary conditions. Finally, the same models that are used here for comparison with distortion data are then compared to experimental residual stress measurements, as discussed in Chapter 5.

4.2 Butt Welding Investigation

4.2.1 Thermal Analysis

It has been shown that the complex heat transfer phenomena in the arc heating and metal transfer zone can be conveniently represented in terms of a single numerical heat source model in order to obtain the temperature history from a transient heat transfer analysis. Studies in the current project have focused on CMn steel plates with a thickness of 6 mm. The case study consisted of two 500 × 250 mm plates joined by a single continuous butt weld to form a single 500 × 500 mm sheet.

Numerical models were constructed for both two dimensional and three dimensional representations. The two dimensional models considered a strip, the plane of which lies normal to the welding direction. This also allowed modelling of half the geometry by taking advantage of the symmetry in geometry and loading. The finite element mesh is shown in Figure 4.1.

Temperature dependent material properties were used for thermal conductivity and enthalpy. The latter was used instead of specific heat in order to smooth the high non-linearity present in the specific heat. This can be done as the finite element solution sets enthalpy as the primary unknown, based on the relation between enthalpy H and specific heat c as a function of temperature T, τ and density ρ [4.2]:

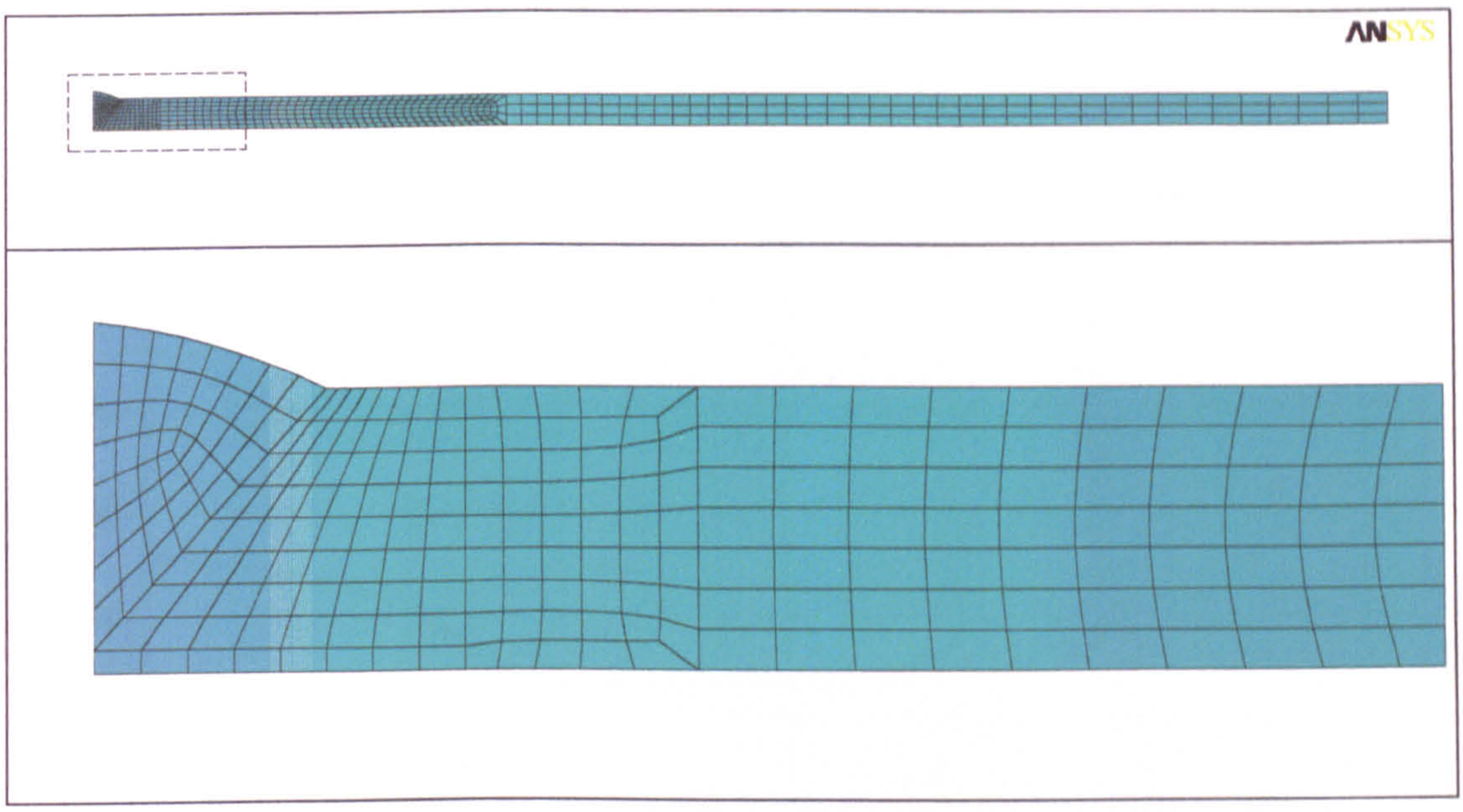

Figure 4.1: Mesh used for the two dimensional numerical models in the butt welding investigation

$$H(T) = \int_0^T \rho c(\tau) d\tau \tag{4.1}$$

Plots of the thermal property data are given in Figures 4.2 and 4.3. A film coefficient accounting for convection and radiation heat transfer modes was applied to the model surfaces using formulations presented in Chapter 3. The analysis was carried out in a transient fashion, varying the load step size in order to capture the different temperature variation gradients exhibited at different stages of the heating and cooling cycles. Three different heat input models were considered (formulations were presented in the previous chapter):

- Volumetric heat input
- Circular Gaussian surface heat input
- Double ellipsoidal heat input

All models embody the 'thermal efficiency' approach presented in Equation (3.8), that is the total heat input in the numerical model is set as a function of the

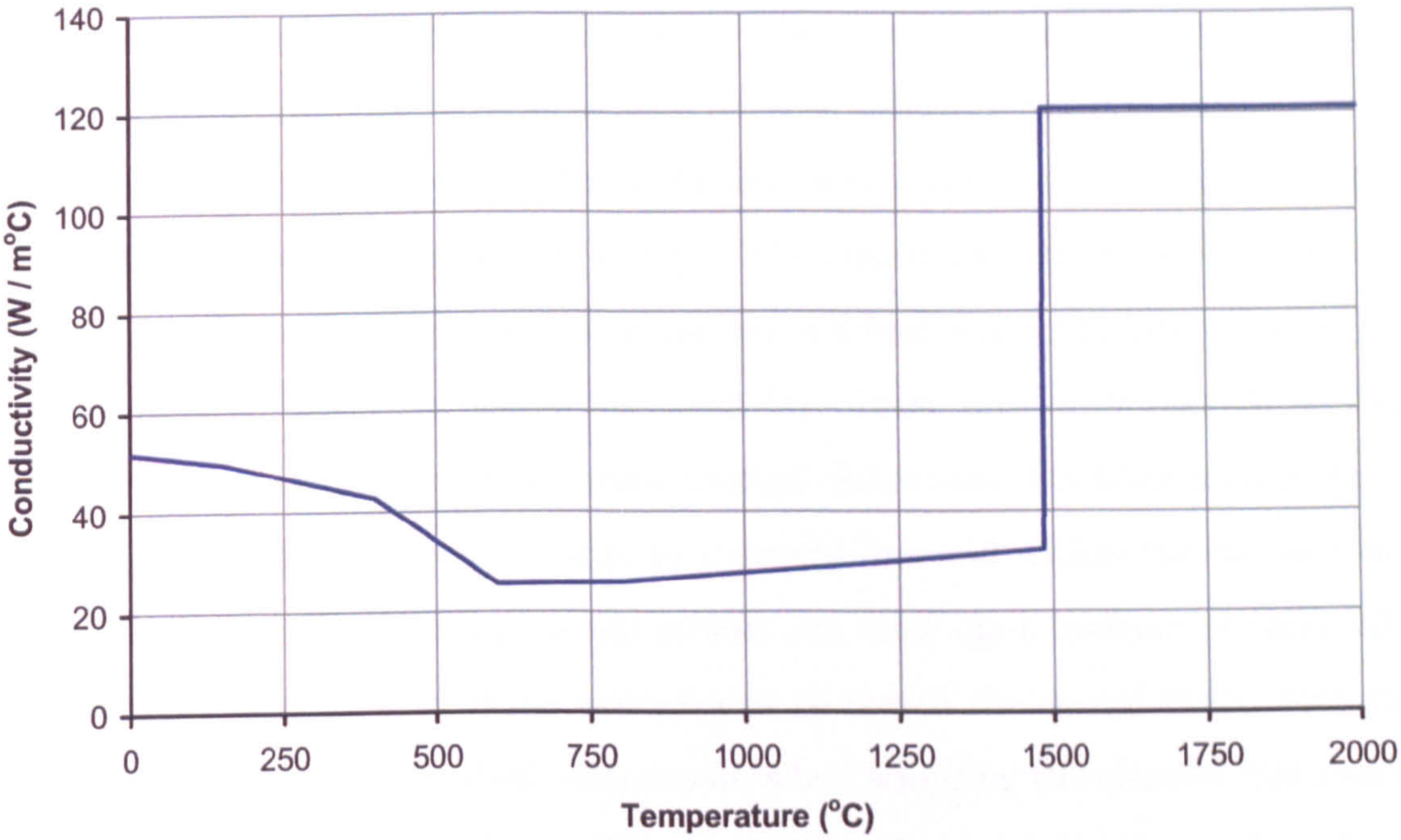

Figure 4.2: Conductivity used in the thermal material models

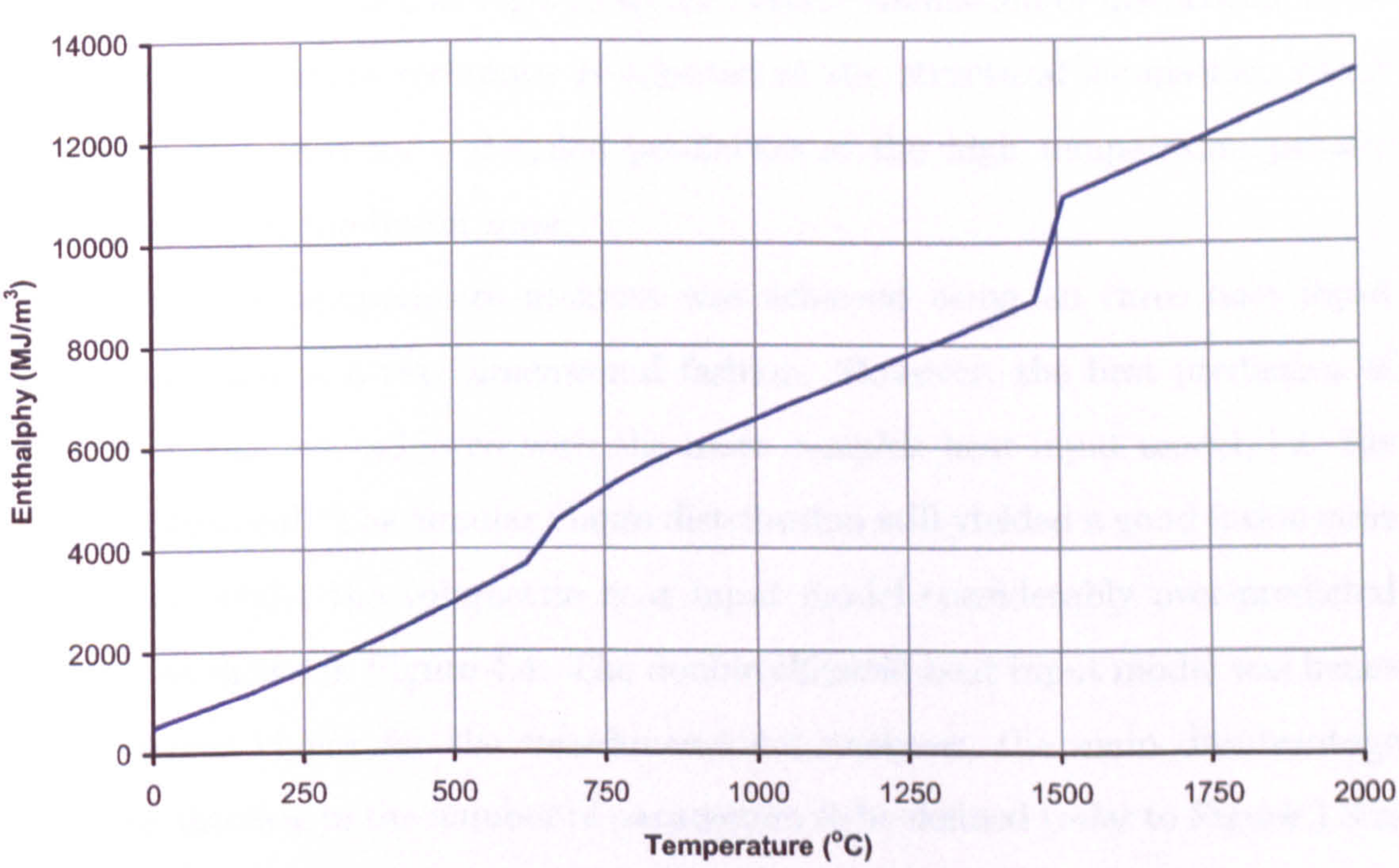

Figure 4.3: Enthalpy used in the thermal material models

electrical power rating noted during welding. This is a limitation on the thermal modelling side as some experimental knowledge must be available prior to commencing the simulation. In order to set a realistic welding efficiency, temperatures at specific points transverse to the weld line were compared with experimental data taken from thermocouple readings. The transverse positions were chosen to capture the region where the longitudinal residual stress exhibits a tensile to compressive variation, as this is the most important area with regards to the development of the contraction forces causing distortion. Detailed temperature variations in regions extremely close to the weld line and within the fusion zone are not of particular interest, as the strains are reset upon melting of material. It is however still an important requirement to match the actual fusion zone as this will provide a more realistic simulation when adopting the element birth and death technique, discussed later. The thermal analysis must hence strike a balance between predicting the correct temperature maxima achieved at transverse points to the weld, and predicting the fusion zone geometry. The former aspect is of greater importance as regards to the correct simulation of distortions, since a cut-off temperature technique is adopted in the structural simulation, which eliminates the need for a detailed prediction of the high temperature profiles exhibited within the fusion zone.

A match in temperature maxima was achieved using all three heat input models, applied in a two dimensional fashion. However, the best prediction of the fusion zone was achieved with the more complex heat input model, i.e. the double ellipsoidal. The circular Gauss distribution still yielded a good fusion zone prediction, whilst the volumetric heat input model considerably over-predicted the size, as shown in Figure 4.4. The double ellipsoid heat input model was hence the preferred choice for the two-dimensional analyses, the main disadvantage being the increase in the number of parameters to be defined (refer to Figure 3.3 in Chapter 3). It also involved a higher amount of scripting as each individual node had to be loaded according to its spatial position in relation to the moving heat

source during the transient analyses. Results for the two dimensional analysis are read as a series of load steps, which represent the longitudinal distances traveled by the heat source during the welding cycle. This is shown schematically in Figure 4.5. An important assumption in using a two-dimensional approach is the lack of heat transfer in the longitudinal direction. This turns out to be a good assumption as the temperature profile resulting from the three-dimensional models has its largest gradient in the transverse direction, showing that most of the heat is indeed transferred through the transverse component.

Heat input modelling consideration varied slightly for the three-dimensional models. In order to keep computational time within feasible limits, mesh density had to be reduced and the resulting mesh is shown in Figure 4.6. This implied a lower number of nodes in regions close to the weld line, which in turn leads to a lower resolution for heat input models based on surface distributions, making these a less attractive option. The volumetric heat input model was hence used for the three dimensional thermal analyses. Prediction of the fusion zone proved to be better than the two dimensional counterpart, even when the heat input region was only based on the initial V-shape weld preparation area. This is due to the added heat flow in the longitudinal direction which, however small, reduced the size over-prediction of the two-dimensional model, making the fusion zone predicted size comparable to the experimental macro graphs. This is shown in Figure 4.7, where a temperature contour plot is plotted for a time step half way through the welding process.

The resulting temperature distributions are presented in Figures 4.8 and 4.9 where maxima and transient temperatures are plotted respectively. Maxima are compared to experimental data [4.1] for this particular welding set-up whilst temperature transients predicted by the numerical models are plotted for the four transverse points under consideration. The plots show how the two and three dimensional models yield similar results, showing that the two dimensional assumption of zero heat transfer in the longitudinal direction is justified. The

assumption is further justified by the fact both two and three dimensional models matched the experimental data using an efficiency of 85%. The profile obtained is typical for this kind of welding process, characterised by a very steep gradient on approach of the heat source and a high gradient transverse to the weld line. Even though convection and radiation effects were included in the model, most of the heat flowed through the plate by conduction.

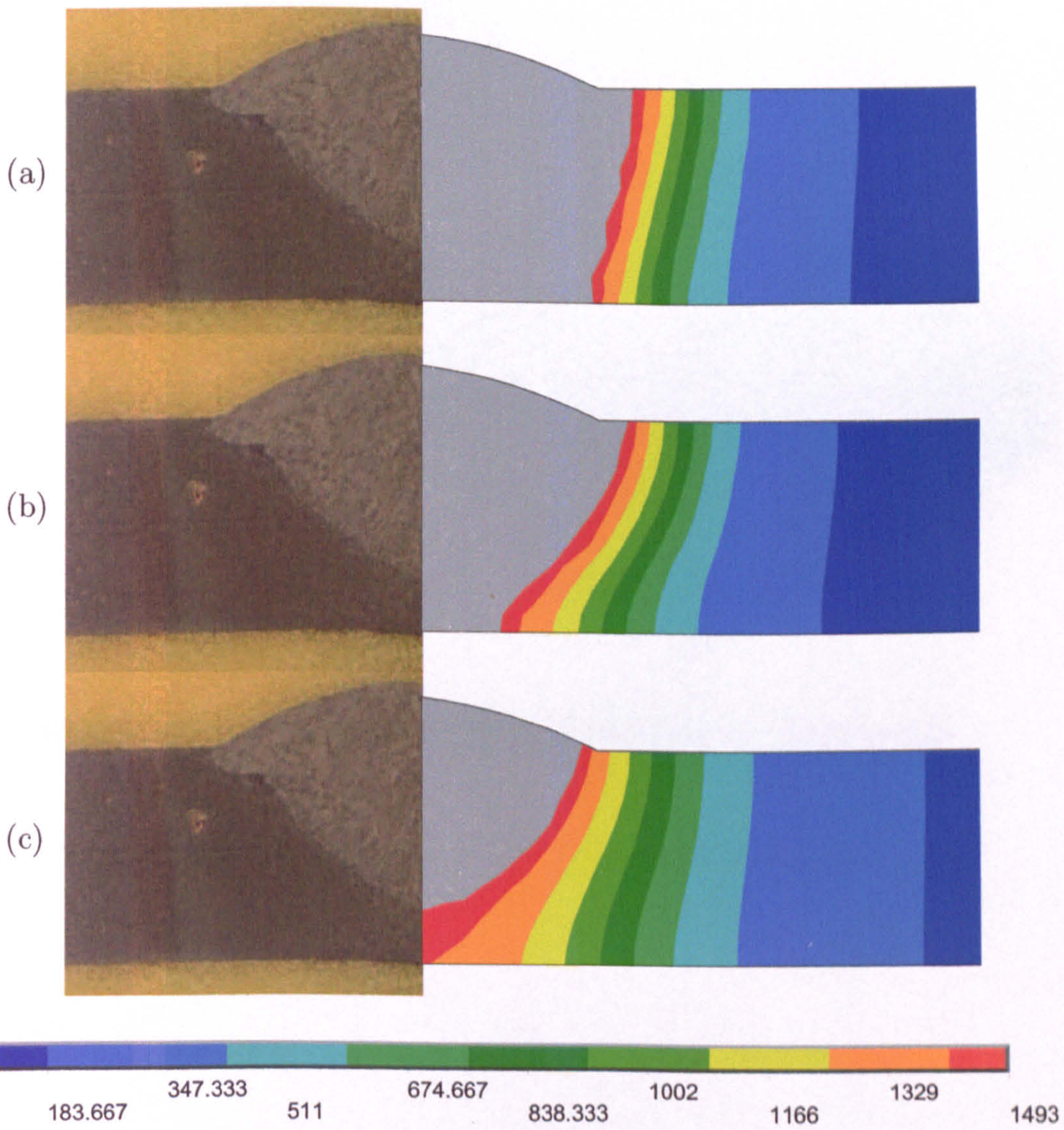

Figure 4.4: Fusion zone prediction for thermal analyses using: (a) Volumetric heat input model (b) Circular Gaussian heat input distribution (c) Double ellipsoidal heat input distribution

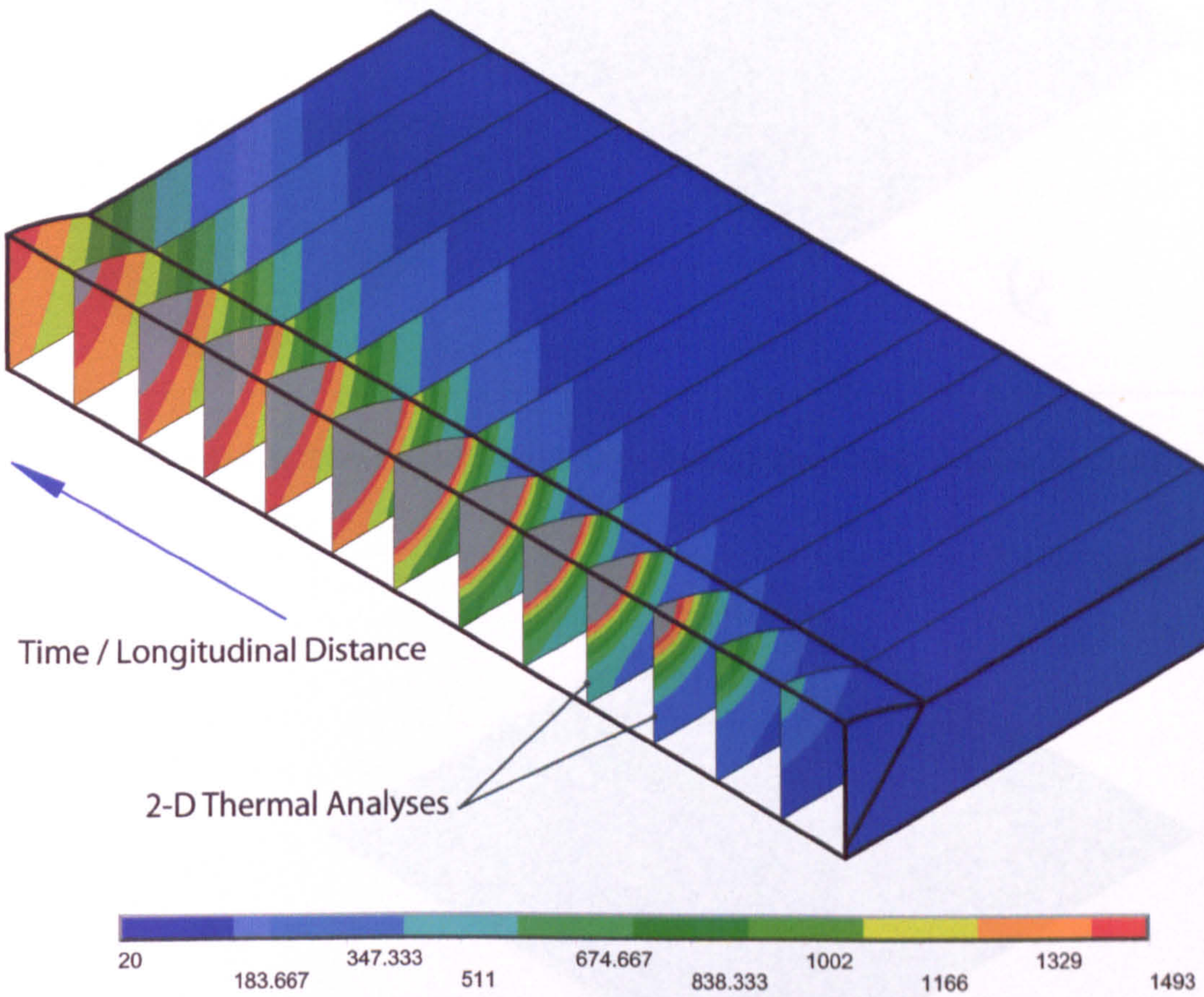

Figure 4.5: Two dimensional thermal analysis results

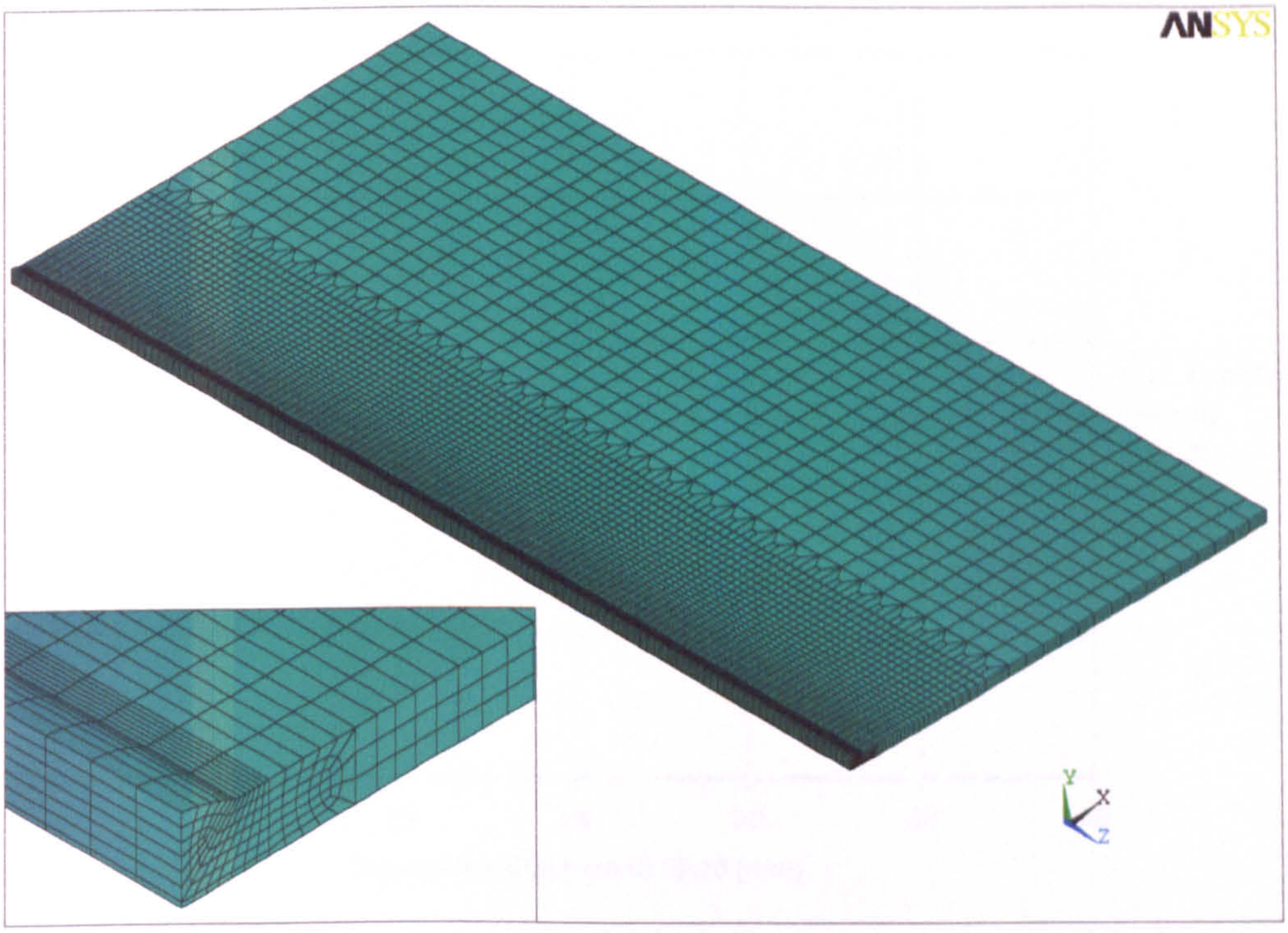

Figure 4.6: Mesh used for the three-dimensional butt welding analyses

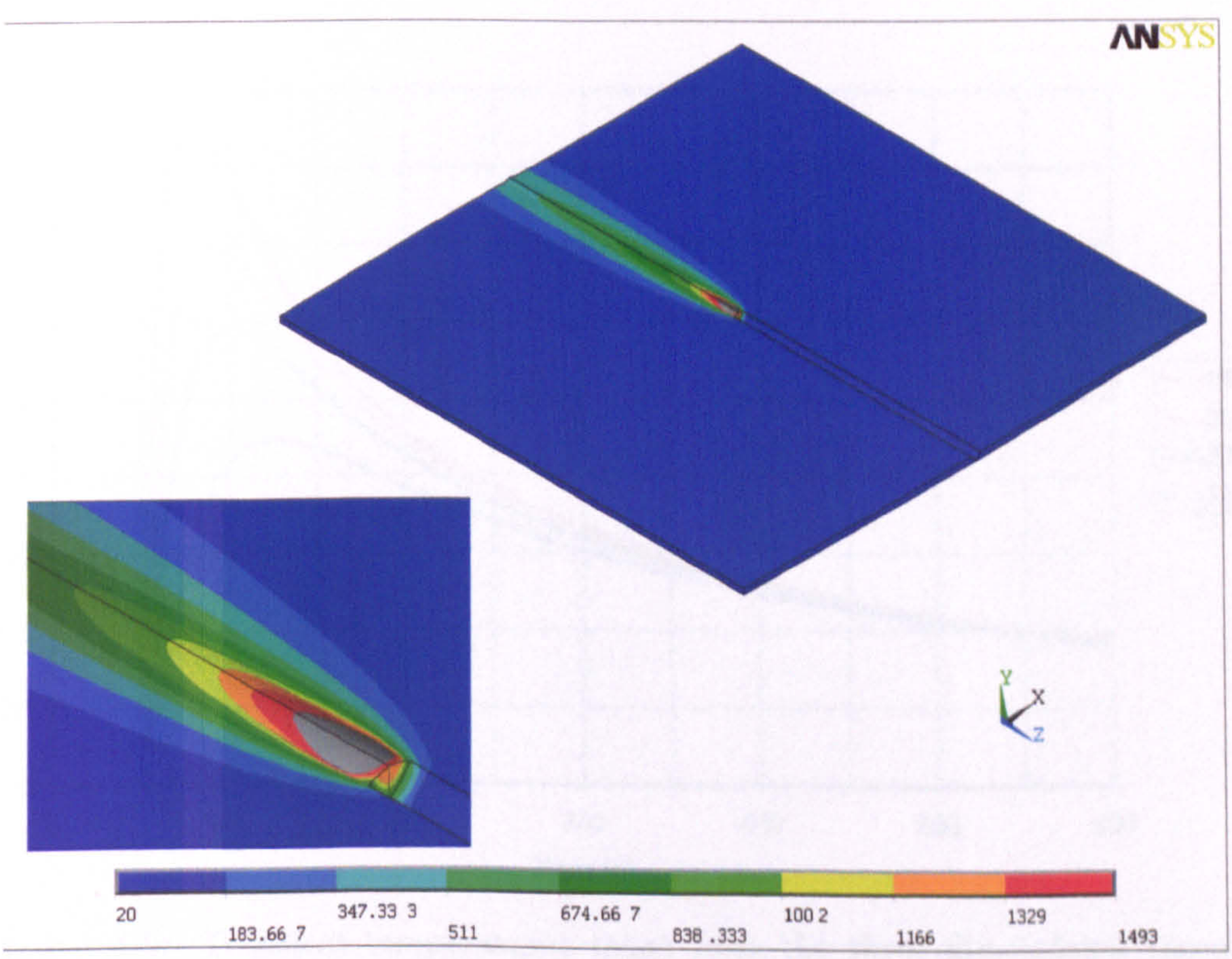

Figure 4.7: Three-dimensional thermal analysis for the butt welding geometry

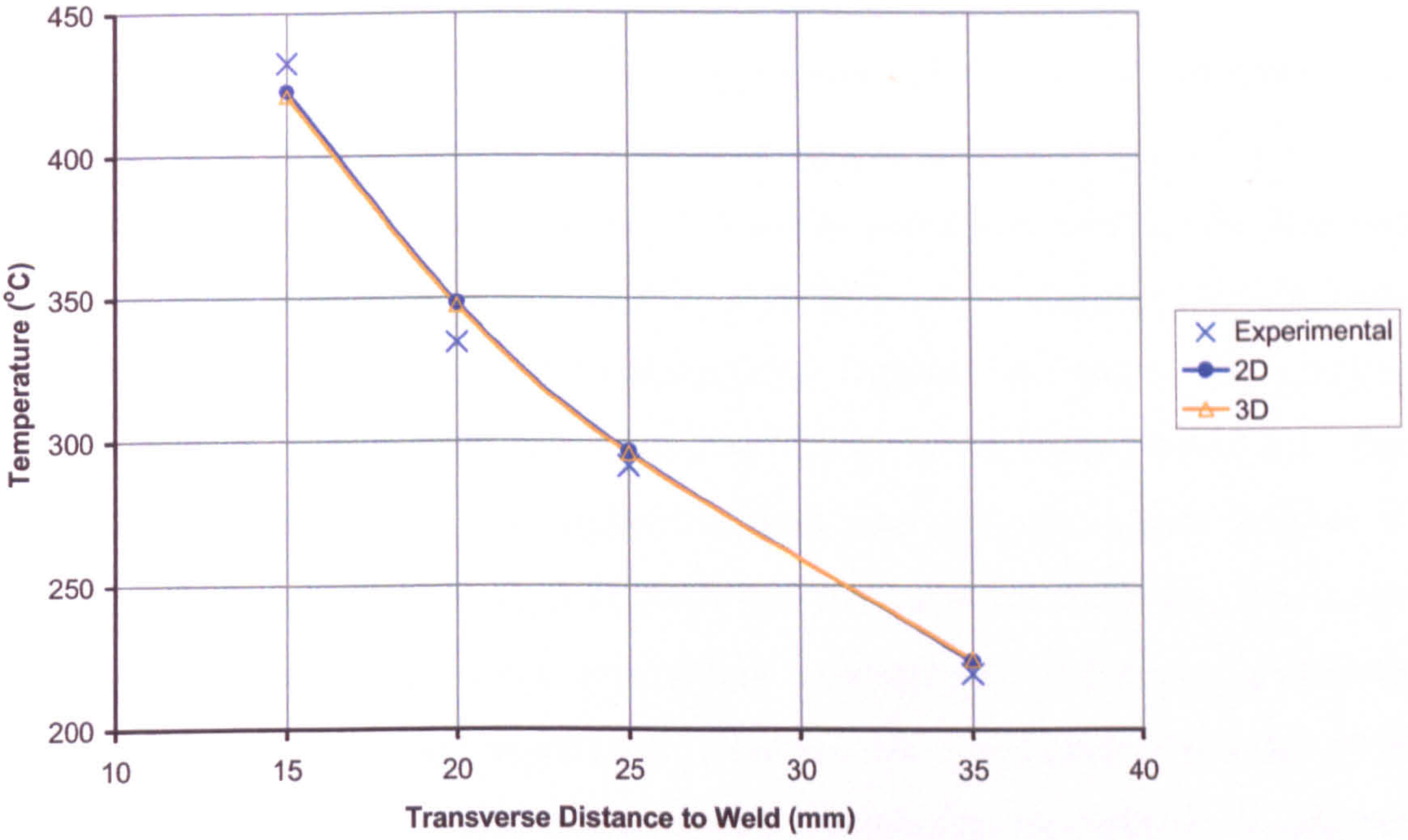

Figure 4.8: Maximum temperature reached throughout welding cycle for the two and three dimensional analyses, compared with experimental data

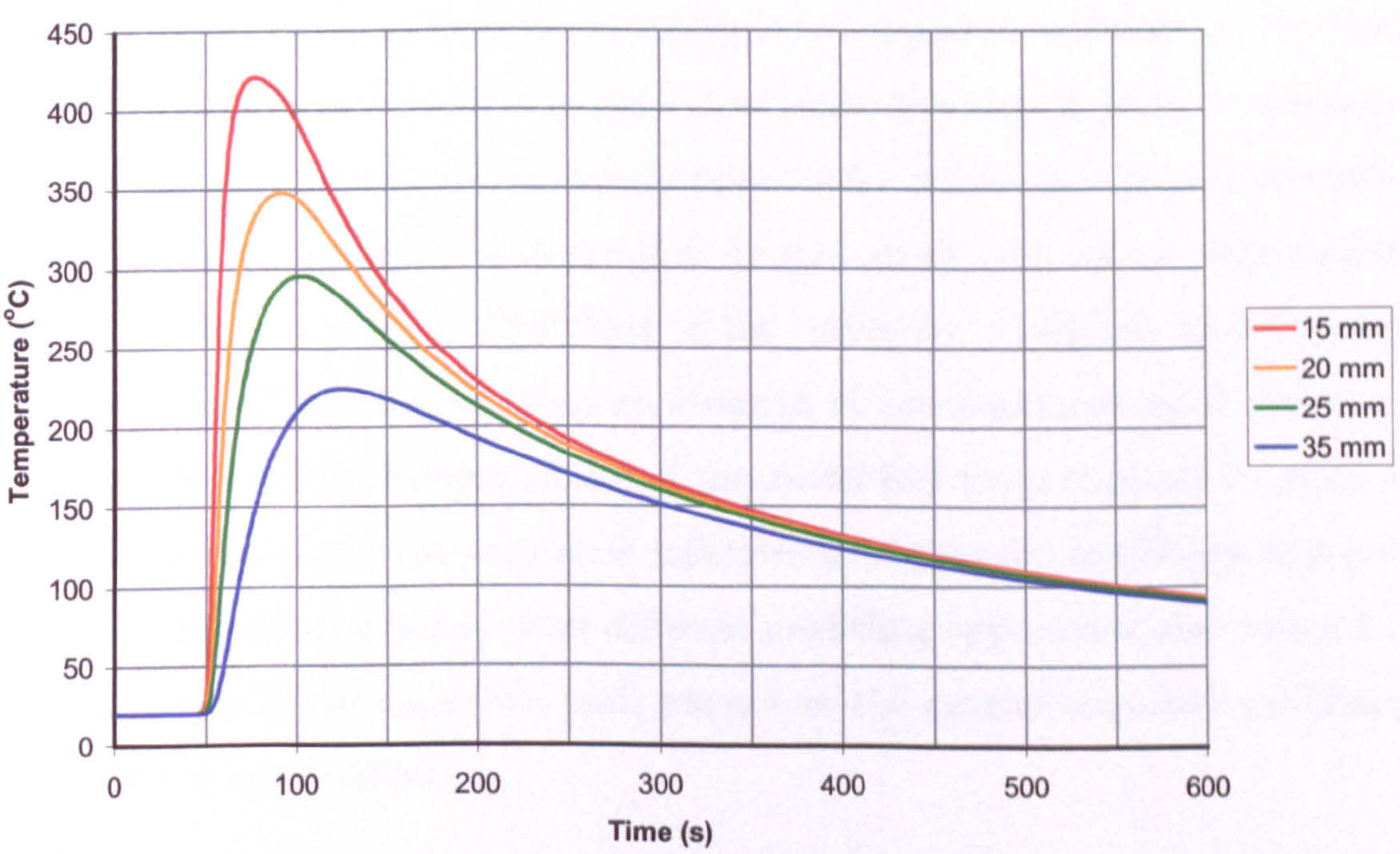

Figure 4.9: Transient temperatures taken from the three dimensional thermal analyses at various transverse distances

4.2.2 Structural Analysis

An un-coupled thermal to structural analysis was carried out. Un-coupling the thermal and structural parts is convenient from the computational point of view as it reduces the number of degrees of freedom present in each of the thermal and structural models. This can be done with little loss of accuracy for this kind of welding configuration, as the deformations experienced during the welding process will not significantly affect the flow of heat in the welded structure. The methodology outlined in the previous chapter was adopted, which consists of tailor made subroutines in order to carry out elasto-plastic analyses. The main uncertainty encountered in this part of the analysis was related to the criteria for element activation and deactivation (element birth and death) together with the choice of boundary conditions to represent conditions encountered during the experimental reference trials. The different strategies investigated are outlined next and compared to experimental reference data in order to determine the optimum simulation technique.

The plates in the computational model were supported notionally at the four corners, with simple restraints in the out of plane direction in order to simulate the pin supports present in the experimental trials. Additional support was provided in the experimental configuration by run-on/off tabs, which were tacked to the plates at the ends. Modelling of the symmetry conditions proved to be problematic. The fusion zone has no strength at the maximum input temperatures and the gravity loading aspect of the model had to be removed, to avoid a requirement to model the somewhat indeterminate restraint conditions imposed by the tack welded end tabs. Five different modelling approaches were tested for the two dimensional approach, with respect to the central boundary condition and element reactivation:

A. As shown in Figure 4.10, the fusion zone elements were determined from the weld preparation shape. These were activated from the onset of the input of heat energy (labeled 'After Weld' in the diagram) but the central

symmetric boundary condition on these elements was activated only after cooling below 600°C. Note that symmetry was not imposed in this model on the small root-face area. Hence, it was assumed that the plates were not continuously connected in this region, which correlates with what happens in the practical weld tests used for comparison. The angular deformation resulting from the delayed imposition of symmetry in the model was much less than typical observations (compare first and third row of Table 4.1). However, the behaviour related well to the experiments in a qualitative sense, in that it was observed that the root areas on either side of the joints moved together during the welding process and were not constrained in the transverse direction.

B. Figure 4.11 shows a variation on this condition, where the root area was assumed to be connected throughout the analysis, but other symmetry conditions were treated as in Model A. This modelling procedure yielded a slightly smaller positive angular displacement tabulated in Table 4.1.

C. Figure 4.12 shows a model where the symmetric boundary condition was maintained throughout the thermal loading. Greater expansion of the upper part of the weld fusion zone during heating generated a negative angular displacement and a large measure of this displacement was retained on subsequent cooling to ambient temperature leading to a final negative distortion. By contrast, overall net negative angular distortion was *not* observed in welding tests for this particular set-up. When the simulated transient deformations were examined at an intermediate stage of the computational cycle, it was clear that the symmetric boundary condition was forcing the centre of the weld to slide vertically during heating. The centreline of the plate, as a result, lifted up during the heating part of the cycle, by an amount much greater than noted during the experiments. Although contraction of the fusion zone eventually took place during cooling, the initial

overshoot was too large to result in the correct net angular distortion at the end of the transient simulation. (Incidentally, modelling the entire plate as a whole i.e. without invoking symmetric boundary conditions, yielded the same results as the present Model C idealisation, as expected).

D. Figure 4.13 shows yet a different approach where de-activation and subsequent re-activation of elements was based on the algorithm presented in the previous chapter, where the criterion is the maximum temperature reached during the thermal simulation rather than the configuration of the weld preparation shape. More specifically, all elements that were predicted to reach a value equal to or higher than a predefined cut-off temperature during the thermal simulation were deactivated at the start of the thermo-elasto plastic simulation and re-activated only when they reached the cut-off temperature. For this approach the cut-off temperature was set to 1493°C (approximately the liquid to solid phase transition temperature for steel) as this appeared to give better matching to the experimental behaviour. The double ellipsoid heat input distribution was used for the thermal analysis so that the cross-section of elements reaching the cut-off temperature matched the fusion zone observed from the macro sections. Symmetric boundary conditions were maintained throughout this simulation with the same adverse effects observed in Model C, resulting in an angular deformation in the opposite sense to the ones observed experimentally (Model D results not shown in Table 4.1

E. Model E is yet another approach, developed in an effort to try and counteract the formation of negative angular distortion resulting from modeling approaches from Models C and Model D. A link element was used, as shown in Figure 4.14, which is set with a zero stiffness in compression, whilst a nominal, high, value is assigned to stiffness in tension. This effectively inhibits any upwards movement of the plate, canceling the initial negative

angular deformations which is incorrectly simulated by Models C & D. The resulting angular deformation matches the reference experimental data in both magnitude and direction (see Table 4.1 rows 1 and 5). The attractive feature of this model is that the element deactivation strategy is derived from the thermal analysis using the double ellipsoid heat input distribution, and hence matches the fusion zone observed in the experimental data.

The above two dimensional modelling techniques are of interest from the computational effort point of view, as they only require a fraction of the time required by their three-dimensional counterparts, whilst still embodying the same level of complexity as regards material models. The plane strain assumption adopted for the simulation, however, means that the plate is assumed to be infinitely long and clamped at the longitudinal ends. This is not in line with the reference experimental data where the plates are of finite length and only supported under their own weight by four pins close to the corners. The constraint imposed by the run on/off tabs is also impossible to model directly using the two dimensional models so that the modifications presented above had to be adopted in order to obtain deformation results in line with the experimental data.

Problems relating to the boundary conditions are considerably diminished when adopting a three dimensional approach. Another improvement is the added information as regards to the longitudinal curvature results, which are of considerable practical interest. The cases considered using three dimensional models were again based on full temperature dependent, elasto-plastic modelling, which implies a substantial penalty in terms of computational time. The two-dimensional models consisted of 524 4-node ANSYS solid element (*plane 42*) [4.3], whilst the three-dimensional models consisted of 12400 8-node ANSYS solid elements (*solid 45*).

Delayed imposition of a symmetric boundary condition could not be implemented in the three-dimensional models, as it is incompatible with incremental travel of the heat source providing the transient thermal input. As with the 2D

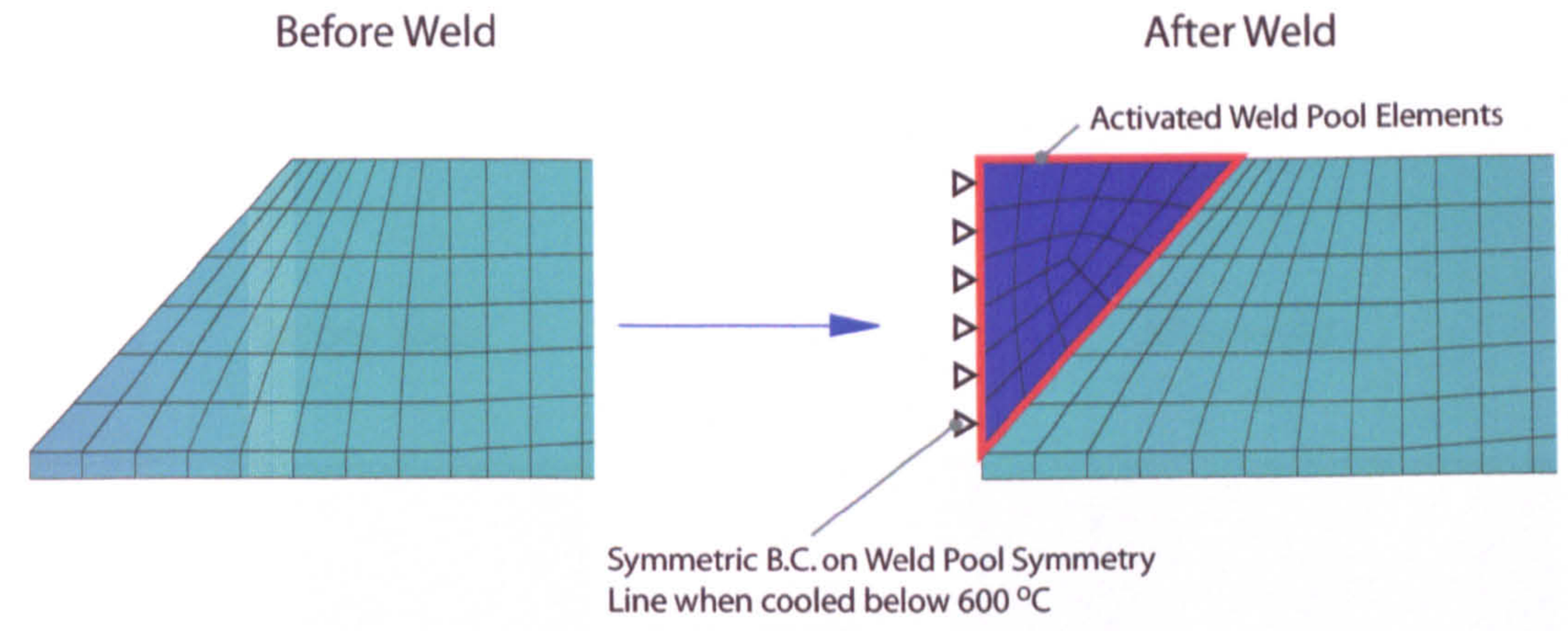

Figure 4.10: Butt welding investigation Model A

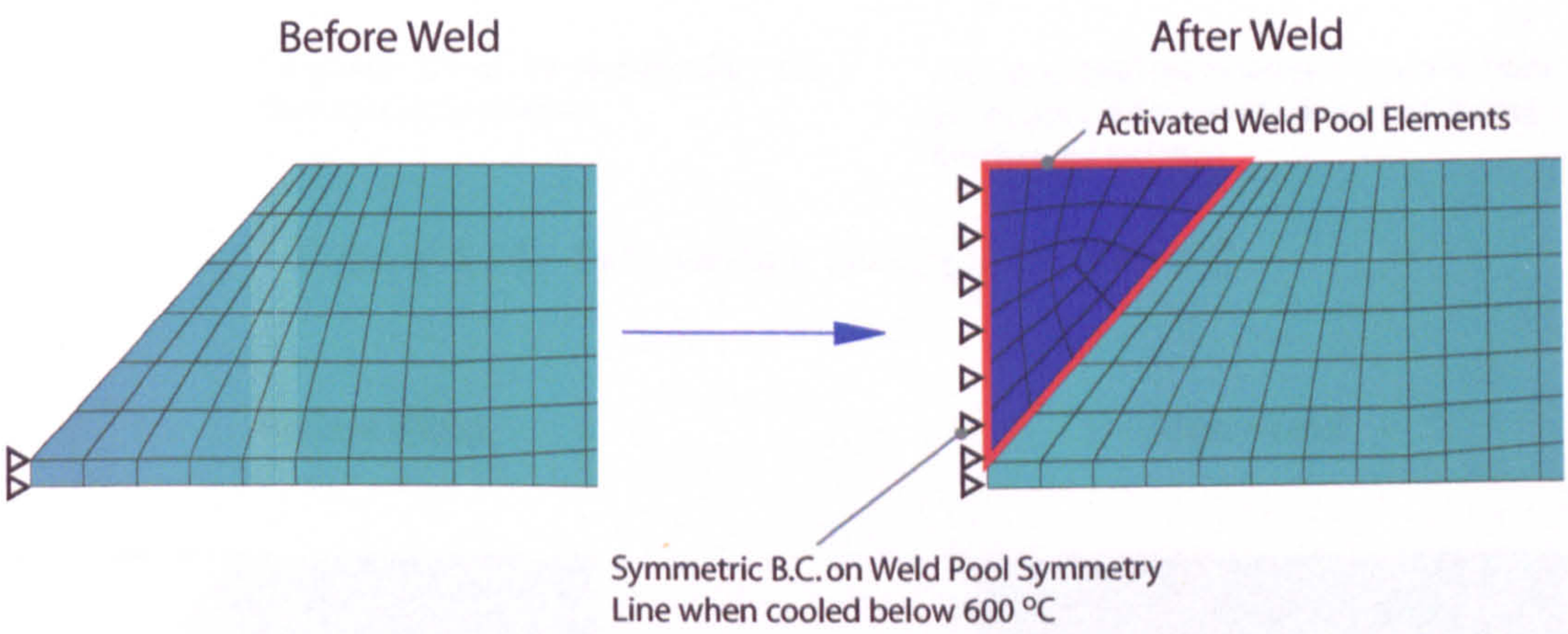

Figure 4.11: Butt welding investigation Model B

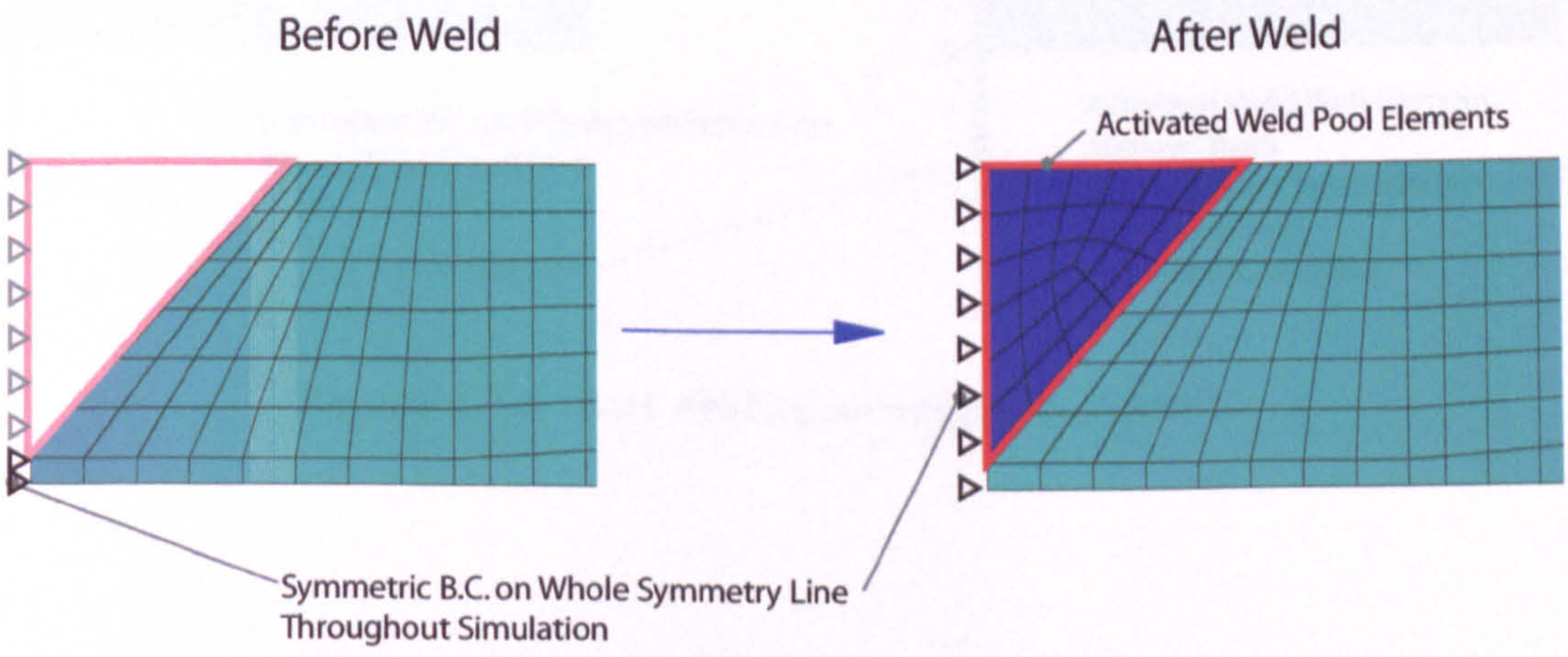

Figure 4.12: Butt welding investigation Model C

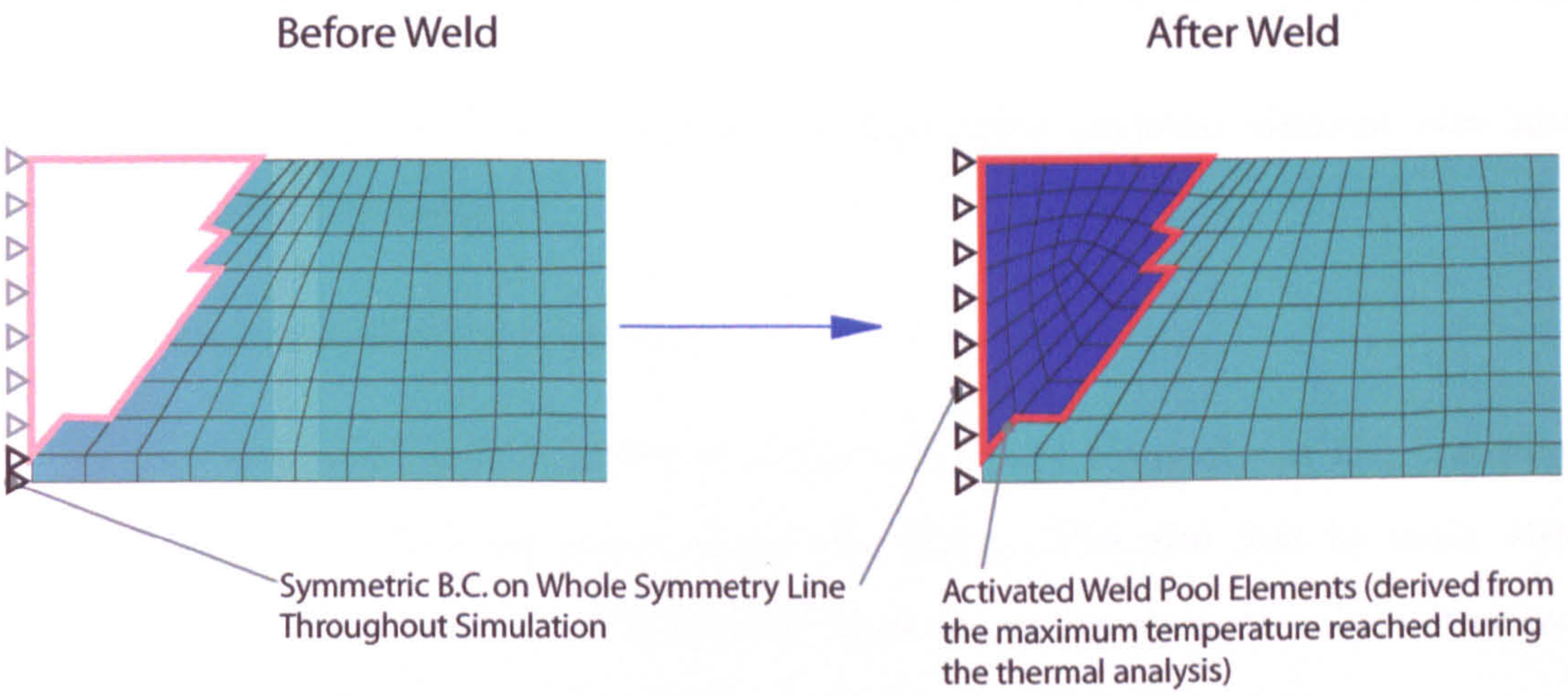

Figure 4.13: Butt welding investigation Model D

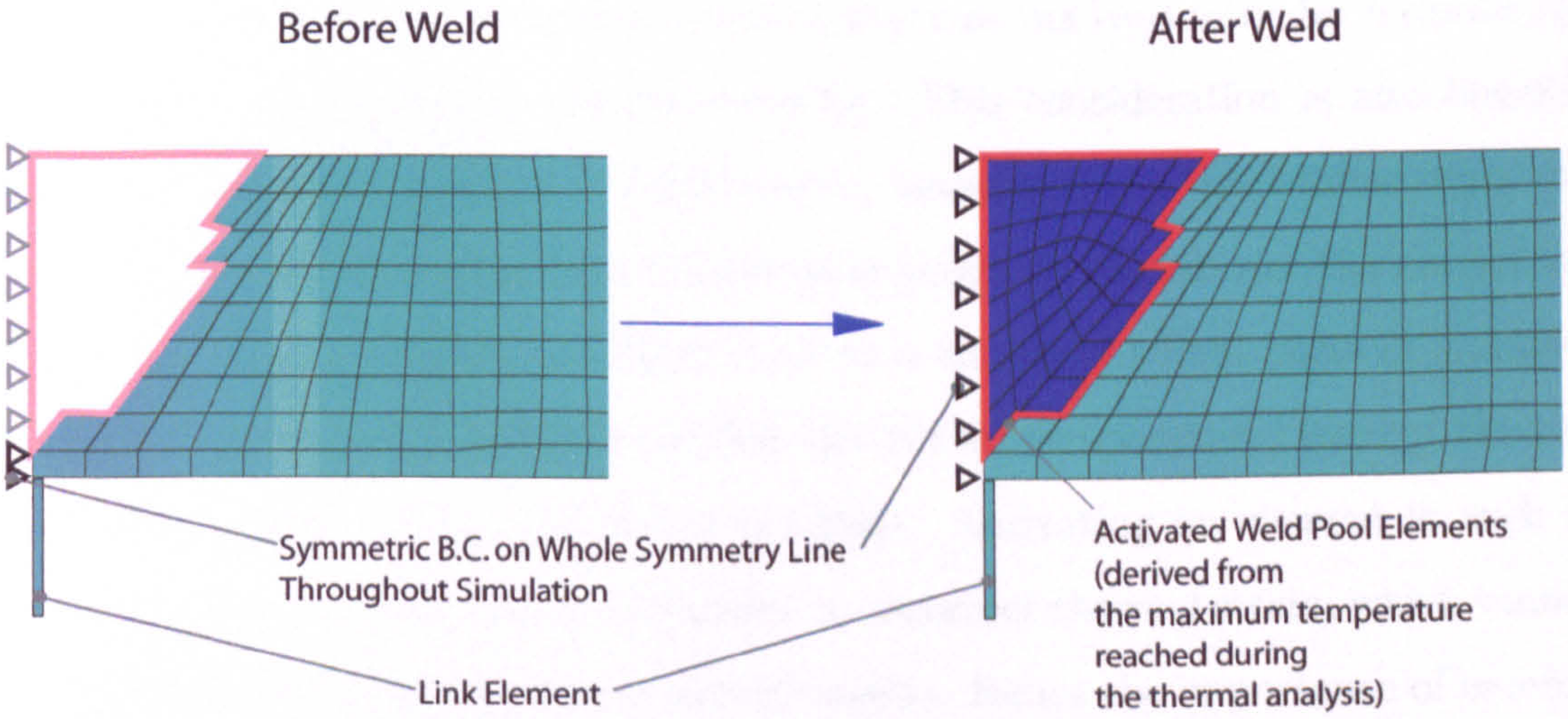

Figure 4.14: Butt welding investigation Model E

analyses, birth and death elements were used to improve simulation of weld material deposition. Due to the highly non-linear nature of the simulations (non-linear material properties and geometry) and the wide range of temperature loading, non-convergence problems were encountered. These were dealt with by adjusting:

- Mesh density to reach a suitable compromise between element size and computational time
- Time intervals for load-steps
- The criterion for re-activation of the weld pool elements as the transient temperature field advanced along the plate. The aim was to make sure that elements were not re-activated until the entire element volume reached temperatures equal to or higher than the cut-off temperature

The last point is of particular importance in ensuring convergence of the structural simulations. Numerical instability can inadvertently be induced by not setting the activation criteria correctly. This consideration is also heavily influenced by the limitation in mesh density present in the three-dimensional finite element model: as the high temperature profile is passed over the structural mesh, the high gradients can easily lead to a situation where parts of a single element have reached and/or exceeded the cut-off temperature, leaving the remaining element volume still below the limit. Activating an element in such a state would mean applying an unrealistic or incorrect thermal strain, which would in turn lead to un-convergence or flawed results. Hence the importance of careful implementation of the reactivation strategy.

Three modelling strategies were investigated for the three dimensional simulations:

F. The symmetric boundary condition was applied in the root face area only, as shown in Figure 4.15, and weld activation was based on weld preparation shape only. The correct pattern of deformation was obtained from this

model, but the computed angular deformation and longitudinal curvature were much greater than the experimental benchmarks (See Table 4.1).

G. Figure 4.16 shows the case where the symmetric boundary condition was applied across the whole thickness (3D version of 2D Model C). The resulting angular deformations took place in a similar sense to model C, i.e. showing negative final curvature and hence not matching the experimental data.

H. Model H is the three-dimensional analogue of the two-dimensional Model D, as the same strategy was used for the activation and deactivation of elements: all elements observed to reach a value equal to or higher than a predefined cut-off temperature during the thermal simulation were deactivated at the start of the thermo-elastoplastic simulation and re-activated only when they reached the cut-off temperature. Similarly to model D, the cut-off temperature was set to 1493°C and symmetry boundary conditions were maintained throughout this simulation across the whole thickness, as shown in Figure 4.17. Compared to the other three-dimensional models F and G, this approach gave better results for angular distortion (see Table 4.1). The resulting longitudinal curvature was similar to the other elastoplastic models but rather greater than the experimental data.

Models F & H yielded the correct mode of deformation, but the best of the three dimensional models was deemed to be Model H (as is Model D for the two-dimensional set). This is because the element birth and death strategy presented in Chapter 3 was adopted, which is representative of the actual fusion zone rather than on the weld preparation area. This is shown in Figure 4.18, where the region exceeding the cut off temperature (and hence the one to be used in the activation / de-activation algorithm) is shown for a single load step. Distortion values were also relatively close to the experimental benchmark for this model.

Quantitative values for angular and longitudinal distortions are tabulated in

Table 4.1. Results are compared to reference experimental data and to a simplified method presented by Camilleri [4.1], described in Chapter 2, comprising of two algorithms, namely the 'Thermal Contraction Strain (TCS)' algorithm for computing the angular deformation and the 'Mismatched Thermal Strain (MTS)' for determining the longitudinal contraction. These algorithms only require a single elastic finite element analysis and are hence very attractive from the computational point of view. Results show the deformation values obtained by applying the algorithms to a three dimensional finite element model with all parameters set equal to the thermo-elasto-plastic models, in order to allow direct comparison.

It can be seen that best comparison was achieved with Models D & H for the two-dimensional and three-dimensional models respectively. These will hence be used to illustrate the effects of distortion and residual stresses. Contour plots for transient and residual temperature, out of plane deformation and longitudinal residual stress are shown in Figures 4.19 to 4.22. Gravity loading was not included as the plates were relatively small. The transient results show an immediate development of the angular deformation in a V-shape. This is in exact agreement with the the reference experimental data [4.1]. At this point the longitudinal residual stresses are still very localised and primarily caused by the restraint imposed by the surrounding material which is still relatively cold. As the heat source reaches the end of the plate (Figure 4.20), angular deformations are still predominant at the heat source position whilst the trailing edges start to cool, contract and develop the longitudinal stress profile that will be present in the residual / final state.

Figure 4.21 shows a load step in which the plate has cooled to a state where most of the material is gaining considerable strength. At this stage the longitudinal contraction forces come into play and start to bend the plate in the longitudinal direction until it assumes the final residual shape shown in Figure 4.22. Final longitudinal and transverse residual stresses are shown in Figures 4.23 and 4.24 respectively, taken for a transverse slice half way along the longitudinal

length and at the plate mid-thickness. A plot showing the variation of longitudinal and transverse residual stress over the entire plate is shown in Figures 4.25 and 4.26 respectively.

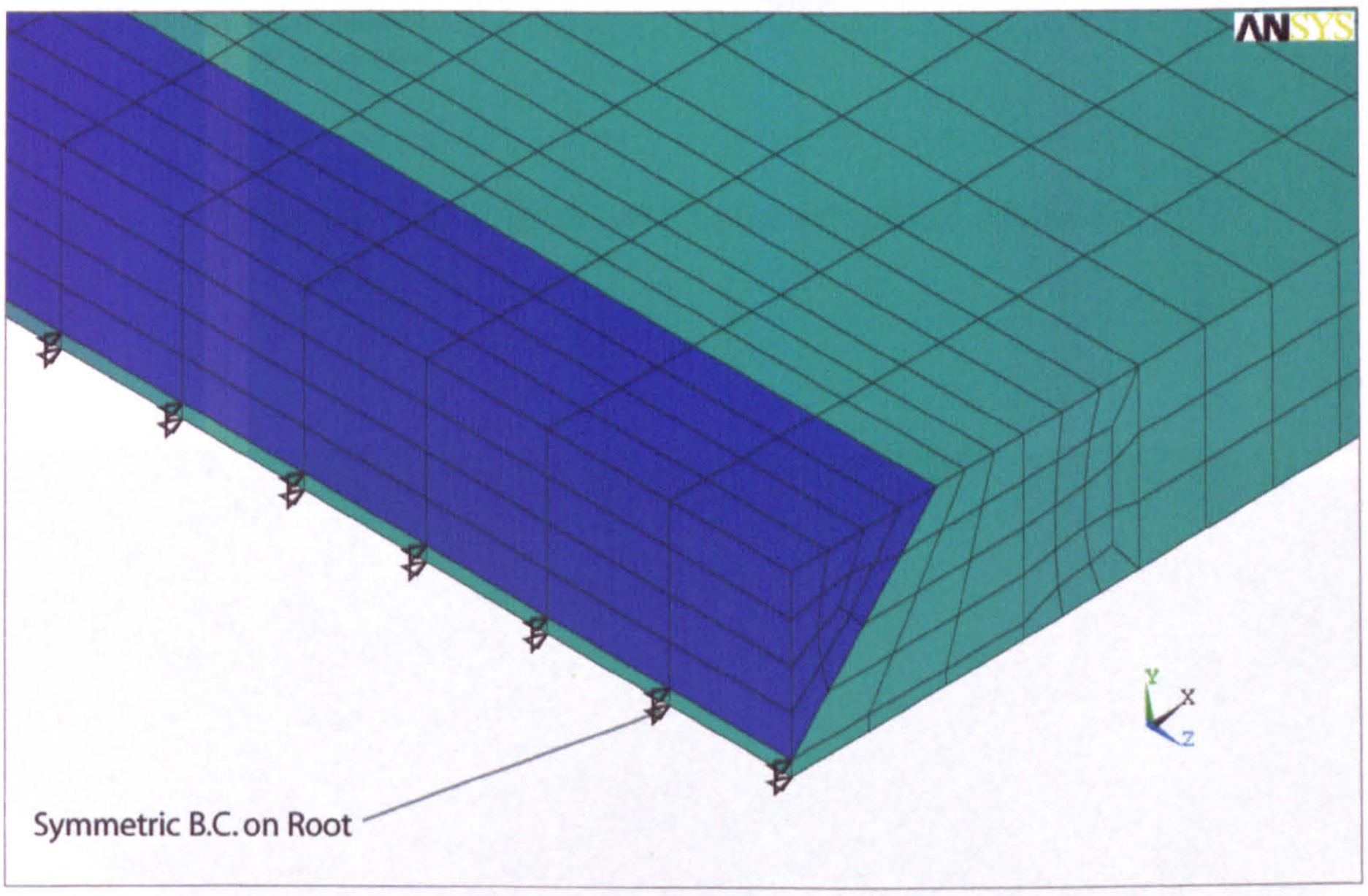

Figure 4.15: Butt welding investigation Model F

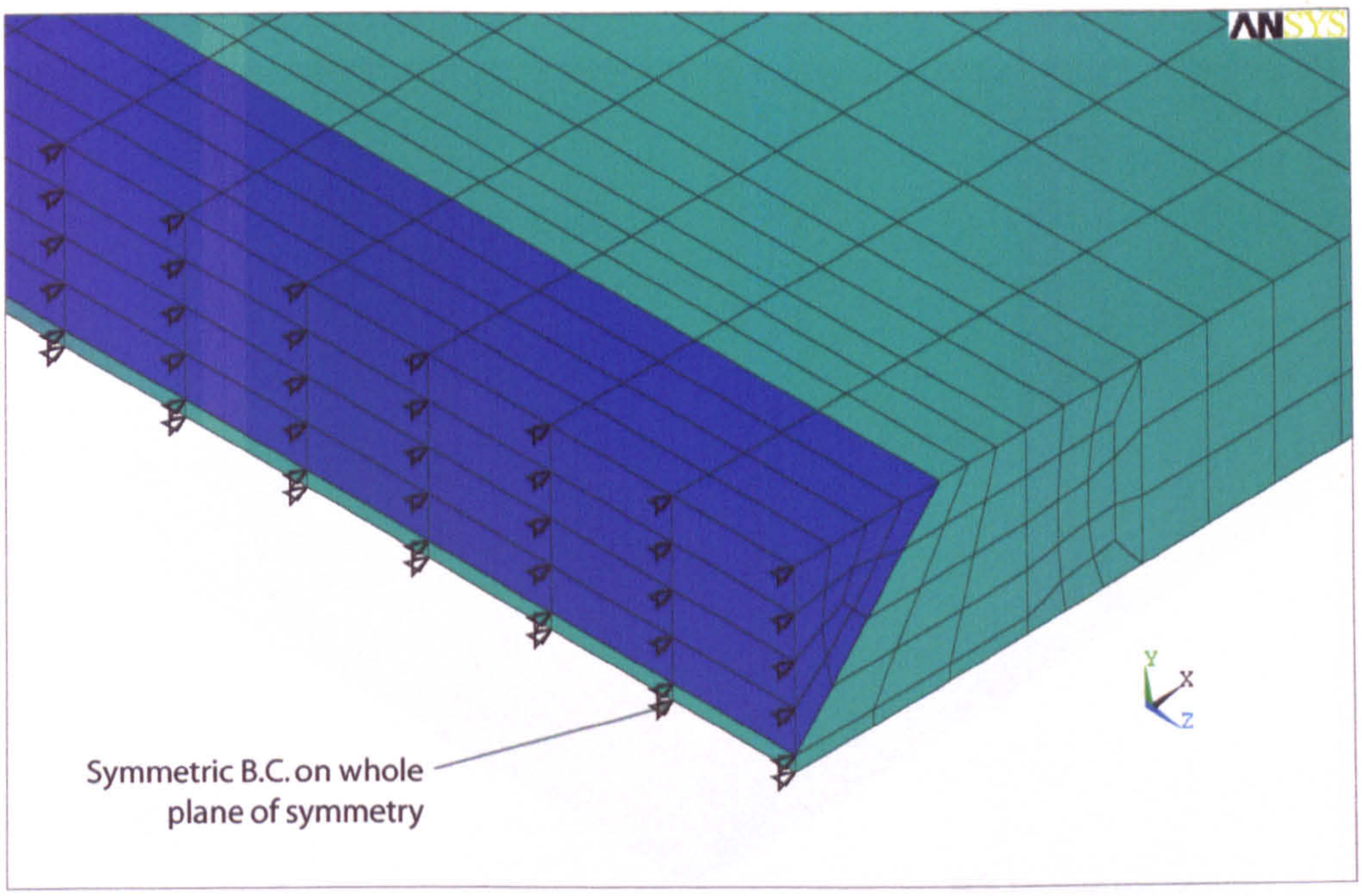

Figure 4.16: Butt welding investigation Model G

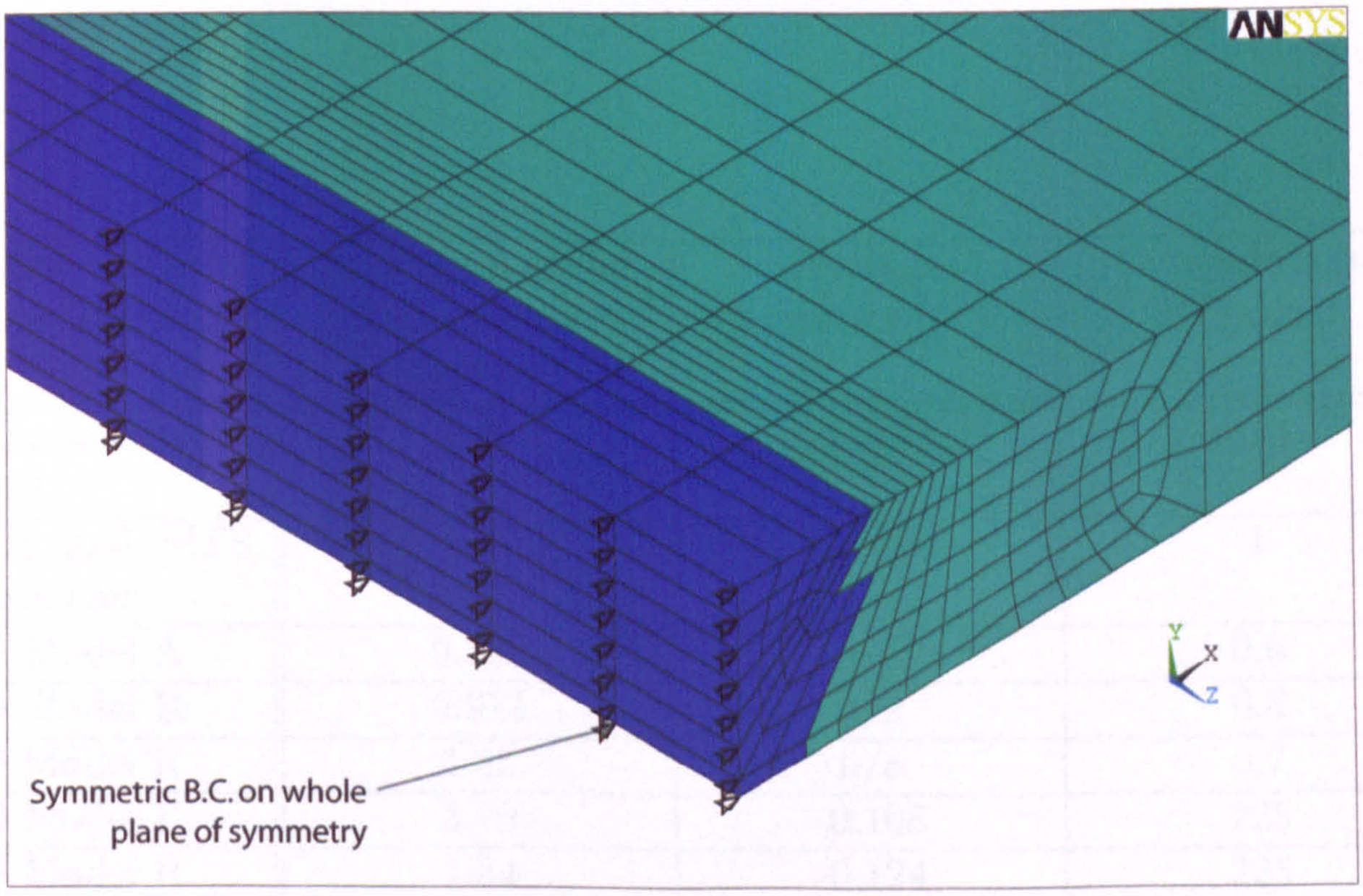

Figure 4.17: Butt welding investigation Model H

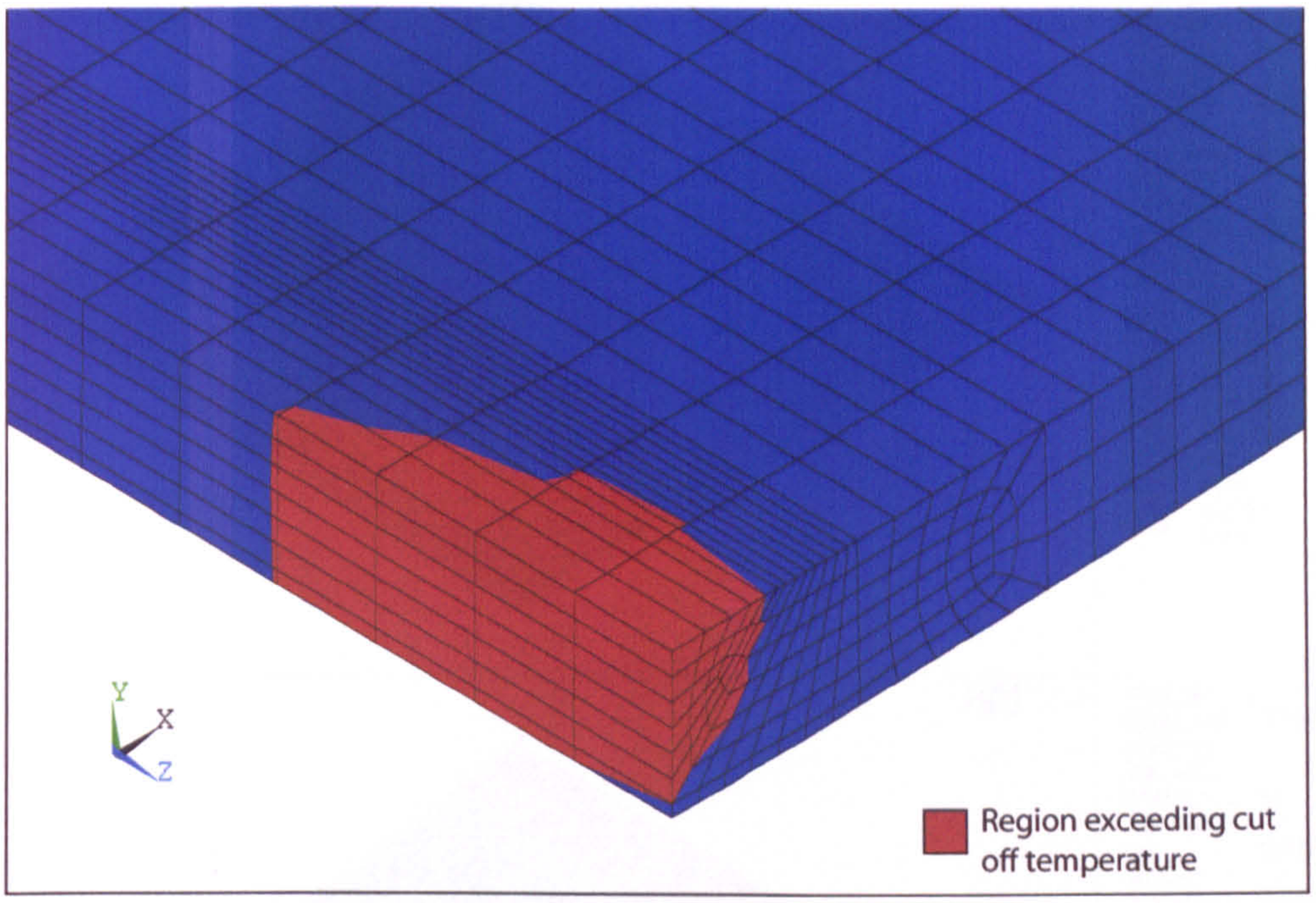

Figure 4.18: Region over which element birth and death criterion is applied for the three dimensional butt welding investigation

Model I.D. / Data Source	Average Angular Deformation (degrees)	Average Curvature (m^{-1})	Computational Ratio
Experimental Data	1.73	-0.0864	n/a
TCS and MTS Algorithm	1.82	-0.0604	1
2D Model A	0.732	n/a	0.6
2D Model B	0.911	n/a	0.6
2D Model E	1.85	n/a	0.7
3D Model F	4.79	-0.108	225
3D Model H	1.84	-0.124	225

Table 4.1: Comparison of average deformation values and computational effort for the butt welding investigation

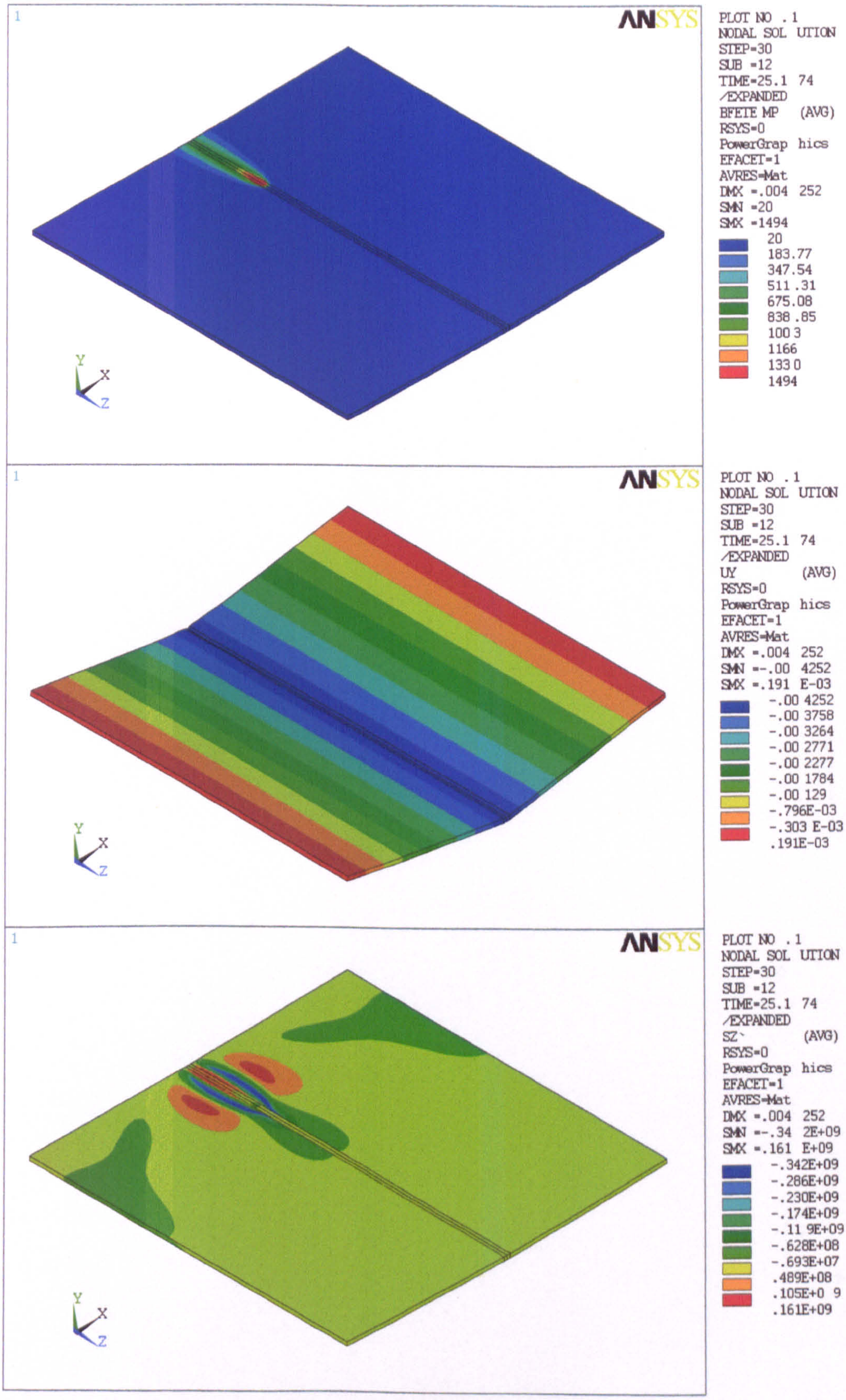

Figure 4.19: Transient response for the butt welding case: initial heating. Top: temperature distribution. Middle: out of plane deformation (graphical representation amplified by a factor of 10). Bottom: longitudinal stress

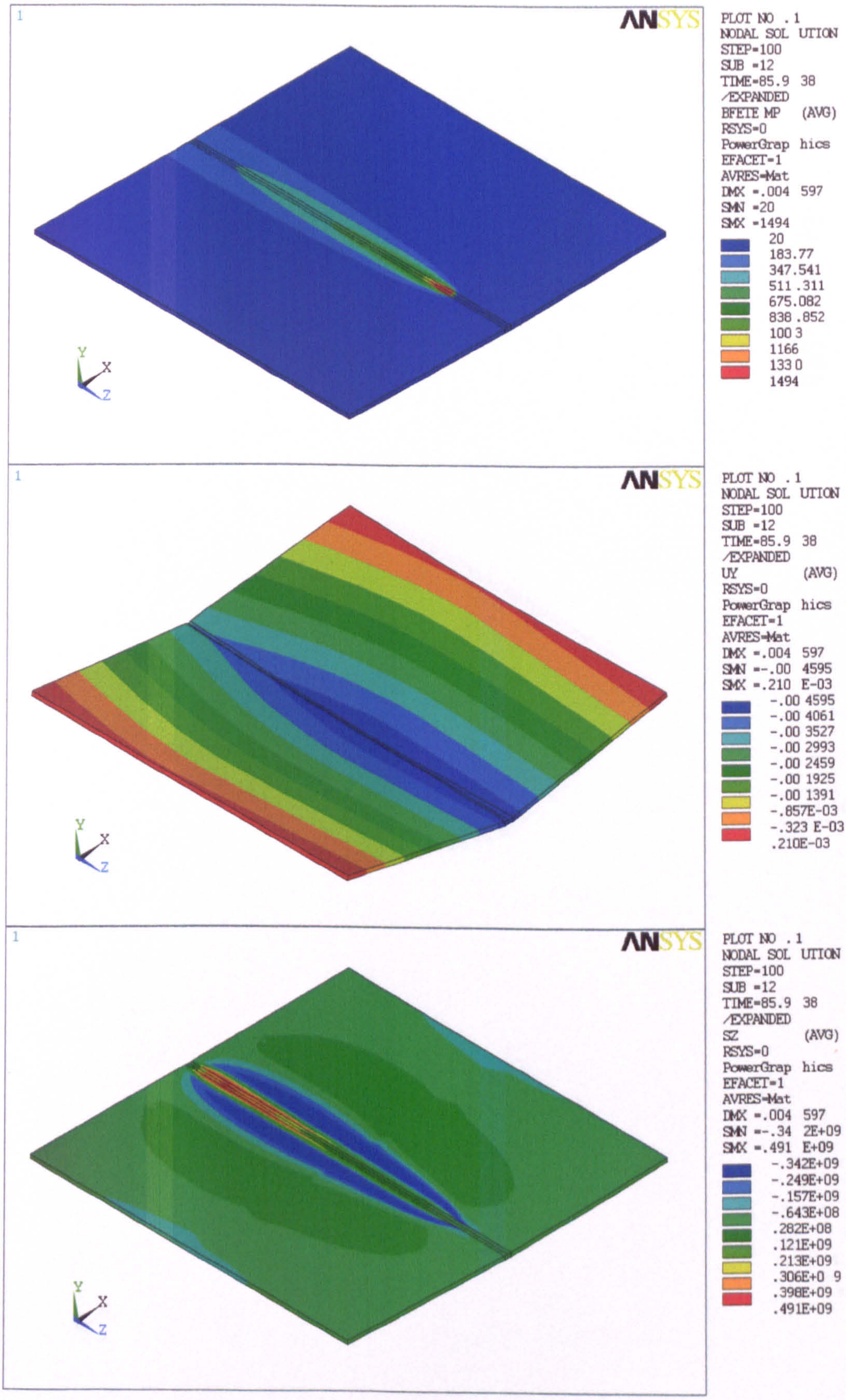

Figure 4.20: Transient response for the butt welding case: subsequent heating. Top: temperature distribution. Middle: out of plane deformation (graphical representation amplified by a factor of 10). Bottom: longitudinal stress

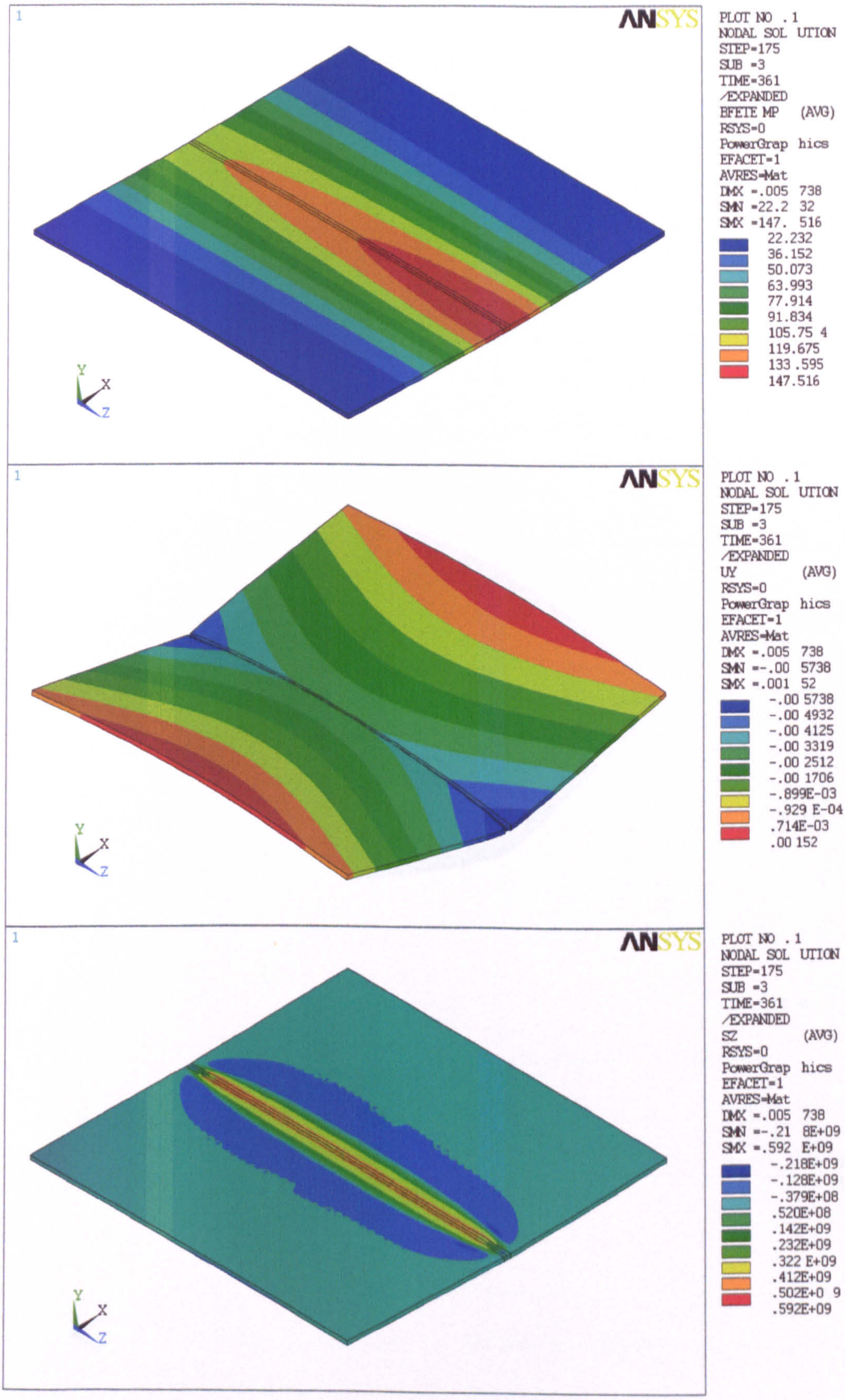

Figure 4.21: Transient response for the butt welding case: cooling. Top: temperature distribution. Middle: out of plane deformation (graphical representation amplified by a factor of 10). Bottom: longitudinal stress

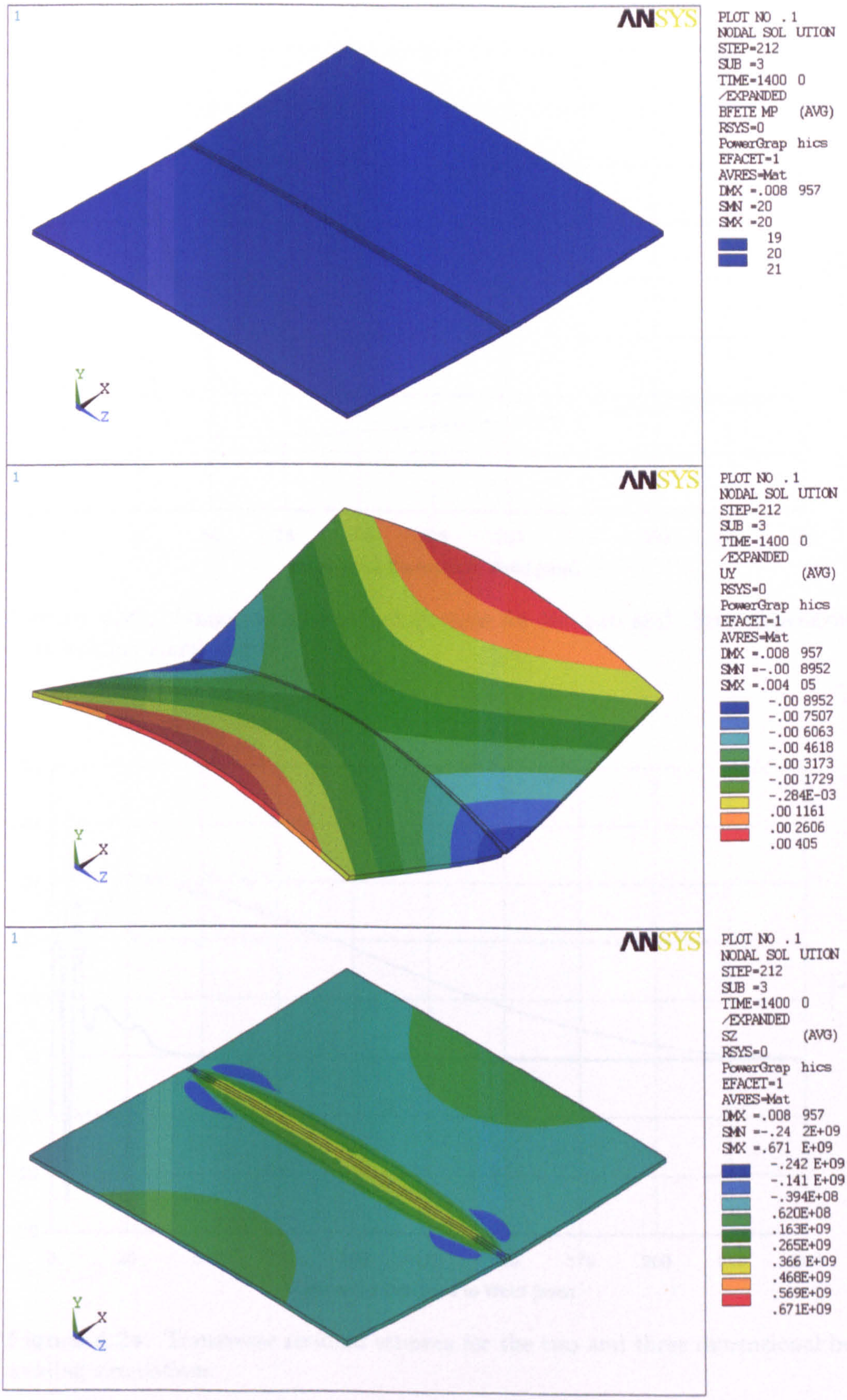

Figure 4.22: Transient response for the butt welding case: final cooling. Top: temperature distribution. Middle: out of plane deformation (graphical representation amplified by a factor of 10) Bottom: longitudinal stress

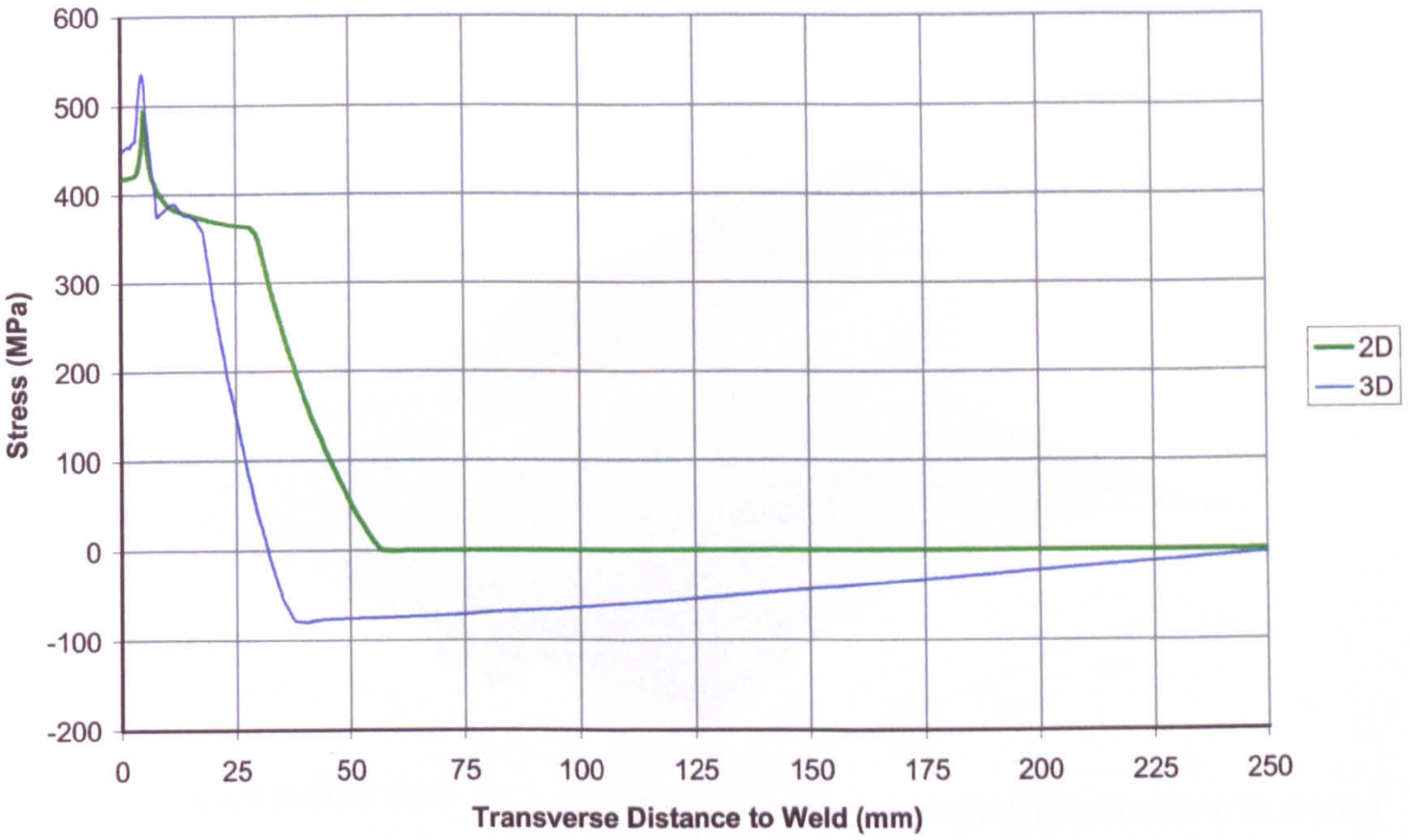

Figure 4.23: Longitudinal residual stresses for the two and three dimensional butt welding simulations

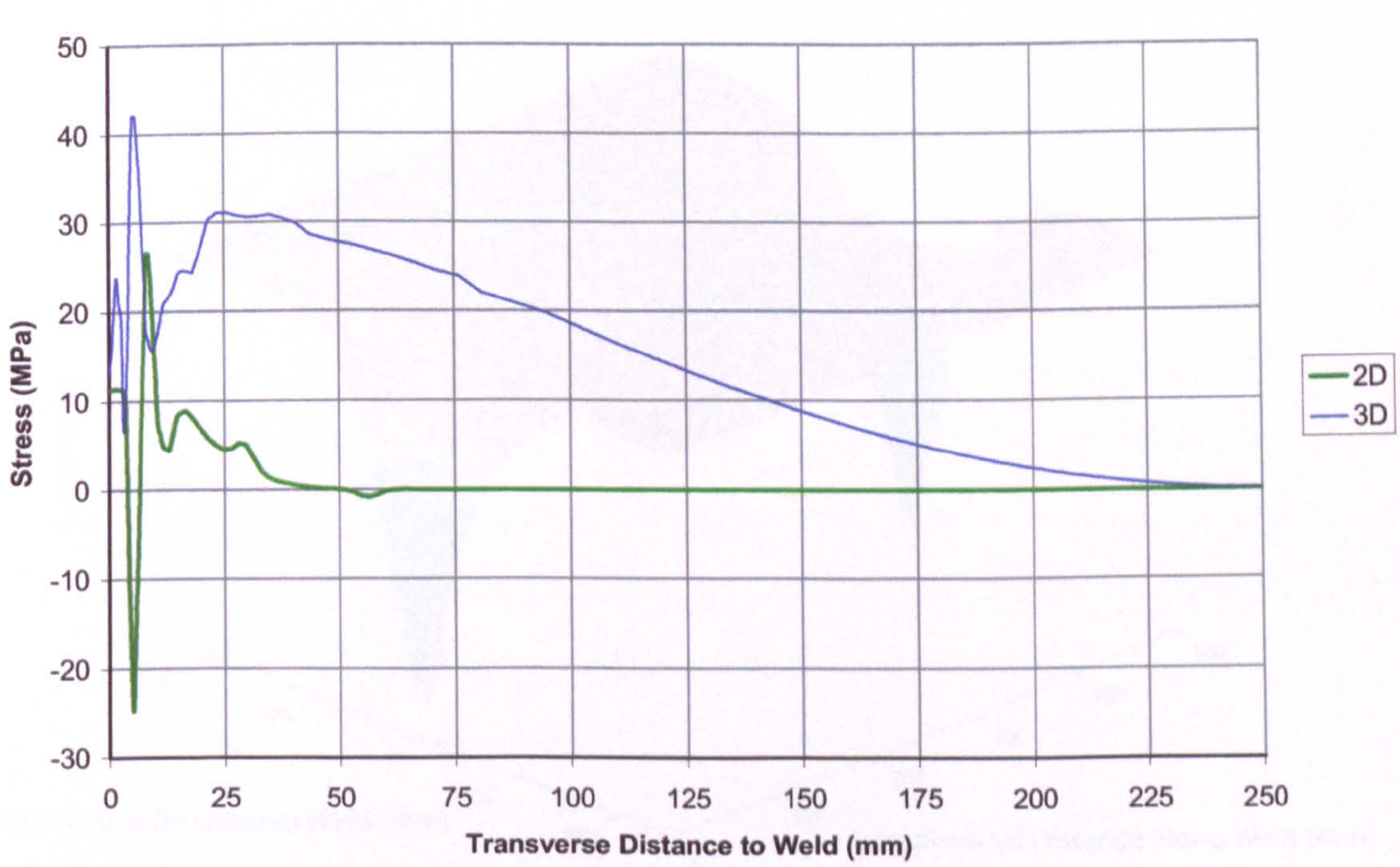

Figure 4.24: Transverse residual stresses for the two and three dimensional butt welding simulations

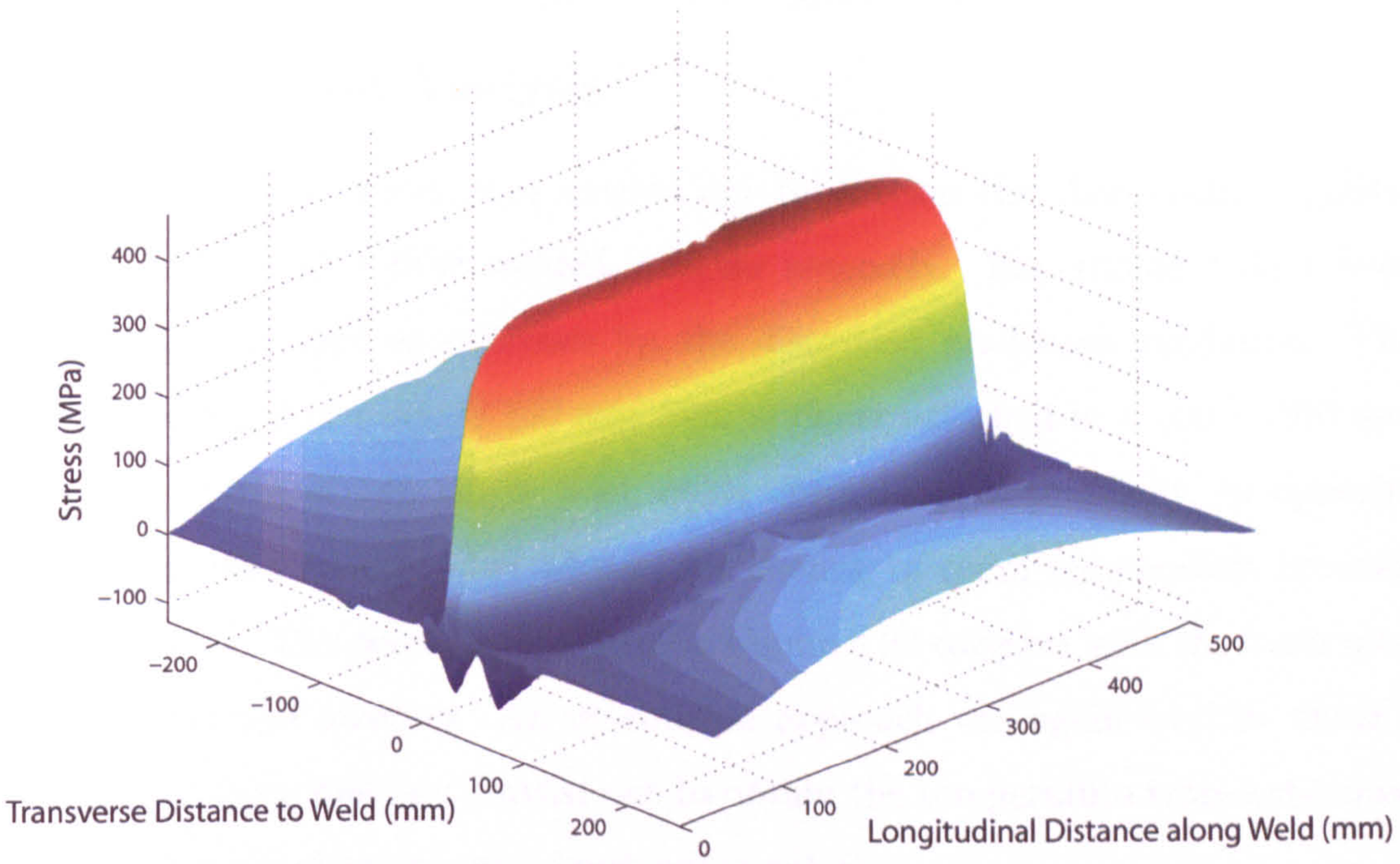

Figure 4.25: Longitudinal residual stress over the entire plate for the butt welding investigation

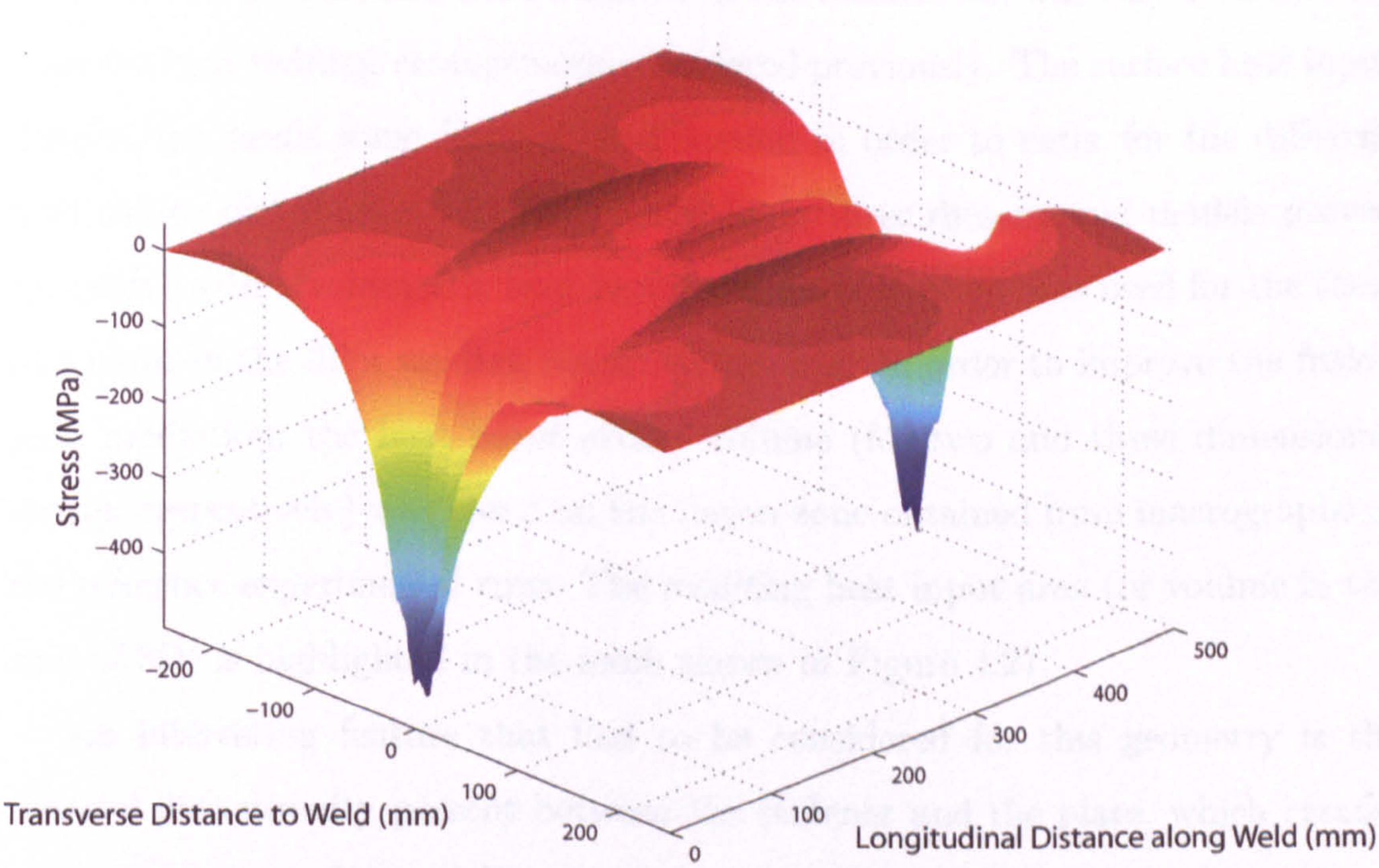

Figure 4.26: Transverse residual stress over the entire plate for the butt welding investigation

4.3 Fillet Welding Investigation

4.3.1 Thermal Analysis

The second set of simulations carried out to develop the thermo-elasto-plastic models dealt with a fillet welded stiffener assembly. Experimental data from [4.1] was again used as reference for the distortion prediction validation. The set-up consisted of a single 150 mm high stiffener attached to a 500 × 500 mm plate by means of two single fillet welds carried out sequentially, in opposite directions, with enough time allowed for cooling to room temperature between the two welds. The geometry is shown in Figure 4.27 together with the mesh used in the numerical analyses. An un-coupled approach was again used in which a thermal analysis was first carried out to obtain the temperature transients, used as input for the elasto-plastic structural simulation.

The fillet welding arrangement is considerably different from the butt weld arrangement. The welding gun has to be placed at an angle meaning that the heat transfer pattern and the formation of the fusion zone will vary considerably from the butt welding arrangement considered previously. The surface heat input distribution needs some form of modification in order to cater for the different heat source distribution. As the butt welding three dimensional models proved successful with a volumetric heat input, the same strategy was used for the thermal input in the fillet welding numerical models. In order to improve the fusion zone prediction, the heat input area / volume (for two and three dimensional models respectively) was based on the fusion zone obtained from macrographs of the reference experimental runs. The resulting heat input area (or volume in the case of 3D) is highlighted in the mesh shown in Figure 4.27.

An interesting feature that had to be considered for this geometry is the thermal discontinuity present between the stiffener and the plate, which creates uncertainty as to the modelling strategy to be adopted at the boundary. Three main approaches were considered when developing the thermal models:

- Merge the nodes so as to assume full heat transfer between the stiffener and the plate
- Use link elements as shown in Figure 4.28 to control the amount of heat transfer expected at the junction
- Leave the nodes unmerged with the assumption that no heat transfer occurs between the two surfaces

The thermal properties of the link element can be changed to effectively control the amount of heat being transferred between the stiffener and the plate. This approach, however, adds to the number of unknown parameters in the analysis and hence to its complexity. Furthermore, macrographs obtained from the reference experimental data clearly showed that a thermal barrier exists at the junction. For this reason the approach with the unmerged nodes was deemed satisfactory and used in the final analyses.

Welding efficiency was again determined by comparison with maximum temperatures reached throughout the welding cycle in the reference experimental data. Figure 4.29 shows the location and labeling of the points under consideration, for which the maximum temperature predictions are compared in Figures 4.30 and 4.31 for weld runs 1 and 2 respectively. Two and three dimensional models were considered as the former are very attractive from the computational point of view. As for the butt welding case study the resulting temperature profile finds its largest gradient in the transverse direction, so that the two and three dimensional simulations yield similar results, as can be seen in Figures 4.30 and 4.31 for the first and second weld runs respectively. The graphs show a very good match using an efficiency of 70 % for the first weld run. The second weld run showed a greater discrepancy for some of the points, which were however still within acceptable limits, using an efficiency of 85 %. Fusion zone predictions are shown in Figure 4.32 for the two dimensional simulations. A very good match was obtained for weld run 1, given the fact that the heat input region was based on fu-

sion zones taken from macrographs. The fusion zone size for weld run 2 is slightly over-predicted but nevertheless follows the pattern observed in the macrographs. The slight over-prediction shows that there is indeed some heat transfer across the gap between the stiffener and the plate. The effect of the thermal barrier can be seen in the discontinuity present in both temperature patterns. A plot of the three dimensional temperature prediction at an intermediate load step in shown in Figure 4.33.

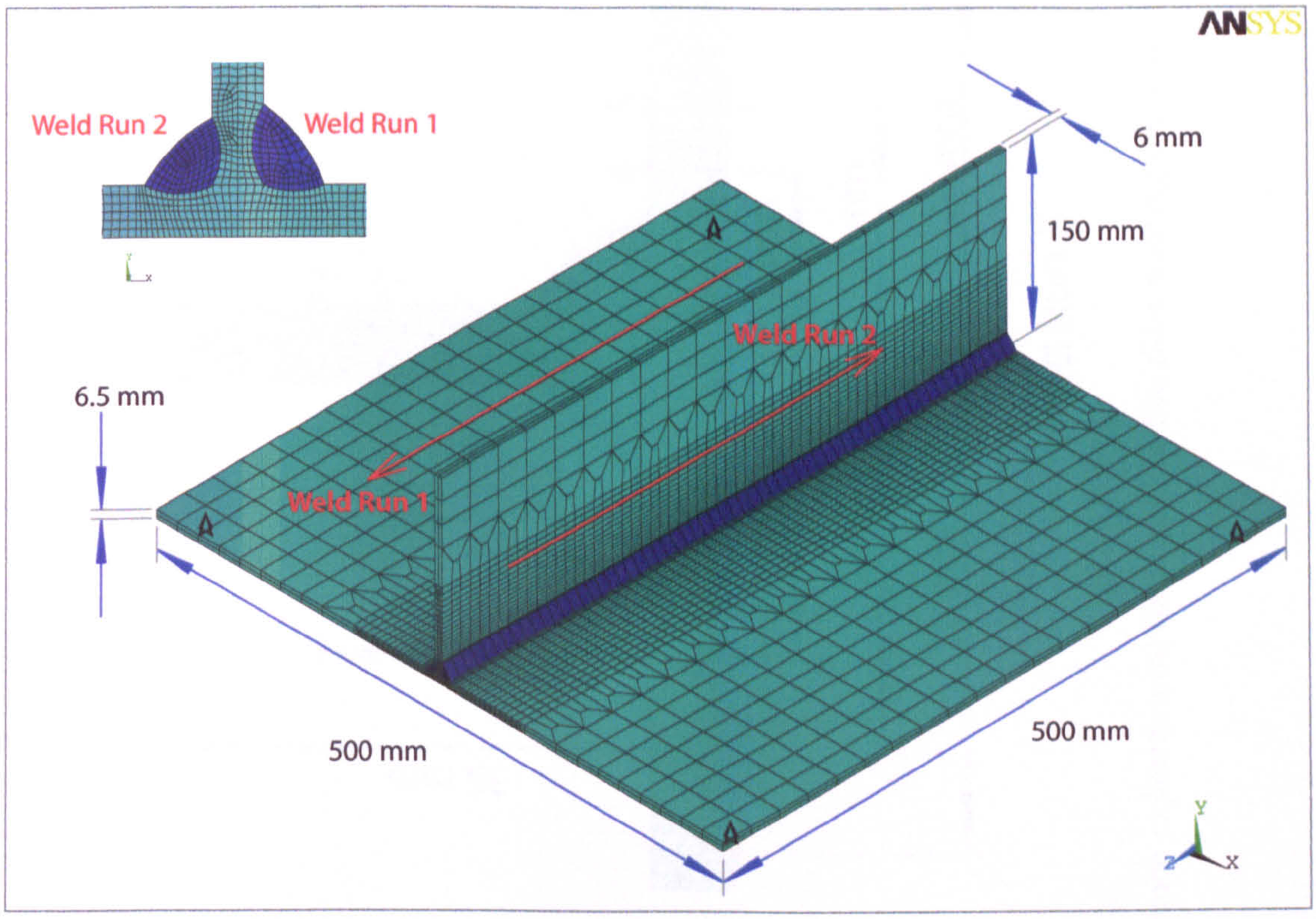

Figure 4.27: Fillet welding case study

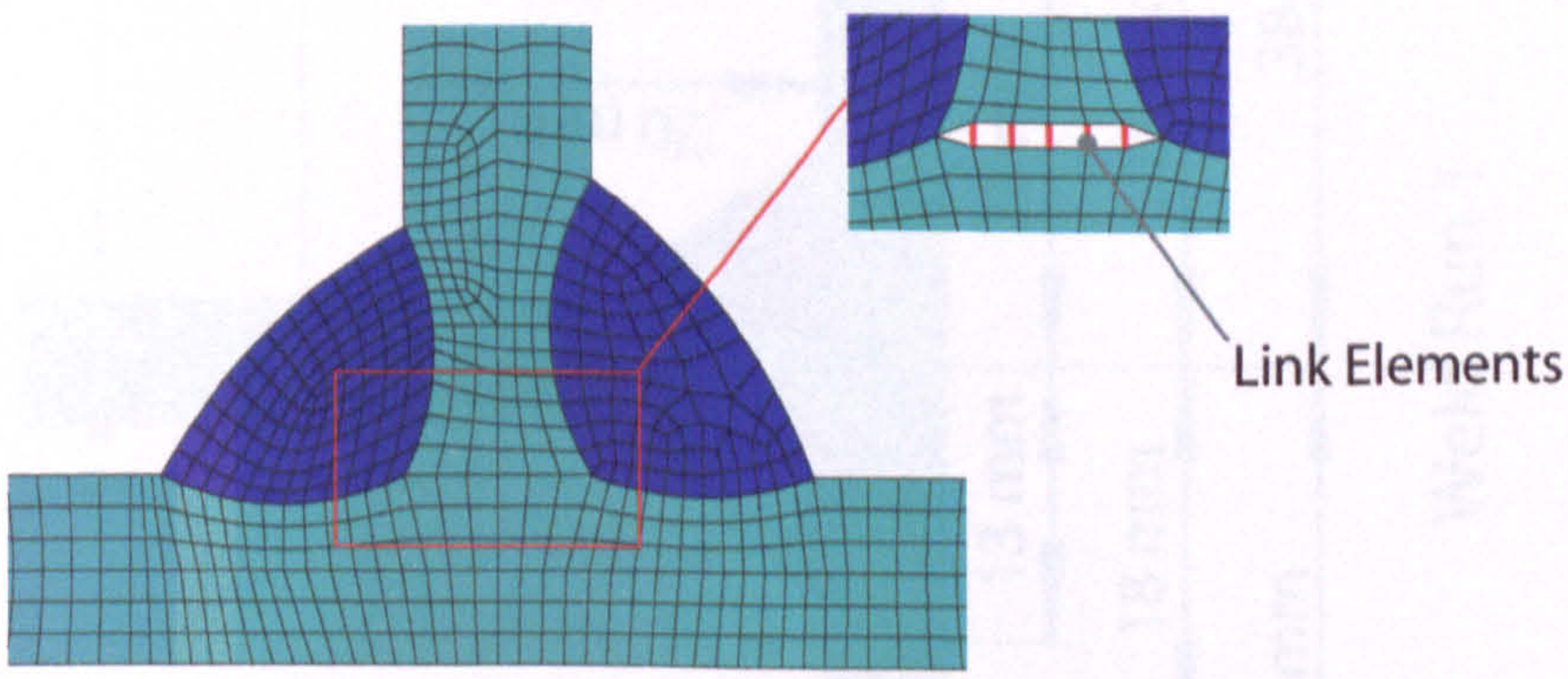

Figure 4.28: Use of link element to simulate thermal barrier in fillet welding investigation (mesh distorted in the detailed view for clarity)

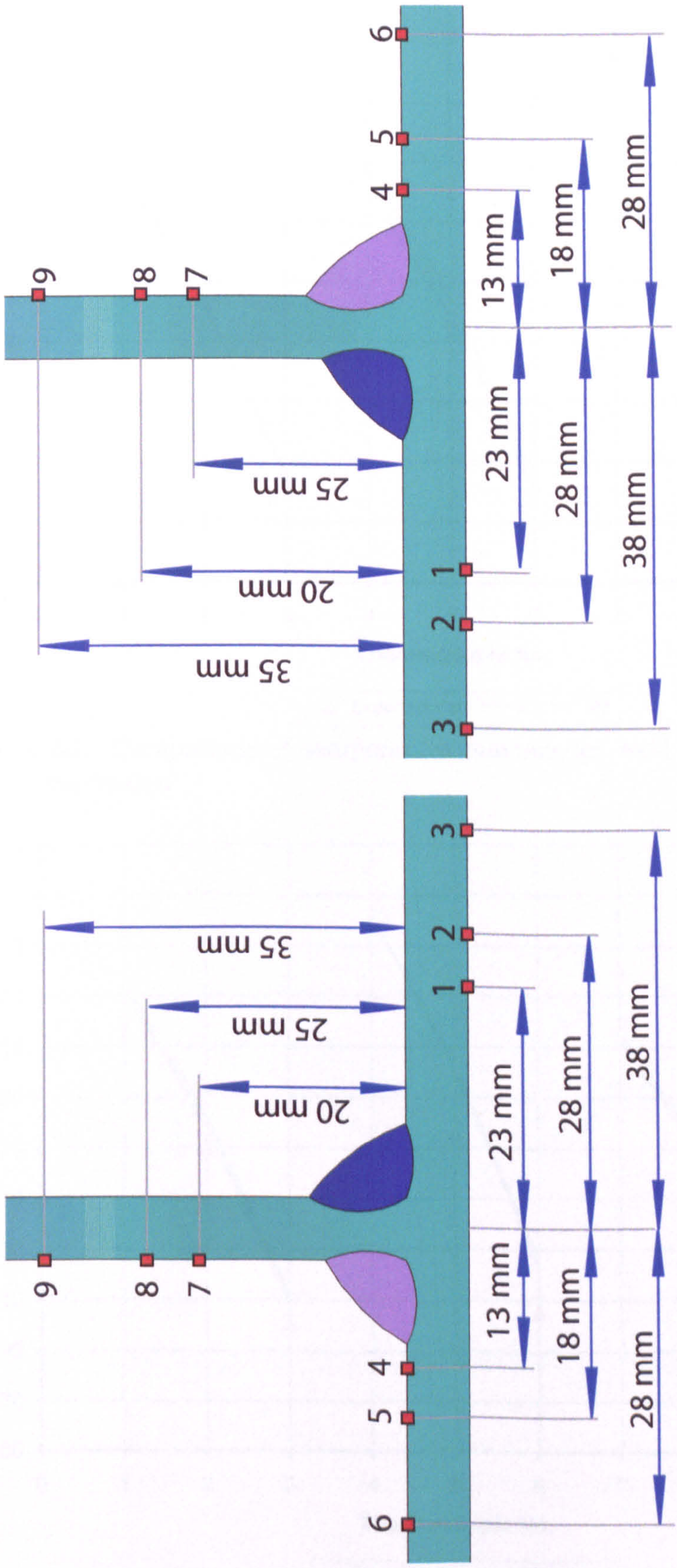

Figure 4.29: Thermocouple placement and labeling of reference experimental data used in the fillet welding investigation

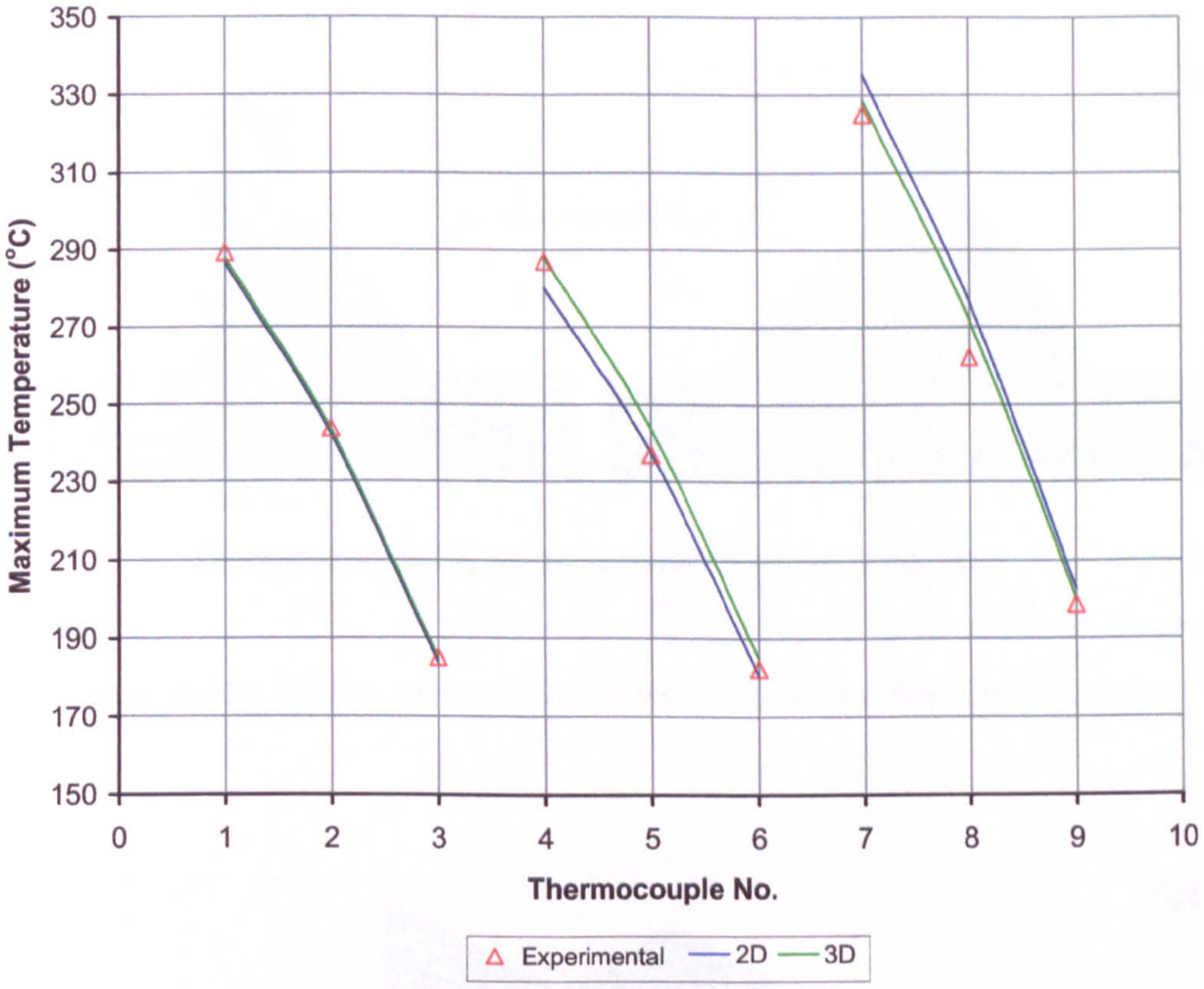

Figure 4.30: Comparison of temperature maxima for weld run 1 of the fillet welding investigation

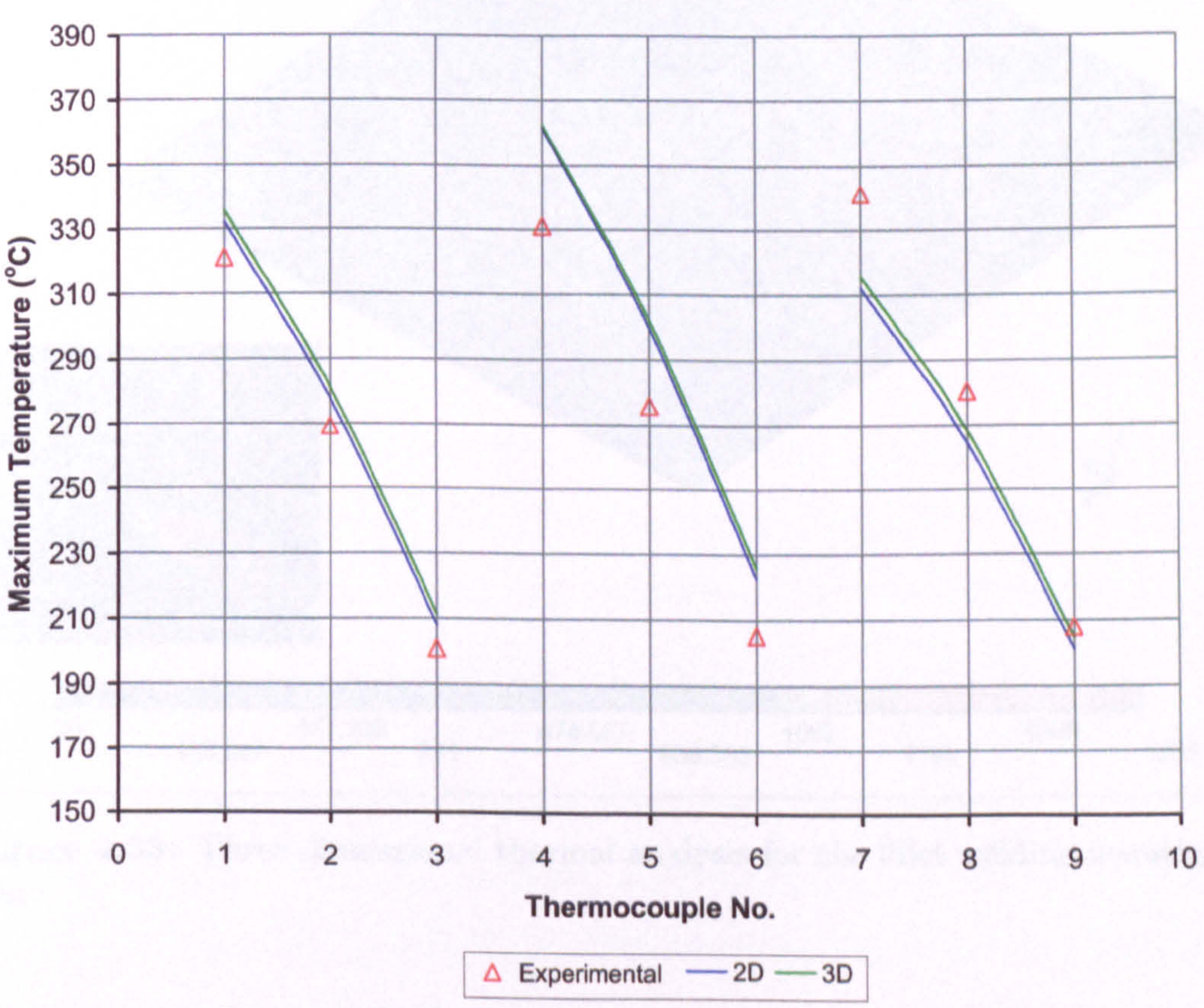

Figure 4.31: Comparison of temperature maxima for weld run 2 of the fillet welding investigation

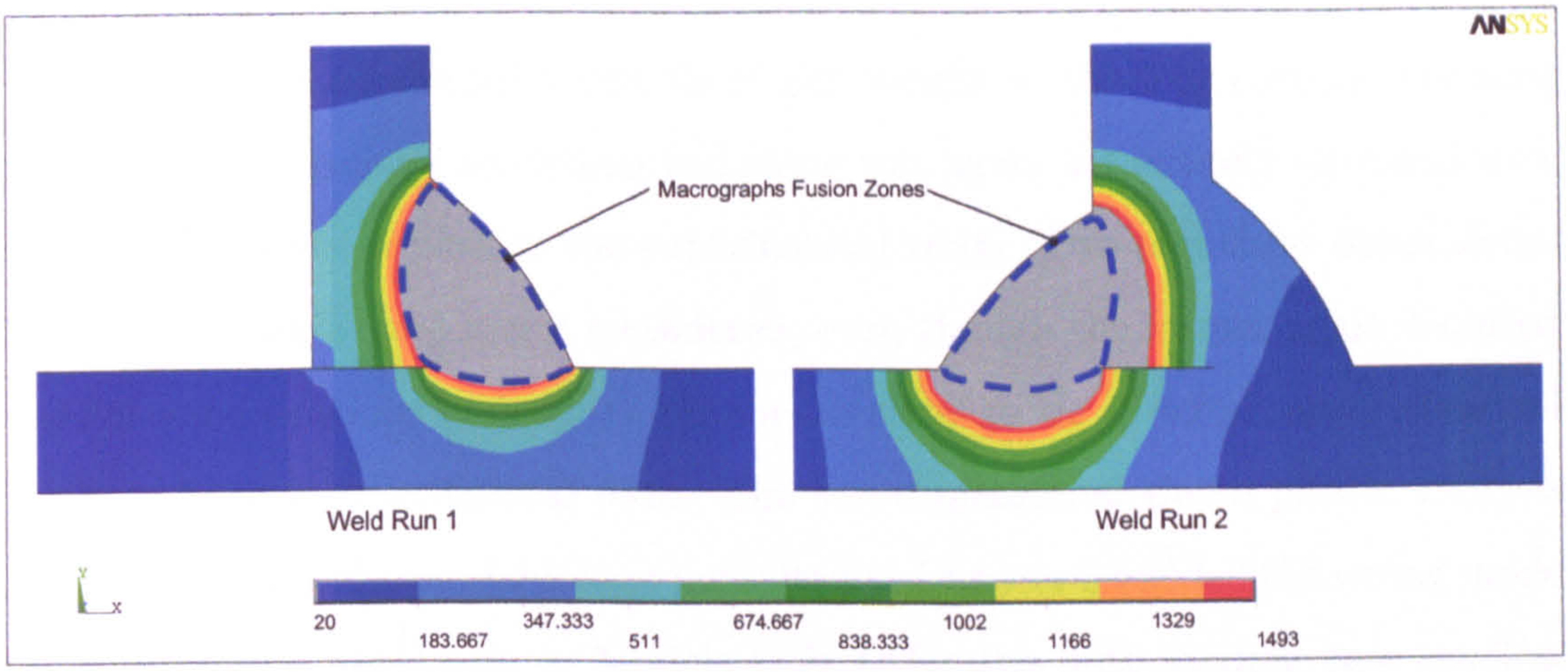

Figure 4.32: Fusion zone prediction for the fillet welding investigation

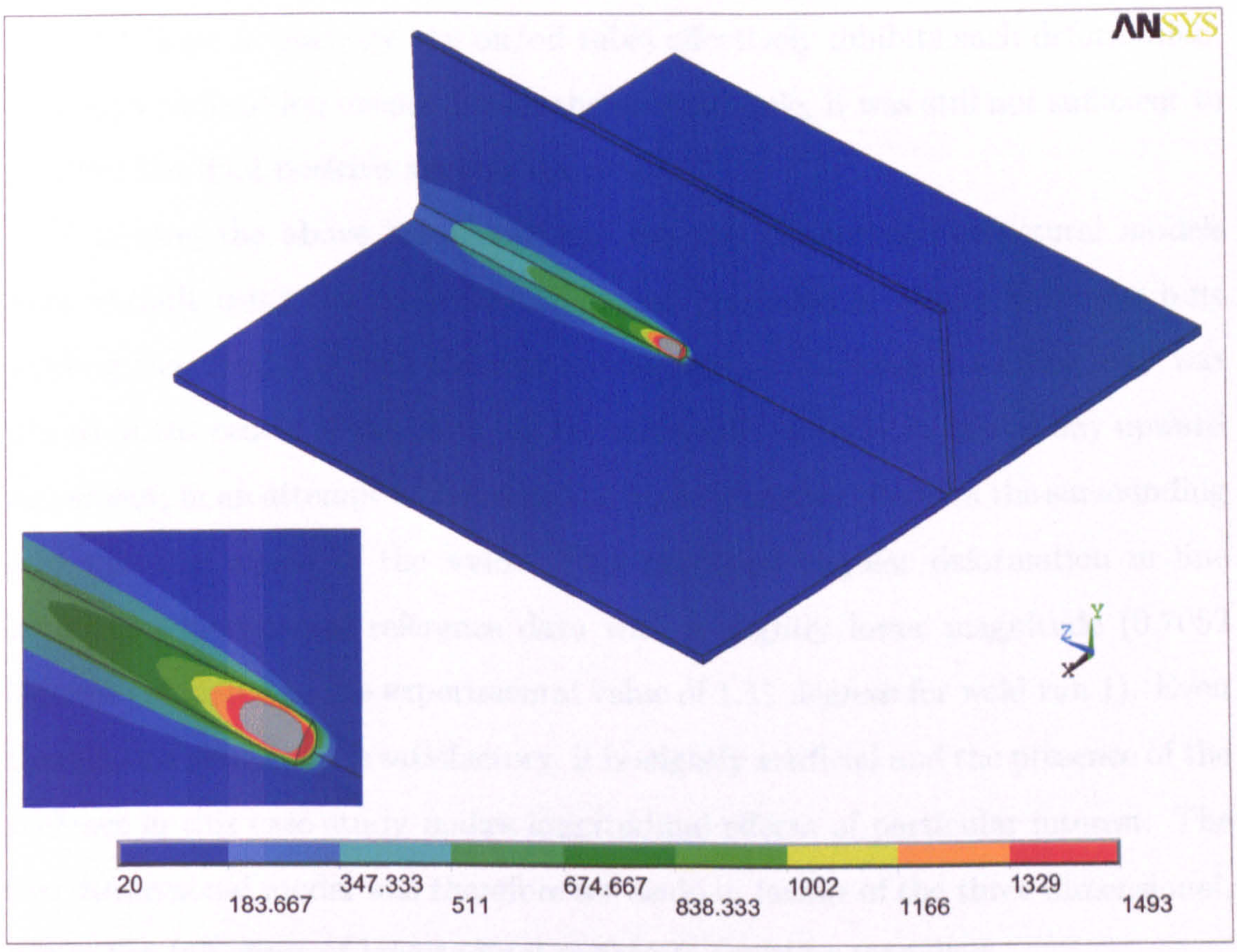

Figure 4.33: Three dimensional thermal analysis for the fillet welding investigation

4.3.2 Structural Analysis

The plates were supported under their own weight at the four corners, meaning that a two dimensional modelling technique was again not entirely representative of the constraints present in the experimental trials. Two and three dimensional structural models were hence considered, even though the former again required special considerations in order to obtain the same mode of deformation observed in the reference experimental data. The two dimensional elasto plastic analysis carried out using the methodology presented in Chapter 3 yielded the wrong mode of deformation, analogous to Models C & D for the butt welding case studies. Expansion in the heating part of the cycle was not restrained in any way in the two dimensional numerical model so that the plate was free to move upwards, contrary to what happens in the experimental trials, where the surrounding cold material (kept in place by run on/off tabs) effectively inhibits such deformation. Although contraction occurs during the cooling cycle, it was still not sufficient to produce the final positive angular distortion.

Following the above considerations, the two dimensional structural models were re-built using the modelling technique presented in Model E for the butt welding case study. A link element having stiffness in tension loading only was placed at the centre of the plate, on the underside, in order to inhibit any upward movement, in an attempt to simulate the undeterminate effects of the surrounding cold material ahead of the weld. This produced angular deformation in line with the experimental reference data with a slightly lower magnitude (0.7052 degrees compared to the experimental value of 1.11 degrees for weld run 1). Even though this prediction is satisfactory, it is slightly artificial and the presence of the stiffener in this case study makes longitudinal effects of particular interest. The two dimensional model was therefore set aside in favour of the three dimensional, where the full effect of longitudinal restraints could be modelled.

As for the two dimensional analyses, material properties were kept the same as for the butt welding investigation. Differences in shape for the fusion zones

of the two weld runs were included, meaning that the numerical models could not take advantage of symmetry. Material deactivation was based on the same algorithms, hence making it equivalent to Model H for the butt welding case study. The models were more computationally intensive as the whole structure had to be included due to the non-symmetric nature of the case study, together with the requirement to include all the transient steps required for heating and cooling of each weld run.

Transient distortion and longitudinal stress results are shown in Figures 4.34 to 4.37. A similar pattern to the butt welding investigation was observed in the initial phases, as angular deformation is formed upon passage of the high heat source. The initial localised stresses are also similar to the butt welding case where the cold surrounding material acts as the primary restraint to form the stresses. As the heat source is passed along the plate, the angular deformation continues, predominantly at the heat source current position. The main difference from the butt welding case is found in the final stages when the longitudinal deformation starts to form. The mechanisms driving the longitudinal distortion are the same, but the structural presence of the stiffener inhibits most of the effect on curvature so that a very small longitudinal curvature is formed in the final residual state. The above transient response matched that observed in the experimental reference data, for both initial and final stages. A match was also obtained for the prediction of the non-symmetric out of plane deformation: the end where the largest negative distortion is observed was the one coinciding with the final (second) weld run, as observed in the experiments.

Figures 4.38 and 4.39 show plots for the residual longitudinal and transverse stress halfway along the plate, through mid-thickness. The main profile for the longitudinal stress is similar to the butt welding case study, characterised by a large central tensile residual stress which quickly turns negative moving away from the weld line. Residual states for both weld runs are plotted. An interesting feature is the asymmetric nature of the residual stress profile due to the first weld

run only. This can be explained in terms of the temperature profile, which is also affected by the thermal barrier at the stiffener/plate junction, and causes the un-symmetric stress pattern. The final residual stress profile shows how the same thing happens in the second weld run, yielding a fairly symmetric final residual stress profile. The transverse residual stress profile shows stress values well below those of the longitudinal counterpart. Again, a bias towards the side corresponding to the first run can be seen in the plot, which is counteracted by the second weld run to form a symmetric residual stress pattern. Plots for the longitudinal residual stresses over the entire plate are shown in Figures 4.40 and 4.41 for the longitudinal and transverse components respectively.

A more quantitative comparison is shown in Table 4.2 where RMS deformation predictions for the best numerical model (i.e. the three dimensional one) are compared with reference experimental data and the simplified algorithm presented in [4.1]. A good match was obtained for out of plane and angular deformation, whilst longitudinal curvatures were very small, due to the presence of the stiffener, and are not tabulated.

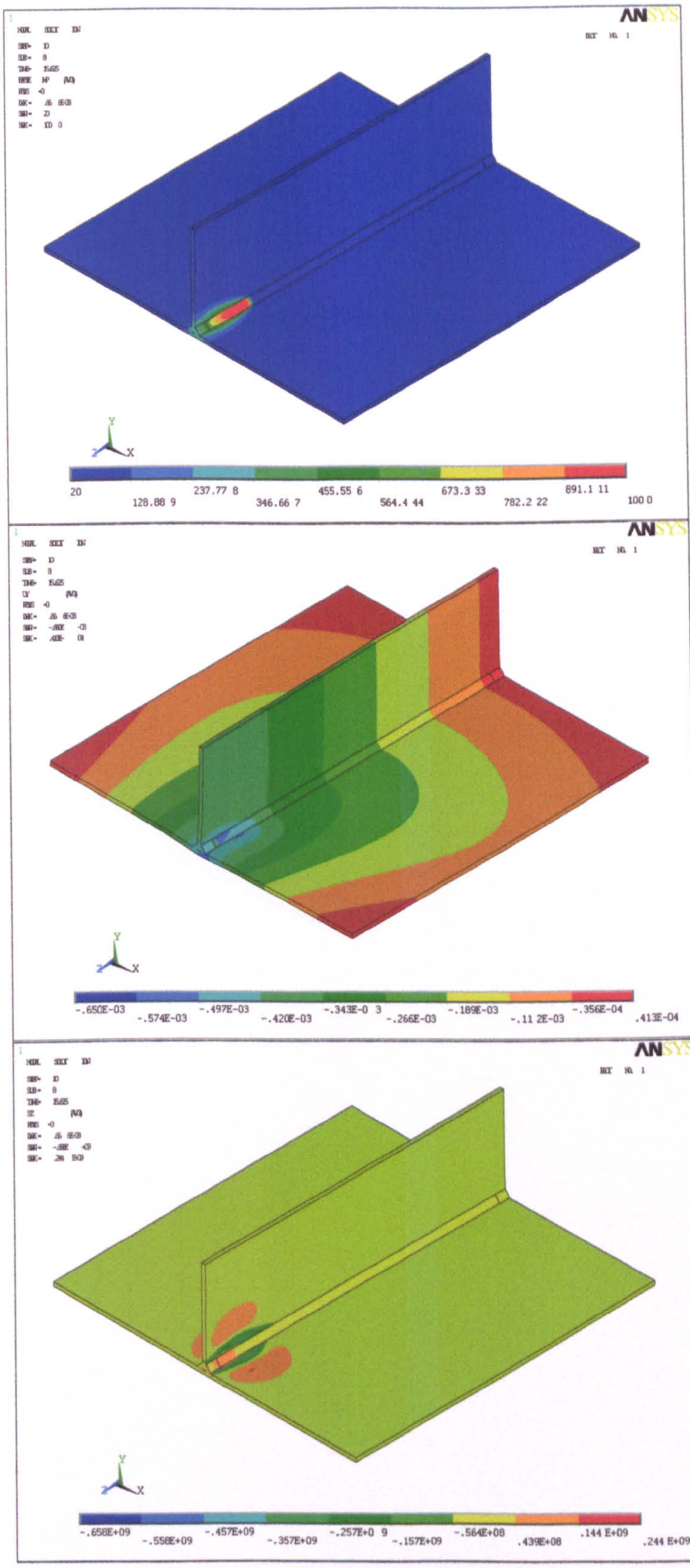

Figure 4.34: Transient response for the fillet welding case: initial heating. Top: temperature distribution. Middle: out of plane deformation (graphical representation amplified by a factor of 10). Bottom: longitudinal stress

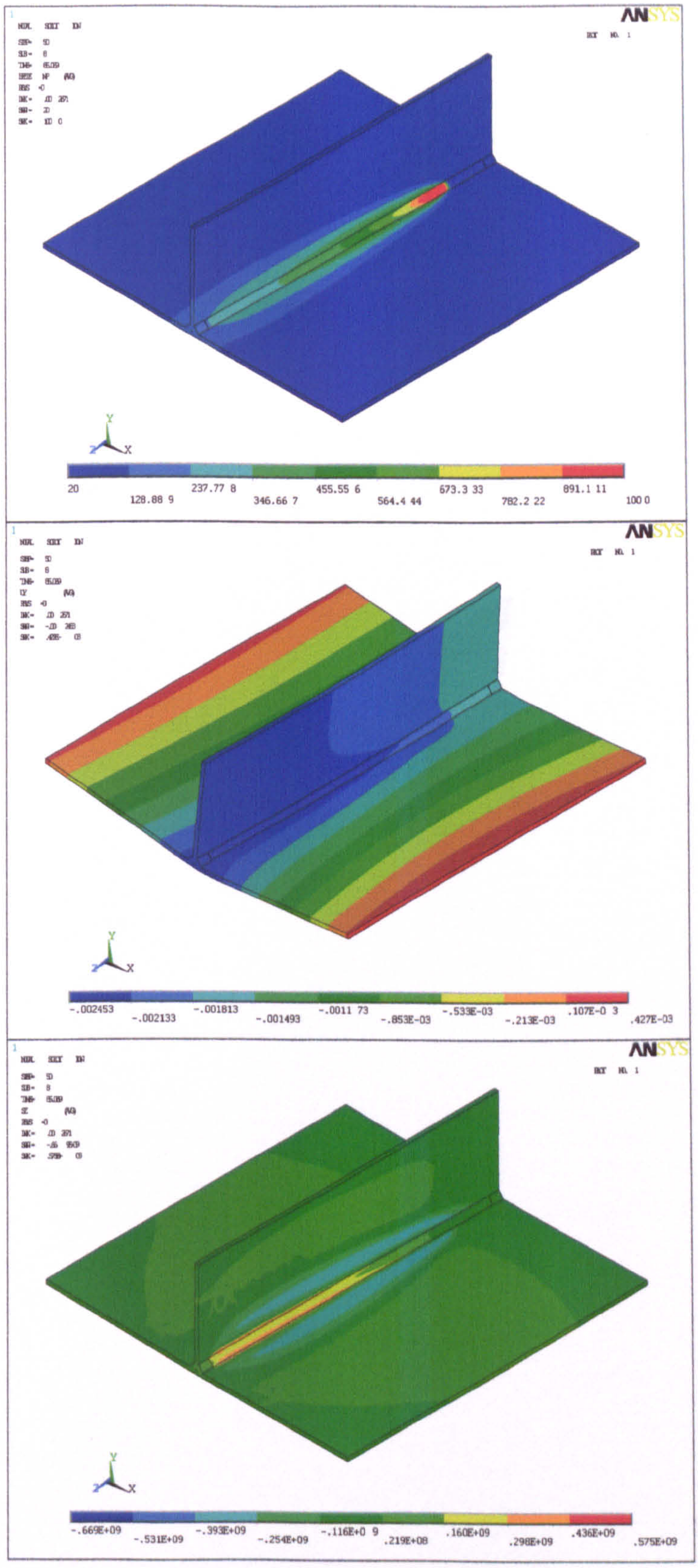

Figure 4.35: Transient response for the fillet welding case: subsequent heating. Top: temperature distribution. Middle: out of plane deformation (graphical representation amplified by a factor of 10). Bottom: longitudinal stress

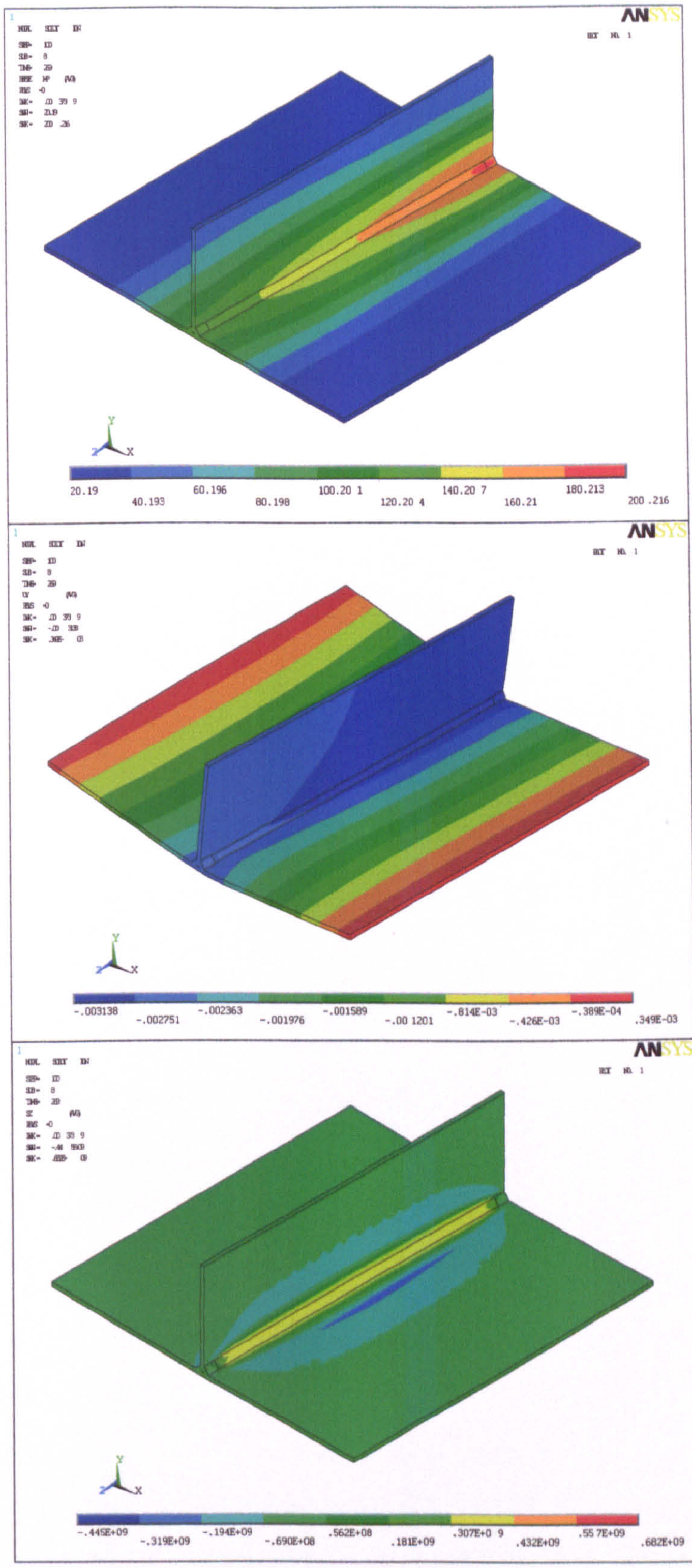

Figure 4.36: Transient response for the fillet welding case: cooling. Top: temperature distribution. Middle: out of plane deformation (graphical representation amplified by a factor of 10). Bottom: longitudinal stress

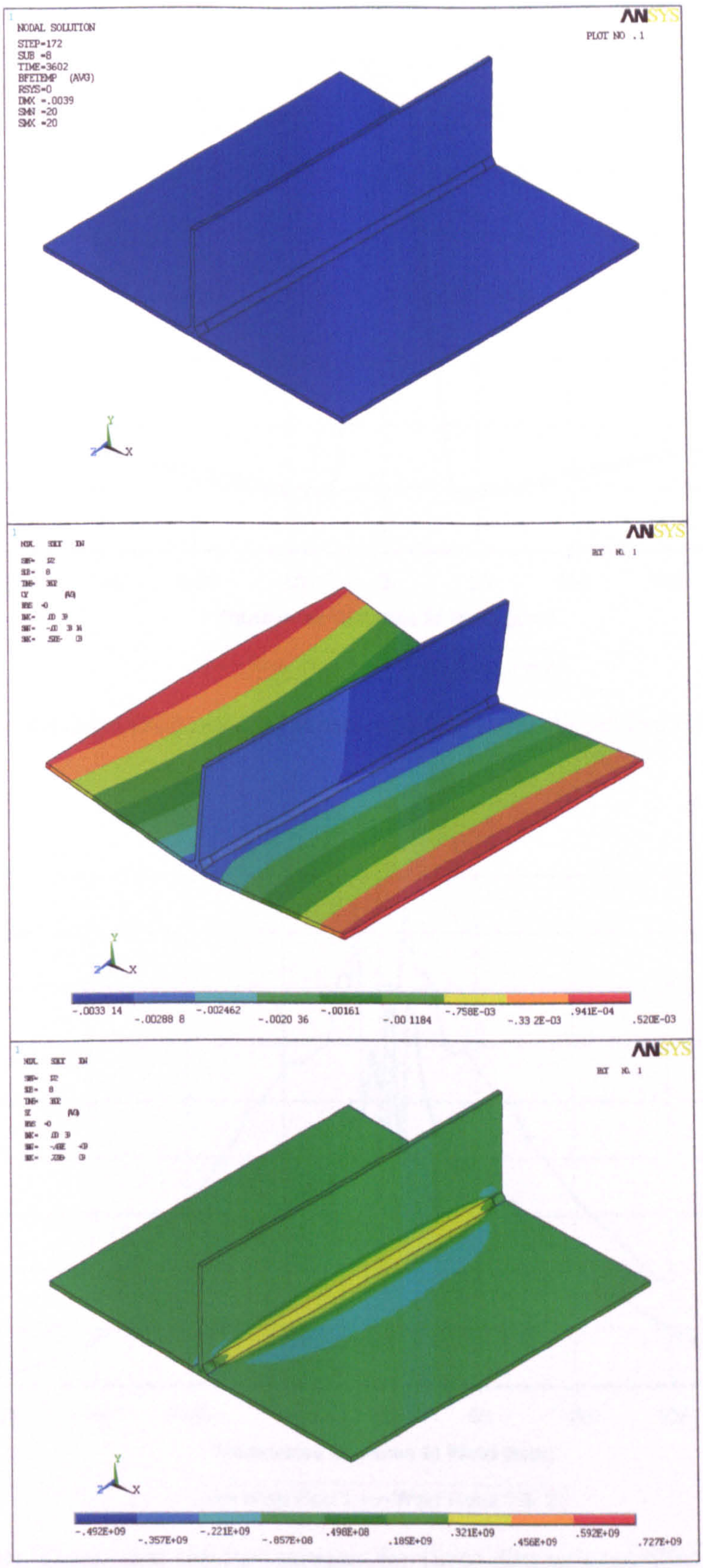

Figure 4.37: Transient response for the fillet welding case: final cooling. Top: temperature distribution. Middle: out of plane deformation (graphical representation amplified by a factor of 10) Bottom: longitudinal stress

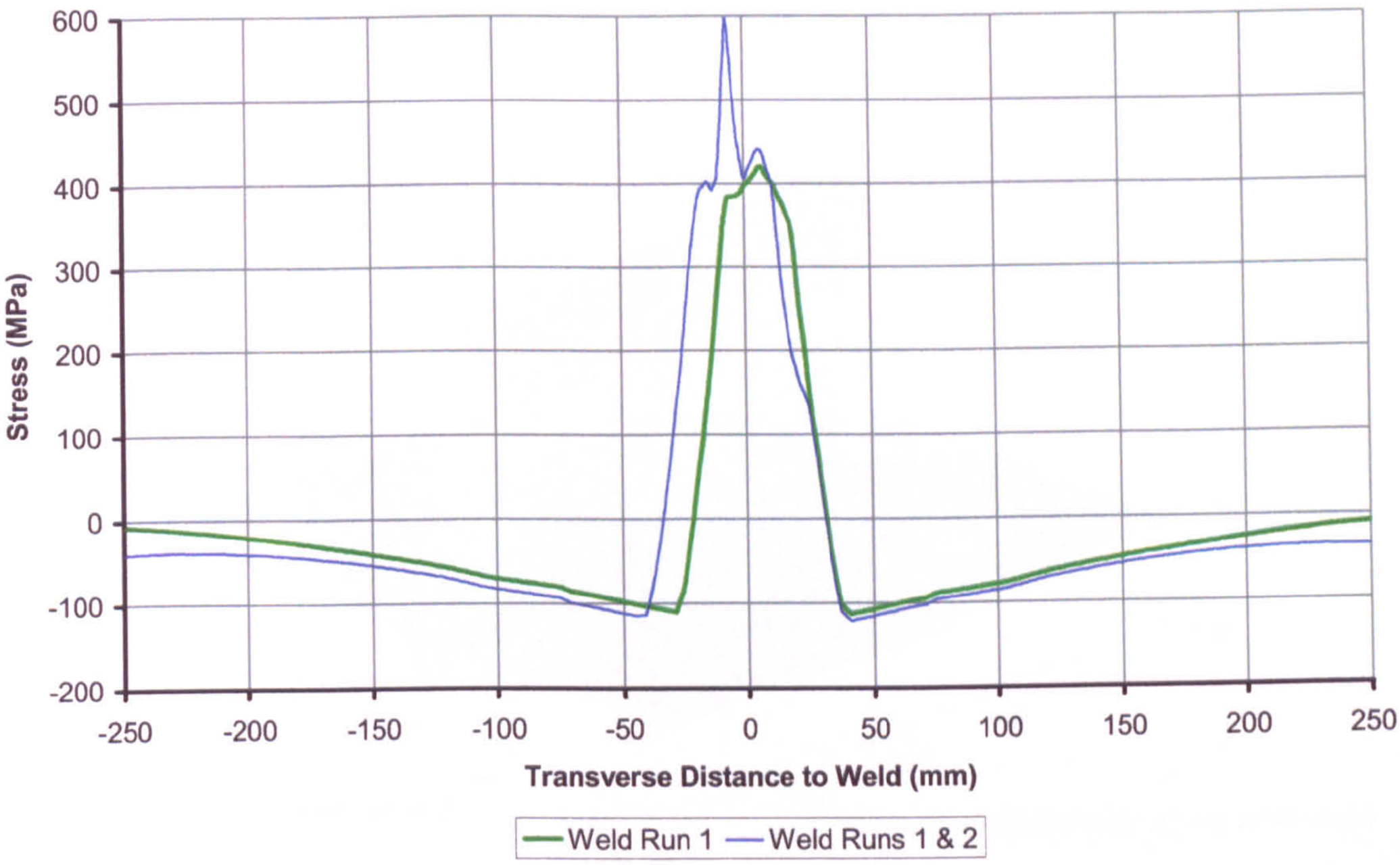

Figure 4.38: Longitudinal residual stresses for the three dimensional fillet welding simulations

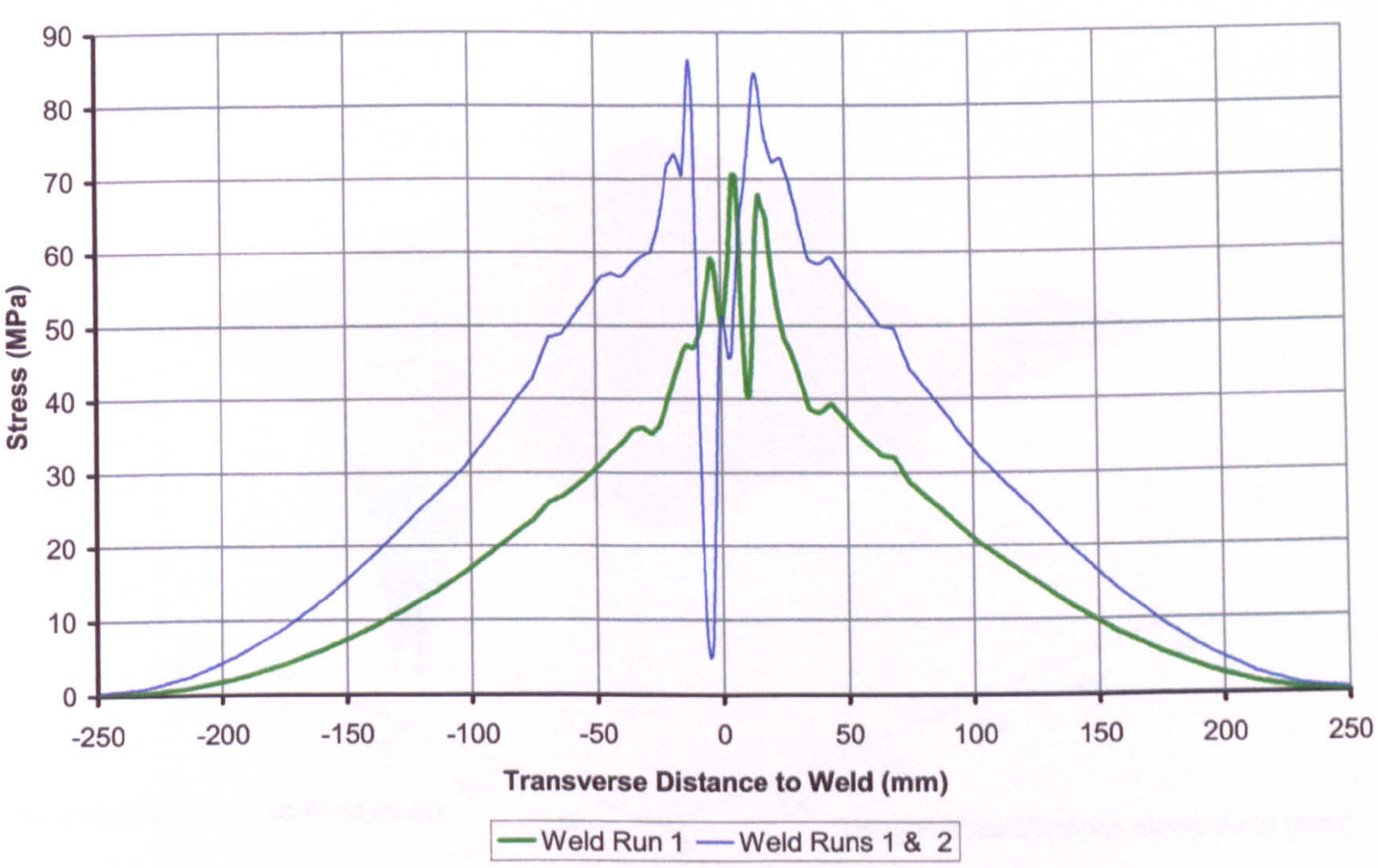

Figure 4.39: Transverse residual stresses for three dimensional fillet welding simulations

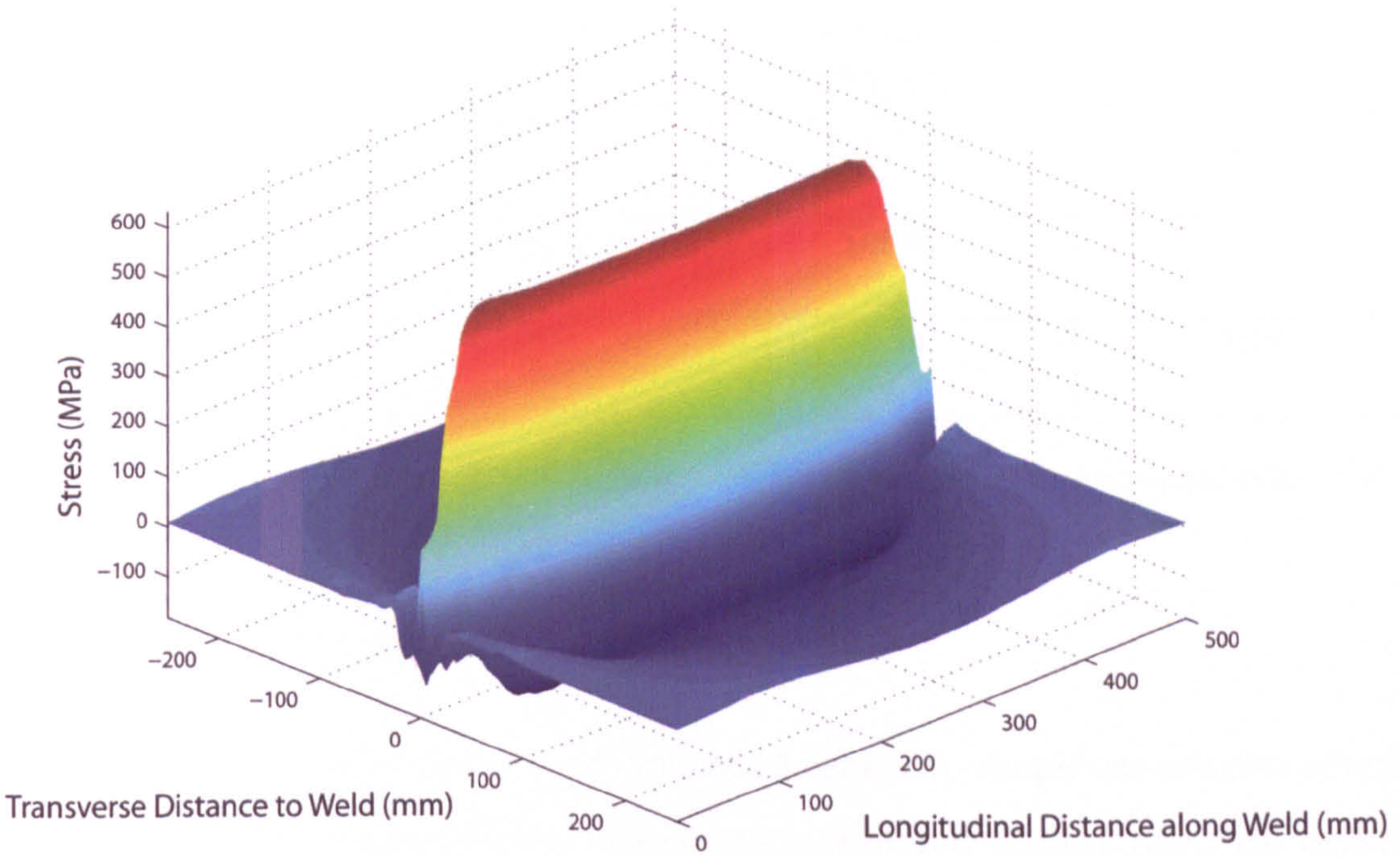

Figure 4.40: Longitudinal residual stress over the entire plate for the fillet welding investigation

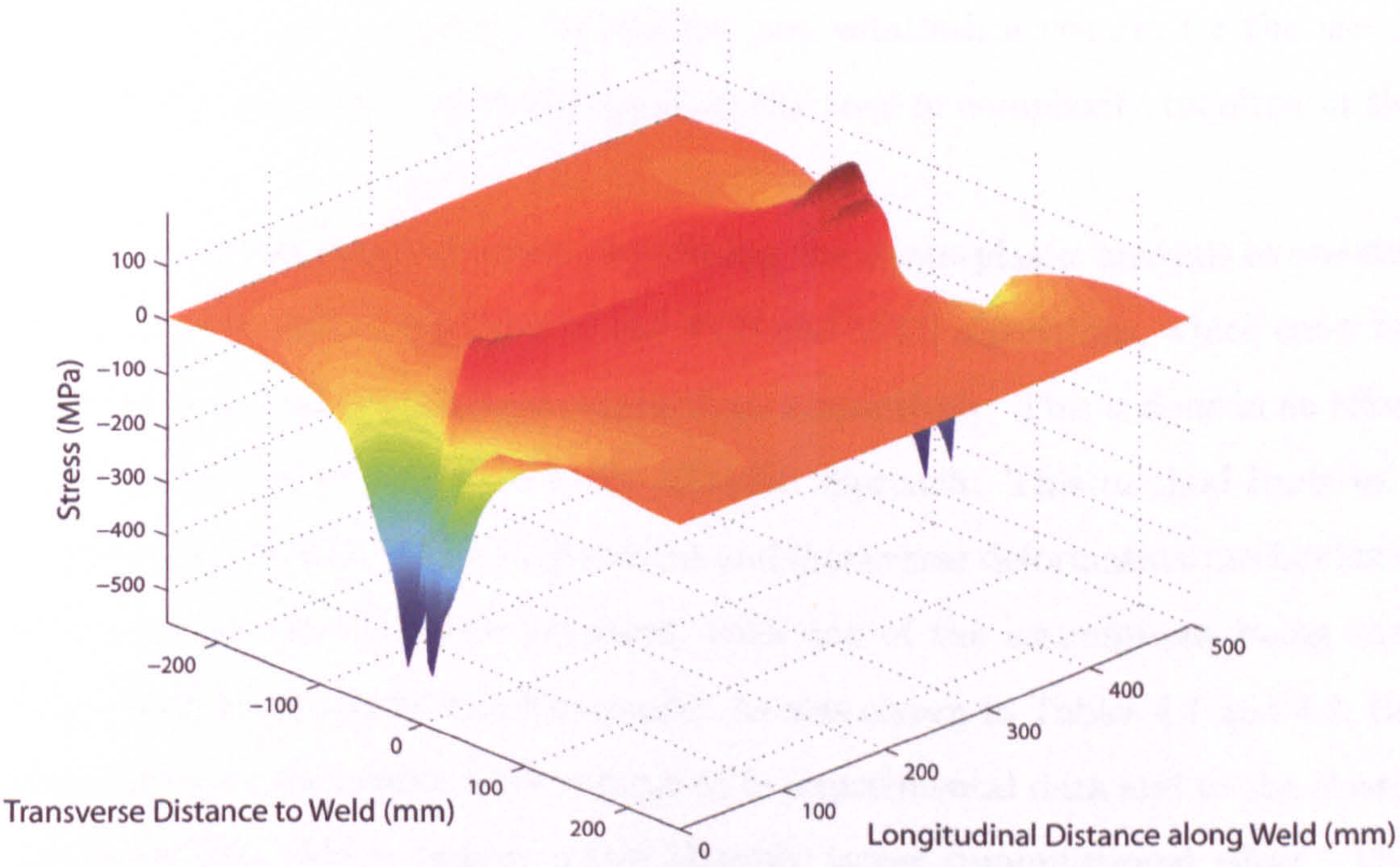

Figure 4.41: Transverse residual stress over the entire plate for the fillet welding investigation

Data Source	RMS Out of Plane Deformation (mm)	RMS Angular Deformation (degrees)	Computational Ratio
Experimental Data	2.74	1.11	n/a
Simplified Algorithm	2.25	0.886	1
Thermo-Elasto-Plastic Models	2.85	1.24	1080

Table 4.2: Comparison of deformation RMS values and computational effort for the fillet welding investigation

4.4 Conclusions

Thermo-elasto-plastic models were developed using two simple case studies of butt welded and fillet welded plates. These were validated against reference experimental distortion data and compared to a more simplified approach developed by Camilleri [4.1], illustrated in Chapter 2. The latter involved a comparison with results obtained using the TCS and MTS algorithms, in an attempt to further validate these simplified techniques, and establish a criteria for the use of the different numerical methods based on the level of complexity required in the results.

The simplified method aimed at reducing the elasto-plastic analysis to one single elastic load step comprising of the TCS and MTS algorithms, which cater for the transverse and longitudinal contractions respectively. This is done in an effort to create the most computationally efficient approach. This method leads to a complete decoupling of the longitudinal and transverse deformation mechanisms. The transient aspect is also removed, with one of the assumptions being that these mechanisms occur simultaneously. As was shown in Tables 4.1 and 4.2, the algorithms are successful, both compared to experimental data and to the elasto-plastic models, which require a considerably larger computational effort. This demonstrates the validity of the assumptions and simplifications adopted in the approach. This is particularly true for mechanisms driving longitudinal effects

(MTS algorithm). The simplified approach as regards to the transverse contraction (TCS algorithm) is however more basic and hence requires more considerations in order to achieve satisfactory results. The thermo-elasto-plastic modelling technique is hence more suited to achieve correct angular distortion predictions, which are usually of significant interest in most fabrication procedures.

In general, good comparisons were obtained for all thermo-elasto-plastic models, compared to both experimental and simplified method data, together with a clear indication of the best modelling approaches to be adopted for distortion prediction. Whilst the simplified approach provides a fast and attractive way of predicting welding induced distortions, the thermo-elasto-plastic models must be used when the following analysis features are required:

- Temperature dependant material properties
- Effects of phase changes
- Plastic response of the material
- Transient aspect
- Constraint on angular contraction, either from clamps or 3D action

All these simulation features considerably extent the computational requirements of the thermo-elastic-plastic models. Some aspects of the results can however only be obtain through the full elasto-plastic models, namely: the induced stresses and the transient deformations, including any instability or buckling that might occur during the welding process.

References

[4.1] D. Camilleri. *Support Tools for the Prediction of Distortion in the Design and Manufacture of Thin Plate Welded Structures.* PhD thesis, University of Strathclyde, Glasgow, 2004.

[4.2] L. E. Lindgren. Finite element modeling and simulation of welding part 2: Improved material modeling. *Journal of Thermal Stresses*, 24:3195–231, 2001.

[4.3] Ansys Inc. *Ansys Documentation*, release 10.0 edition.

Chapter 5

Experimental Measurement Techniques

5.1 Introduction

The previous chapter has described development and application of the simulation methodology on simple cases of butt and fillet welding. The results were compared with experimental data relating to temperature and distortions. Whilst these are of great importance for the validation of the numerical models, it is also of interest to compare the model predictions against measurements of residual stress. This further validation is of particular value as the transient elasto-plastic finite element models provide a picture of the induced stresses for both the transient and residual states.

A number of techniques exist for the measurement of residual stress in structures and their application extends beyond welding induced stresses. It is generally of interest to understand both qualitatively and quantitatively the nature of stresses induced by manufacturing processes, both for cases where they are beneficial or where they are detrimental.

The hole drilling method was adopted in the current investigation for simple cases of butt and fillet welding in order to compare with results obtained from the thermo-elasto-plastic models. This served as a validation for the finite element analyses, especially with regards to the adequacy of the complexity level adopted

in the material model.

The final set of experimental measurements presented here deals with the evaluation of the coefficient of thermal expansion of the material and the uniaxial stress-strain response. These are not measurements taken for validation purposes, but represent a crucial set of input parameters for the correct application of the numerical models.

5.2 Residual Stress Measurement Technique

5.2.1 Introduction

Residual stresses are stresses that exist in a structure which is not subject to external forces. They are hence self equilibrating and are usually induced in the structure by some kind of manufacturing process. Classification of residual stresses is closely related to the distance, or characteristic length, over which the stresses equilibrate, and hence to the spatial resolution being investigated. These are classified in the following three categories [5.1]:

- Type I stresses σ_I: the characteristic length is comparable to the structure's dimensions
- Type II stresses σ_{II}: the characteristic length is comparable to the grain size
- Type III stresses σ_{III}: the characteristic length is less than the grain's dimension

These are shown schematically in Figure 5.1 where a hypothetical variation of stress is plotted against distance at a microscopic scale such that variations within grains and from grain to grain are noticeable. It is clear how Type II and III stresses are closely linked to the material microstructure and include effects such as differences in properties for different grain orientations, effects of dislocations etc. Even though Type II and III stresses balance out over regions in

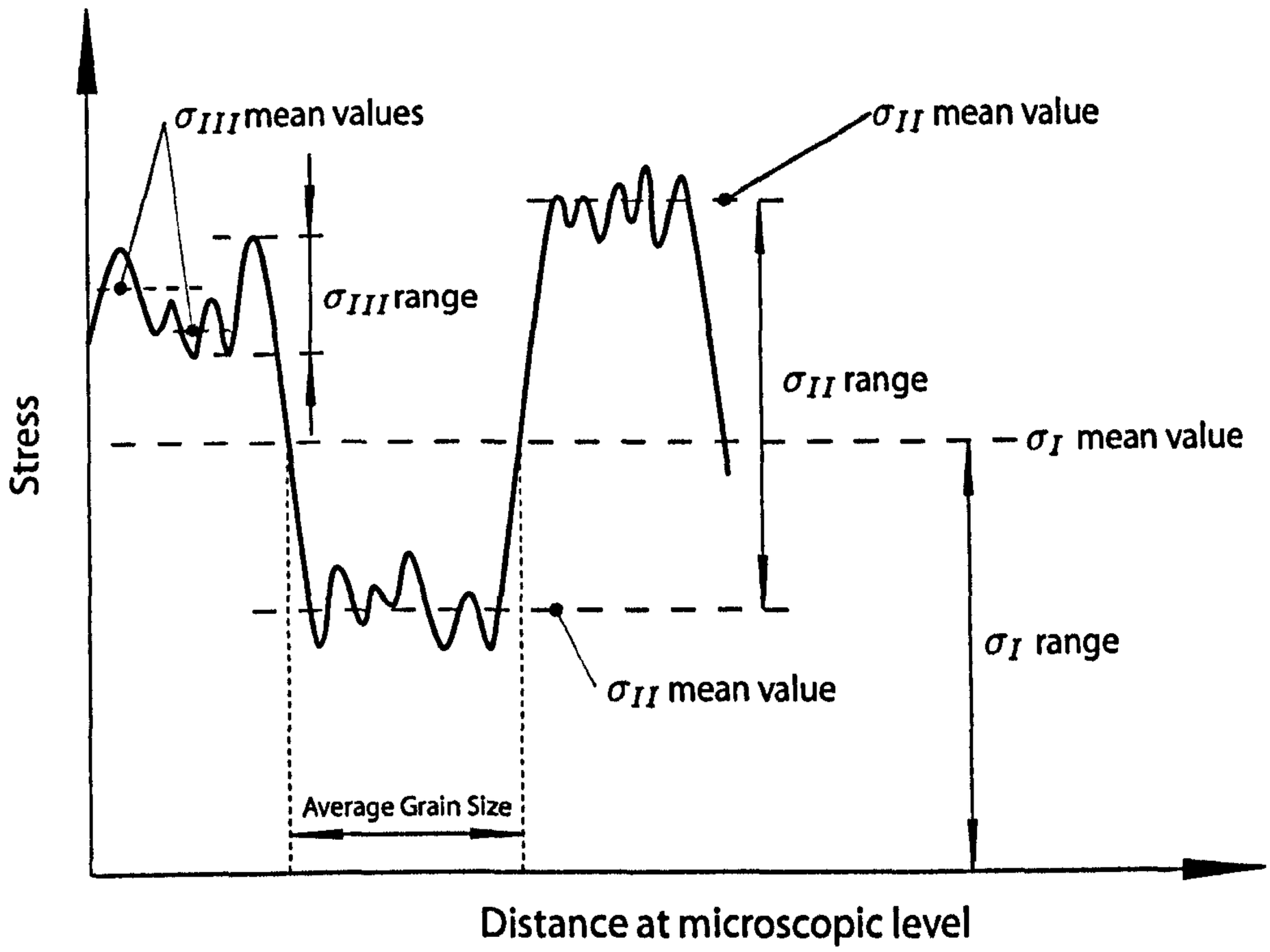

Figure 5.1: Classification of residual stresses based on characteristic length

the order of magnitude equal to the grain size, they might still carry cumulative effects in regions of larger size up to the phase boundary. This can be seen by considering the Type II stress in the longitudinal direction $\sigma_{z,II}$ split up for phase related components $\langle\sigma_{1,II}\rangle$ and $\langle\sigma_{2,II}\rangle$. Integrated over the sampling area A the following relation holds (adapted from Withers et al [5.2]):

$$\begin{aligned} 0 &= \int_{A_z} \sigma_{z,II} dA \\ &= \int_{A_1} \sigma_{z,II} dA_z + \int_{A_2} \sigma_{z,II} dA_z \\ &= f_A \langle\sigma_{1,II}\rangle + (1 - f_A) \langle\sigma_{2,II}\rangle \end{aligned} \tag{5.1}$$

Where f_A, $(1 - f_A)$ are the area fractions $\frac{A_1}{A}$ and $\frac{A_2}{A}$ over which the different stresses act. It can be seen how, even though Type II stresses must balance over the small grain size characteristic length, their effects carry a cumulative value

within the sampling area, which essentially is a background residual stress due to that particular phase. It is hence important to understand whether the residual stress measurement sampling area is large enough so that Type II and III still average to zero. Material removal techniques (such as the hole-drilling method) remove macroscopically sized regions so that the reading would reflect Type I stresses only. This is convenient in the current project as Type I stresses are of most interest. These are the stresses that induce the contraction forces and trigger the welding induced deformations.

There are several residual stress measurement techniques, ranging from non destructive techniques such as neutron diffraction and magnetic methods, to other destructive (or partially destructive) techniques such as hole-drilling and sectioning methods. The choice of measurement technique depends on a number of factors, the most noteworthy are:

- Feasibility to carry out destructive or non-destructive measurements
- Sample size and shape
- Resolution required for the measured residual stress

For the current investigation, the hole-drilling method proved to be an adequate choice, as destructive tests could be carried out on the welded samples. Furthermore, the size and shape of the test pieces did not pose any problems for the use of residual stress measurement apparatus and the spatial resolution offered by this method was deemed to be adequate.

5.2.2 Apparatus & Procedure

The hole-drilling method consists of removing material by means of a stress free process such as an abrasive stream of air and powder. It is important to use such a stress free process as other more conventional cutting processes can induce further residual stresses that would invalidate the readings. The combination of

material removal and residual stresses originally present in the structure causes relaxation around the drilled hole. Measurements taken by means of strain gauges are then used to calculate the residual stress originally present. As will be shown in the following sections, the position at which the relaxing strains are measured is critical for the correct determination of the residual stresses. For this reason specialised strain gauges (Vishay 062UL) were used, which have the three necessary strain gauges laid out on a single sheet together with markings for the hole's position. These are shown in Figure 5.2. Each strain gauge was wired in a quarter-bridge fashion as they each carried independent strain values, with a three wire arrangement to compensate for wire-length effects. A standard strain gauge rosette for residual stress measurements (model CEA-06-062UL-120 from Vishay) and a balancing / measurement device was used in order to measure the three strain values for each drilled depth.

The apparatus used is shown schematically in Figure 5.3 and consists of:

- A fixture to keep the rotating cutting head firmly in place
- A rotating cutting head through which air and abrasive powder are mixed to create a cutting stream
- Optical measurement equipment (not shown in the diagram) used for alignment and measurement of the drilled hole and placed in the position to be occupied by the rotating cutting head
- Air compressor and powder mixer (not shown in the diagram)

As will be shown in the following sections, the hole diameter is of great importance in the calculation of the residual stresses from the strain gauge data. Whilst the aim is not to achieve a specific value, it is important that the resulting hole dimensions fall within certain limits (which are still very small) since correct relaxation of the stresses will only be achieved within these limits. This is

also due to the fact that calculation of the residual stresses is based on calibration data obtained from the literature and this naturally only lies within certain boundaries.

The stream of abrasive powder and air is of a smaller diameter than the required final hole diameter. The drilled hole is hence obtained by the rotation of the cutting head. This leaves excess material at the hole centre, which however does not impinge on the surrounding material relaxation and hence on the results (see Figure 5.4). The hole diameter can hence be controlled by two main parameters:

- The offset of the rotating head from the hole axis
- The width of the air powder jet at the plate surface

The first can be mechanically set on the drill head and was kept constant throughout the experiments. The width of the air powder jet is on the other hand readily changed by adjusting the height between the nozzle and the plate surface. The apparatus manual suggests a height of 1.5mm but it was found that setting the height to this value did not yield satisfactory results. A calibration procedure had to be employed by varying the height of the nozzle until a hole diameter was obtained within the required limits. The variation of height with hole diameter was highly non linear due to large variation in the flow diameter as it exits the nozzle.

Accuracy of the positioning and measurement of the hole is critical to achieve correct results. For this reason optical equipment was used for alignment and measurement. The equipment is tailor-made to fit in the fixture so that, once aligned, the cutting head will occupy the same position. The optical device had cross-hairs embedded in the viewfinder for alignment purposes, the view being magnified by a factor of 3.44. Measurements in the plate surface plane were accomplished by a moving cross-hair positioned by means of a micrometer-screw-gauge thimble and ratchet knob fitted in the optical device. A vernier scale

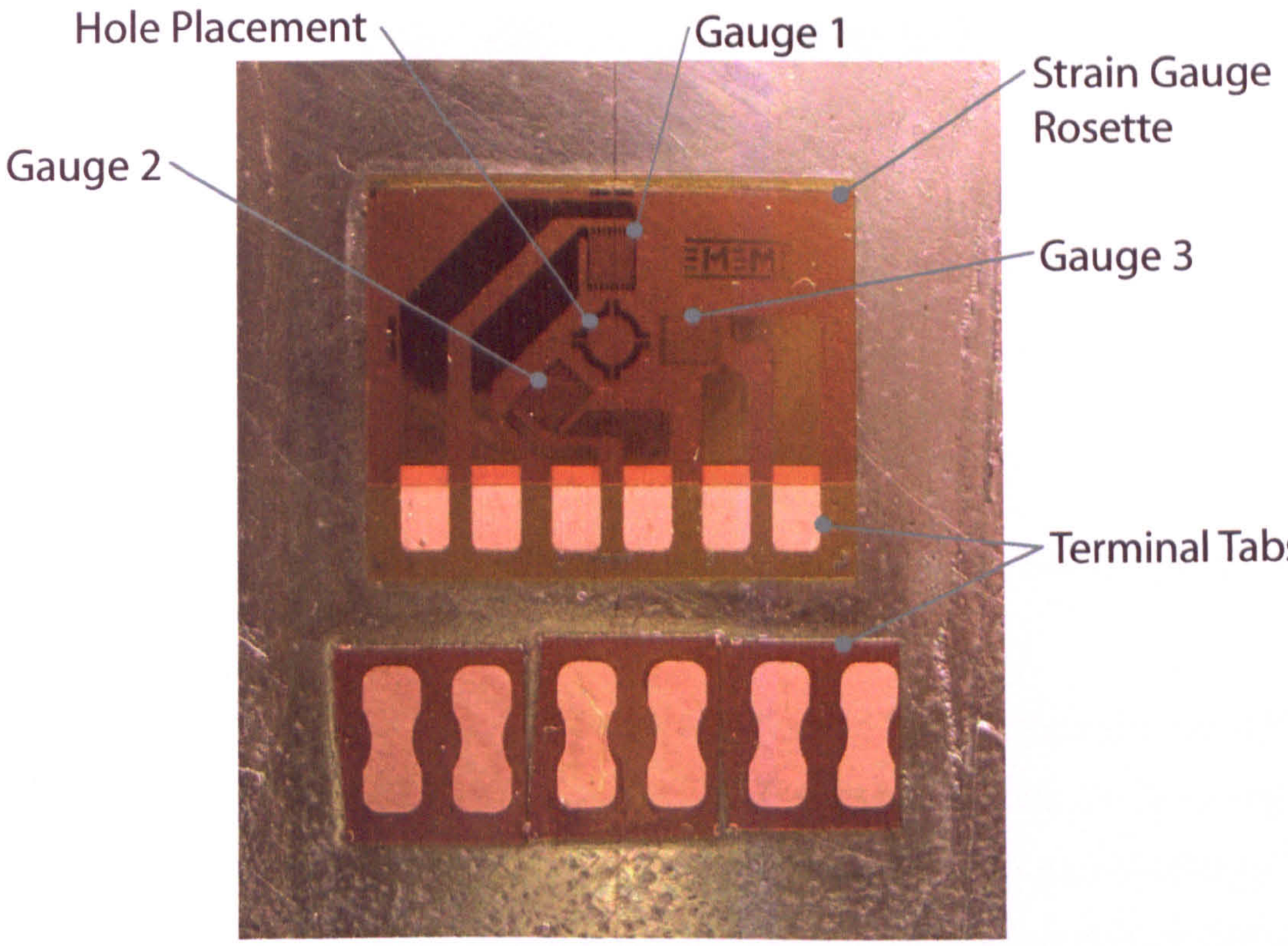

Figure 5.2: Strain gauge set-up for the hole-drilling measurements

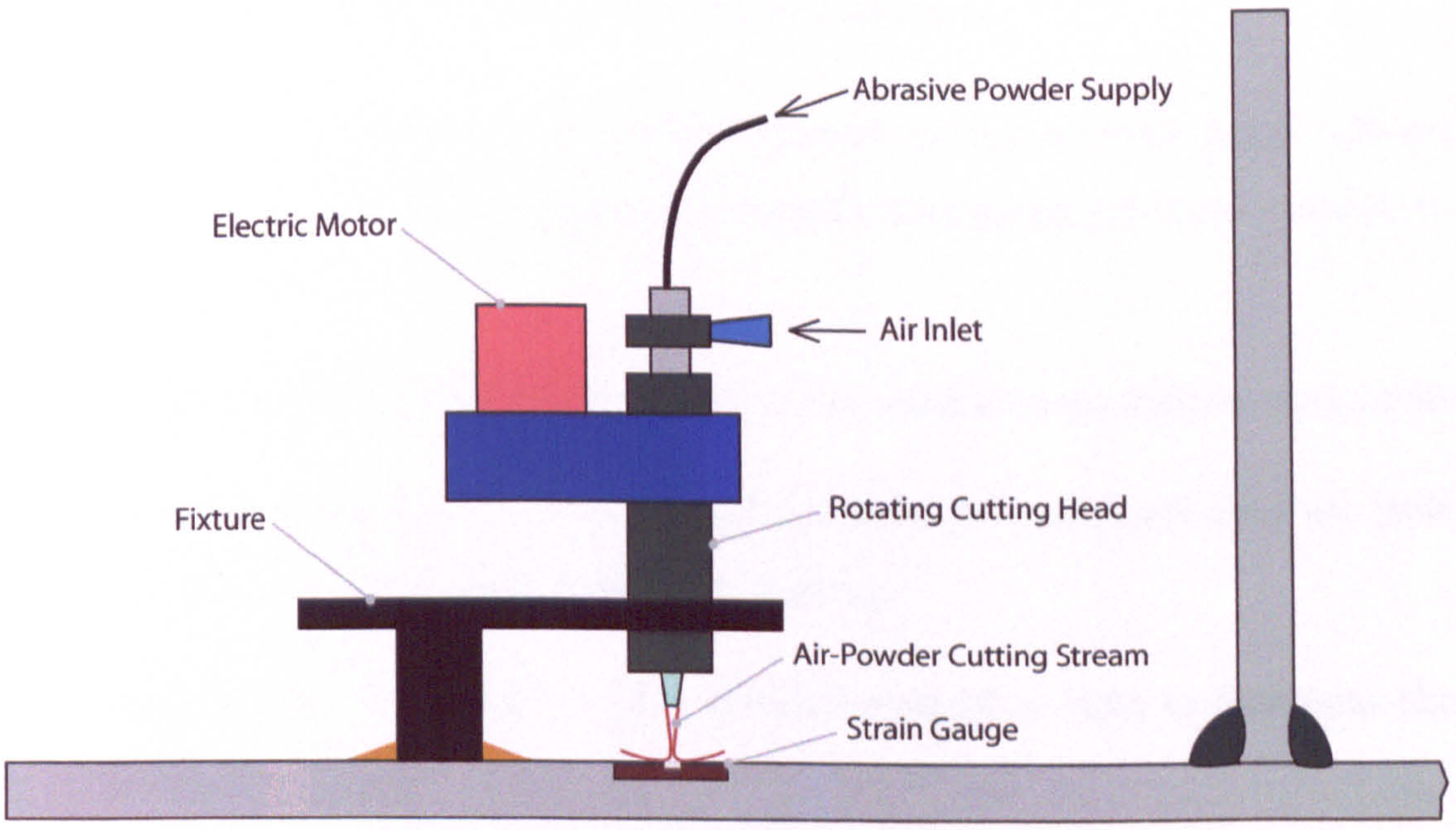

Figure 5.3: Hole drilling experimental set-up

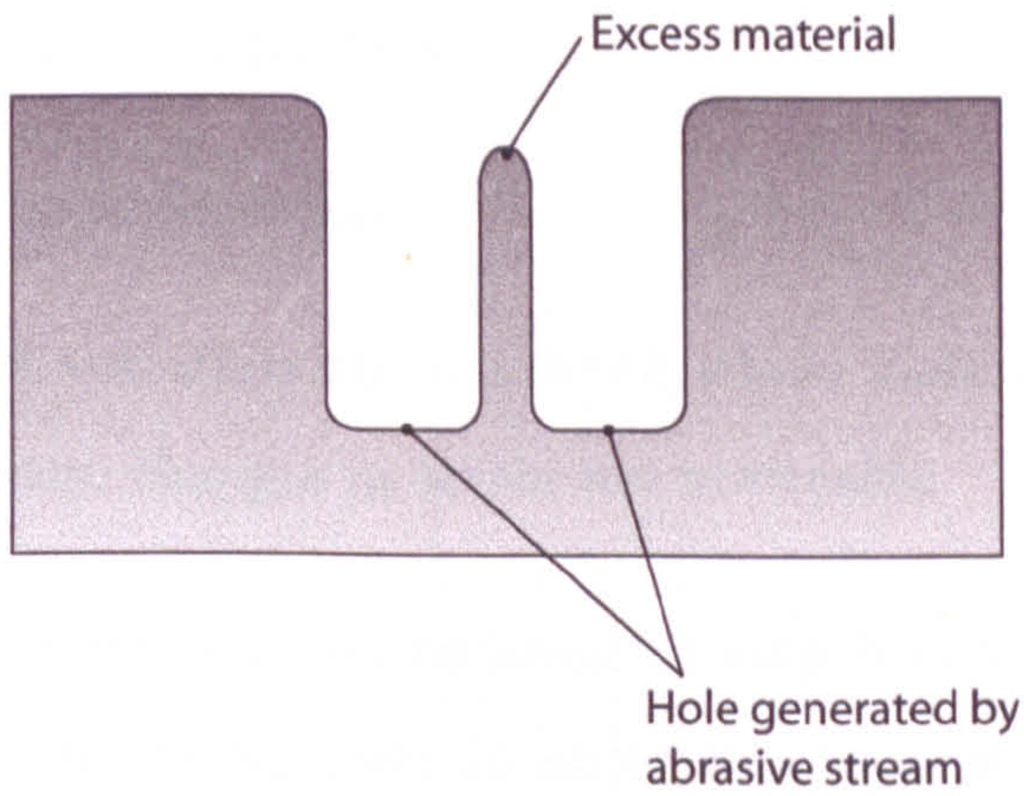

Figure 5.4: Schematic representation of a typical section obtained with the rotating cutting head

allowed measurements with a resolution of 0.01mm. Measurements in the normal direction from the surface (i.e. for the hole depth) were taken by focussing the image of the plate on the optical device. The thimble for focus adjustment also had a vernier scale so that, starting off with a zero reading focussed on the plate surface before drilling, the depth could be read off the scale by re-focussing on the newly formed surface at the bottom of the hole.

The following experimental procedure was adopted:

1. Prepare the surface at the points of interest and apply strain gauge rosettes (complete with wiring for simultaneously measuring the three strains in each rosette)

2. Align the head onto plate by means of the optical measurement equipment

3. Take the height reading with the optical device focussed onto the plate (this would serve as the hole depth zero reading)

4. Measure the strains prior to any material removal in order to determine the initial strain state

5. Replace the optical head with the drilling head

6. Remove a thin layer of material

7. Measure the change in strain

8. Repeat the last two steps up to a depth where material relaxation is complete and no more changes in strain are noticeable

The amount of material to be removed in step 6 is critical. On one hand enough material has to be removed in order to obtain a noticeable change in strain, on the other the depth should not be too much as this will reduce the total number of readings to be taken. This is because the total depth of the hole is limited due to the fact that the material relaxation reaches a plateau.

Preparation of the surface is carried out with the standard procedure for strain gauges with careful consideration as to not induce any stresses in the material, which would obviously affect the final result. For this reason the surfaces were ground and polished by hand until a satisfactory surface finish (close to mirror surface) was achieved.

5.2.3 Calculation Theory

An understanding of the theory underlying the material relaxation around the drilled hole is essential in order to understand how the recorded data is used to calculate residual stresses. Detailed discussion on theory and calculation using different measurement techniques is presented in [5.3]. The following is a discussion relating to the methods used for the current investigation.

In the first instance an idealised case must be considered, for which the stresses around the hole can be described by the measured strains according to the geometrical configuration of the gauges. A through hole is considered for which a standard ASTM type clockwise hole drilling strain gauge rosette is used. The strain around the hole ε can be expressed in terms of the maximum σ_{max} and minimum σ_{min} residual stresses using the following relation:

$$\varepsilon = (\sigma_{max} + \sigma_{min})\,\bar{A} + (\sigma_{max} - \sigma_{min})\,\bar{B}\cos 2\phi \tag{5.2}$$

Where ϕ is the angular position of the strain gauges and $\bar{A}$ and $\bar{B}$ are calibration coefficients. For an idealised measurement at an infinitesimal small point, the coefficients take on the following form:

$$\bar{A} = -\frac{1+\upsilon}{2E}\left(\frac{r_a}{r}\right)^2 \tag{5.3}$$

$$\bar{B} = -\frac{1+\upsilon}{2E}\left[\frac{4}{1+\upsilon}\left(\frac{r_a}{r}\right)^2 - 3\left(\frac{r_a}{r}\right)^4\right] \tag{5.4}$$

Where r is the radial position, r_a the hole radius and E and υ elastic properties of Young's Modulus and Poisson's ratio respectively. The above relation cannot however be used in practice, as the size of the strain gauge must be taken into consideration. Furthermore, the drilled hole could not be made through the entire plate thickness as the stresses would be completely relieved at a lower depth.

For blind holes, no analytical solutions such as the one described above exist. The calibration coefficients $\bar{A}$ and $\bar{B}$ must therefore be obtained by either experimental calibration or literature containing data obtained from finite element calculations. As a first step, Equation (5.2) is inverted to give residual principal stresses σ_{max} and σ_{min} and angle ϕ in terms of measured strains ε_{g1}, ε_{g2} and ε_{g3}:

$$\sigma_{max,min} = \frac{\varepsilon_{g3} - \varepsilon_{g1}}{4\bar{A}} \pm \frac{\sqrt{(\varepsilon_{g3} - \varepsilon_{g1})^2 + (\varepsilon_{g3} + \varepsilon_{g1} - 2\varepsilon_{g2})^2}}{4\bar{B}} \tag{5.5}$$

$$\phi = \frac{1}{2}\arctan\left[\frac{\varepsilon_{g3} + \varepsilon_{g1} - 2\varepsilon_{g2}}{\varepsilon_{g3} - \varepsilon_{g1}}\right] \tag{5.6}$$

The above equation can hence be used to determine the calibration coefficients to be used in the residual stress calculation. It is convenient to group the strain components in the following sets of equations, denoted $\bar{p}$, $\bar{q}$ and $\bar{t}$ for a rosette of the type used in the current investigation:

$$\bar{p} = \frac{(\varepsilon_{g3} + \varepsilon_{g1})}{2} \tag{5.7}$$

$$\bar{q} = \frac{(\varepsilon_{g3} - \varepsilon_{g1})}{2} \tag{5.8}$$

$$\bar{t} = \frac{(\varepsilon_{g3} + \varepsilon_{g1} - 2\varepsilon_{g2})}{2} \tag{5.9}$$

Next an $x - y$ coordinate system of stresses (σ_x, σ_y and τ_{xy}) is established so that the x-direction stress σ_x is parallel to the Gauge 1 axis. In this way the stresses can be re-written in terms of parameters $\bar{P}$, $\bar{Q}$ and $\bar{T}$ which are not related to strain gauge type/geometry:

$$\bar{P} = \frac{(\sigma_y + \sigma_x)}{2} \tag{5.10}$$

$$\bar{Q} = \frac{(\sigma_y - \sigma_x)}{2} \tag{5.11}$$

$$\bar{T} = \frac{\tau_{xy}}{2} \tag{5.12}$$

Parameters $\bar{P}$, $\bar{Q}$ and $\bar{T}$ are also related to the calibration coefficients $\bar{A}$ and $\bar{B}$ through the strain gauge measurements $\bar{p}$, $\bar{q}$ and $\bar{t}$ by the following simple relations:

$$\bar{P} = \frac{\bar{p}}{2\bar{A}} \tag{5.13}$$

$$\bar{Q} = \frac{\bar{q}}{2\bar{B}} \tag{5.14}$$

$$\bar{T} = \frac{\bar{t}}{2\bar{B}} \tag{5.15}$$

The above relations only apply under the assumption that the residual stress is uniform with thickness. From the finite element models it could be seen that the variation in stresses throughout thickness is small when compared to the one across the plate surface. It was hence deemed sufficient to use these relations in order to compute the residual stress measurements. Furthermore, calibration coefficients $\bar{A}$ and $\bar{B}$ are usually provided in terms of $\bar{a}$ and $\bar{b}$ in order to include elastic material properties of Young's Modulus E and Poisson's ratio υ using the following relation:

$$\bar{a} = \frac{2E\bar{A}}{1+\upsilon} \tag{5.16}$$

$$\bar{b} = 2E\bar{B} \tag{5.17}$$

Calibration coefficients are provided in [5.3] in terms of the hole radius and depth. The following relations can then be used to conveniently extract the required stresses from the measured data:

$$\sigma_{max,min} = \bar{P} \pm \sqrt{\bar{Q}^2 + \bar{T}^2} \tag{5.18}$$

$$\tau_{max} = \sqrt{\bar{Q}^2 + \bar{T}^2} \tag{5.19}$$

$$\phi = \frac{1}{2} \arctan\left(\frac{-\bar{T}}{-\bar{Q}}\right) \tag{5.20}$$

$$\sigma_x = \bar{P} - \bar{Q} \tag{5.21}$$

$$\sigma_y = \bar{P} + \bar{Q} \tag{5.22}$$

$$\tau_{xy} = \bar{T} \tag{5.23}$$

The following procedure is hence adopted for the residual stress calculation :

1. Measure residual strains ε_{g1}, ε_{g2} and ε_{g3}

2. Evaluate $\bar{p}$, $\bar{q}$ and $\bar{t}$ with Equations (5.7), (5.8) and (5.9)

3. Obtain calibration coefficients $\bar{a}$ and $\bar{b}$ by experimental calibration or available finite element calculations

4. Using elastic material properties E and υ calculate $\bar{A}$ and $\bar{B}$ with Equations (5.16) and (5.17)

5. Compute $\bar{P}$, $\bar{Q}$ and $\bar{T}$ with Equations (5.13), (5.14) and (5.15) ($\bar{P}$, $\bar{Q}$ and $\bar{T}$ represent the required residual stresses grouped in a convenient form, see Equations (5.10), (5.11) and (5.12))

6. All residual stress quantities can be obtained from $\bar{P}$, $\bar{Q}$ and $\bar{T}$ with Equations (5.18) to (5.23)

The above procedure details calculation for a single measurement at a single hole depth. For the set-up used in the current investigation, the maximum useful

depth before all the stresses are relieved is approximately equal to 0.4 times the strain gauge rosette mean diameter, equal to 5.13mm for the current investigation, giving a maximum useful depth of 2.05mm. The relief of strains as a function of depth is shown in Figures 5.5, 5.6 and 5.7 where functions of relieved strains $\bar{p}$, $\bar{q}$ and $\bar{t}$ are plotted against normalised hole depth for one of the drilled holes. A number of readings can be taken up to this depth. For such incremental data Step 5 is calculated in a weighted average manner using the following:

$$\bar{P} = \frac{\sum(\bar{A}\bar{p})}{2\sum(\bar{A}^2)} \tag{5.24}$$

$$\bar{Q} = \frac{\sum(\bar{B}\bar{q})}{2\sum(\bar{B}^2)} \tag{5.25}$$

$$\bar{T} = \frac{\sum(\bar{B}\bar{t})}{2\sum(\bar{B}^2)} \tag{5.26}$$

Where summations are carried out for the number of readings taken at the different depths. For the current investigation calibration coefficients $\bar{a}$ and $\bar{b}$ were obtained from [5.3] from data obtained by finite element calibrations.

When the stress across the thickness is not uniform, other calculation procedures must be employed. The successful use of these methods is however highly dependent on the experimental procedure and errors, together with the type of residual stress field present in the structures. The available calculation procedures are:

- Integral Method: good for non-uniform stress fields but very sensitive to strain measurement errors
- Power Series Method: good for smoothly varying stress fields but cannot pick up very localised stress variations
- Incremental Strain and Average Stress Method: only possible when experimental calibration is available. They are approximations of the Integral

Method and must be used with care

The Integral Method is analogous to the uniform stress field approach, the main difference being that for every hole depth increment the resulting stress distribution is made up of a number of components along the depth. This implies that Equations (5.13), (5.14) and (5.15) in the above procedure are replaced by a matrix system of equations embodying a number of components for each calibration coefficient. Experimental evaluation of the calibration coefficient is not feasible since it is very difficult to produce known layered stress fields.

The Power Series Method is based on the idea of dividing the stress field into a power series for which the corresponding coefficients are available from finite element calibrations. In practice the series is only limited to the second term giving a stress field that varies linearly with depth. Similarly to the Integral Method the depth for stress calculation is limited to 0.3 to 0.4 times the strain gauge rosette mean diameter.

After reviewing the methods for non uniform stress across thickness, together with the knowledge from the numerical models that the variation of stress across the thickness is relatively small, the uniform stress calculation procedure was adopted for the current investigation.

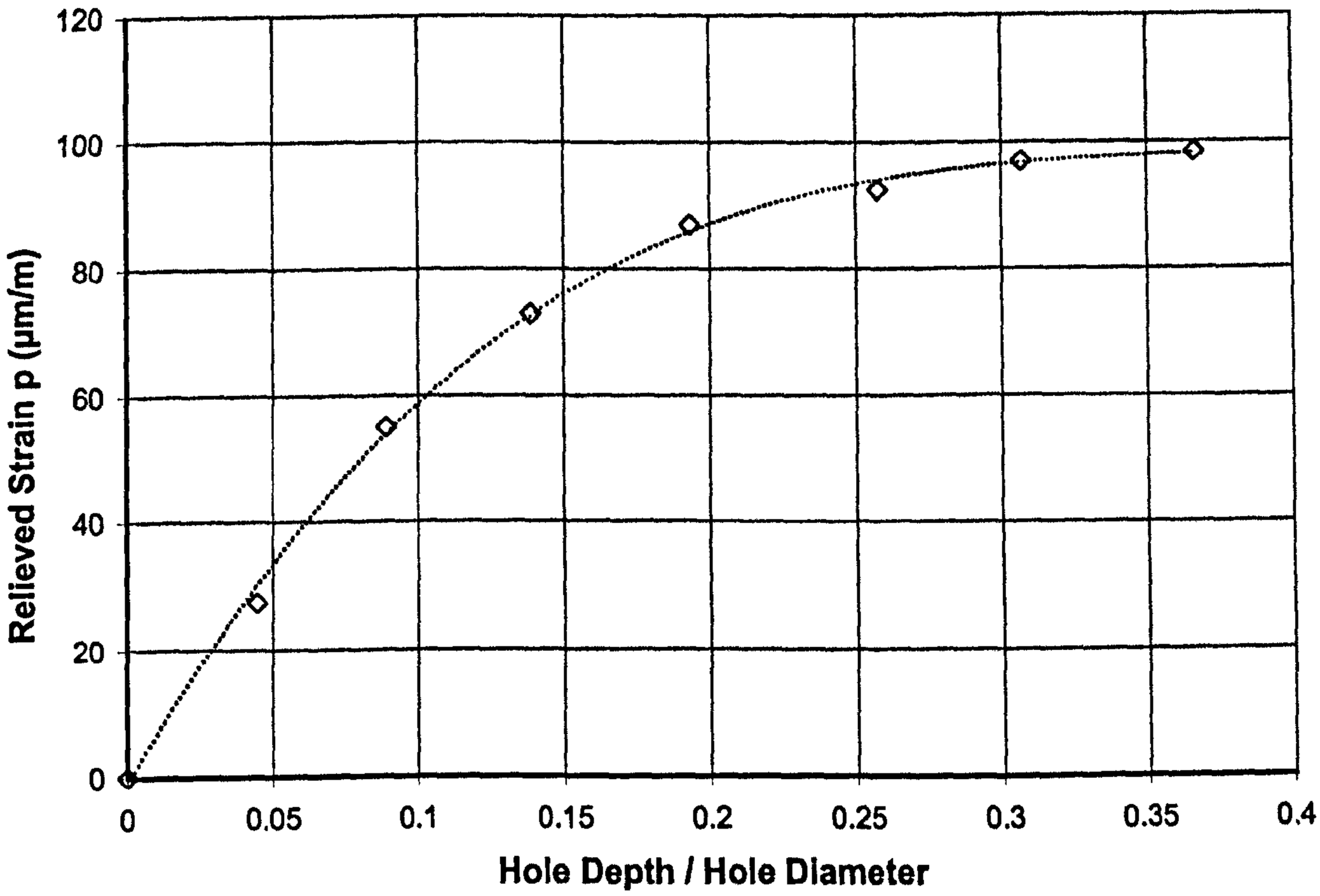

Figure 5.5: Relief of strains with increase of hole depth. Values computed for $\bar{p}$, see Equation (5.7) (taken from one of the strain gauge rosette readings)

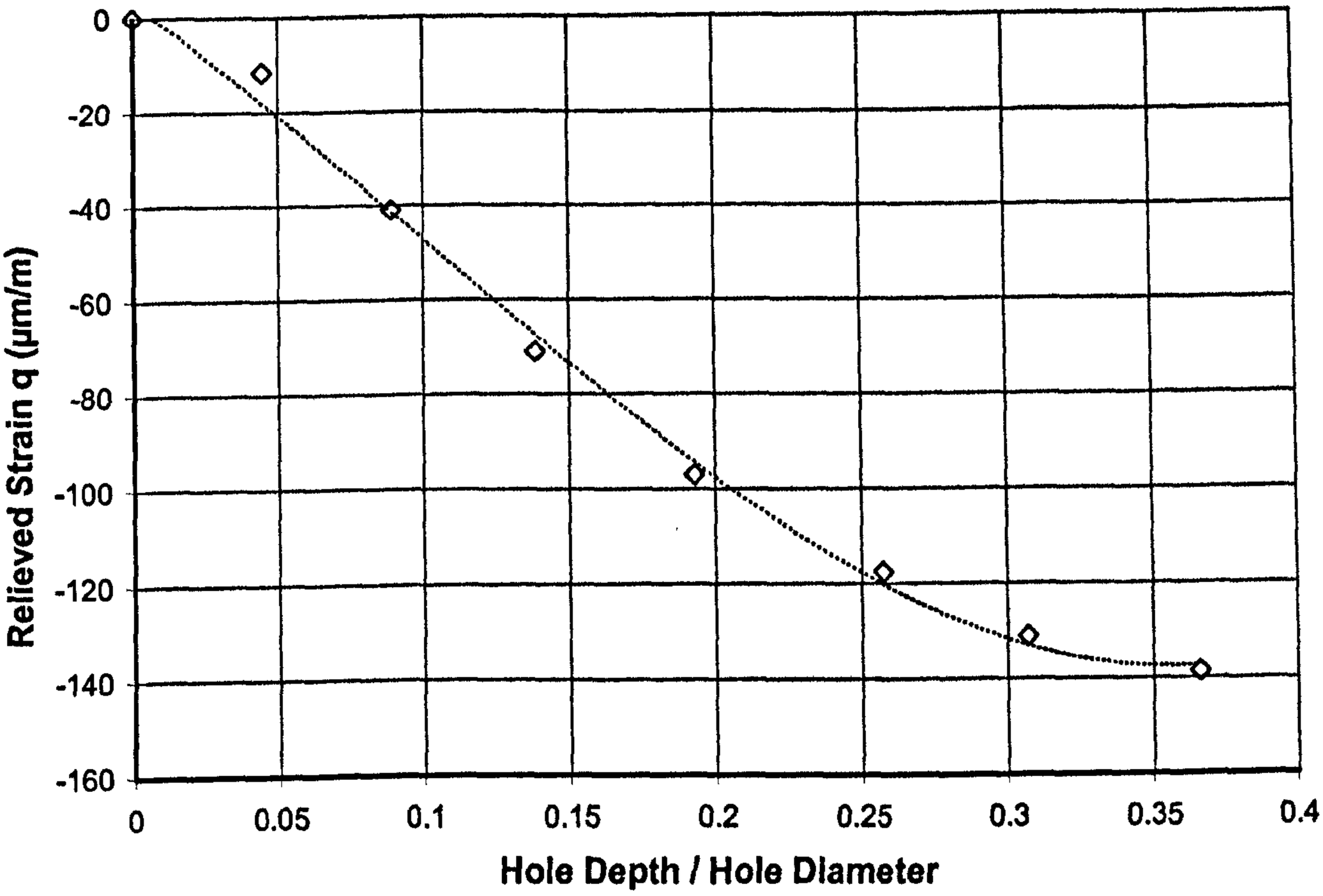

Figure 5.6: Relief of strains with increase of hole depth. Values computed for $\bar{q}$, see Equation (5.8) (taken from one of the strain gauge rosette readings)

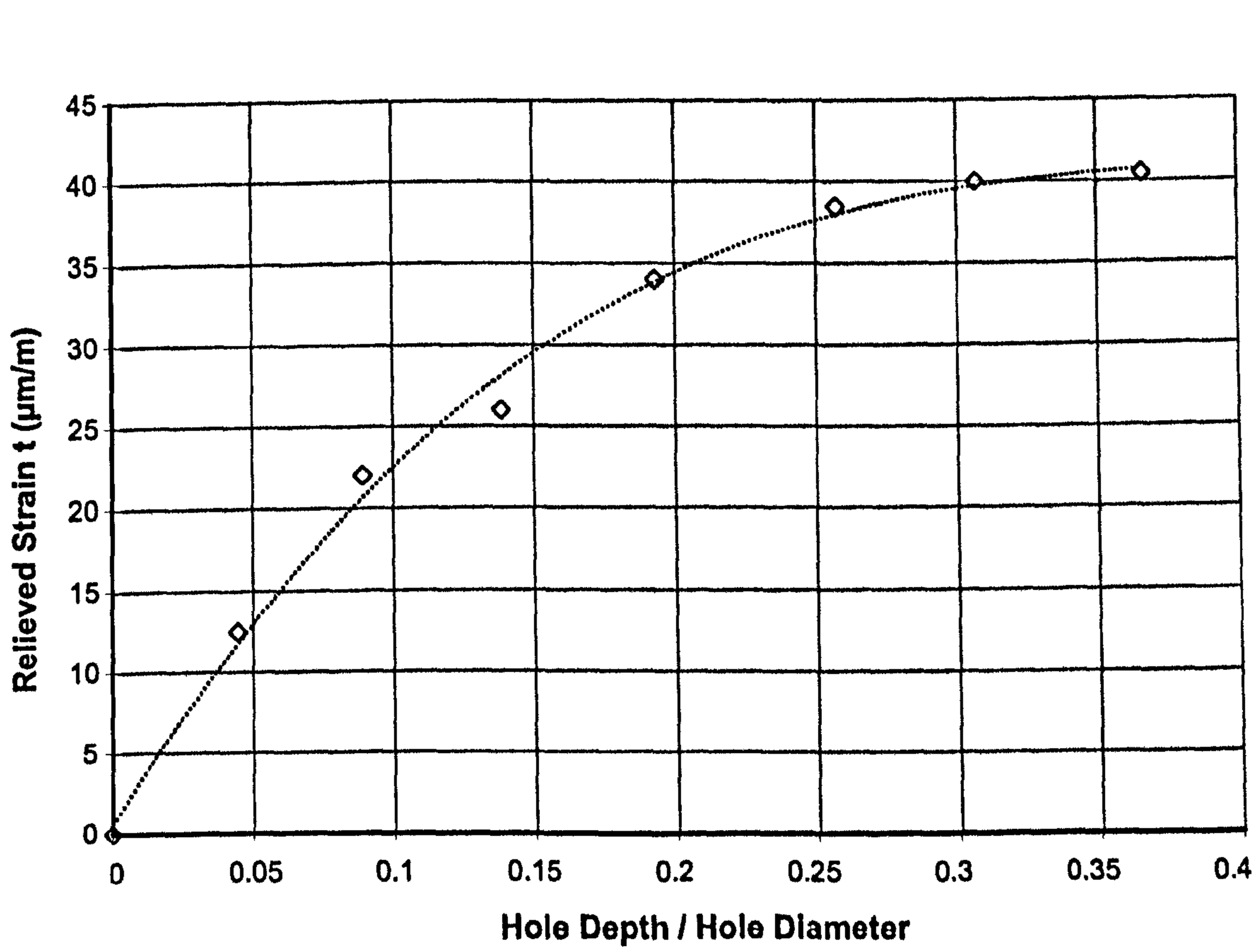

Figure 5.7: Relief of strains with increase of hole depth. Values computed for $\bar{t}$, see Equation (5.9) (taken from one of the strain gauge rosette readings)

5.2.4 Fillet Welding Results

Measurements were taken on 500 × 500 mm plates with a 15cm stiffener, attached by two single pass fillet welds. The strain gauges were all placed in the middle of the plate by varying the transverse position from the weld centre line. Different longitudinal positions were not considered as most of the variations occur in the transverse cross section. Three plates were considered for the measurements, with 8, 11 and 14 strain gauge rosettes on Plates 1, 2 and 3 respectively, giving a total of 33 readings. The welding conditions of the three plates were similar and could hence be compared to the same numerical model. This is shown in Figures 5.8 and 5.9 for longitudinal and transverse residual stresses respectively.

Longitudinal stresses are the largest and of most interest. Figure 5.8 shows results obtained for all measured plates. An average path is plotted for better comparison with the Finite Element prediction. A good match was obtained with differences approximately within a 100 MPa range. The following features are of main interest in comparing measurement with predictions:

- A very good match was obtained in the region close to the weld, which is of great importance as regards to the contraction forces inducing distortion
- The width of the central region matched on both sides of the stiffener, i.e. for both weld runs
- The point of *inflexion* where the stress profile sharply changes direction (roughly at $x = \pm 50$ mm) matched, although from there onwards the finite element prediction converges faster towards the zero stress line
- Far field stresses matched less well: measurements give a greater negative longitudinal stress than calculated

It is also of interest to note how the hole drilling measurements were unable to detect the stresses in the plastic region developed on the weld line due to strain

hardening effects. This was expected as it is inherent for this kind of residual stress measurement technique.

Transverse stresses exhibit a very different profile (see Figure 5.9). Lower magnitudes can be seen for both the measurements and the predictions, both lying within an approximate range of 100 MPa. In the finite element predictions the curve is translated into the positive region, ranging from a zero value at the extreme edges to a central positive maximum. Measurements also increased from the plate edges to the centre, but remained negative except for a few data points from Plate 2. It can also be noticed how the transverse stress data points exhibit a greater variation from plate to plate than the longitudinal stress points, especially close to the weld line. This is due to the greater dependency of the transverse stresses on the actual weld fusion zone, which varies from plate to plate. Smaller variation is exhibited for the far field stresses. Transverse stresses should, in theory, fall to zero at the plate edges, where the material is free and there is no restraining material to provide a force that induces residual stresses. This, as expected, can be seen in the finite element predictions. The hole drilling measurements showed a non zero value close to the one side of Plates 2 and 3. This unexpected result can be attributed to additional residual stresses originally present in the material, which were probably due to the cutting process used in the manufacture of the plates.

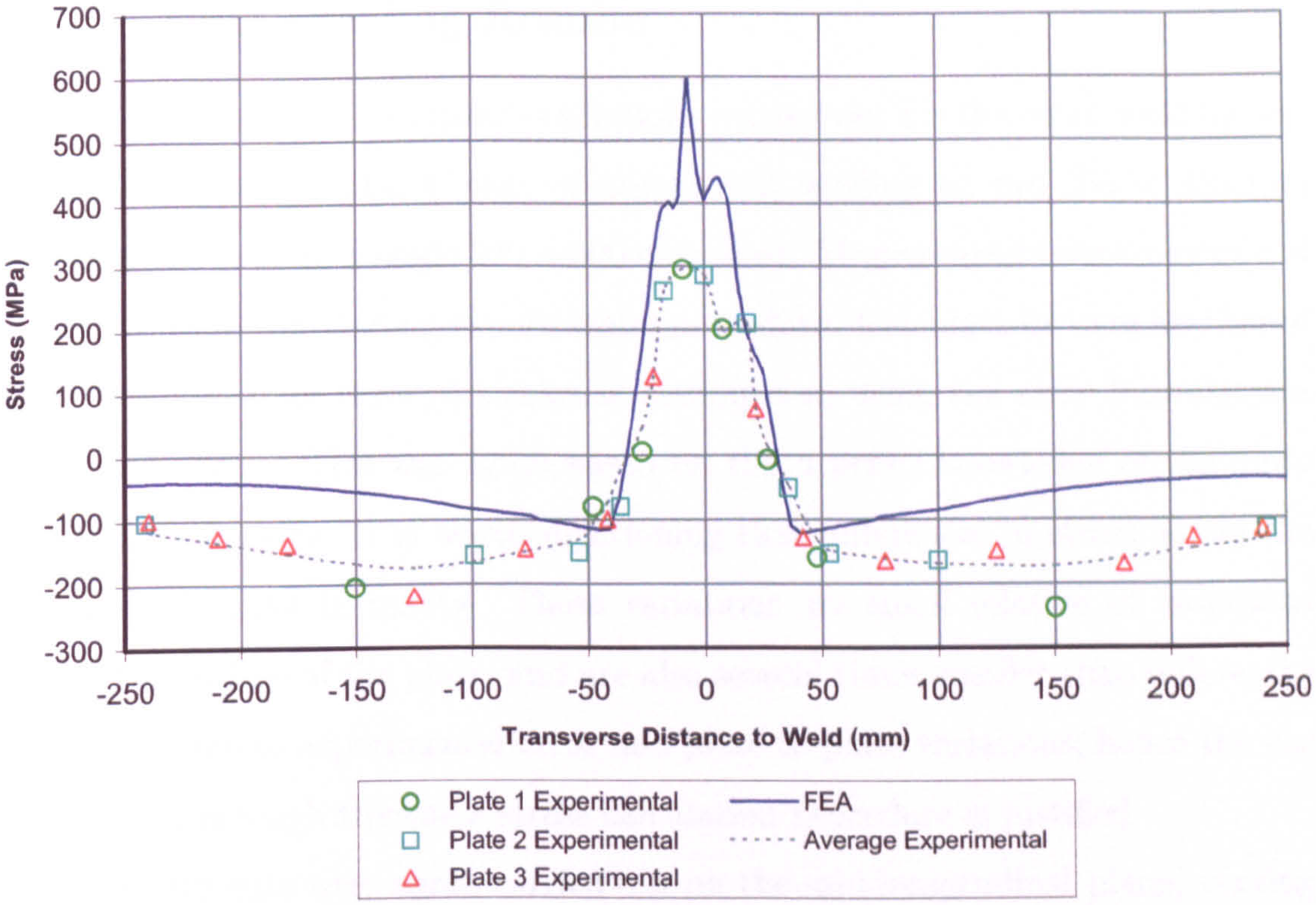

Figure 5.8: Longitudinal residual stress measurements on fillet weld set-up. Comparison with Finite Element prediction

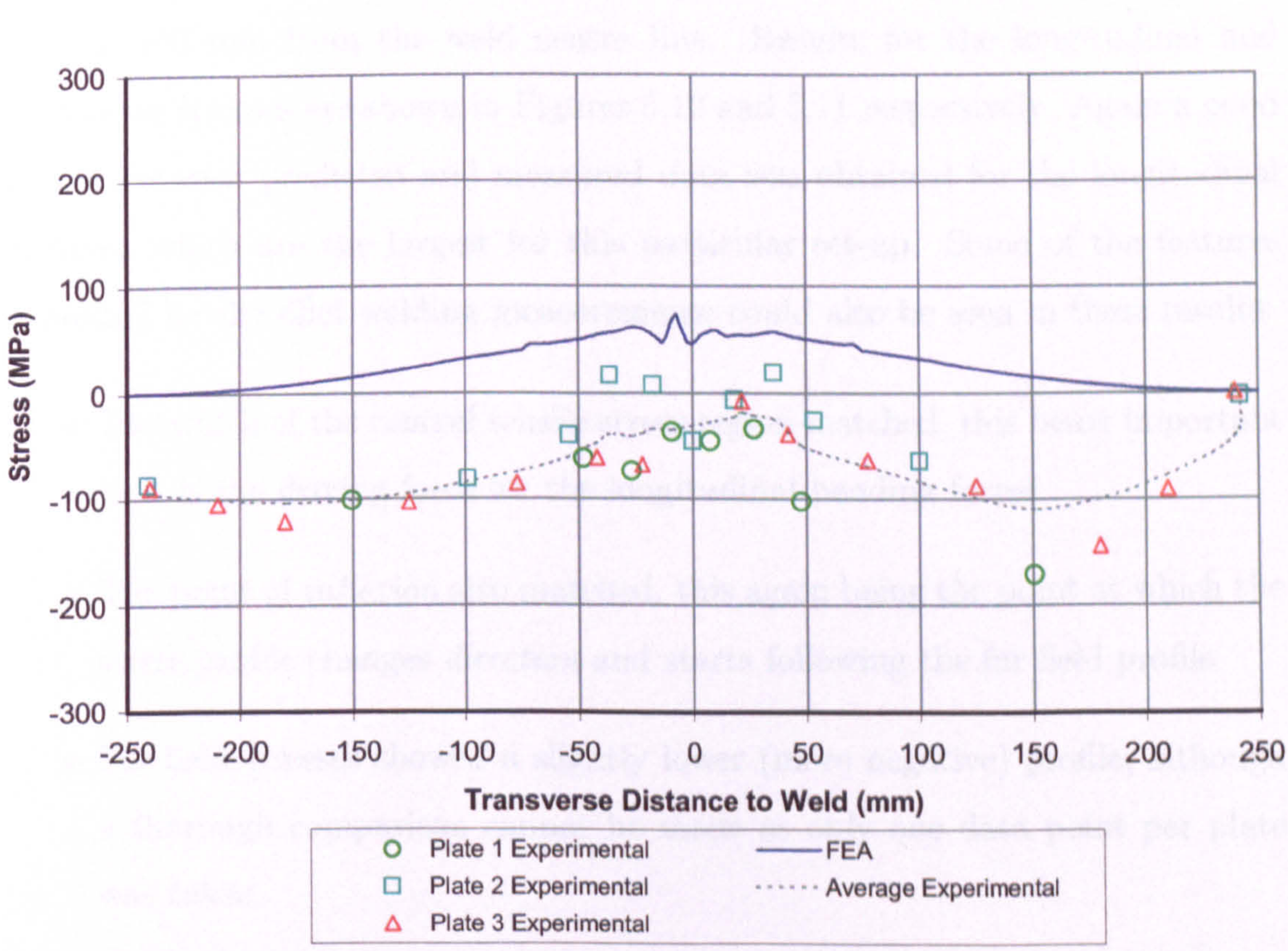

Figure 5.9: Transverse residual stress measurements on fillet weld set-up. Comparison with Finite Element prediction

5.2.5 Butt Welding Results

It is also of interest to compare predictions carried out for the other welding set-up presented in Chapter 4, that of simple butt welding on two 500 × 250 mm plates joined to form a single 500 × 500 mm sheet. Measurements were carried out using the same hole drilling experimental procedure. Calculations were also based on a uniform stress through thickness assumption, using the same formulations presented above. This was again based on the *a priori* knowledge of the finite element predictions. It is worth mentioning that differences in stress across the thickness do exist in reality. These variations are small relative to variations across the surface of the plate, and are also several times smaller than differences in stresses due to experimental error and plate to plate variations; hence the use of constant through thickness stress calculation procedure is justified.

Measurements were again carried out on the mid-longitudinal plane, varying the distance transverse to the weld centre line. Four plates were considered with four strain gauge rosettes placed on each plate at transverse distances of 5, 20, 45 and 150 mm from the weld centre line. Results for the longitudinal and transverse stresses are shown in Figures 5.10 and 5.11 respectively. Again a good match between predicted and measured data was obtained for the longitudinal stresses, which are the largest for this particular set-up. Some of the features exhibited by the fillet welding measurements could also be seen in these results:

- The width of the central tensile stress region matched, this being important as it is the driving force for the longitudinal bending forces
- The point of *inflexion* also matched, this again being the point at which the stress profile changes *direction* and starts following the far field profile
- Far field stresses showed a slightly lower (more negative) profile, although a thorough comparison cannot be made as only one data point per plate was taken

Similarly to the fillet welding set-up, measurements could not pick up stresses in excess of the yield point which are found in the finite element results in regions very close to the weld line and are due to strain hardening effects.

Transverse stresses did not match as well and, similarly to the fillet weld measurements, resulted in negative measurement, opposed to the positive values obtained from the finite element predictions. Values were smaller in magnitude compared to the longitudinal stress values, and exhibited a greater variability from plate to plate. This implied a greater dependence on the actual weld / fusion zone shape.

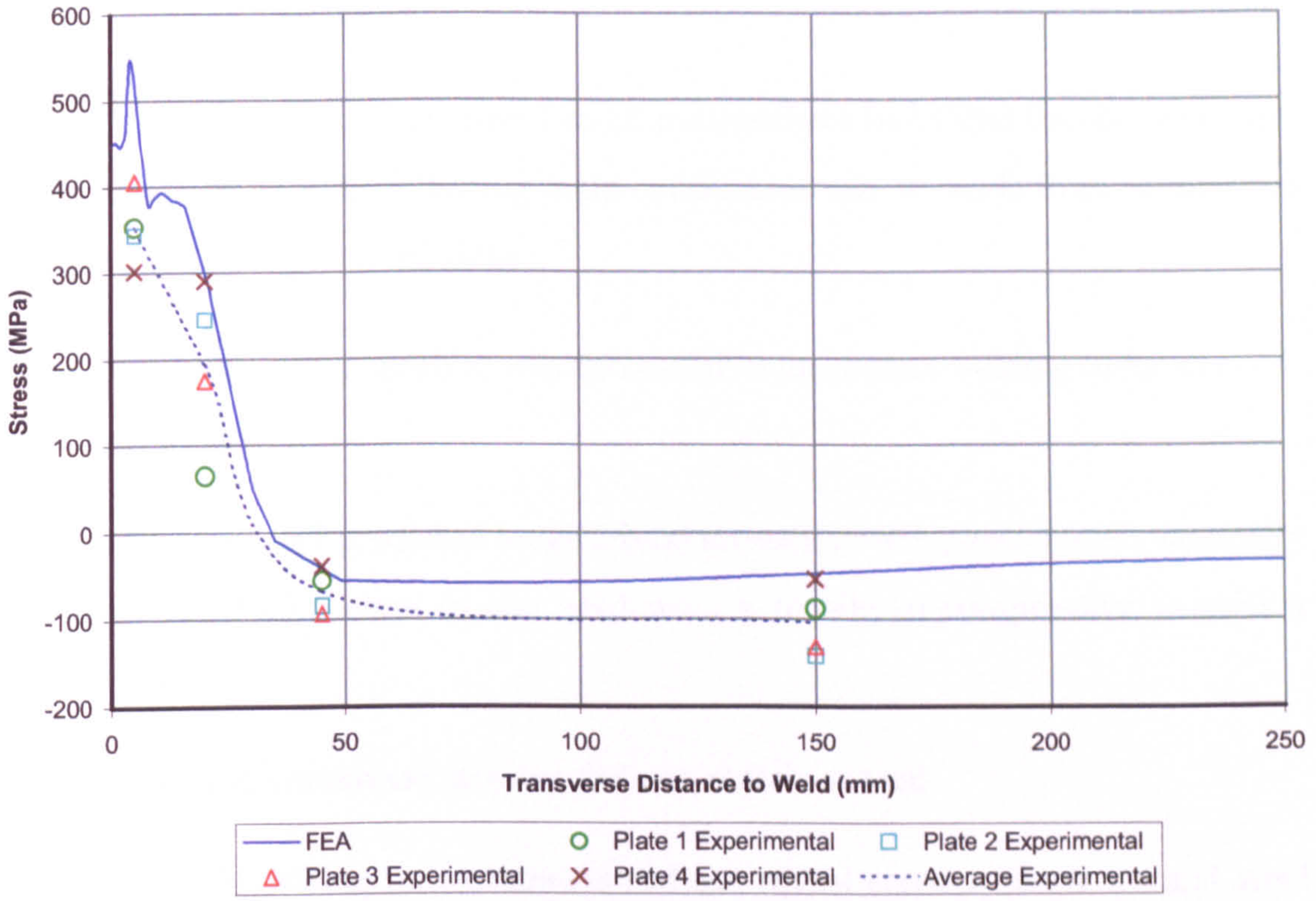

Figure 5.10: Longitudinal residual stress measurements on welding set-up. Comparison with Finite Element prediction. (Half of the plate was considered owing to symmetry)

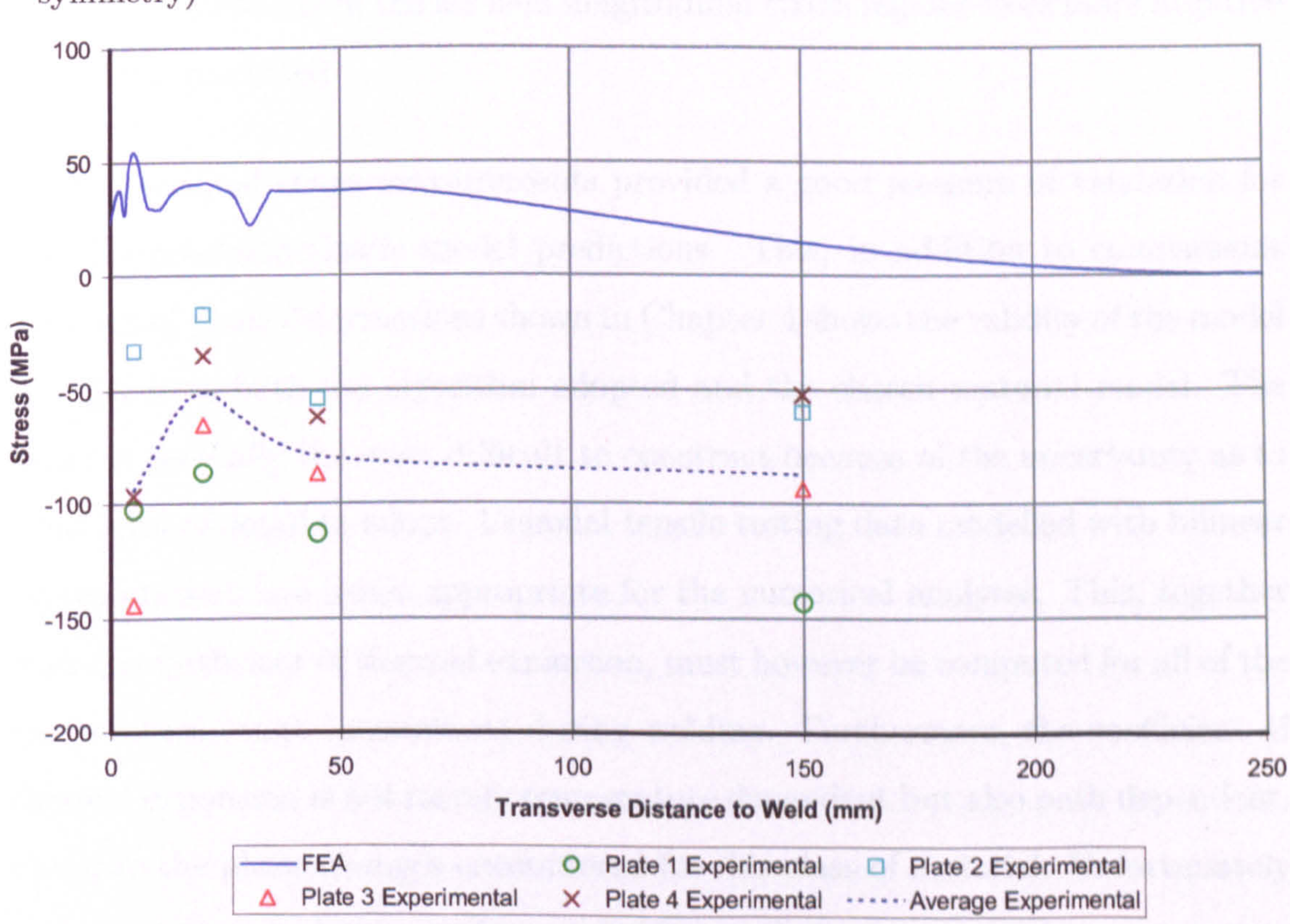

Figure 5.11: Transverse residual stress measurements on butt welding set-up. Comparison with Finite Element prediction. (Half of the plate was considered owing to symmetry)

5.2.6 Conclusions

The hole drilling technique proved to be a convenient technique for the configurations investigated. The following main conclusions can be made from comparison of measured and predicted data:

- The hole drilling method was successful in measuring welding induced residual stresses
- Measured and predicted longitudinal stresses gave a good match, especially for the region close to the weld were a tensile to compressive transition occurs
- Measured transverse stresses did not match as well
- The hole drilling measurements did not reveal stresses above normal yield for this material
- Measurements in the far field longitudinal stress regions were more negative than predicted

The residual stress measurements provided a good measure of validation for the thermo-elasto-plastic model predictions. This, in addition to comparisons with out of plane deformations shown in Chapter 4 shows the validity of the model as regards to both the algorithm adopted and the chosen material model. The latter is generally the most difficult to construct because of the uncertainty as to what level of detail to adopt. Uniaxial tensile testing data modelled with bilinear representations are hence appropriate for the numerical analyses. This, together with the coefficient of thermal expansion, must however be computed for all of the temperature range encountered during welding. Furthermore, the coefficient of thermal expansion is not merely temperature dependent but also path dependent, owing to the phase changes encountered for this class of material. Unfortunately such data is not always readily available, so that experimental measurements

had to be carried out. The following sections describe quasi-static dilatometry measurements carried out to determine the coefficient of thermal expansion and presents results obtained for uniaxial testing carried out at different temperatures.

5.3 Dilatometry Measurements

5.3.1 Introduction

Dilatometry measurements were required in order to obtain temperature dependent values for the coefficient of thermal expansion. Two sets of results were obtained for the class of materials used throughout the investigation: one set was carried out at the University of Strathclyde with available apparatus, whilst the other was obtained from industrial partners Corus. The following sections present results obtained, together with an investigation on the effect of using a path dependent coefficient of thermal expansion for the current investigation. This showed only a slight variation in the numerical results leading to the adoption of the temperature dependent (non-path dependent) values in the numerical material models.

5.3.2 Procedure & Results

A dilatometer type PL-TMA STA 1640 from Labtherm Science was used to measure the coefficient of thermal expansion. It consisted of an enclosed chamber fed with a controlled atmosphere and heated through the required thermal cycle. Argon was fed in the chamber in order to minimise oxidisation of the sample that leads to the formation of a thin layer of extra material, hence disrupting the very delicate readings for material dilation. Measurements are captured by a transducer connected to a computerised control system. The tip of the transducer reaching the heated chamber is made up of a ceramic material in order to minimise it's effect in the expansion measurements. The thermal cycle could be preset from the computerised control unit but was limited to a maximum heating / cooling rate of $30\frac{°C}{min}$ which is not as much as the actual heating / cooling rate

experienced by some parts of the plates during the welding process.

Samples were taken from actual welded plate, both from regions far away from the weld to represent the base material and from the weld line itself. The values for the different material models were assigned to the respective elements in the numerical model using the algorithm presented in Chapter 3. A total of 12 samples (5 from the weld material and 7 from the base plate) were considered in order to obtain a good average for weld and parent material coefficients. A typical plot obtained from one of the base plate samples is shown in Figure 5.12. The plot yielded the expected overall profile for this type of material, which is characterised by the plateau obtained in the cooling part due to phase transformations. The major deficiency encountered with these results was the lack of expansion in the initial heating phase, caused by backlash triggered by the very low extensions encountered in this stage of heating. Notwithstanding this, the cooling part is of greater interest as regards to the development of welding induced residual stresses and distortions and is the one that will be used for the numerical material model. The coefficient of thermal expansion, defined in Chapter 3, Equation (3.21), is extracted from the extension vs. temperature plots using the following:

$$\alpha_{in}(T) = \frac{d\,(\delta l/l)}{dT} \tag{5.27}$$

Where δl and l are extension and original sample length respectively. The coefficient of thermal expansion is therefore nothing but the gradient of the plots divided by the sample original length. Considering the cooling part of the plot, it can be seen that three distinct values can be extracted where the gradient is constant, i.e. two values for the high temperature ($\simeq$ 800°C – 1200°C) and low temperature ($\simeq$ 20°C – 600°C) expansions and one for the phase transformation range ($\simeq$ 600°C – 800°C). The latter was taken to be zero in order to simplify the numerical model.

Further data was obtained from commissioned results, of which a sample plot

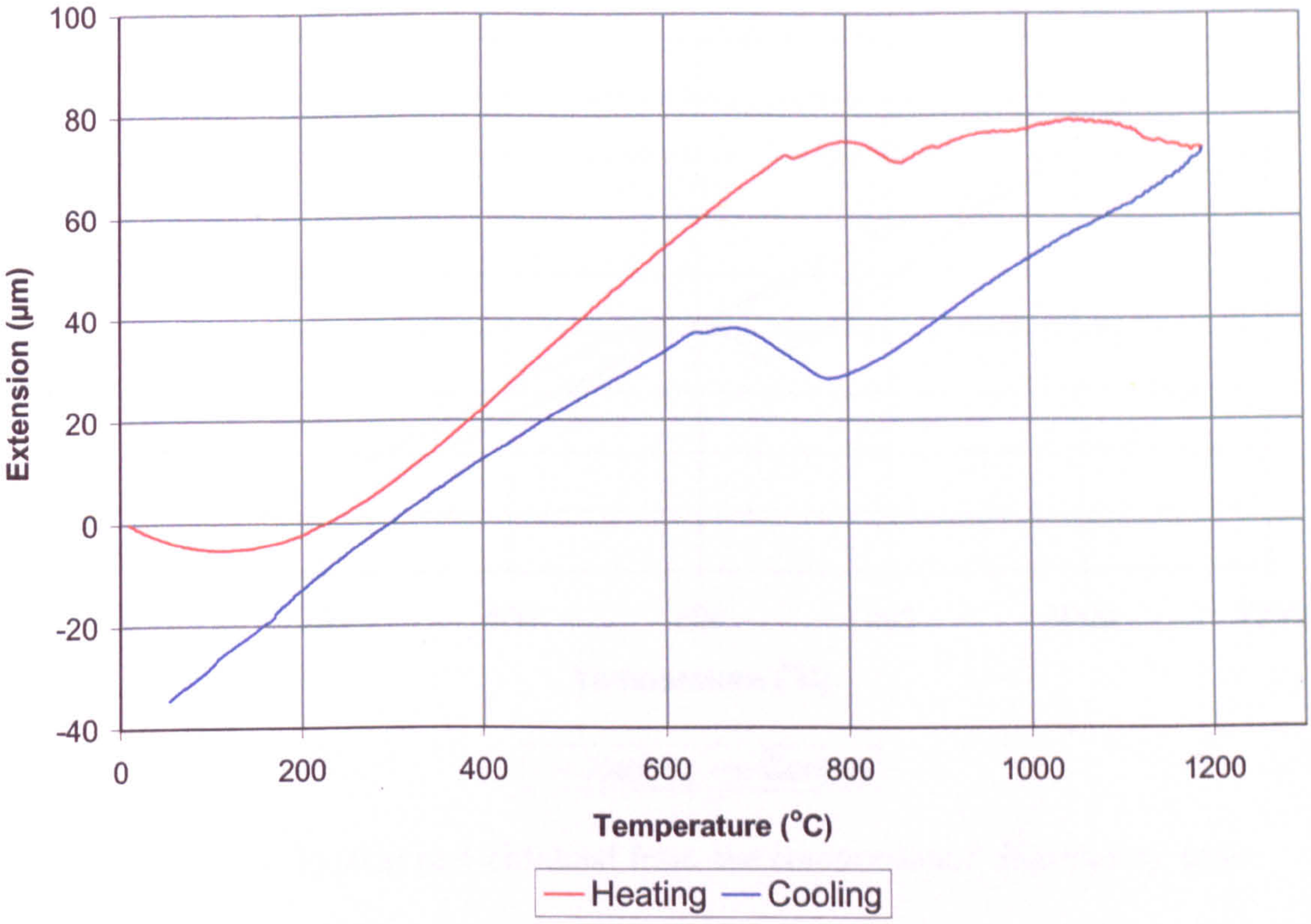

Figure 5.12: Typical plot obtained from the in-house dilatometry tests

is shown in Figure 5.13. The same features, typical for this class of material, can be see and again three distinct values for the coefficient of thermal expansion could be extracted. These are shown in Figure 5.14 where the coefficients have been extracted for both parent and weld materials using averaged values from the available samples. The values were taken from the cooling cycle and applied to the two material models used in the analysis, i.e. the one for elements representing the fused zone (weld material) and the ones for the remainder of the plate (parent material). Path dependency was not included, as it was deemed unnecessary for the level of complexity required by the models. A minor investigation on the effect of using path dependent coefficients was carried out, outlined in the next section.

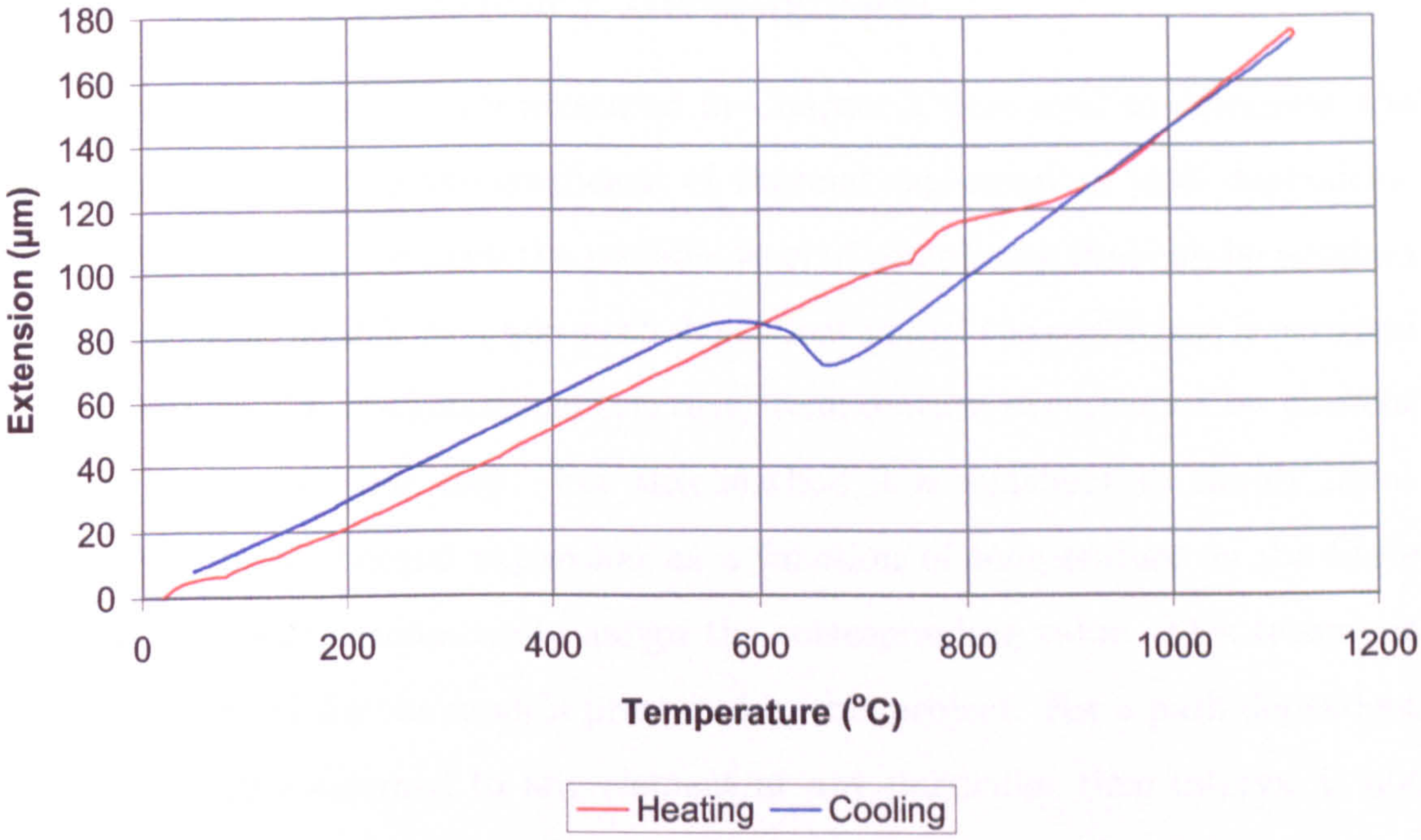

Figure 5.13: Typical plot obtained from the commissioned dilatometry tests

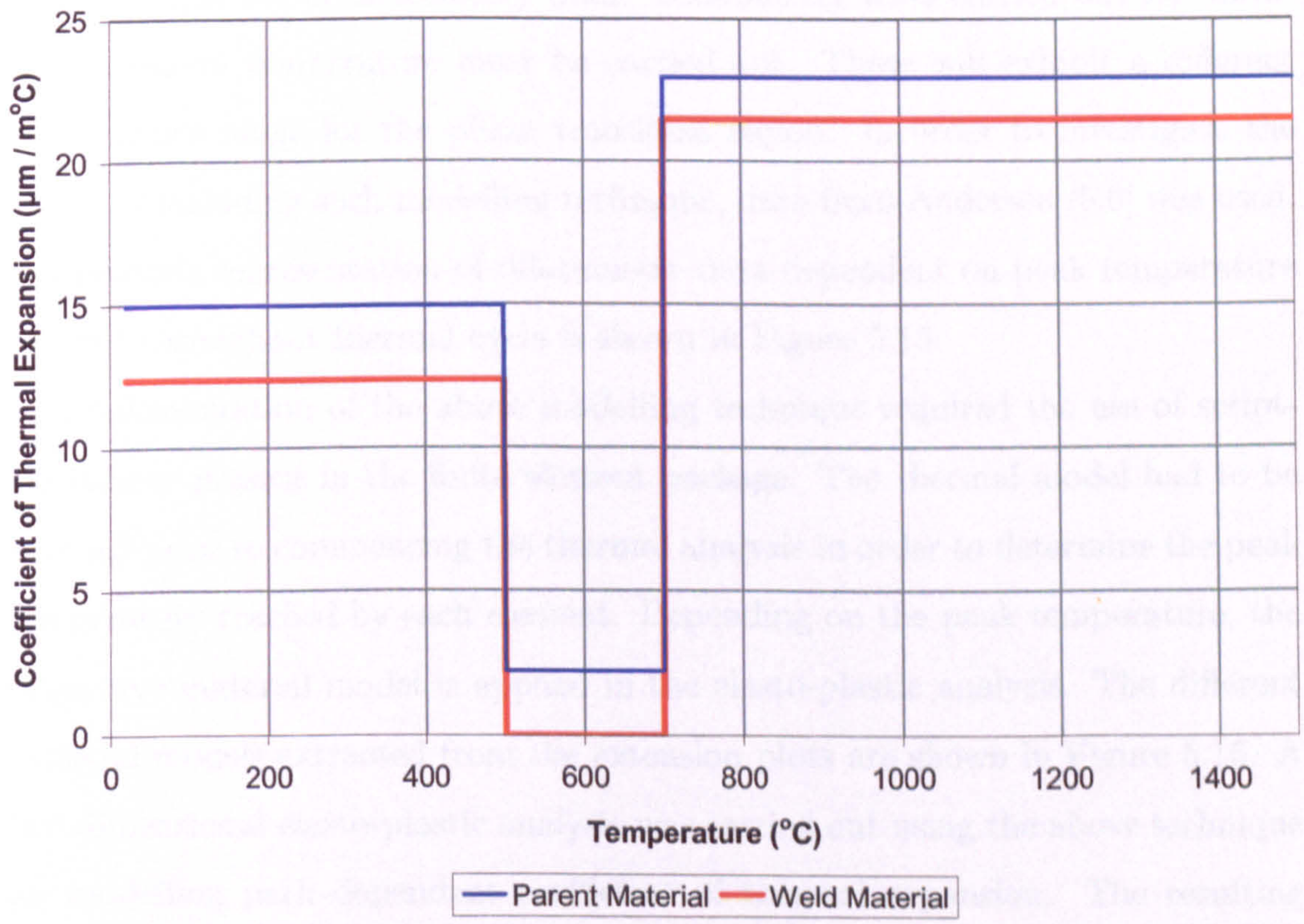

Figure 5.14: Coefficient of thermal expansion extracted from averaged dilatometry readings

5.3.3 Path Dependency Investigation

The two-dimensional models presented in Chapter 3 were used to determine the feasibility of modelling the coefficient of thermal expansion as path dependent. Lindgren [5.4], [5.5] discusses the possible level of complexity that can be adopted for the material model. In a non-path dependent model the coefficient is assigned only based on the instantaneous (current) temperature experienced by element in that particular time step. For this method it is sufficient to simply input the coefficient of thermal expansion as a function of temperature as the finite element code will automatically assign the corresponding value. This technique proved successful for the models presented in this project. For a path dependent model the value assigned to any element at any particular time interval is not only dependent on the current temperature but also on the peak temperature reached throughout the welding cycle. This modelling approach clearly requires a much larger set of dilatometry data. Dilatometry tests carried out for different maximum temperature must be carried out. These will exhibit a different temperature range for the phase transition region. In order to investigate the effects of including such modelling technique, data from Andersen [5.6] was used. A schematic representation of dilatometry data dependent on peak temperature reached throughout thermal cycle is shown in Figure 5.15.

Implementation of the above modelling technique required the use of scripting facility present in the finite element package. The thermal model had to be scanned prior to commencing the thermal analysis in order to determine the peak temperature reached by each element. Depending on the peak temperature, the respective material model is applied in the elasto-plastic analysis. The different material models extracted from the extension plots are shown in Figure 5.16. A two-dimensional elasto-plastic analysis was carried out using the above technique for modelling path dependent coefficient of thermal expansion. The resulting numerical model is shown in Figure 5.17 where the plotted mesh shows the resulting distribution of material models. This analysis was compared to the same

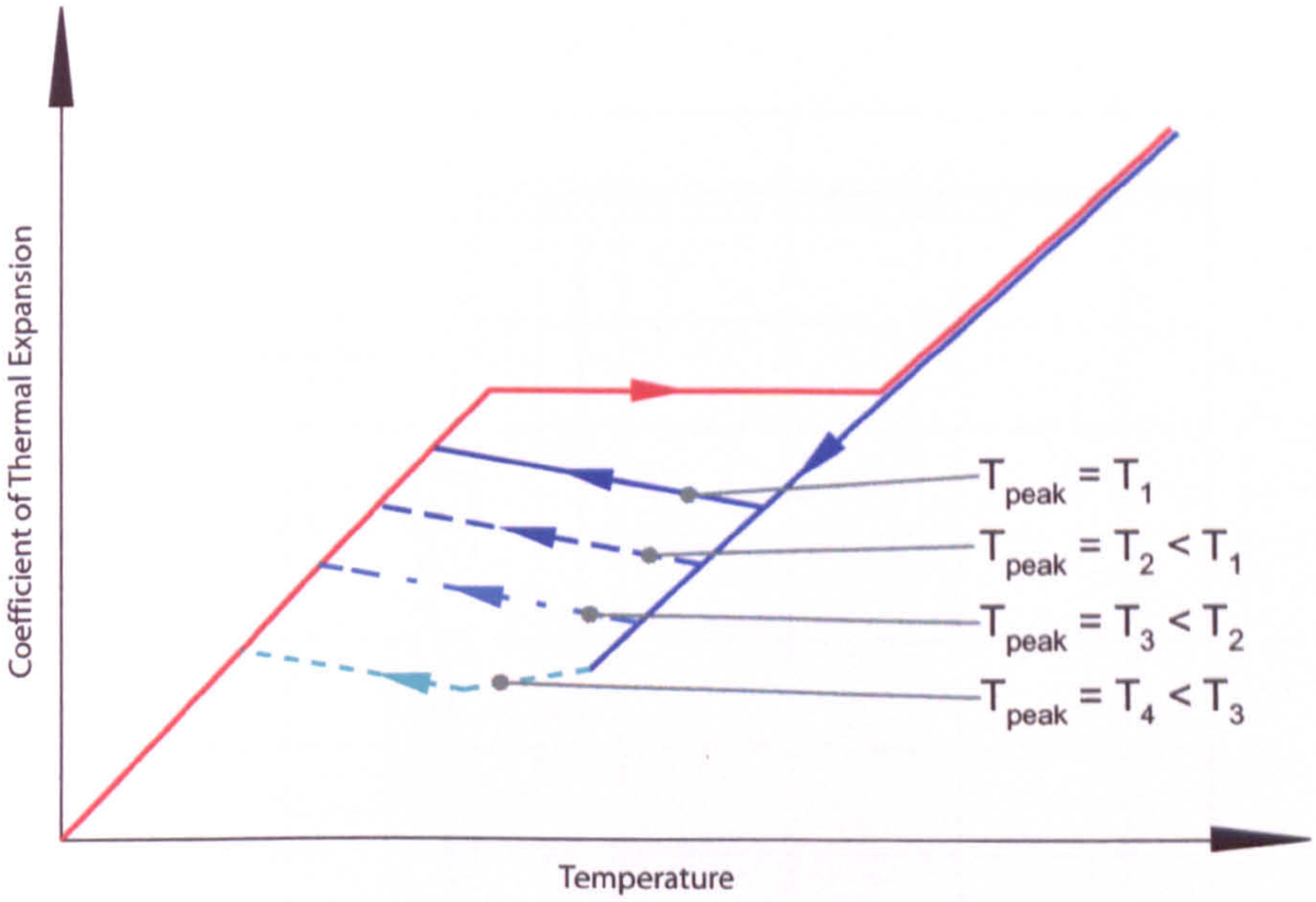

Figure 5.15: Schematic representation of the coefficient of thermal expansion dependent on peak temperature reached throughout the thermal cycle

run carried out with a non-path dependent model, i.e. one coefficient of thermal expansion vs. temperature curve applied to all elements. The data for the latter was taken from the coefficient curve relating to the base plate metal in the path dependent model. This allowed for direct comparison and hence evaluation of the effects of using a path dependent modelling technique. Predicted longitudinal and transverse stresses are shown in Figures 5.18 and 5.19 respectively.

The plots show the high similarity in predicted stresses for models using path dependent and non-dependent coefficients. It is also evident from Figure 5.17 how few of the elements were in fact modified by the non-path dependent algorithm. This implies that a much finer mesh would be required to better simulate the path dependent effects. This is however not feasible for dimensions used in the current investigation. Furthermore, a much larger set of dilatometry data would be required, carried out with a more advanced apparatus which allows heating and cooling cycles representative of the actual welding process.

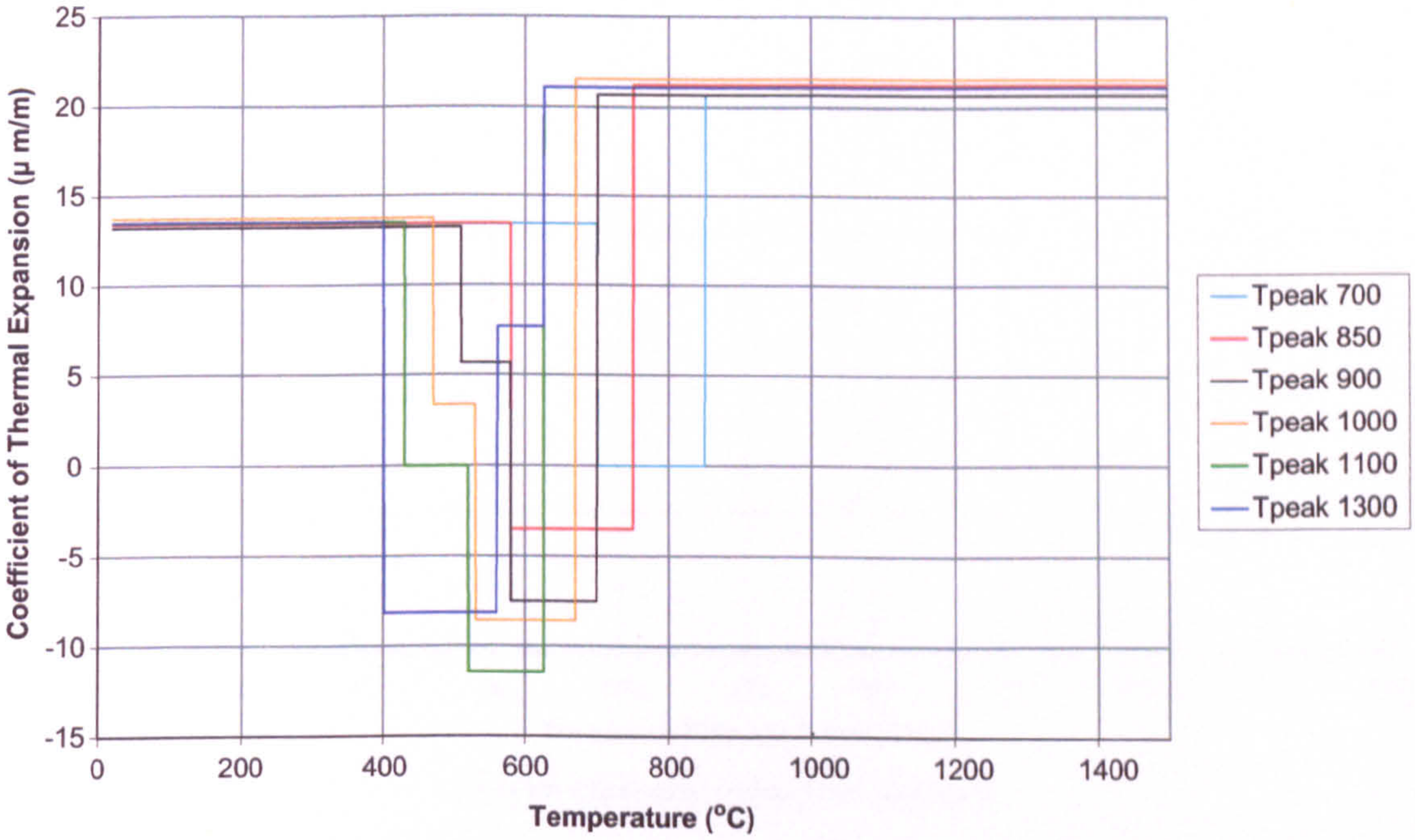

Figure 5.16: Coefficient of thermal expansion as a function of temperature for different peak temperatures reached throughout thermal cycle

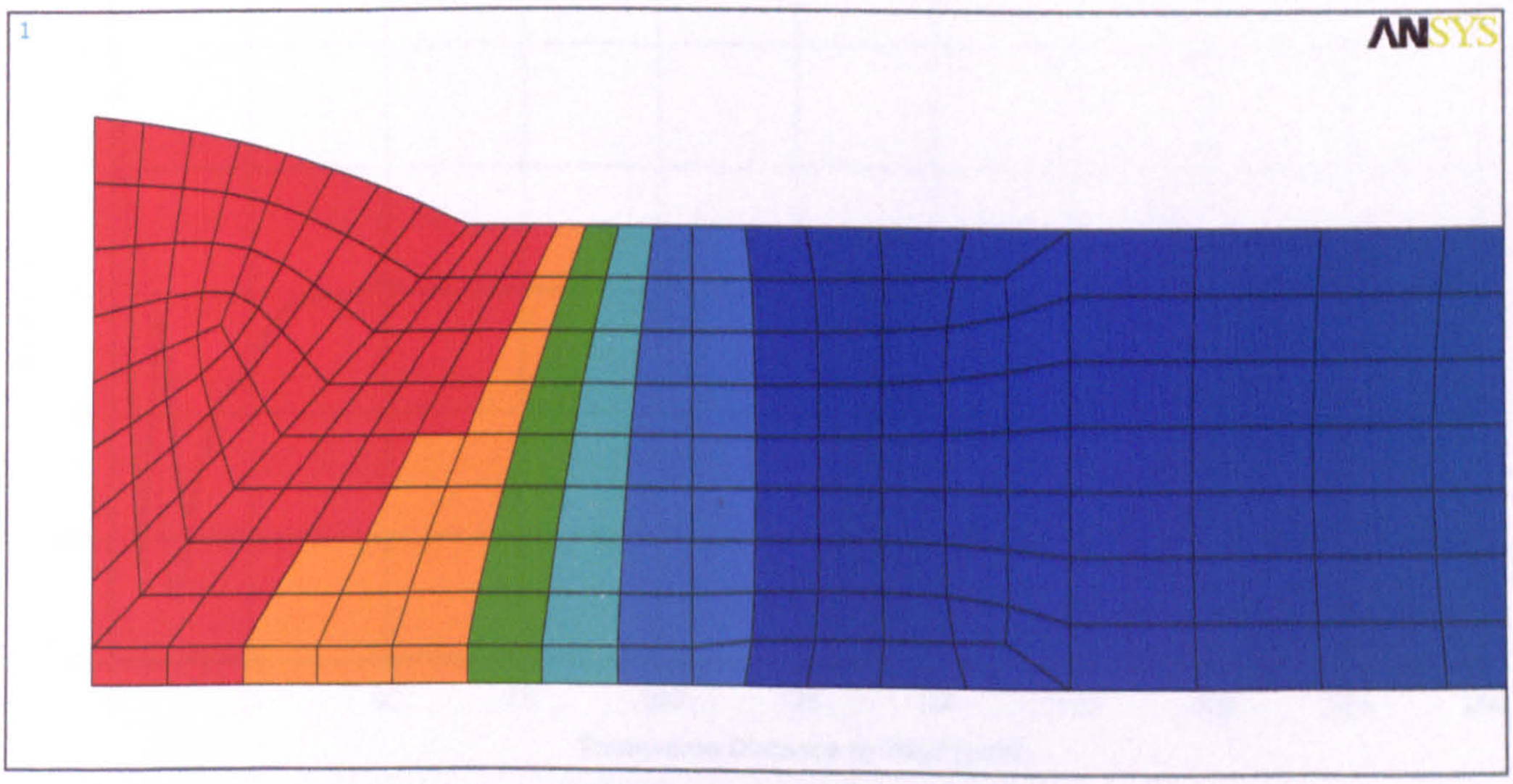

Figure 5.17: Application of different material models (different colours) for the coefficient of thermal expansion depending on peak temperature reached throughout thermal cycle

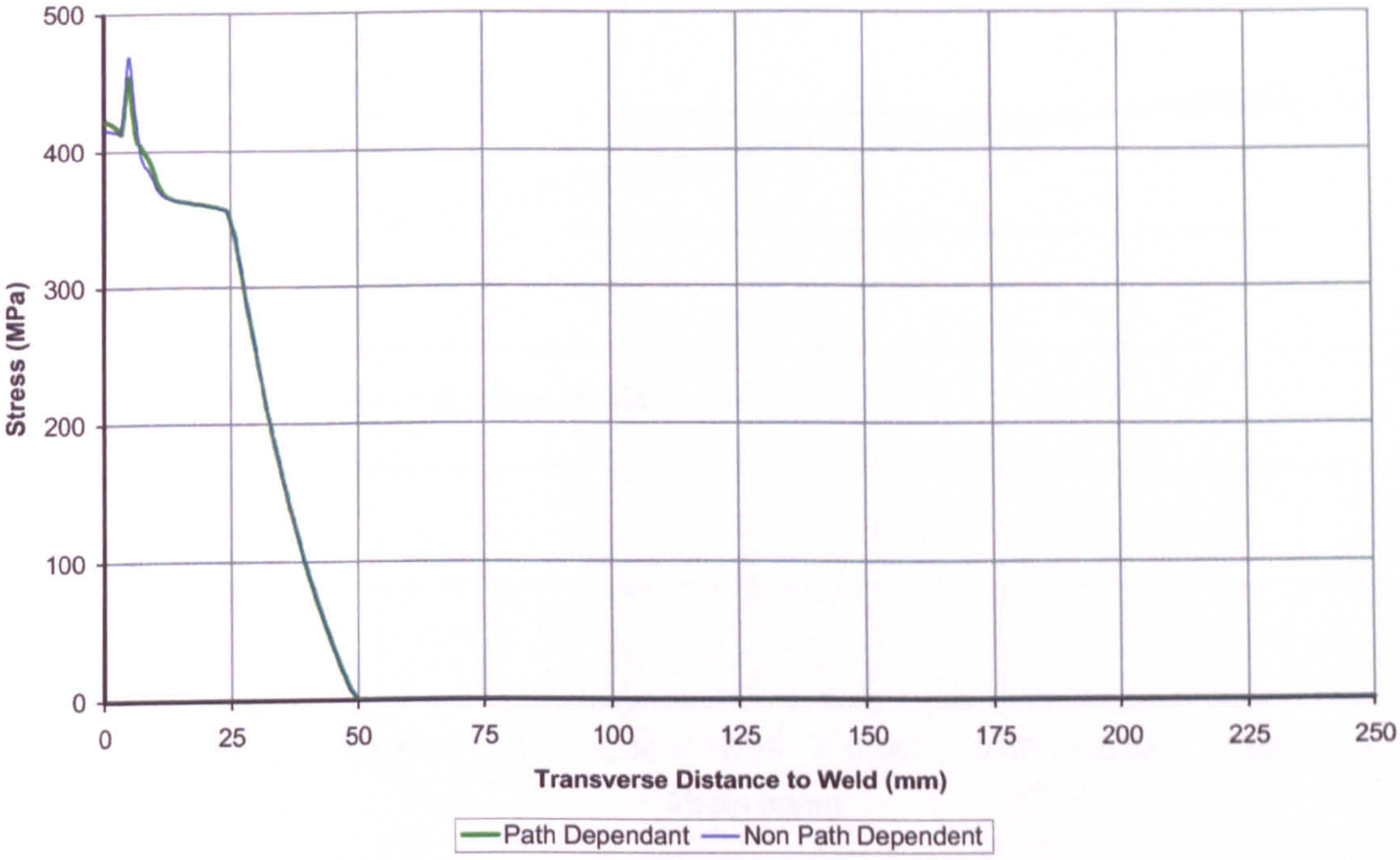

Figure 5.18: Longitudinal residual stress predicted by two-dimensional thermo elasto plastic model for path dependent and non dependent coefficients of thermal expansion

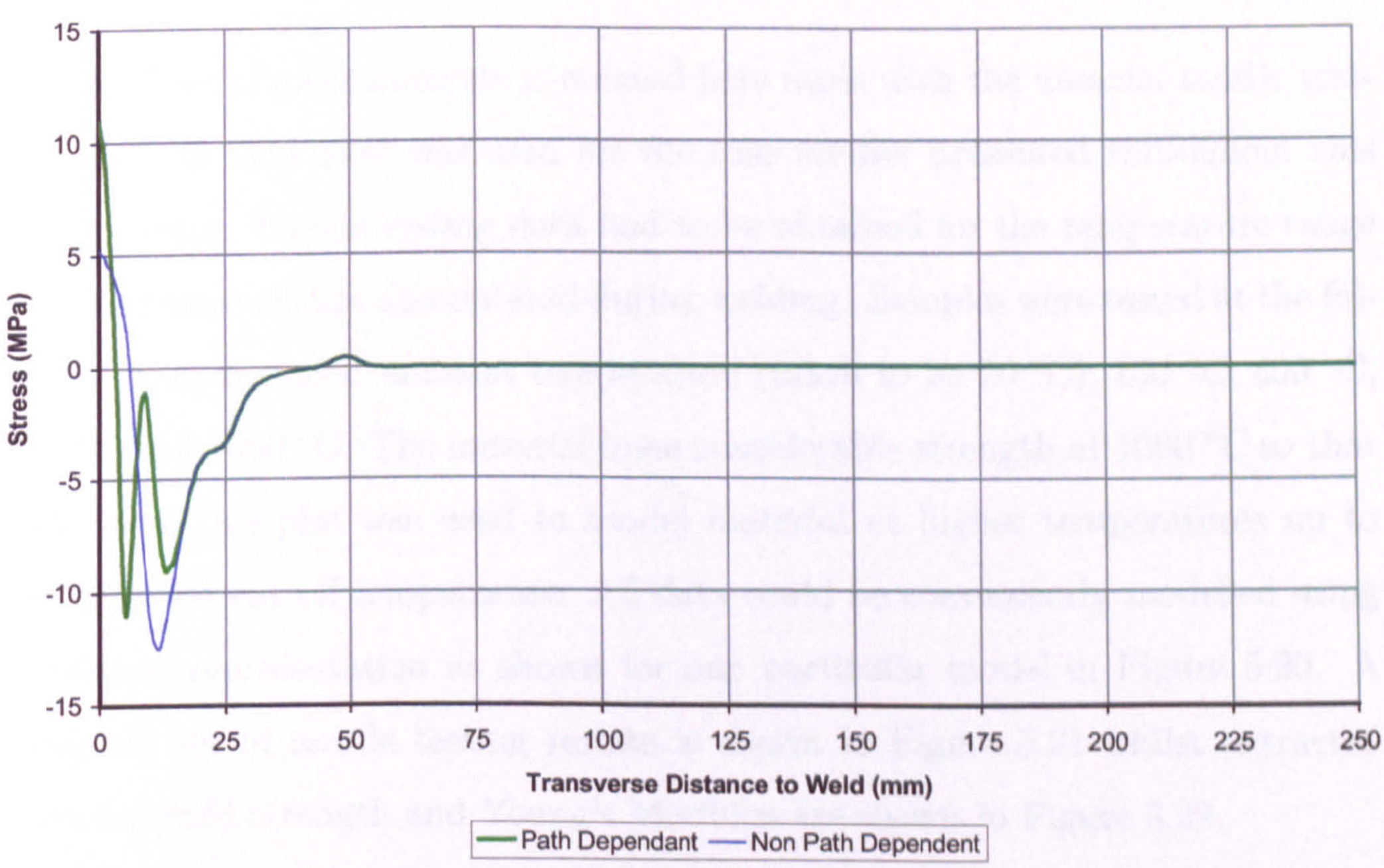

Figure 5.19: Transverse residual stress predicted by two-dimensional thermo elasto plastic model for dependent and non path dependent coefficient of thermal expansion

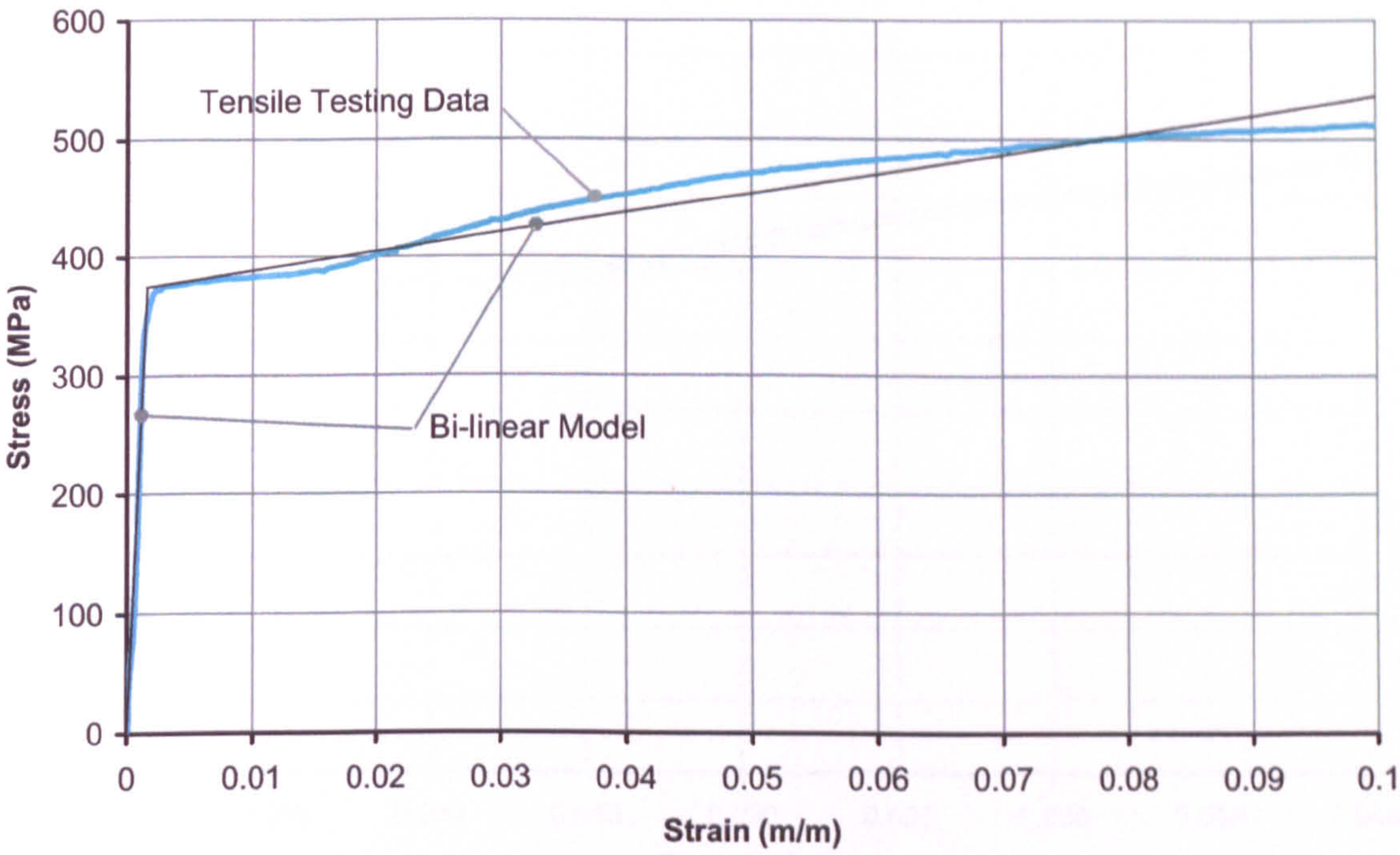

Figure 5.20: Bilinear model extracted from the stress strain uniaxial tensile testing data

5.4 Tensile Testing

The final set of measurements presented here deals with the uniaxial tensile testing. DH 36 mild steel was used for the case studies presented throughout this investigation. Tensile testing data had to be obtained for the temperature range representative of that encountered during welding. Samples were tested at the following temperatures: ambient temperature (taken to be 20 °C), 150 °C, 400 °C, 600 °C and 1000 °C. The material loses considerable strength at 1000 °C so that data from this plot was used to model material at higher temperatures up to the assumed cut-off temperature. All data could be conveniently modelled using a bilinear representation as shown for one particular model in Figure 5.20. A complete set of tensile testing results is shown in Figure 5.21 whilst extracted data for yield strength and Young's Modulus are shown in Figure 5.22.

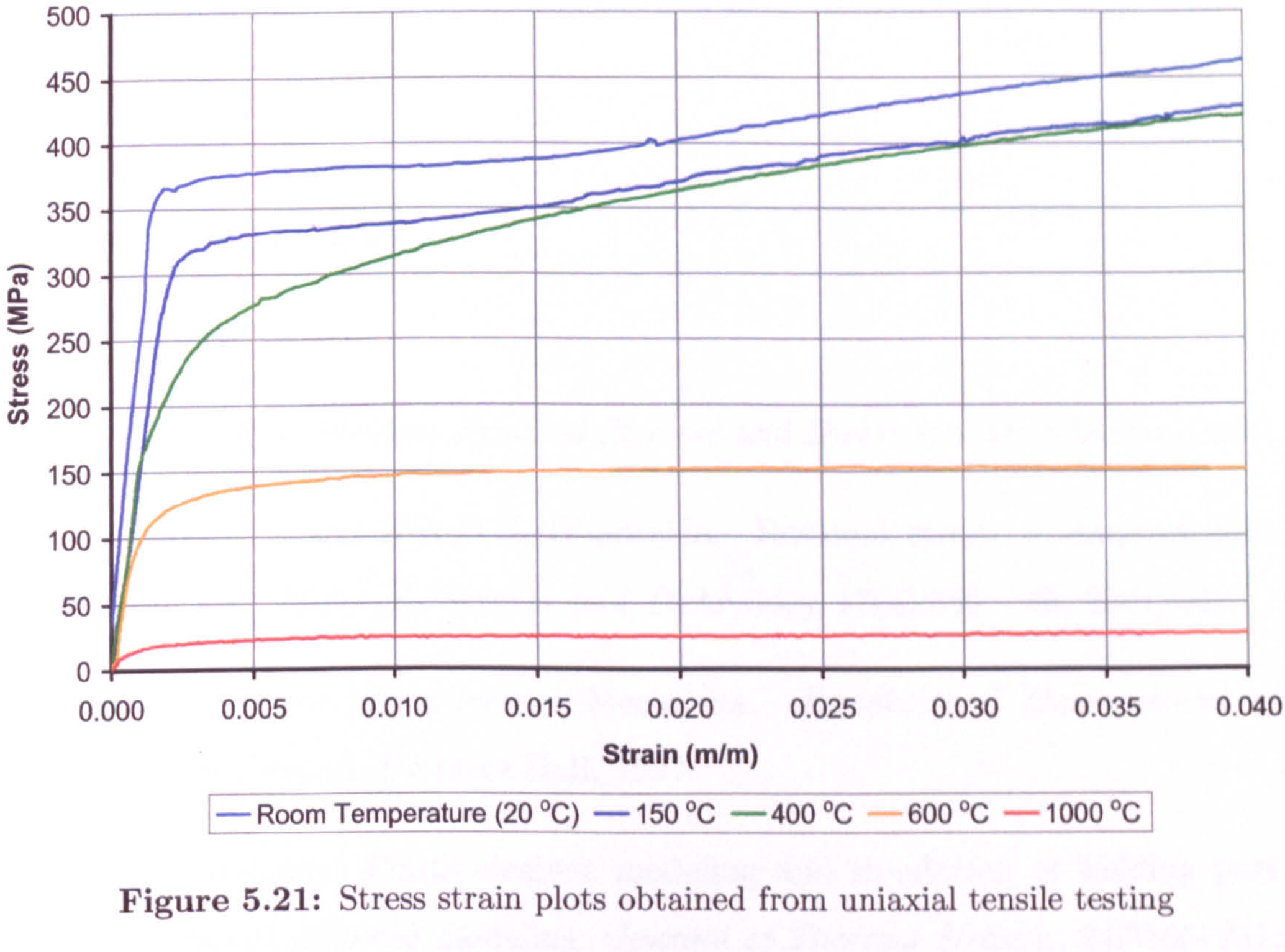

Figure 5.21: Stress strain plots obtained from uniaxial tensile testing

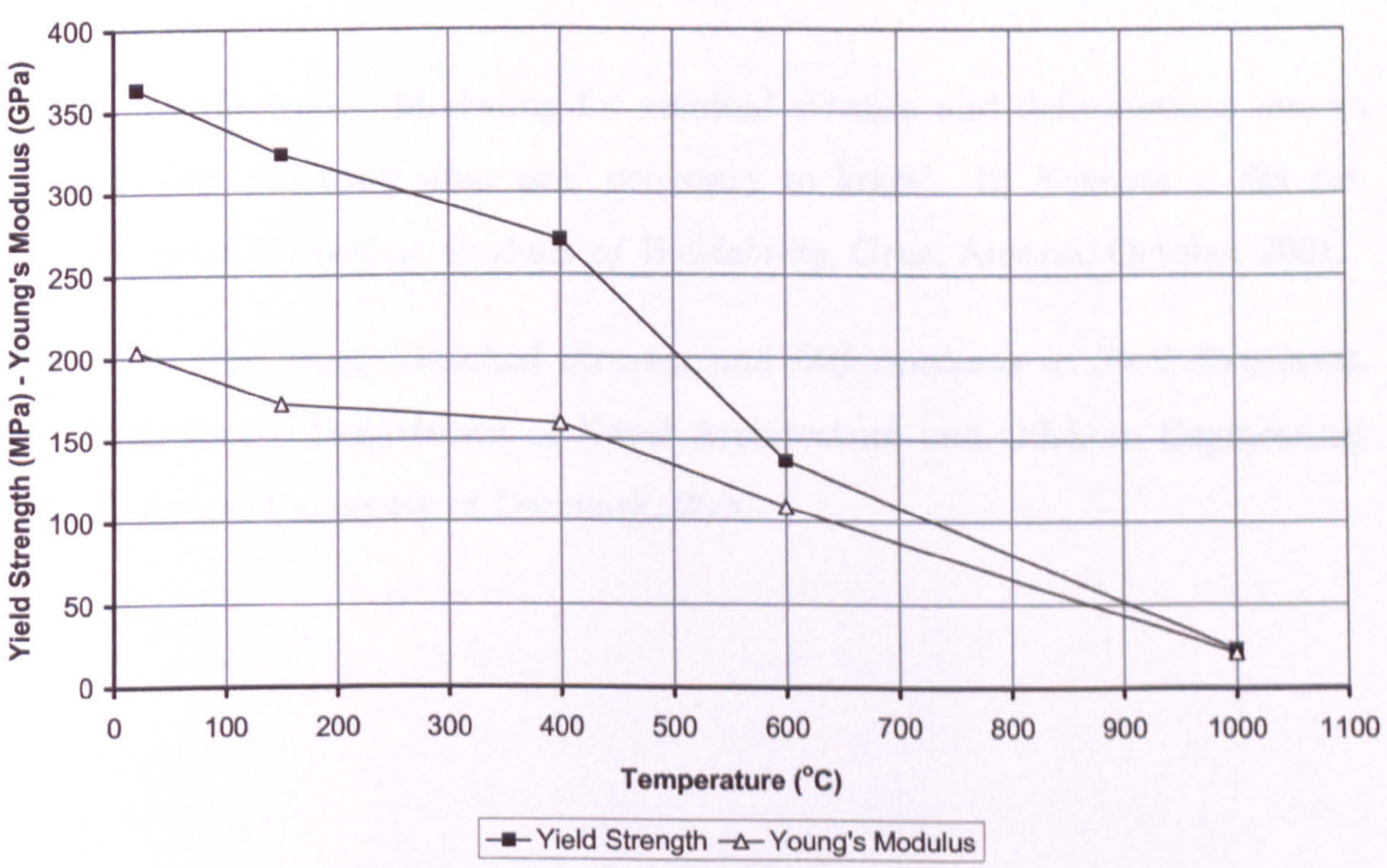

Figure 5.22: Yield strength and Young's modulus extracted from the tensile testing data

References

[5.1] Dieter Radaj. *Welding Residual Stresses and Distortion.* DVS Verlag, 2003.

[5.2] P.J. Withers and H.K.D.H. Bhadeshia. Residual stress. 1. measurement techniques. *Materials Science and Technology*, 17(4):355 – 65, 2001/04.

[5.3] Inc Society for Experimental Mechanics. *Handbook of Measurement of Residual Stresses.* Prentice Hall, 1997.

[5.4] L. E. Lindgren. Finite element modeling and simulation of welding part 2: Improved material modeling. *Journal of Thermal Stresses*, 24:3195–231, 2001.

[5.5] L. E. Lindgren. Modelling for residual stresses and deformations due to welding. 'knowing what isnt' necessary to know'. In *Keynote at 6th Int. Seminar Numerical Analysis of Weldability*, Graz, Austria, October 2001.

[5.6] L. F. Andersen. *Residual Stresses and Deformations in Steel Structures.* PhD thesis, Department of Naval Architecture and Offshore Engineering, Technical University of Denmark, 2000.

Chapter 6

Investigation of Fabrication Procedures affecting Welding Induced Residual Stresses and Distortions, Application to Industrial Scenarios

6.1 Introduction

The previous chapters have illustrated the use of simulation for the prediction of induced residual stresses and distortions in cases dealing with continuous butt and fillet welding of thin plates. These methods were developed using general purpose finite element software in order to keep their applicability wide in scope. It is generally recognised that there are several factors that contribute to the development of residual stresses and distortion, and it is not always possible to include all of them in numerical studies. Even the factors that can be simulated satisfactorally, using the methods presented earlier, are often kept constant or disregarded in order to to simplify the analysis.

The current chapter sets out to investigate two factors that are often disregarded, namely: the effect of restraints imposed on the structure during welding, and the tack welds that are placed prior to the deposition of a full continuous weld. The investigation is carried out on the basis of the validation given in

Chapters 3 and 4 on simple cases of butt welding and fillet welding.

Interest in these two aspects of welding distortion stems directly from industry. The use of restraints during welding is a practice that is usually carried out in the sub-assembly stage, since it is the most obvious and practical remedy to contain problems of distortion for consecutive assembly stages. It is therefore of interest to simulate such practice in order to determine whether, and to what extent, the beneficial effects outcome the detrimental ones, and to see if a best practice can be deduced from the simulation results.

In the case of tack welds, most research work dealing with the prediction of welding induced distortion and residual stresses attribute little importance to the processes and parameters affecting the initial conditions of the structure. This, however, is not always justified as, for instance, it has been previously demonstrated that the shape of the structure prior to full welding has an important effect on the final distortion. This is especially true when one considers that the use of simplified modelling techniques has revealed modes of deformation that usually depend highly on the initial shape of the plate/structure. Since the tack welds are essentially the last manufacturing process before the full weld is laid out, it is of interest to investigate the effects this operation has on the final residual stresses and distortions and try to establish a best practice scenario to minimise unwanted distortions and residual stresses.

6.2 Tack Weld Investigation

6.2.1 Case Study Description

Tack welds are short welds placed prior to completion of the main continuous joining welds in the structure. They are usually made with the same welding process as used on the final joint. This results in a weld with similar qualities to the final one, but usually with smaller dimensions. Their main purpose is to keep the adjoining components in the structure in place so that it can be conveniently handled during the final welding process and any spacing is preserved.

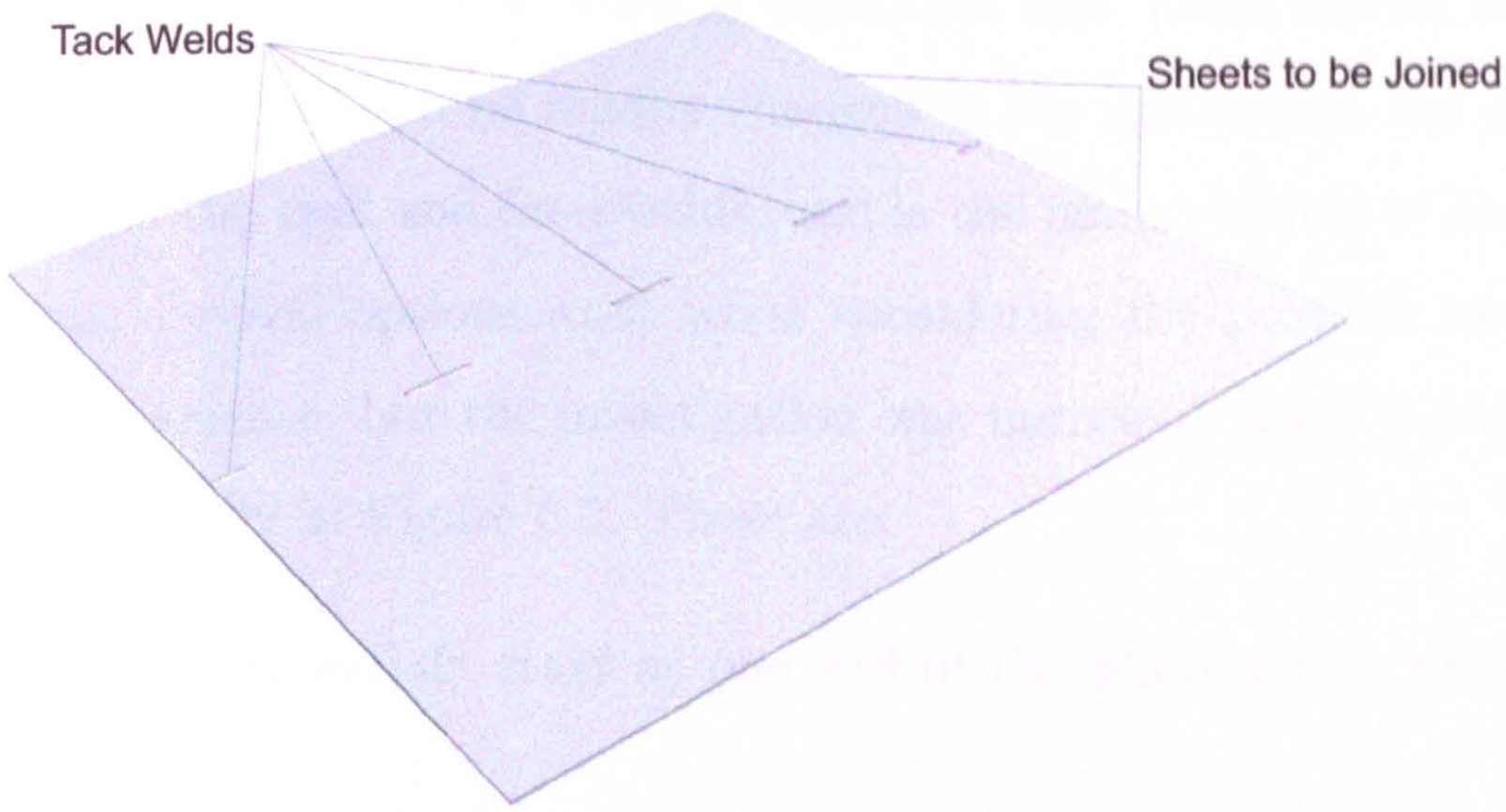

Figure 6.1: Tack welds on rectangular plates

Some researchers have considered the effects of tack welding through experiments and numerical simulation. Abid et al [6.1] investigated the effects of tack welds on a welded pipe flange joint. In their numerical models the authors did not consider the welding of the tacks as such, but placed them as "existing / activated" elements in the model, before starting the structural simulation of the actual main welding process. Hence, the main effect of the tack welds on the computed deformations related to their placement, relative to the start-stop positions in the main welds.

Jonsson et al [6.2] also investigated the effects of tack welding by means of experimental and numerical analyses. Their work focussed on the influence of the tack welding procedure on the change in gap width between the two plates. This is considered to be an important effect, of especial interest for the automation of welding processes. The tack welding procedure was found to strongly influence the change in gap during the final full weld.

The current investigation focuses on tack welds employed prior to butt welding rectangular plates. These are laid out as shown in Figure 6.1 on two 450 × 900 mm plates, 4 mm thick, joined to form a single 900 × 900 mm sheet. The investigation was carried out experimentally and numerically, using the methods validated in previous chapters. The main uncertainty encountered in industry with regards

to this procedure concerns the order in which the tack welds should be placed. This is something that can be readily changed to try and reduce the distortion caused by both the tack and final welds, and is the main variable of the current investigation. Several options exist when considering the possible variation in tack welding sequence, but the investigation was narrowed down to three cases, shown schematically in Figure 6.2. These are:

- Case 1T - Sequential: start at one end of the plate and move along the length
- Case 2T - Ends First: start at the two ends of the plate, continue from the middle and move outwards in a circular fashion
- Case 3T - Centre First: start from the middle of the plate and move outwards in a circular fashion

The sheets had to be kept together prior to the tack welding in order to handle them during the experiment. They were joined by three to four small spot welds placed on one side of the sheets. Although the three combinations for the tack welds were the main variable for the current investigation, the placing of the spot welds turned out to have a strong influence on the final results. This was not anticipated and led to a more complex outcome for the distortion results as explained later.

6.2.2 Thermal Transients Experimental Investigation

For the experimental trials, nine plates were considered in total, three for each case. The thermal effects were captured in two stages. Firstly, a small plate was manually tack welded by a skilled welder in order to obtain an initial typical example of such welds. The welds were carried out with the same equipment and settings that would be used to make tack welds on large sub-assemblies. This plate was then sectioned in order to obtain macrographs of the tacks. Although it is difficult to achieve identical tack welds, the macro-sections provided a good

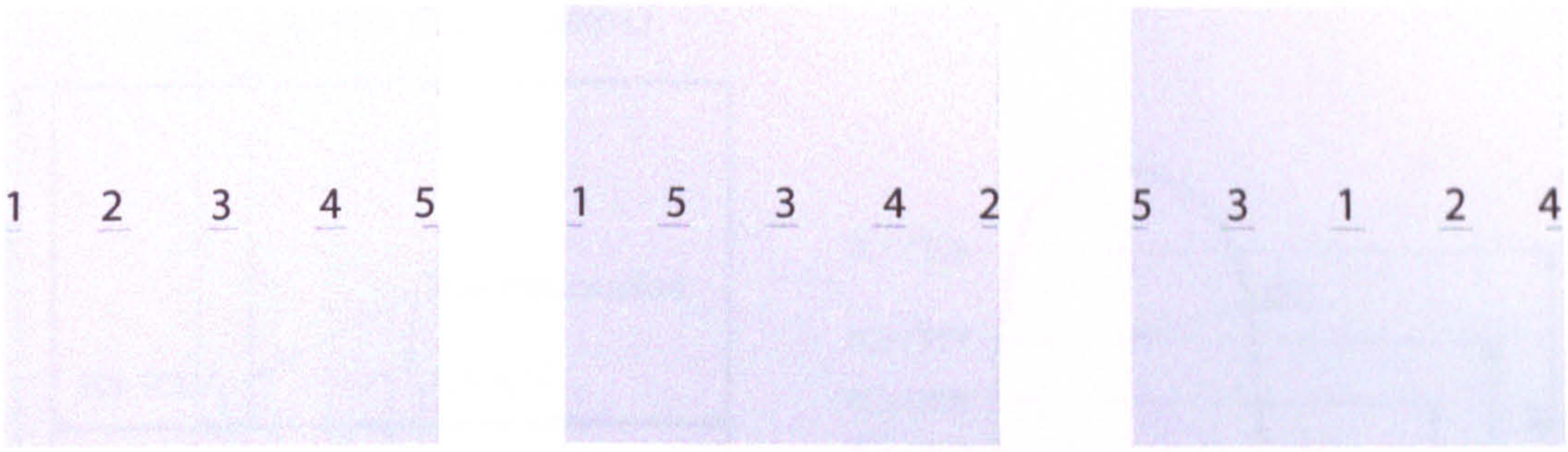

Figure 6.2: Tack Sequences Investigated

starting point as they gave the shape, together with the amount of penetration of the weld. This was particularly useful when setting up the finite element model in the initial stages.

The second phase consisted of the main experimental trial where the plates were tack welded with the three different sequences. The welding was again carried out manually by a skilled welder in order to reproduce conditions encountered during intermediate stages of a typical shipbuilding sub-assembly operation. During tack welding of three of the plates the temperature transients were monitored using thermocouples placed in the positions shown in Figure 6.3. Mineral insulated thermocouples type K were used and these were fitted half-way through the thickness of the plates. Thermocouples were fitted in plates assigned to a different tack welding sequence. These were placed next to two of the tack welds as shown, in order to determine whether the temperature transients of the different tacks interacted.

Results for the temperature transients are shown in Figures 6.4, 6.5 and 6.6 for plates 1, 2 and 3 respectively. It can be noticed that these exhibit a similar pattern to those encountered in previous experimental investigations, showing that the process is indeed similar to the one used for continuous welds. Each graph consists of ten paths, five for each longitudinal position (refer to Figure 6.3). Transient patterns for thermocouples having the same transverse positions (TC1 and TC6,

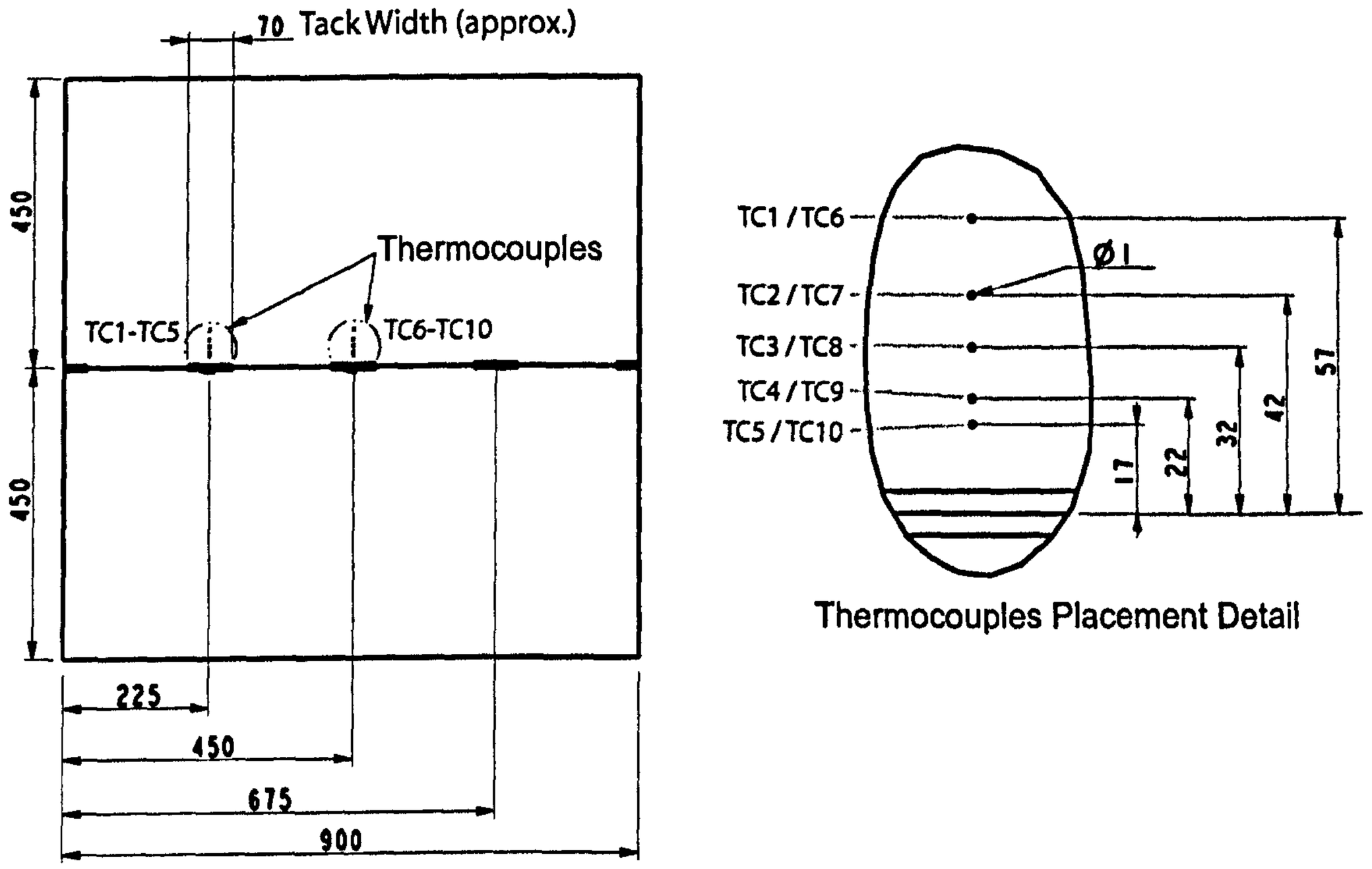

Figure 6.3: Thermocouple positions for the tack welding investigation

TC2 and TC7 etc) should, in theory, exhibit similar patterns, only shifted in time. In practice differences occurred, most noticeable from a comparison of the maximum temperatures reached throughout the cycle (Figure 6.7 (a)). These differences are expected because of the variability of the process, which was carried out in a manual fashion. The largest variations were encountered in transverse positions closest to the weld. This is to be expected as the highest temperatures are those that are dictated by the localised effects of the welding process, which are bound to be slightly different for each tack weld. Nonetheless the data is still useful for the purpose of simulation and the investigation presented here. As shown in Chapter 4 the driving force for the distortions are the maximum temperatures achieved during the entire weld cycle. It is hence of interest to compare these with predictions obtained from Finite Element Analysis (discussed later); this is shown in Figure 6.7.

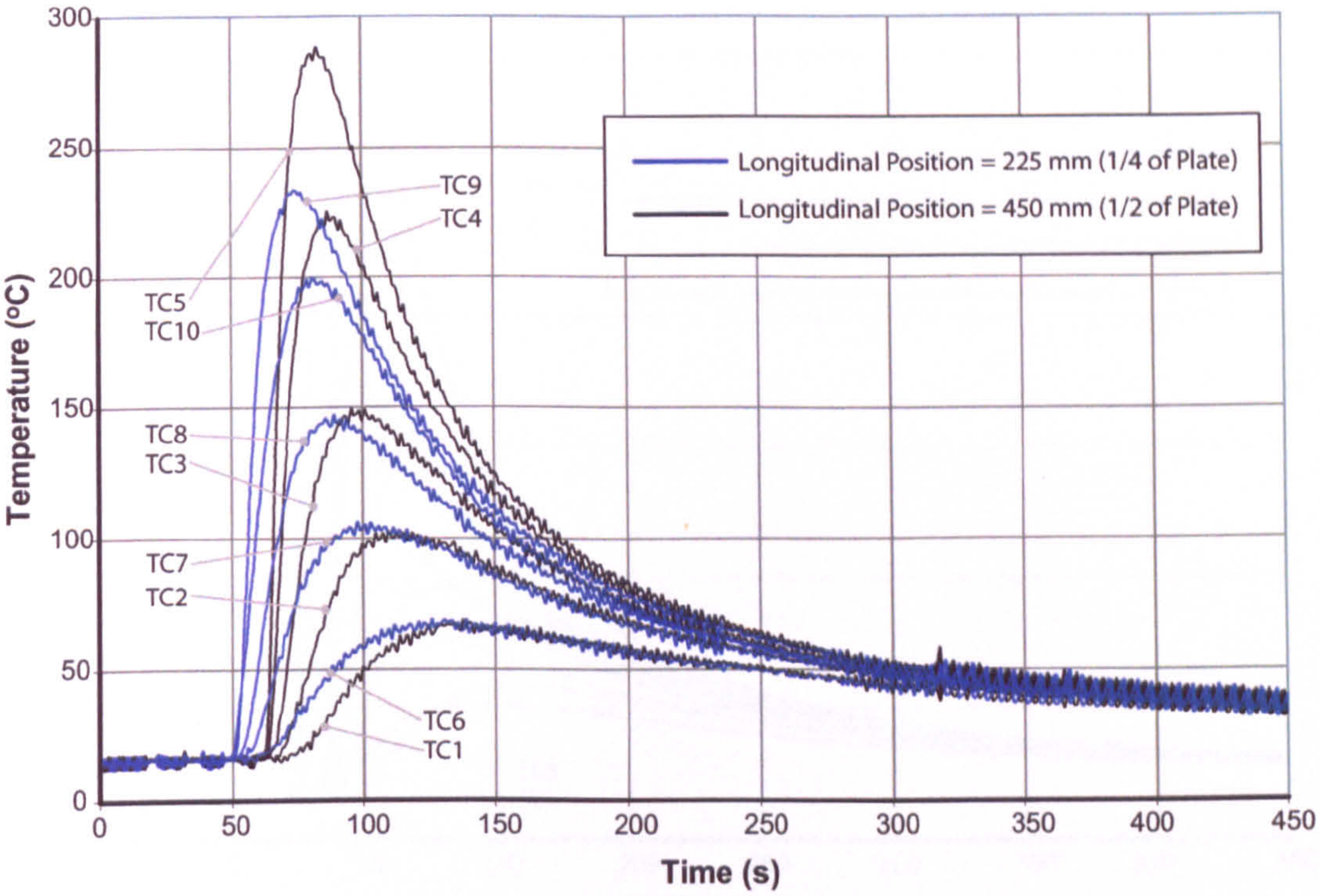

Figure 6.4: Temperature transients for the tack welding trials - Plate 1

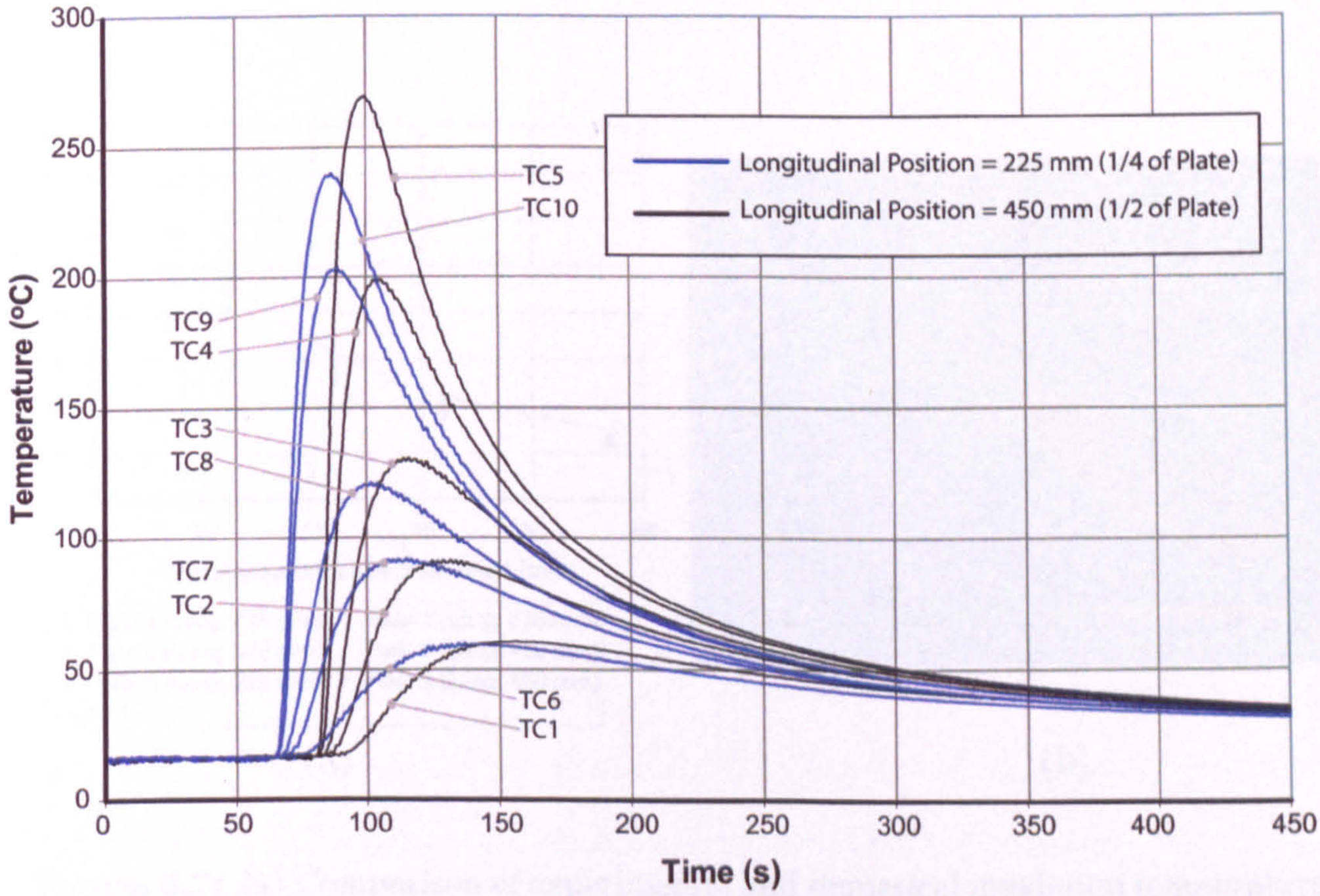

Figure 6.5: Temperature transients for the tack welding trials - Plate 2

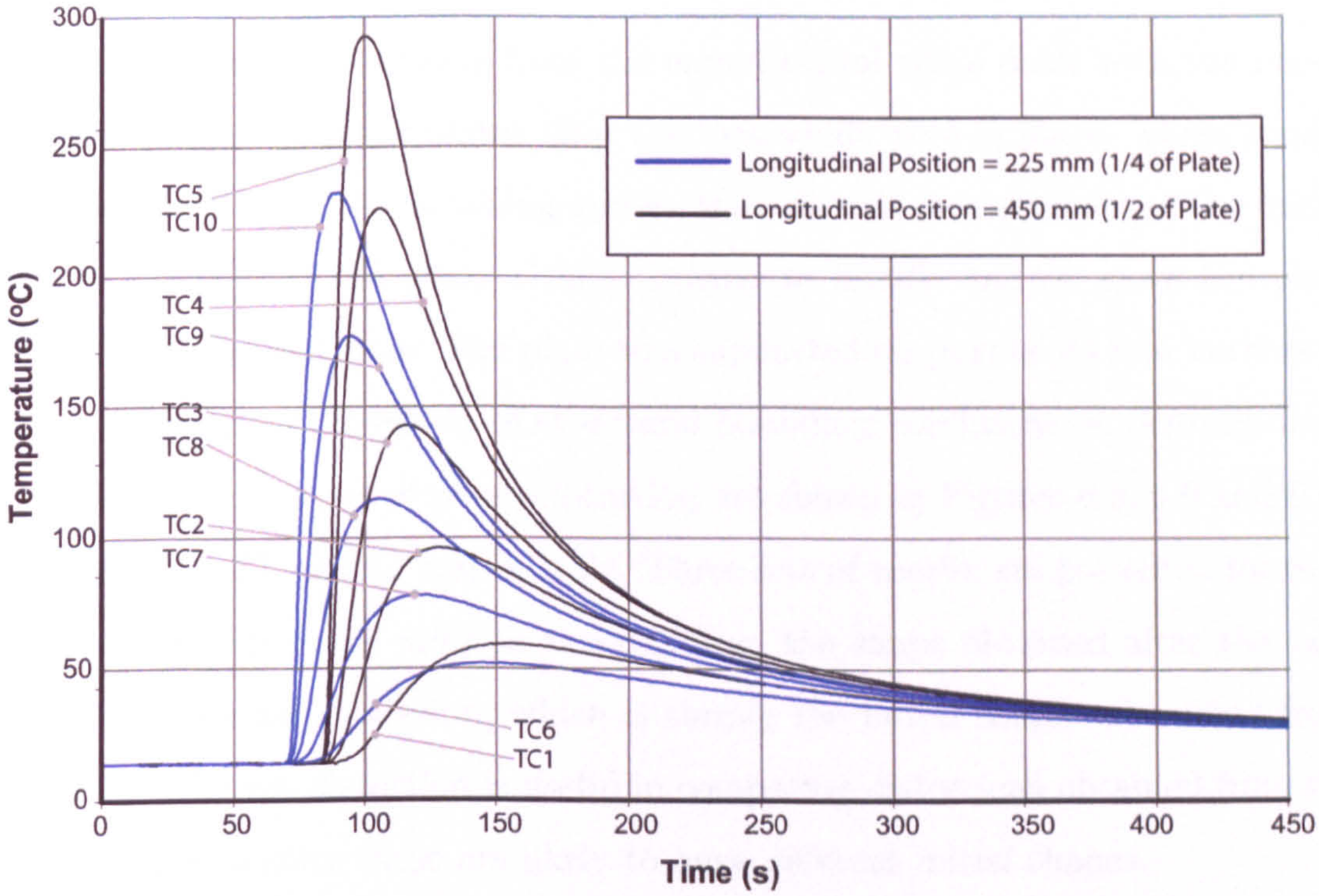

Figure 6.6: Temperature transients for the tack welding trials - Plate 3

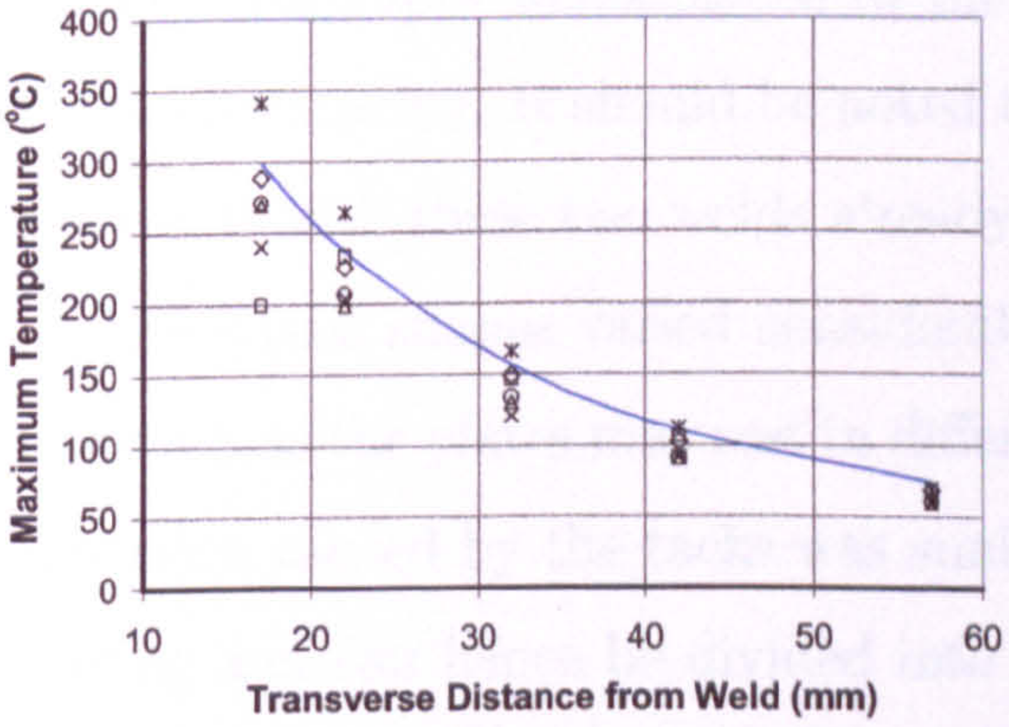

(a)

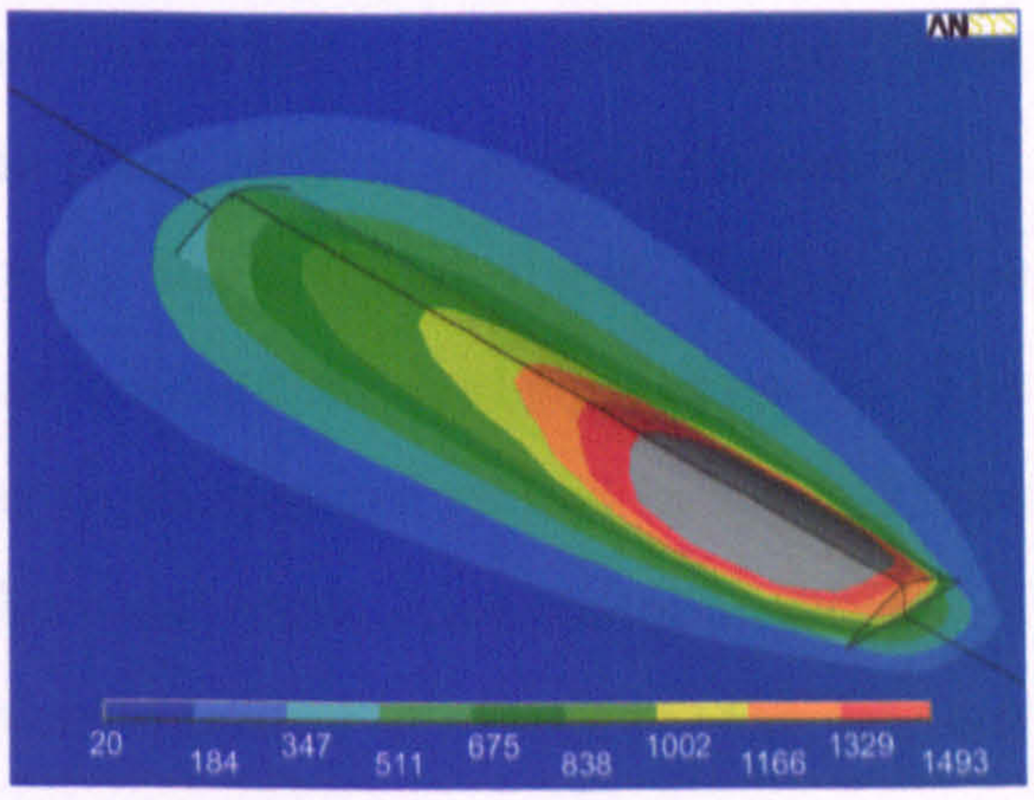

(b)

Figure 6.7: (a) Comparison of experimental and numerical maximum temperature transients. (b) Contour plot of predicted temperature field for a single tack weld

6.2.3 Out of Plane Distortion Experimental Investigation

The next set of results taken from the experimental trials dealt with the out-of plane deformation of the plates after the tack welds were in place. These results were acquired by a laser scanning system that allowed measurement of the initial and final shape of the plate without having to handle and/or move the plate before or after weld runs. The plate was supported on pins at its four corners in order to minimise the effects of structural boundary conditions on deformations.

Results for the out of plane distortion are shown in Figures 6.8, 6.9 and 6.10 for Cases 1T, 2T and 3T respectively. Three sets of results are presented for each case: the initial shape prior to tack-welding, the shape obtained after the tack welds and the net distortion, which is simply the initial shape subtracted from the final. The net distortion is useful in comparing distortions obtained from the different plates since these are likely to have different initial shapes.

Since the plates were supported before tacking under their own weight on four points only, they had to be held together initially in order to place them on the rig and handle them during the experiments. This retention was effected by two or three small spot welds placed at the ends of the edges to be joined (i.e. prior to the main tacks). It should be noted that the 'initial shape' given in the figures was taken with these two welds already in place, with the sheets held together.

The initial shapes varied considerably for the different plates. This is to be expected, as the plates may rest in different orientations on the pin supports. The distortion caused by the tacks was similar to the pattern caused by normal butt welding and can hence be divided into the usual three main components of out-of-plane, angular and longitudinal distortion. Looking at results for the net tack distortion, two main trends for the out of plane deformation can be noticed. For plates 5, 6, 4, 7, 8 and 9 the plates distorted in the direction favoured by sagging under gravity between the end supports, producing predominantly longitudinal distortion. For the remainder of the plates (1, 2 and 3) the opposite happened, distortion took place upwards in the transverse or angular sense with a much

larger mean value. Such significant differences were initially unexpected and turned out to be influenced by the placement of the initial spot welds, as these were different for the plates exhibiting the larger out of plane distortions. The latter were the ones for which the tack welds were placed on the same side of the plate as the spot welds. For the remainder of the plates all the tack welds were instead placed on the opposite side from the spot welds. Root mean square values for the out of plane, angular and longitudinal distortion are shown in Figure 6.11.

It is apparent how the method of retaining the plates prior to the tack welding is critical for the final outcome of the induced distortions. Placing these initial spot welds on the opposite side of the tack welds yielded considerably lower distortions and is therefore a better approach.

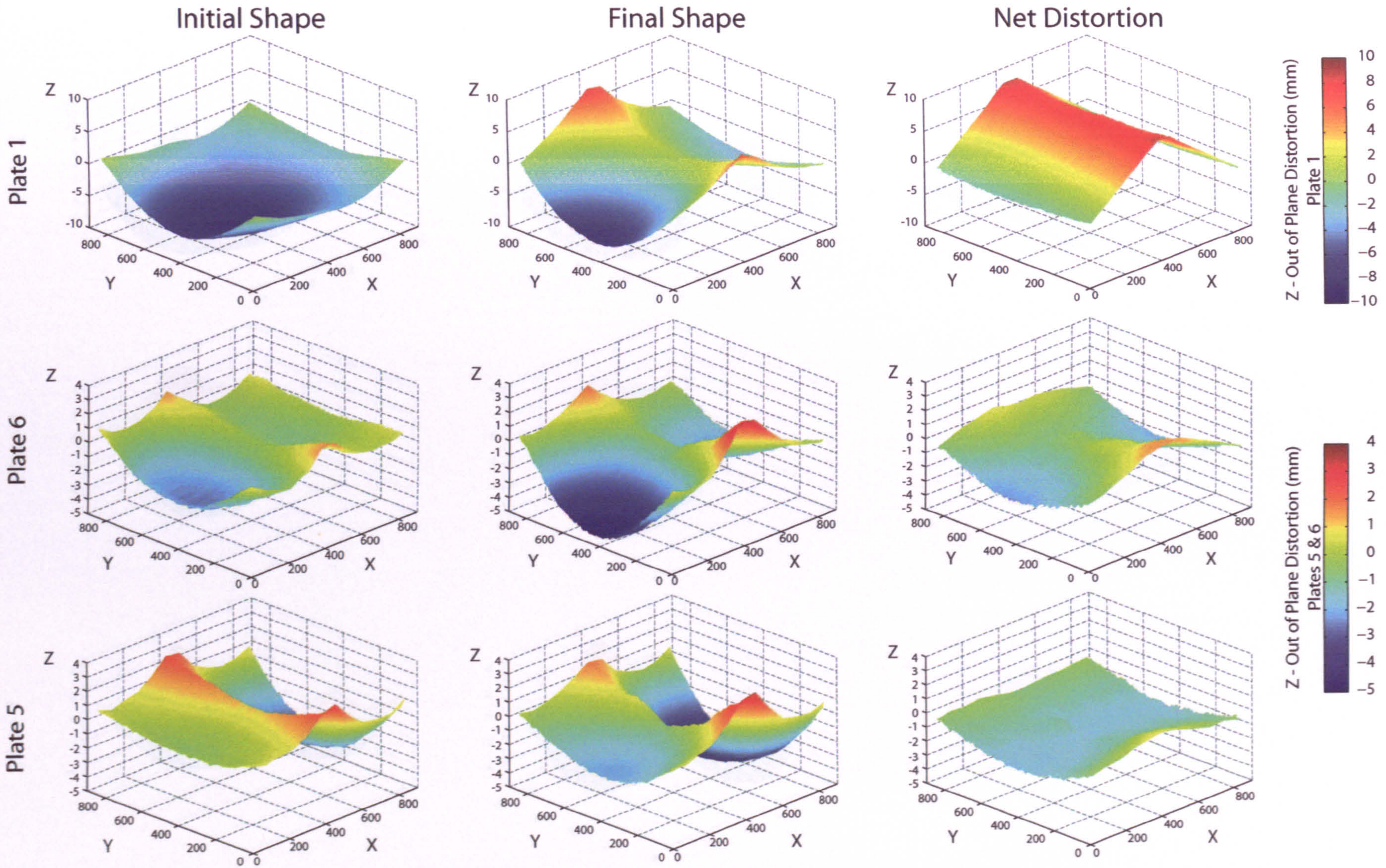

Figure 6.8: Case 1T - Sequential - Out of plane distortion for the tack welding investigation. Legend: Z - Out of plane deformation (mm); Y - Along weld (mm); X - Transverse to weld (mm)

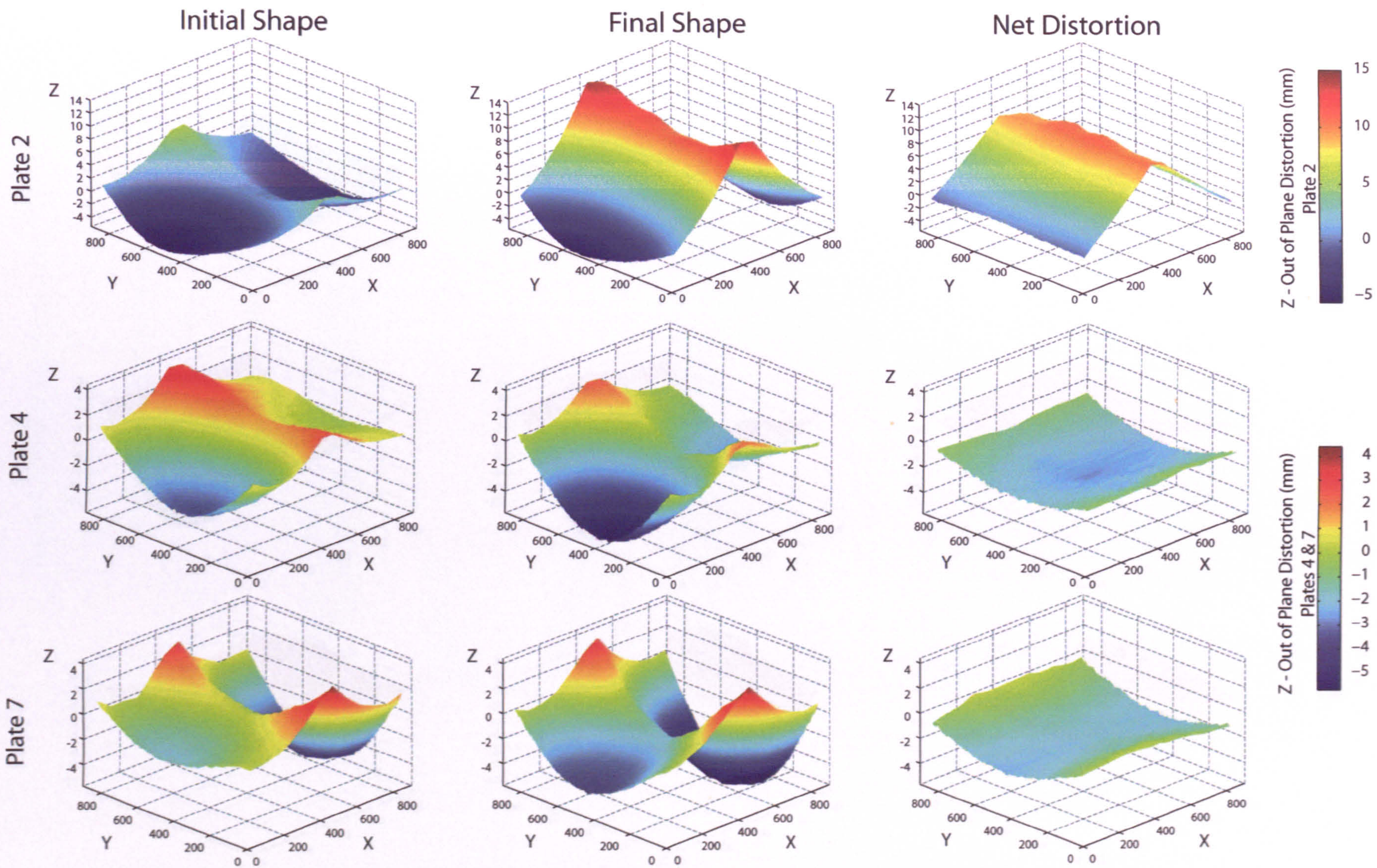

Figure 6.9: Case 2T - Ends first - Out of plane distortion for the tack welding investigation. Legend: Z - Out of plane deformation (mm); Y - Along weld (mm); X - Transverse to weld (mm)

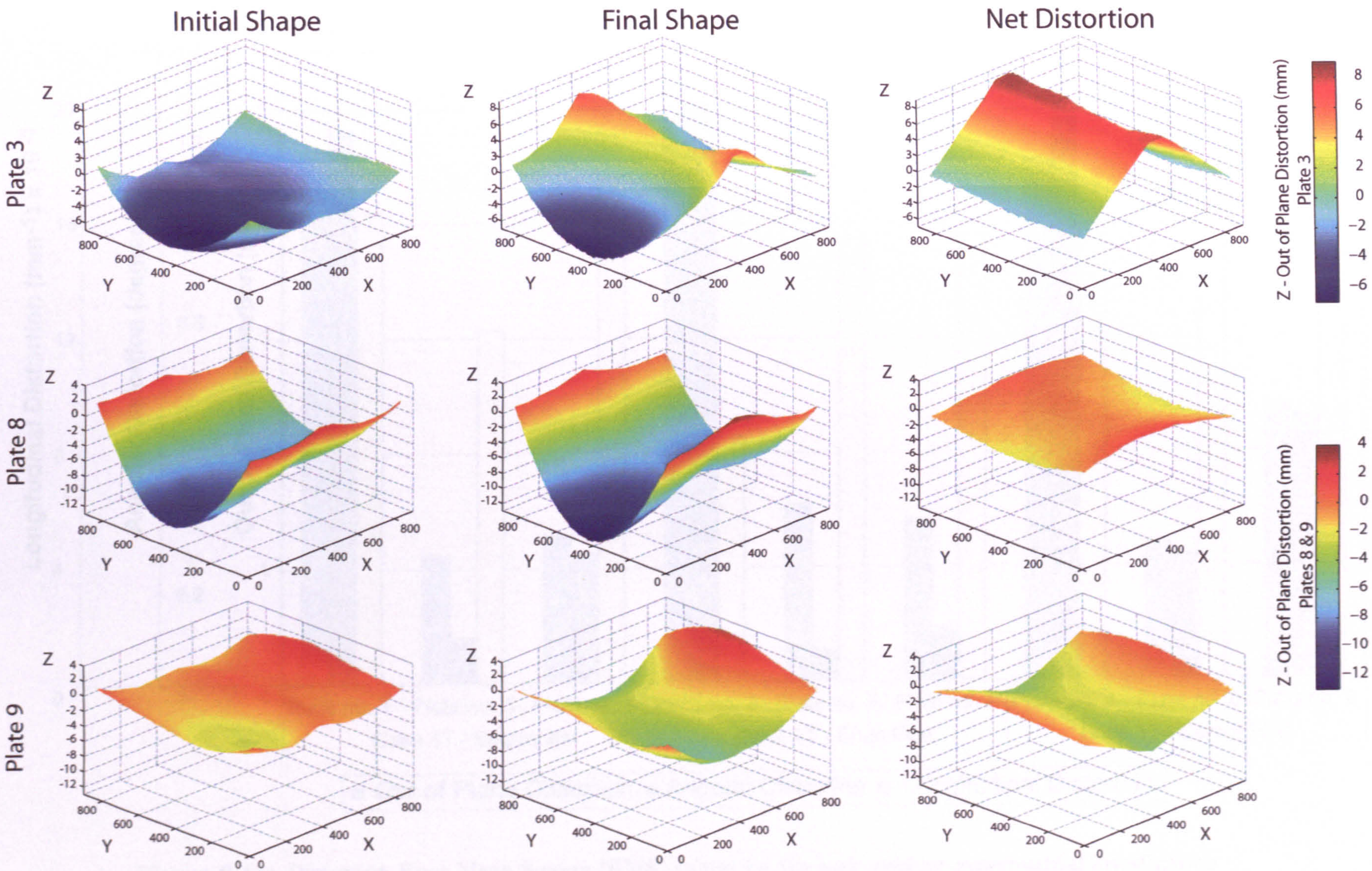

Figure 6.10: Case 3T - Centre first - Out of plane distortion for the tack welding investigation. Legend: Z - Out of plane deformation (mm); Y - Along weld (mm); X - Transverse to Weld (mm)

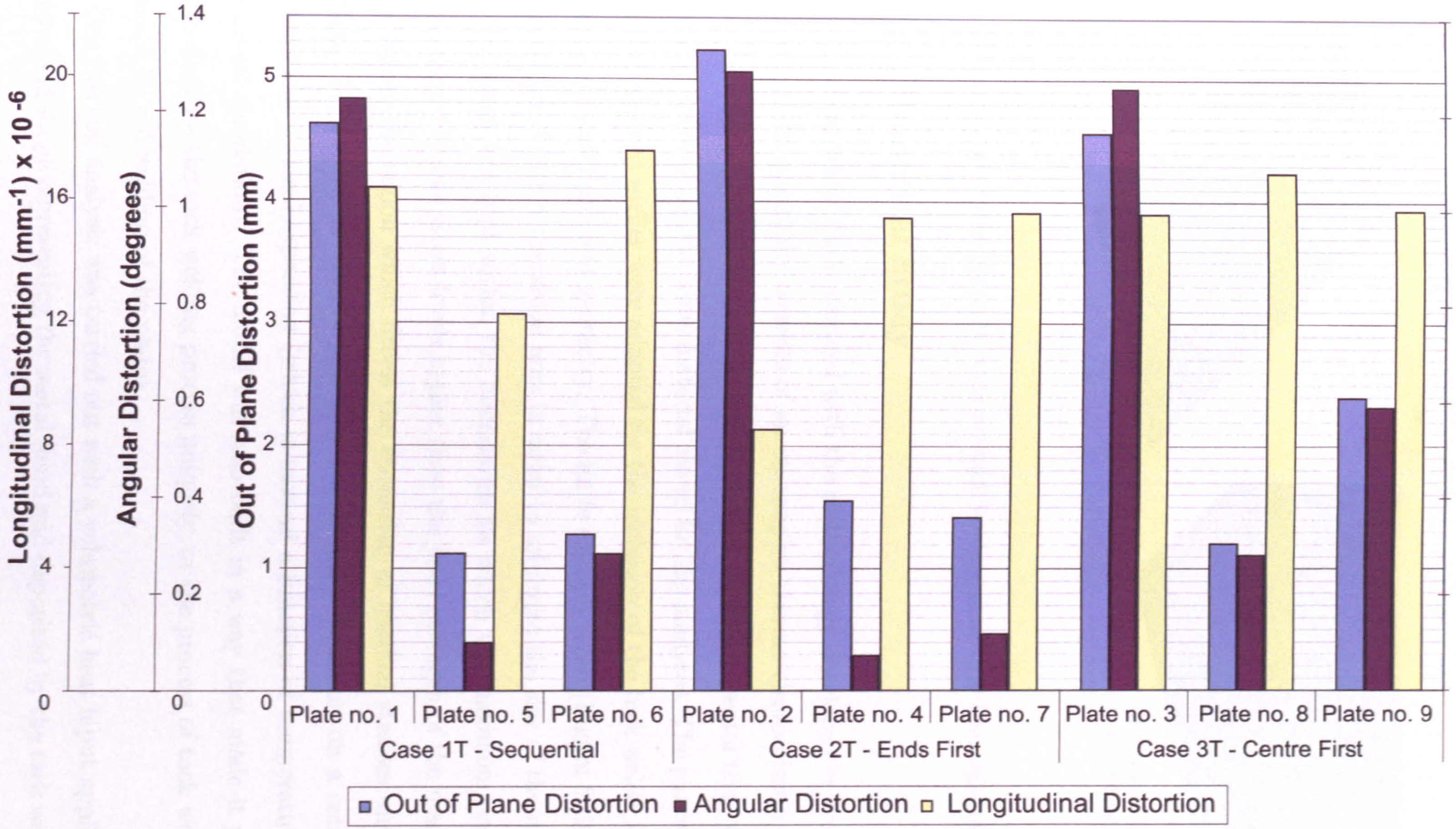

Figure 6.11: Distortion Root Mean Square (RMS) values for the tack welding experimental investigation

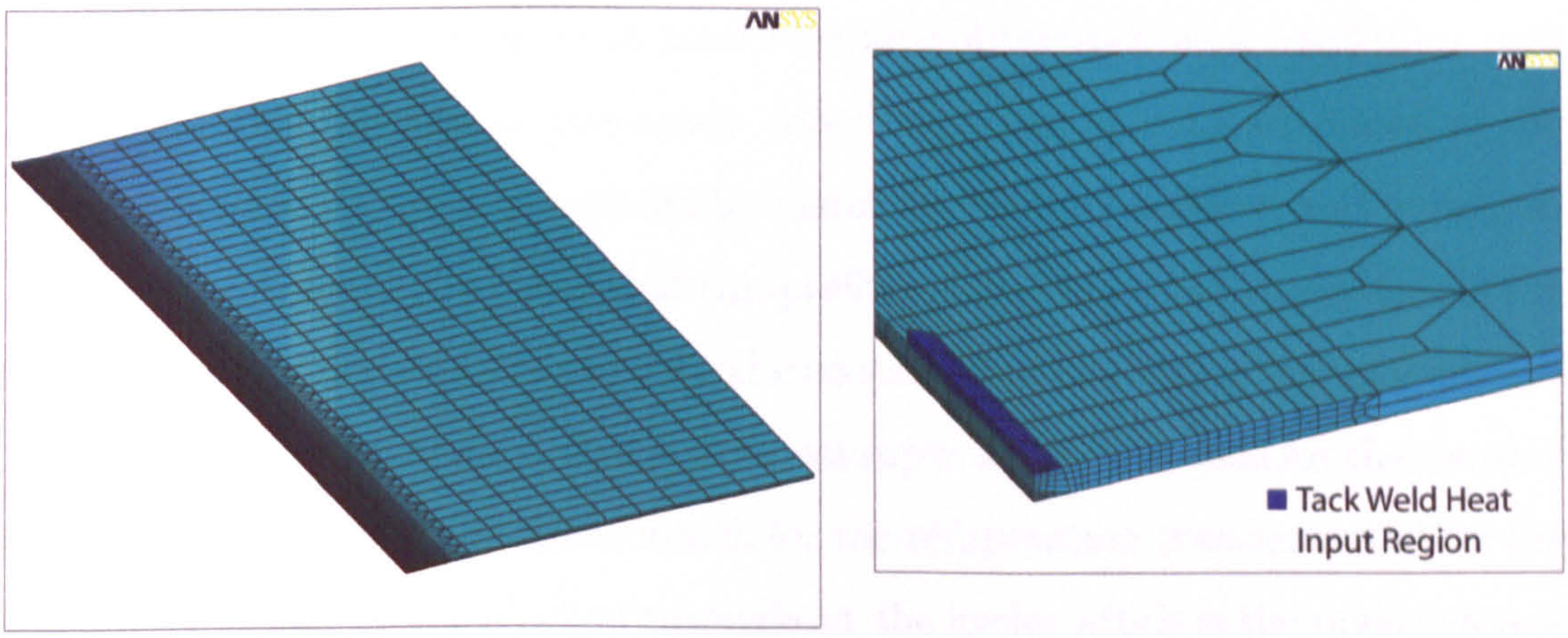

Figure 6.12: Finite Element mesh for tack welding numerical investigation

6.2.4 Numerical Study

The numerical study was performed with the methodology developed in previous chapters, which essentially consists of an un-coupled thermo-elasto-plastic simulation. The same class of material was also used for the experimental trial, which made it possible to use the same material model for the analyses. The parametric models developed earlier were adapted for the inclusion of the tack welds, which required a slightly different geometry. The finite element mesh (Figure 6.12) was again designed with a transition area in order to minimise the size of the model. The fine mesh was kept within the boundaries for which the maximum temperature reached causes stress levels higher than the yield strength of the material, since this is the region which drives the formation of residual stresses and distortion. This could be done *a priori* by basing the calculation on a constant coefficient of thermal expansion (which is instead a function of temperature for the actual simulation). The model was also built in a way that made it possible to simulate the tack welding process uniquely, or the process of tack welding followed by full welding of the plates.

The thermal analysis was carried out with a volumetric heat input applied to an idealised shape representing the metal fused and deposited by the tack welding

process. This shape was based on macro sections obtained from a small plate tack welded for this purpose as previously described. The thermal efficiency of the welding process was then computed by matching up the predicted and measured fused zones. It should be noted that this preliminary study was independent of the main trials, but nevertheless proved to be successful in predicting the temperature transients of the main trials. Hence this heat input model was used for the thermal analysis and yielded a very close match for the temperature transients and for the maximum temperatures reached throughout the cycle, which is the main interest (Figure 6.7). Comparison of experimental and predicted fusion zone is shown in Figure 6.13. The simple heat input model provided a good match, which is however made easier by the *a priori* knowledge of the area to which the heat input must be applied. This prediction is not however the main focus of the analysis as, for the purpose of far-field (global) residual stresses and distortions, the match of the maximum temperatures reached throughout the cycle is more important.

Once the temperature transients have been established, the next part of the simulation can be carried out. The algorithm presented in Chapter 3 was implemented. The thermal results file is first scanned to determine which elements have exceeded the cut off temperature. These elements are then deactivated (killed) at the start of the transient structural analysis, only to be re-activated as the heat source is advanced along the plate. The cut off temperature for these analyses was taken to be 1493°C. The remainder of the analysis was also carried out in a manner similar to the simulation techniques presented earlier. Half of the plate was modelled by exploiting the symmetry of the case study. This created constraint in the transverse direction, whilst the plate was constrained in the thickness direction at the two (four in reality) points where the pin supports are found. The numerical model also requires another constraint in the longitudinal direction in order to avoid rigid body motion of the solution, and this was done by simply fixing one node in the middle of the plate in the longitudinal direction. Gravitational loading was included as the plate is large enough for this to have

an effect. Results for the out of plane deformation and the longitudinal residual stresses are shown in Figures 6.14, 6.15 and 6.16 for the three cases investigated.

It can be seen that the computational result show a match in the mode of deformation for plates 4 to 9, i.e. for the plates whose spot welds were on the opposite side from the tack welds. A comparison of root mean square (RMS) values is shown in Figure 6.17, where the type of deformation for plates 1, 2 and 3 is denoted Mode I, whilst the type of deformation for the remainder of the plates is denoted as Mode II. Again the finite element predictions are closer to Mode II for both out of plane and angular distortion. Longitudinal distortion was similar for both modes with the exception of Case 2T (Ends First), which was the only case in which the Mode I distortion was lower than the predicted one.

The predicted residual stresses are also shown in Figures 6.14, 6.15 and 6.16 where contours of the predicted longitudinal stresses (the largest for this kind of set-up) are plotted for the whole plate and shown in detail for a single tack weld. The pattern for longitudinal stress is similar to the one usually observed in continuous welds. The effect is however localised and the tack welds were sufficiently spaced for residual stresses of each tack not to interfere with each other. Figure 6.18 shows a comparison of longitudinal and transverse residual stresses for the different tack welds, i.e. at different longitudinal positions along the plate. Tacks 1 and 2 are taken at the plate edges and show a different stress profile from the other tacks.

6.2.5 Conclusions

The following main conclusions were drawn from the experimental and numerical investigation:

- The simulation techniques developed in previous chapters proved successful in simulating the tack welding process
- Two modes of deformation were observed from the experiment, these being

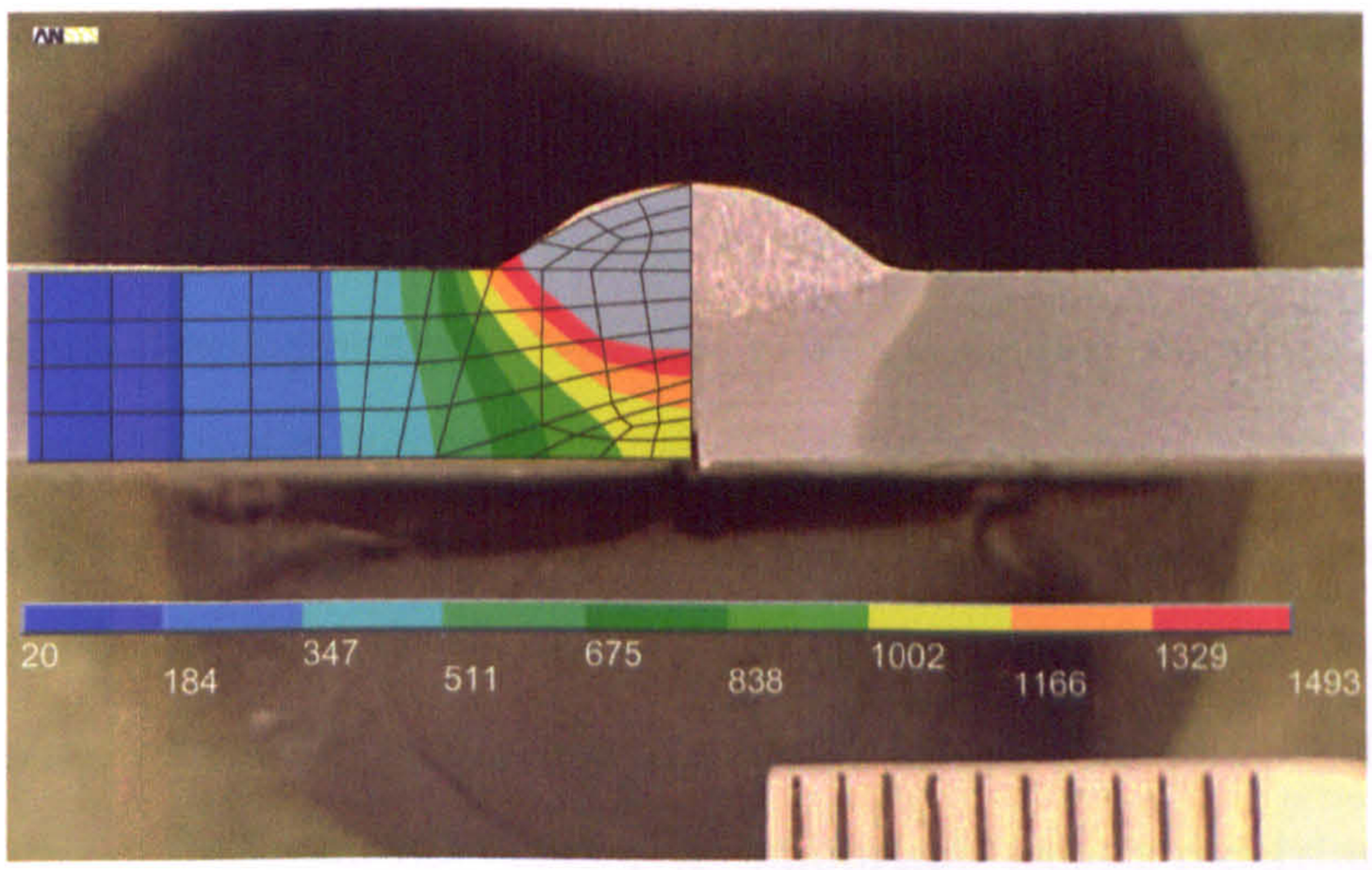

Figure 6.13: Tack weld investigation. Comparison of experimental and predicted fusion zone

determined by placement of the tack welds relative to the spot welds, i.e. on the same side or opposite side

- The Finite Element models predicted one form of deformation, with a relatively close match when comparing RMS distortion values
- The tack welds should be placed on the opposite side of the plate from the spot welds in order to obtain the mode of deformation with the smallest distortion
- Case 1T (Sequential) proved consistently to be the best sequence to adopt in order to minimise distortion, from both the experimental and numerical studies (although differences for this size of plate were small)
- Residual stresses were almost identical for all cases (a graph showing a comparison is not presented as they would yield identical plots)
- Different tacks also yielded the same residual stress profile, with the exception of Tacks no. 1 & 2, which must yield different plots as they are at the plate edges

It should be pointed out that the differences between the Cases (1T, 2T and 3T) were in fact quite small when looking at RMS values of distortion. However the plates are relatively small when compared to sub-assembly structures encountered in shipbuilding practice where larger deformations would be expected. It hence still is of interest to compare the differences obtained in the tack welding investigation for the different cases. Also, a much larger than expected variation was seen between plates exhibiting Mode I and Mode II forms of deformation, which emphasises the importance of the initial shape / conditions in relation to final outcome of deformation. This is an important aspect recurring throughout the various investigations carried out in the current project.

The effect of the spot welds was initially assumed to be minimal but they turned out to have a strong influence on the final results. Looking at the various initial shapes it can be noted that the spot welds yielded consistent modes of distortion, meaning that their influence lay mainly in the restraint offered during the subsequent tack welding process. The drastic difference in shape between deformation Modes I and II suggests a reversal in the *hinge point* offered by the structure to the transverse contraction of the tack welds.

Residual stresses turned out to be almost identical for all tacks and for the three cases, with the exception of the tacks lying on the plate edges. This is due to the lack of surrounding restraining material which inevitably leads to a different stress profile.

It must also be noted that, although this study set out to include aspects affecting welding distortion that were previously not given much attention (i.e. tacks), the simulations by no means cover all aspects that are present during this process and that can affect the final outcome of the deformation. This is especially true for larger subassemblies where there are other aspects not included in the simulations presented here that could affect the outcome of residual stresses and distortion (for instance any intermediate measures that could be taken between tack weld completions).

(a)

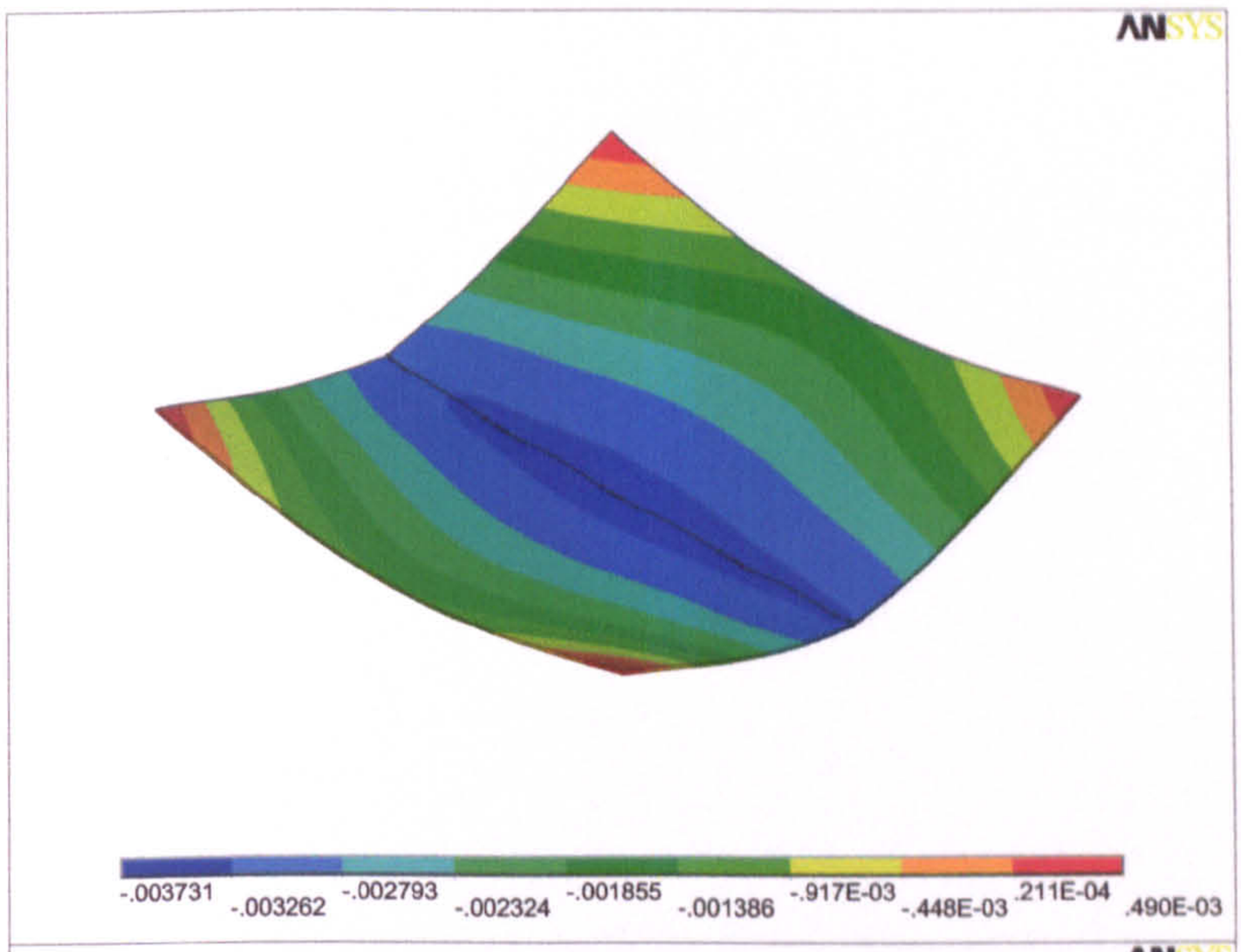

(b)

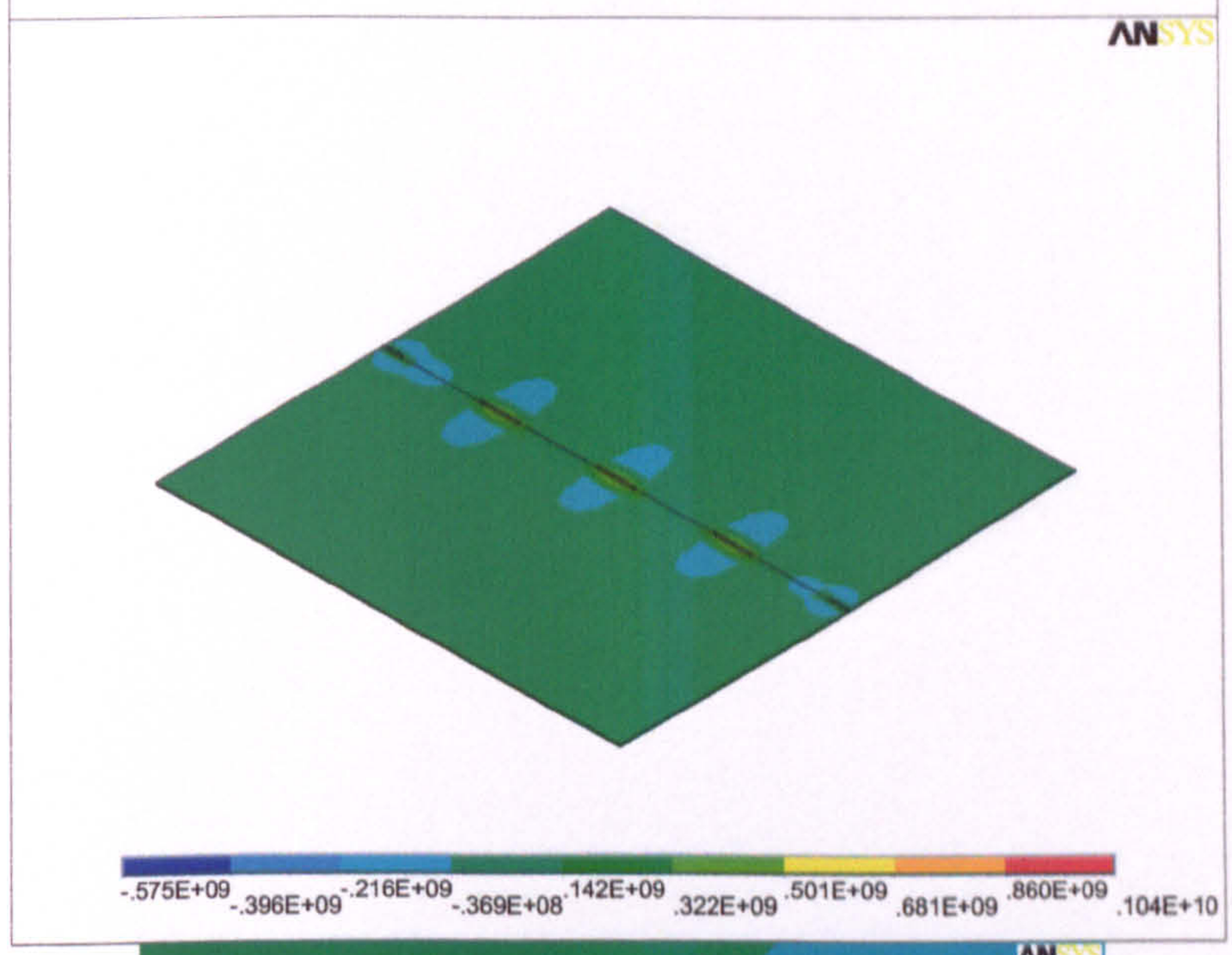

(c)

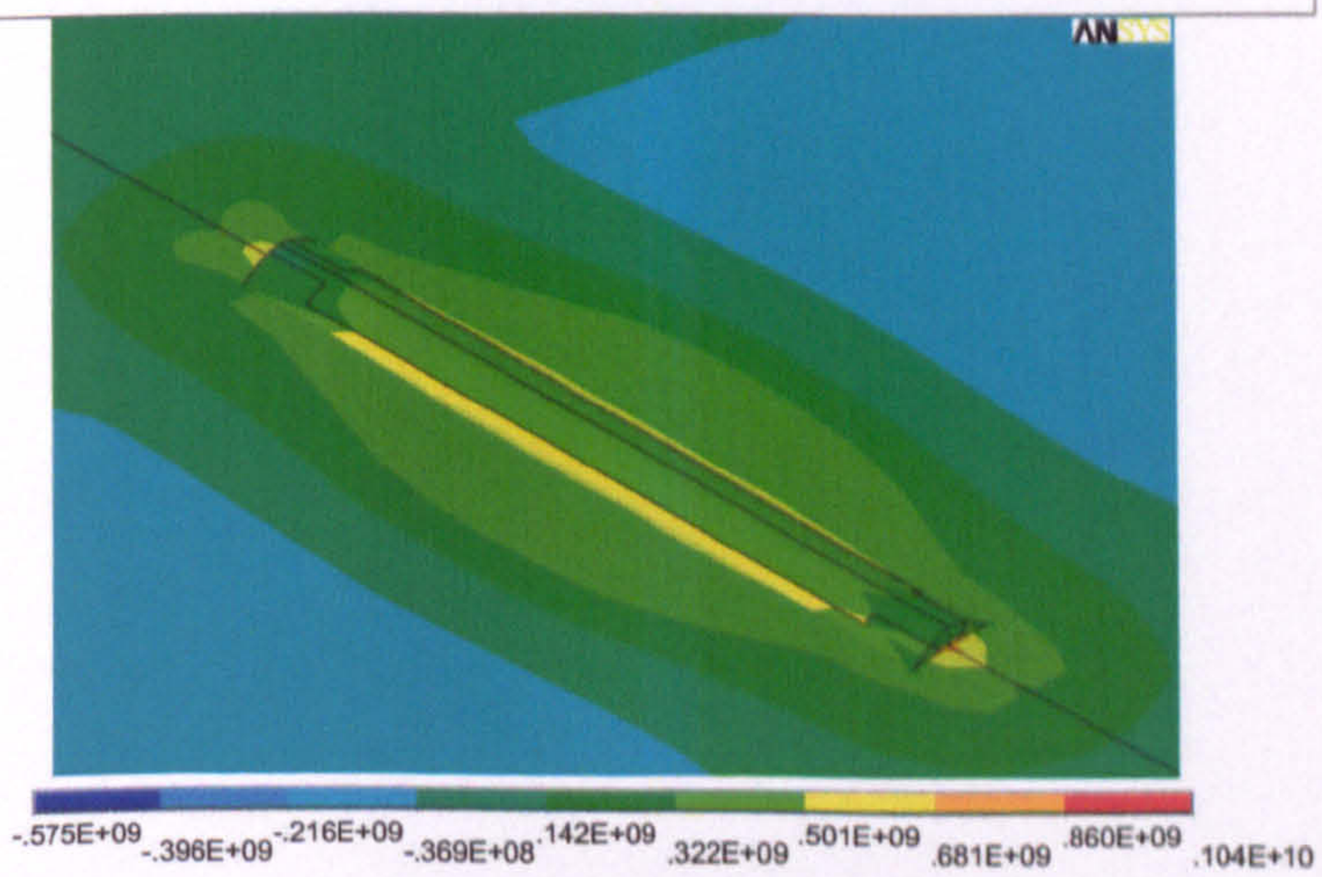

Figure 6.14: Tack investigation Case 1T - Sequential, numerical results. (a) Out of plane distortion (m) (graphical representation amplified by a factor of 40). (b) Longitudinal residual stresses (Pa). (c) Detail for longitudinal residual stresses on a single tack weld (Pa)

(a)

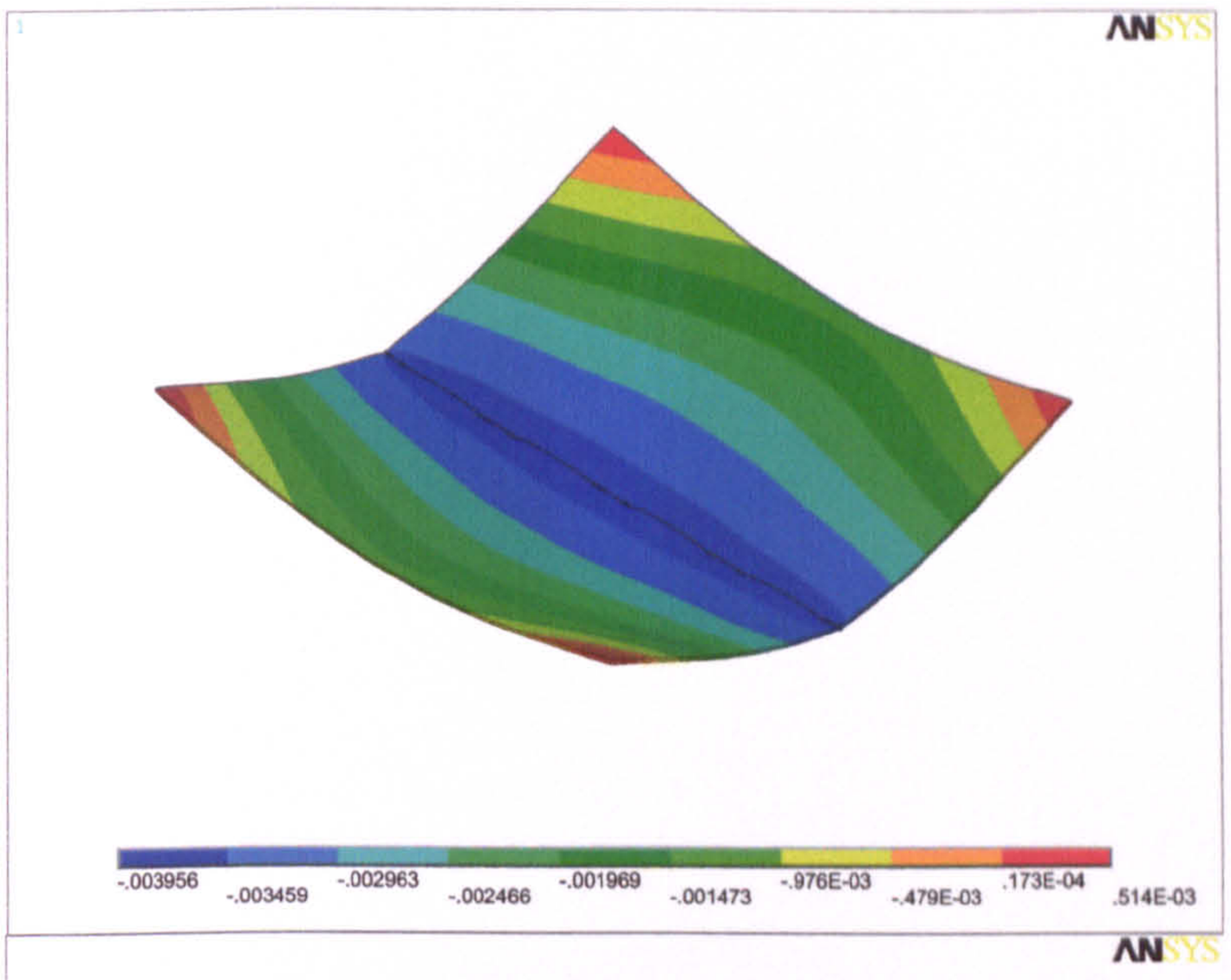

(b)

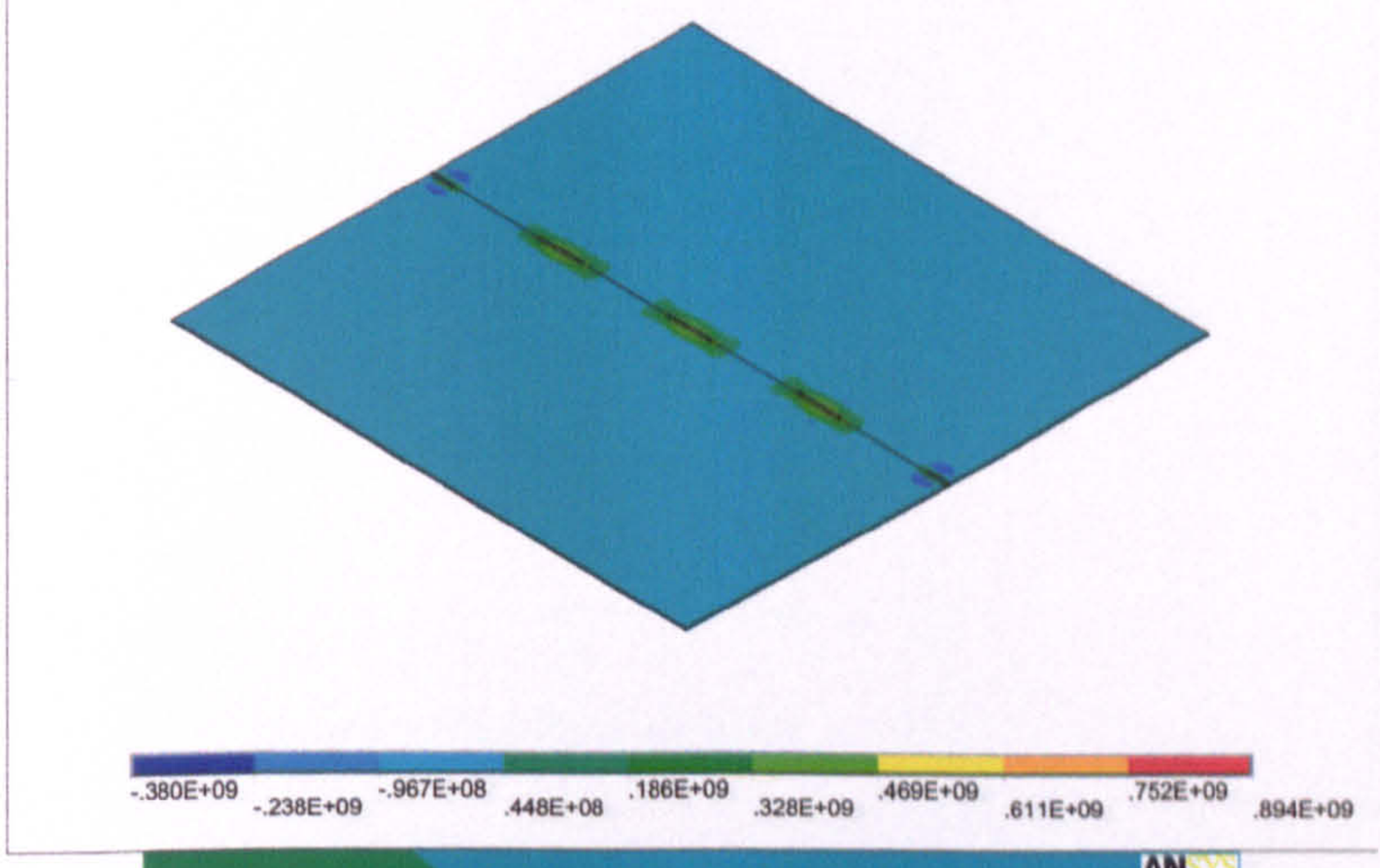

(c)

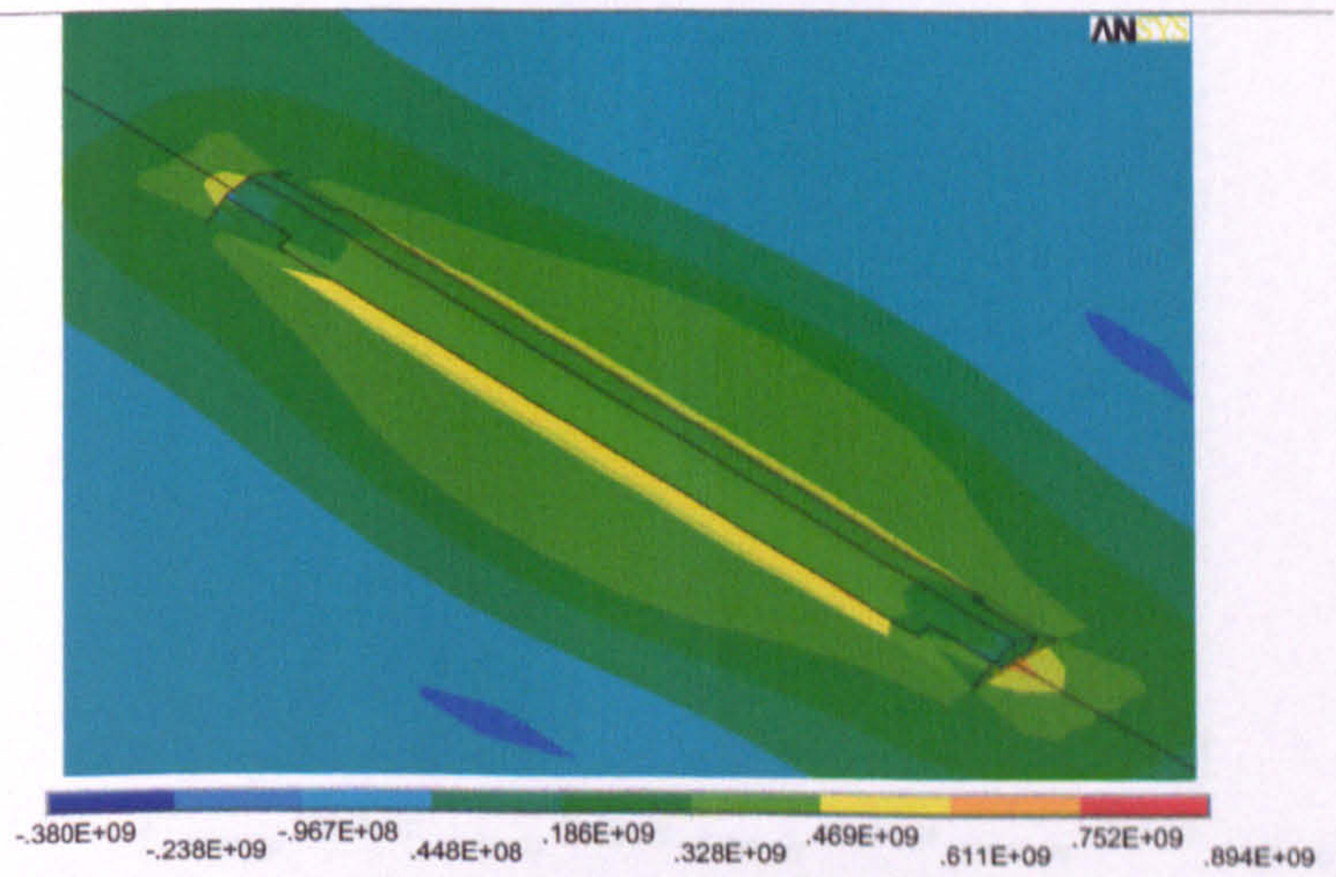

Figure 6.15: Tack investigation Case 2T - Ends first, numerical results. (a) Out of plane distortion (m) (graphical representation amplified by a factor of 40). (b) Longitudinal residual stresses (Pa). (c) Detail for longitudinal residual stresses on a single tack weld (Pa)

(a)

(b)

(c)

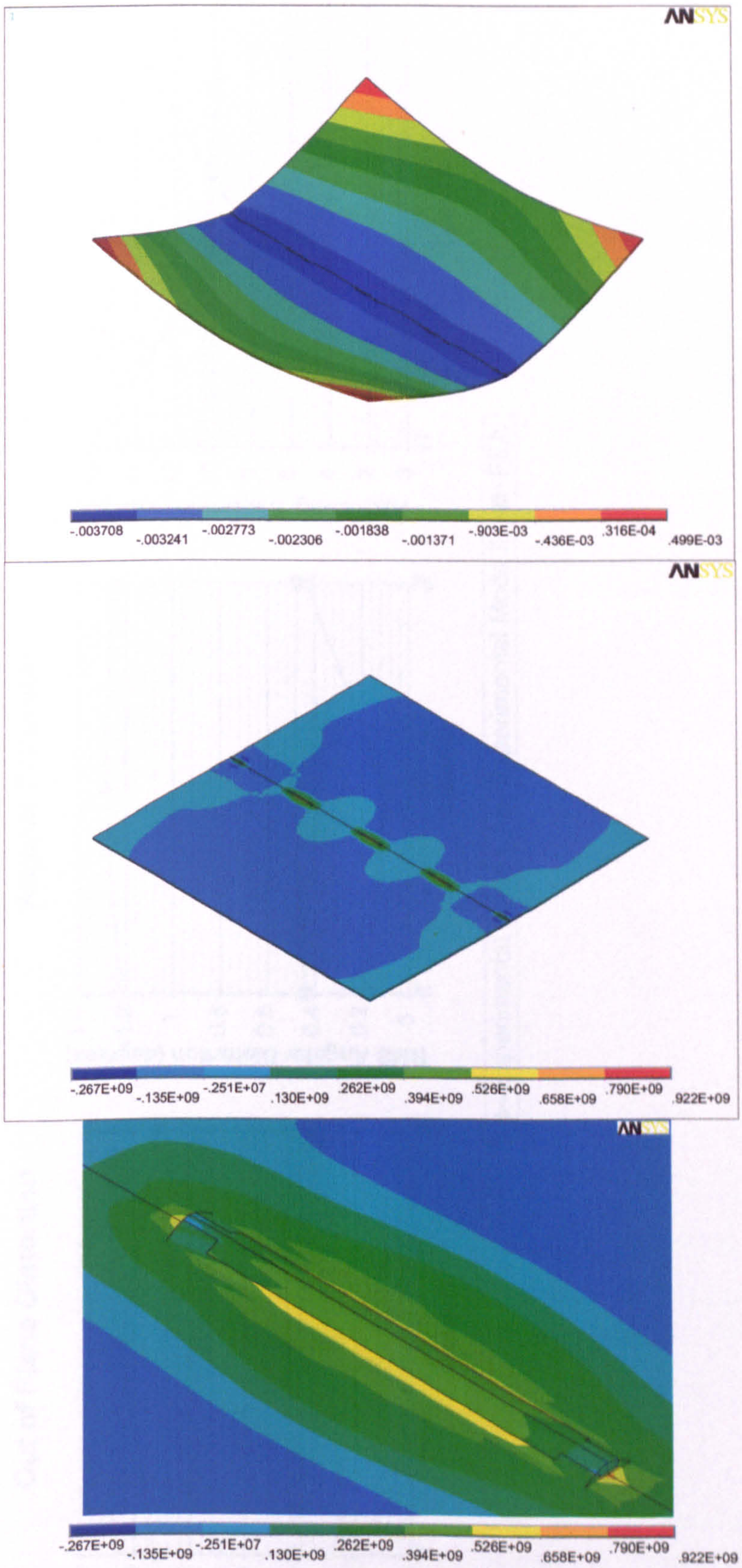

Figure 6.16: Tack investigation Case 3T - Centre first, numerical results. (a) Out of plane distortion (m) (graphical representation amplified by a factor of 40). (b) Longitudinal residual stresses (Pa). (c) Detail for longitudinal residual stresses on a single tack weld (Pa)

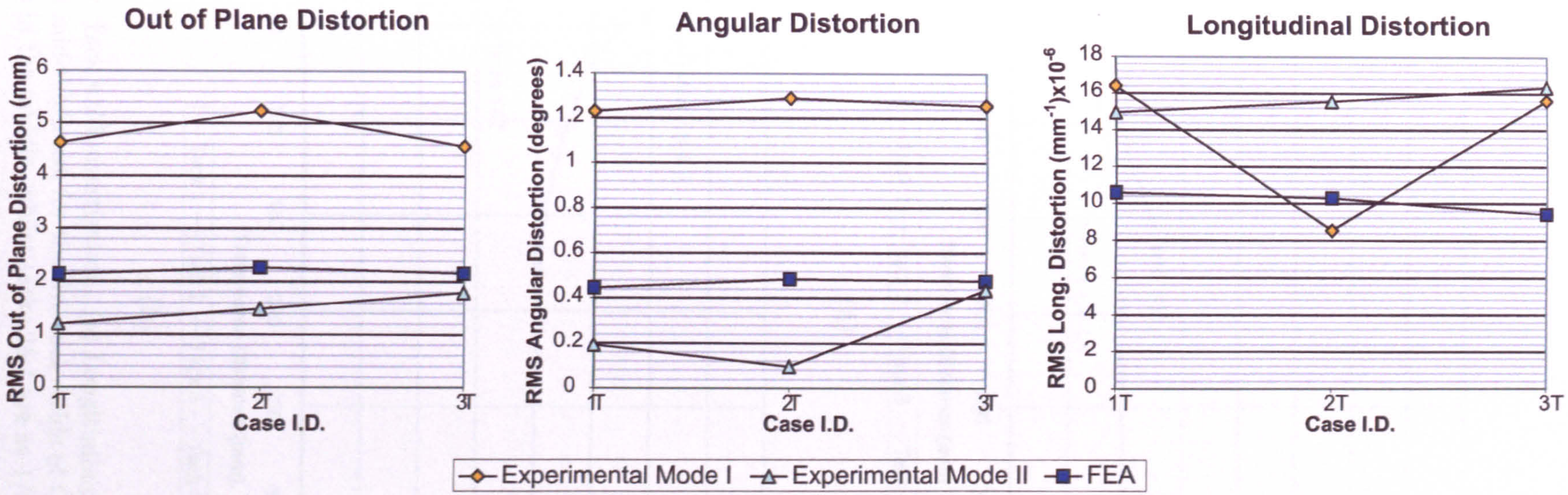

Figure 6.17: Tack welding investigation. Comparison of experimental and numerical RMS values

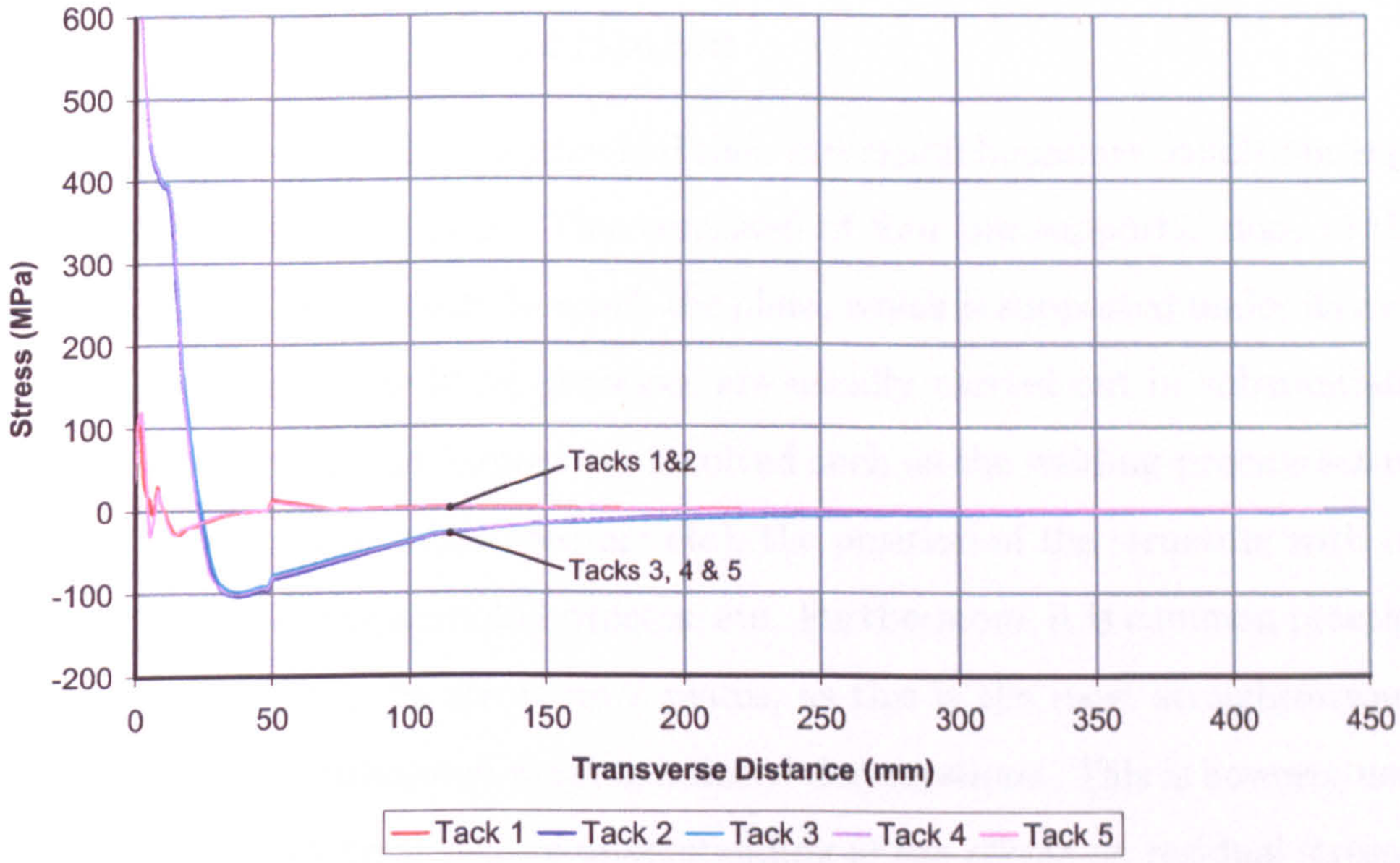

(a)

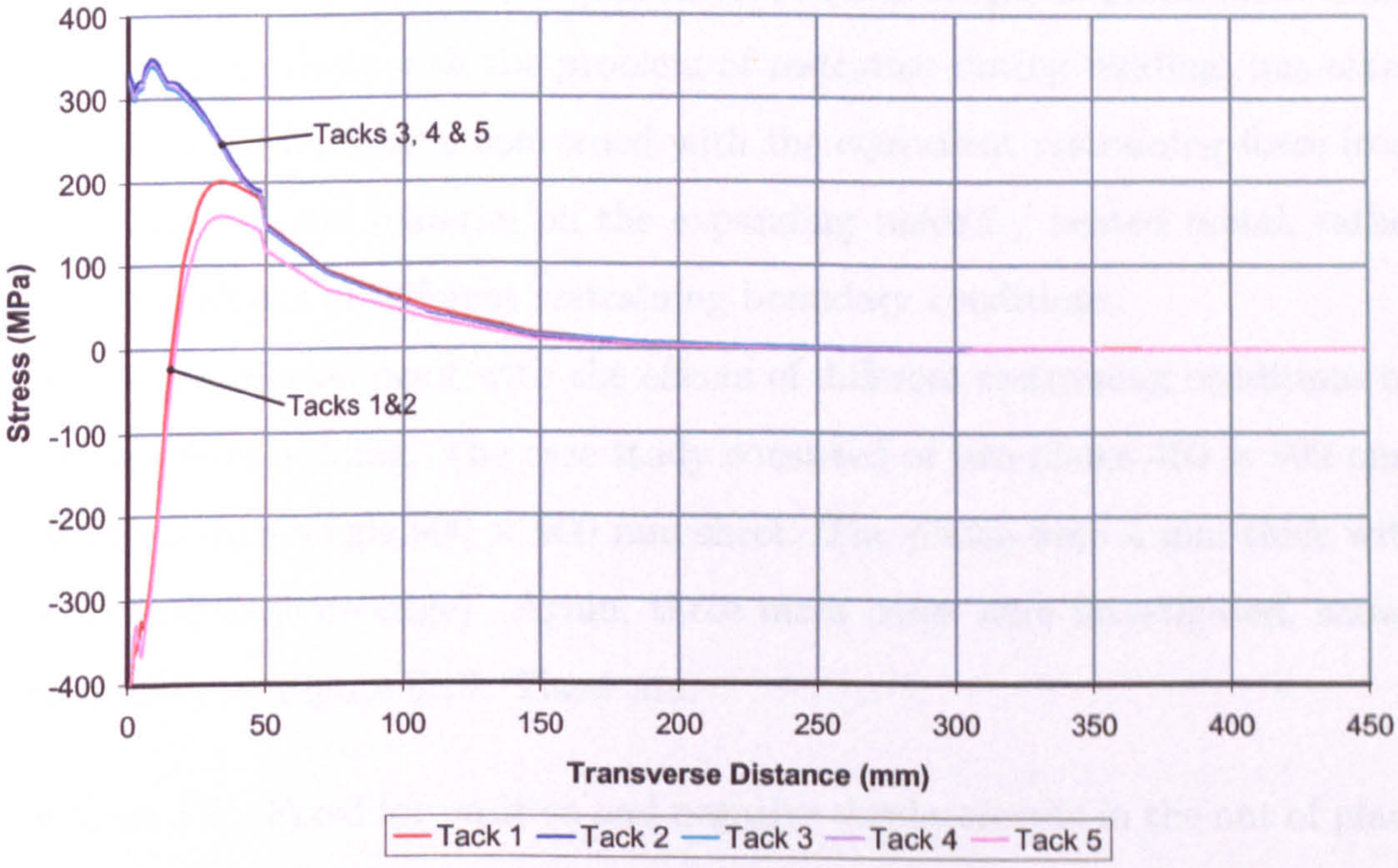

(b)

Figure 6.18: Tack weld investigation. (a) Longitudinal and (b) Transverse residual stresses at mid-thickness, for the five tack welds of Case 1T. Tack 1&2: plate's edges. Tack 3 in the middle, whilst tacks 2&4 are at 1/4 lengths from the edges

6.3 Restraint Investigation

6.3.1 Case Study Description

All the models presented so far have had their structural boundary conditions kept to the simplest possible form. This consisted of four pin supports, close to the corners and adjusted initially to touch the plate, which is supported under its own weight. However real welding processes are usually carried out in substantially different scenarios. Many factors are involved such as the welding process set-up (manual, robotic arm, submerged arc etc), the position of the structure with respect to the rest of the assembly process, etc. Furthermore, it is common practice to purposely restrain the structure / plates, as this is the most straightforward way to contain any unwanted welding induced deformations. This is however usually done without a great deal of understanding of the effects on residual stresses or even on whether the deformations are actually reduced or merely kept under control until the sub-assembly is passed on to other stages of production. Some researchers have dealt with the problem of restraints during welding, but many (e.g. [6.3], [6.4]) have been concerned with the equivalent restraining force from the surrounding cold material on the expanding welded / heated metal, rather than on the effects of different restraining boundary conditions.

This investigation dealt with the effects of different restraining conditions on continuous butt welding. The case study consisted of two plates 450 × 900 mm, welded to form a single 900 × 900 mm sheet. The plates were 4 mm thick with no weld prep (square edge). Again, three main cases were investigated, shown schematically in Figure 6.19. These are:

- Case 1R - Fixed for positive and negative displacements in the out of plane direction at four corners
- Case 2R - Resting on the floor unconstrained
- Case 3R - Resting on the floor and fully constrained at four corners

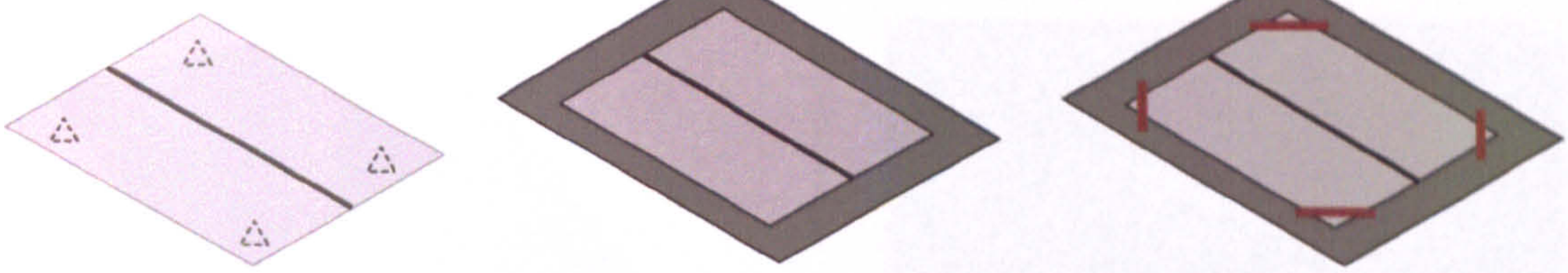

Figure 6.19: Restraint Cases Investigated

The investigation for the restraint conditions was carried out almost entirely through numerical analyses. Welding parameters were obtained from experimental data extracted during welding trials of a similar set-up to ensure the simulation parameters yielded reliable results. Hence, the welding efficiency was established by comparison with thermal transients and the thermal analysis, followed by the structural analysis carried out on the three cases. The effects of the different restraining / boundary conditions on welding induced residual stresses and distortions was the main aim of the analyses.

6.3.2 Thermal Analysis

As mentioned above, the thermal analysis was based on experimental trials carried out on plates with the same geometry and welding set-up. Similarly to the tack welding investigations the thermal input model was kept to a simple volumetric heat input. This, together with the adoption of a welding efficiency parameter, proved to be adequate in predicting the maximum transients. The shape of the volumetric heat input was again based on macrographs of sectioned plates, which yielded a close match in predicted and actual fusion zone (see Figure 6.21), although it should be noted that this prediction is not as important as the one for maximum transients. The mesh used is shown in Figure 6.20, and again makes use of a transition region in order to keep the fine mesh within the region that

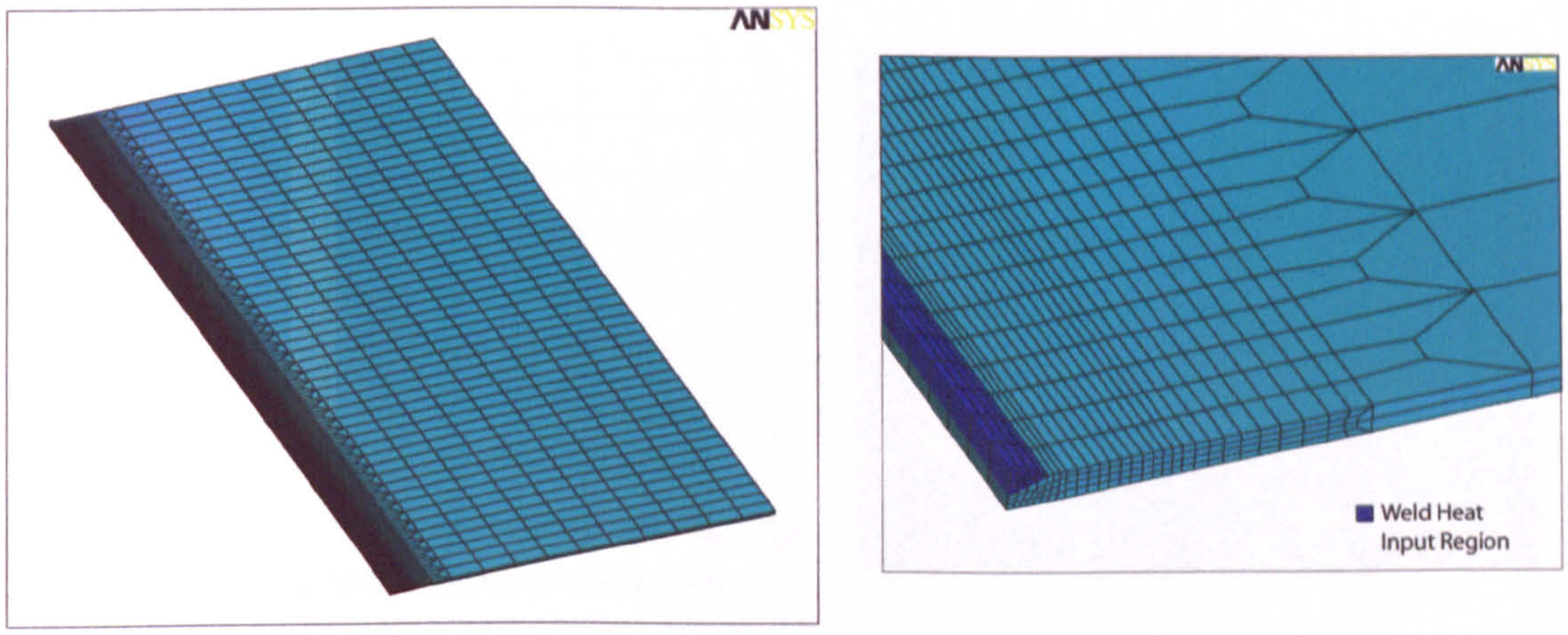

Figure 6.20: Restraint Investigation: Finite Element Mesh

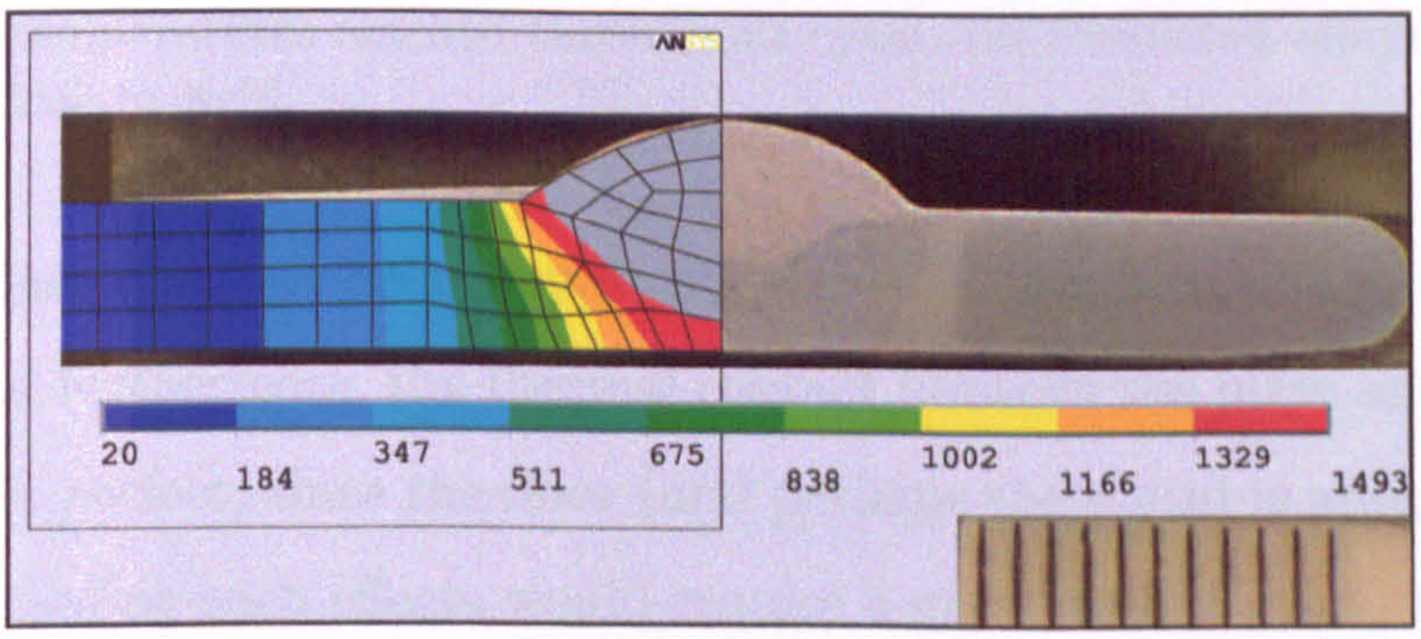

Figure 6.21: Restraint investigation. Comparison of experimental and predicted fusion zone

experiences a strain equal or lager than yield.

Figure 6.22 shows a comparison of the predicted and actual maximum temperatures reached throughout the welding cycle using a welding efficiency of 82% together with a contour plot of the predicted temperature distribution (note the level of discretisation in simulating the weld metal deposition). Once the temperature transients were established, the structural simulation could be carried out. The thermal model was consistent for all three cases investigated. This implies that the thermal boundary conditions were also constant. This constitutes a simplification for Cases 2R and 3R, since the thermal contact that might exist between the plate and the floor was not included. This can be justified in two

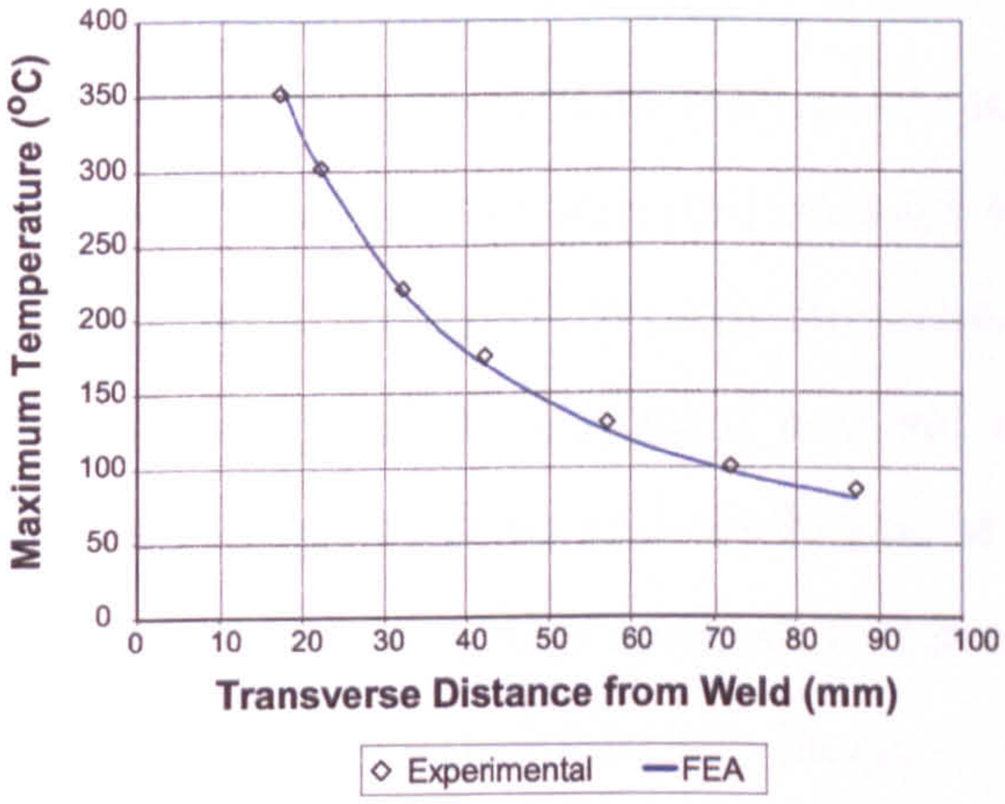

(a)

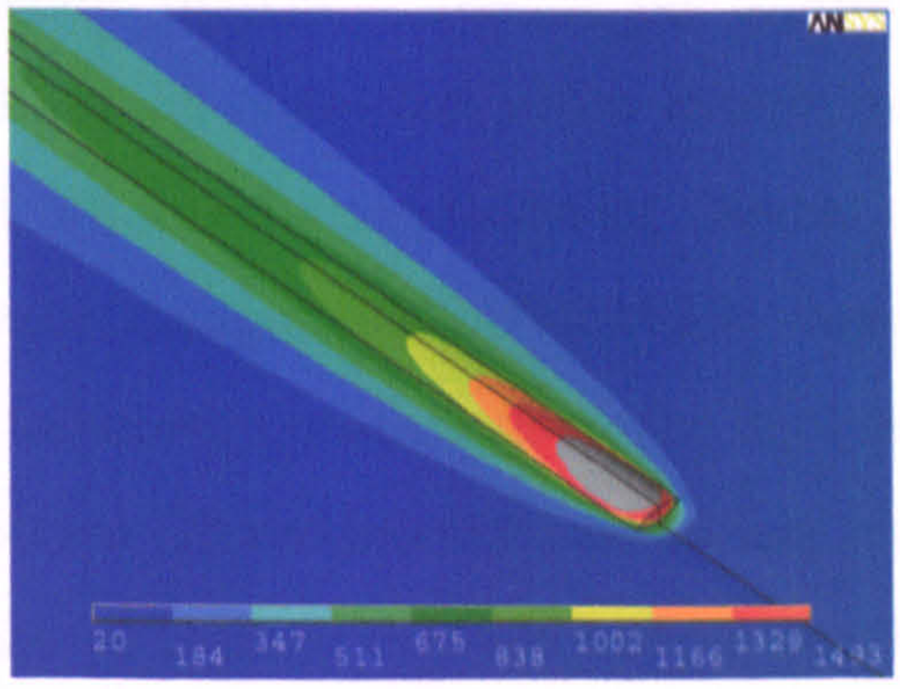

(b)

Figure 6.22: Restraint Investigation: (a) Comparison of predicted and actual maximum temperatures reached throughout cycle. (b) Predicted temperature distribution close to weld

ways: the heat flow has been previously shown to occur predominantly within the plate and furthermore, the thermal contact between the plate and the floor is definitely not perfect, since the floor (and perhaps the plate) is always uneven in practice. Including such effects would require a great deal of validation therefore and is out of the scope of this analysis.

6.3.3 Structural Analysis

The structural analysis was again carried out using the same simulation strategies as presented in previous chapters. An elasto-plastic transient analysis was performed using the same non-linear material properties presented earlier to model the parent and weld materials. Element birth and death was used to simulate material deposition with a cut off temperature (taken to be 1500°C) technique based on the algorithm presented in previous chapters.

The new aspect that was included in this investigation was the simulation of the plate resting on the floor, i.e. idealised rigid flat surface. Two methods were investigated, the first being the use of contact elements. The relevant surfaces on the finite element model were designated as the contact surfaces so that the finite

element software could assign contact elements to them. During the solution phase the contact elements were made to follow an algorithm which determines whether the surfaces come into contact and adjusts the displacement degrees of freedom accordingly. It is clear that this method requires a substantially larger computational effort, adding a new set of unknown parameters to the analysis such as contact stiffness and coefficient of friction. Nevertheless a preliminary run was performed using this method, but it was soon realised that the computational time required was prohibitively large.

The second method made use of standard line structural element *link 10* [6.5], which has a dual stiffness feature: different stiffness values can be specified for tension and compression loadings. This feature is most commonly used in applications requiring the simulation of cables. For this investigation the link elements were employed to simulate the floor by setting their stiffness to a very high value in compression and to zero in tension. Hence, by placing the link elements on the underside of the plate, the plate was effectively inhibited from moving downwards, providing a basic but effective means of simulating the constraint imposed by the floor. The link elements were joined at one end to the nodes corresponding to the plate underside, whilst the other end was fixed in all directions. This method resulted in a considerably lower computational effort when compared to the use of contact elements, but still provided a satisfactory representation of the constraint of the floor on the plate. The main omission is the lack of constraint in the longitudinal direction, i.e. that provided by the floor friction. However, this is of little relevance for the purpose of welding induced residual stresses and distortion.

Some measures had to be taken in order to ensure convergence of the analysis. The stiffness in compression has to be set to a large value, but this has to be kept within limits in order to avoid running into numerical problems. For the same reason the stiffness in tension cannot be set to zero, but to a relatively small value. In addition, in order to minimise the number of degrees of freedom of

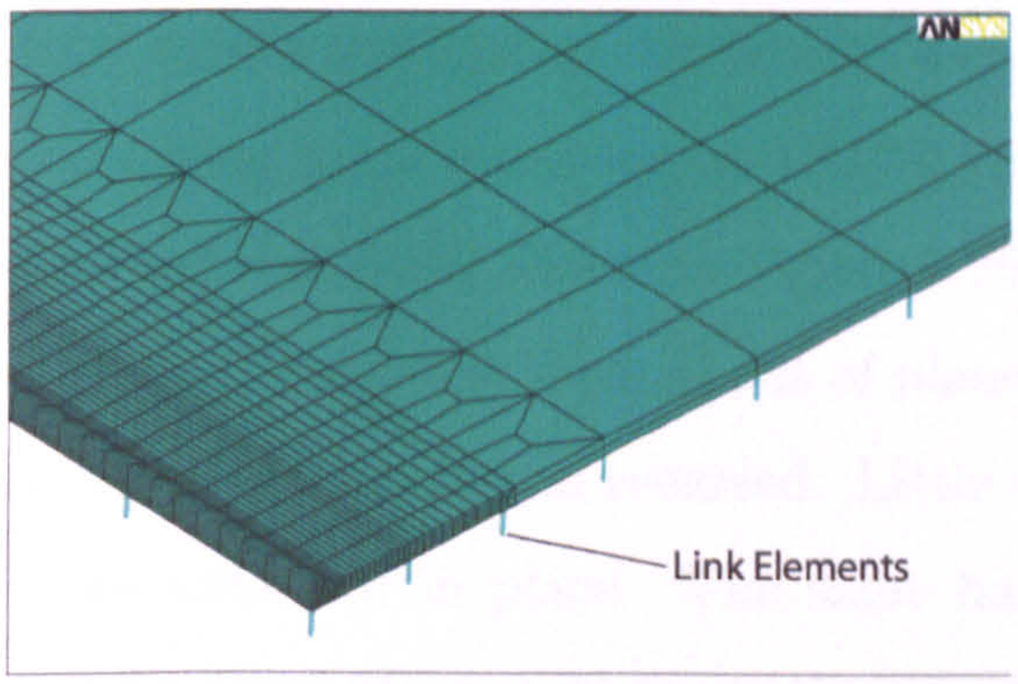

Figure 6.23: Restraint investigation: mesh showing link elements to simulate floor

the model, link elements were not assigned to each and every node on the plate underside, but to a smaller number, keeping the distance between link elements relatively small. The resulting mesh is shown in Figure 6.23. For Case 1R the analysis proved to be very similar to those presented in earlier chapters since the supports were of the same kind. This can therefore be considered as a benchmark for Cases 2R and 3R where the structural boundary conditions were changed.

Results for the out of plane distortion are shown in Figure 6.24 for all cases. For Case 1R and 2R only the final out of plane contour plot is shown whilst for Case 3R the three final stages of the simulation are shown: the time at which the plate has cooled to room temperature after welding but has the constraints still applied to it; the time at which the constraints at one end are removed and the time at which both constraints are removed. Cases 1R and 2R presented the usual longitudinal and angular modes of deformation, with only slight differences in magnitude. A different mode of deformation was instead obtained for Case 3R. Due to the symmetric nature of the analysis, Figures 6.24 (d) and (e) effectively show the effects of removing both constraints at once for each end. Upon completion of welding, when the plate has cooled to room temperature, little or no deformation occurred, as the restraints were still in place. As one end was released, the plate immediately distorted upwards. The same happened for the other constraints yielding the final mode of deformation shown in Figure 6.24 (e).

Similarly to the tack weld investigation, quantitative comparison of the deformations was done by taking room mean square (RMS) values of out of plane, angular and longitudinal deformations, shown in Figure 6.25. As already noticeable from the contour plots, the greatest form of out of plane distortion occurred for Case 3R when one set of restraints was removed. Little or no distortion was seen when the restraints were still in place. The same happened for the longitudinal distortion, whilst Case 1R proved to be the worst as regards angular deformation.

To compare effects on residual stresses, a slice at mid-thickness and half way along the plate was considered. Figure 6.26 shows a plot for the final longitudinal residual stress for the three cases investigated. All three paths closely follow each other. Slight differences can be seen in the region close to the weld, where values exceed the material yield strength. Case 3R gave a slightly lower residual stress than the other cases, but greater differences can be seen in Figure 6.27 where the different stages of Case 3R are compared. The stage in which the plate is still clamped exhibited a distinctly higher stress profile in regions close to the weld. The transition region from the yield values to far field stresses followed the same path, whilst the far-field region exhibited a different profile: whilst the un-clamped phases showed the usual transition to negative values (necessary for equilibrium, i.e. to balance out forces), the phase for the clamped case hardly reached any negative values. This is because the restraints were still providing the reaction forces necessary for equilibrium. This profile is also similar to the ones exhibited in two-dimensional analyses, where the stress profile does not exhibit any negative values.

6.3.4 Conclusions

The following main conclusions are drawn from the numerical restraint investigation:

- The techniques developed in previous chapters proved successful in simulat-

ing welding induced residual stresses and distortion under different restraining conditions (although no experimental investigation was carried out to provide direct validation)

- Link elements provided a convenient technique to simulate the restraint of the floor

- Restraining the structure did not provide a clear reduction in deformations

- The mode of deformation is reversed for Case 3R (the case where restraints are imposed on the structure)

- Taking the final stage of Case 3 as the relevant comparison, residual stresses for all three cases proved to be fairly similar

- Case 3R resulted in a higher residual stress (considerable for the transverse direction) in the stage when welding was completed but restraints were still in place

The analysis for the case with restraints proved to be problematic because of the increased susceptibility of the structure to buckle. Since the analyses were carried out in a transient fashion it was possible to note a buckling phenomenon occurring roughly half way through the analysis of Case 3R.

Restraining the structure did not prove to be beneficial. The extra boundary conditions imposed on the structure yielded higher values of residual stress, which resulted in increased out of plane and longitudinal deformations upon release of the restraints.

When the plate is merely supported at four corners, the combination of the passage of the high heat source and gravity effects generate a gull-wing angular contraction. This lowers the line of action of the weld relative to neutral axis and causes the longitudinal contraction force to act well below the original flat horizontal line. As a consequence the longitudinal deformation takes up the shape shown in Figure 6.24 (a) and (b) for Cases 1R and 2R. In Case 3R, the restraint

placed on the structure effectively inhibits the plate from assuming a gull-wing shape in the angular sense. Furthermore, the plate cannot move downwards because of the restraint provided by the floor. The result is that deformations occur in the positive out of plane direction leading to an inverted V shape (opposite to Cases 1R and 2R) in the angular form. This deformation is even more accentuated at the plate ends (see Figure 6.24 (c)), where there is less surrounding, and hence restraining, material in the longitudinal direction. Releasing the plate from this initial state yields the mode of deformation shown in Figure 6.24 (d) and (e), which is in the opposite direction of the other two cases.

As mentioned above, the line of action of the force relative to the original mid-thickness horizontal line is considerably different for the restrained and unrestrained cases. In the unrestrained Cases 1R and 2R, the angular deformation occurs immediately as the heat source is passed over the plates, so that the line of longitudinal action is immediately lowered. For the restrained case, the line of action of the longitudinal contraction force is kept closer to the original flat line up to the point when the constraints are removed. This creates further instability and, in practice some uncertainty as to which mode of deformation a restrained welded structure might take up. There is also a higher susceptibility to buckling, as the structural scenario is essentially that of an almost flat plate on which a contraction force is being imposed. This is true for both the transient and the residual states of deformation. The transient models were in fact able to capture such instability / buckling effects that occurred when the heat source was at a position approximately three quarters of the length along the plates. This is however only of relative importance, as the shape prior to the release of the clamps is the main driving factor for the final residual deformation.

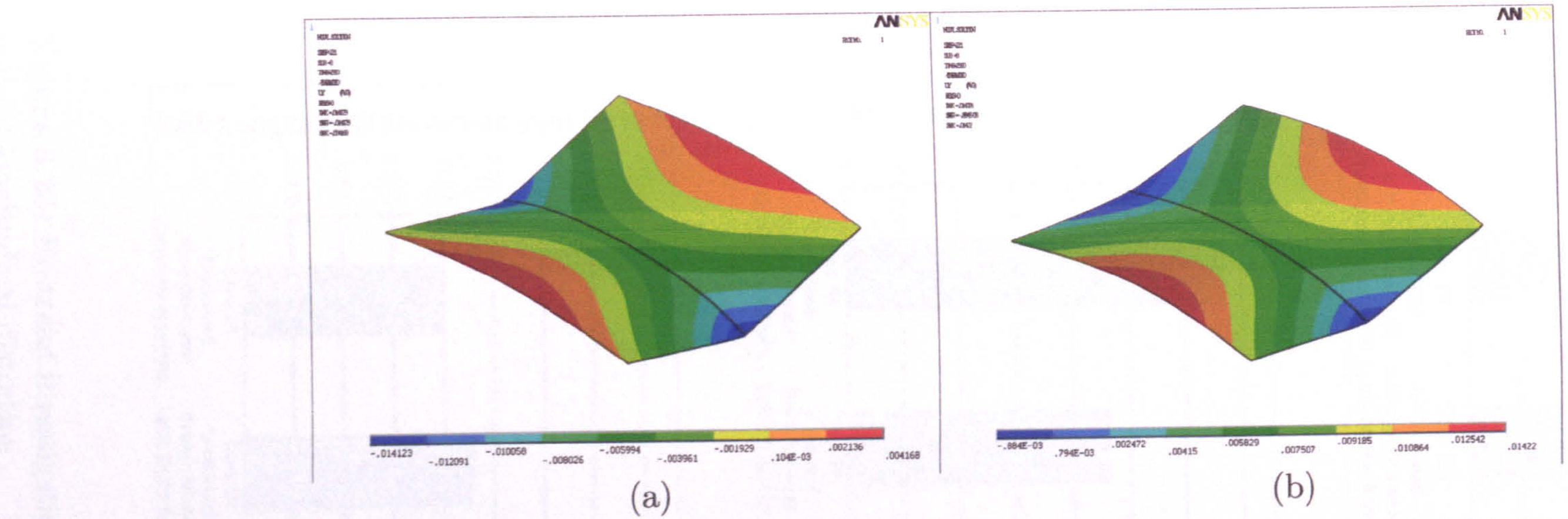

(a) (b) (c) (d) (e)

Figure 6.24: Restraint investigation: residual out of plane distortions for (a) Case 1R (b) Case 2R (c) Case 3R after weld with all restraints still in place (d) Case 3R with restraints removed at one end (e) Case 3R with restraints of both ends removed

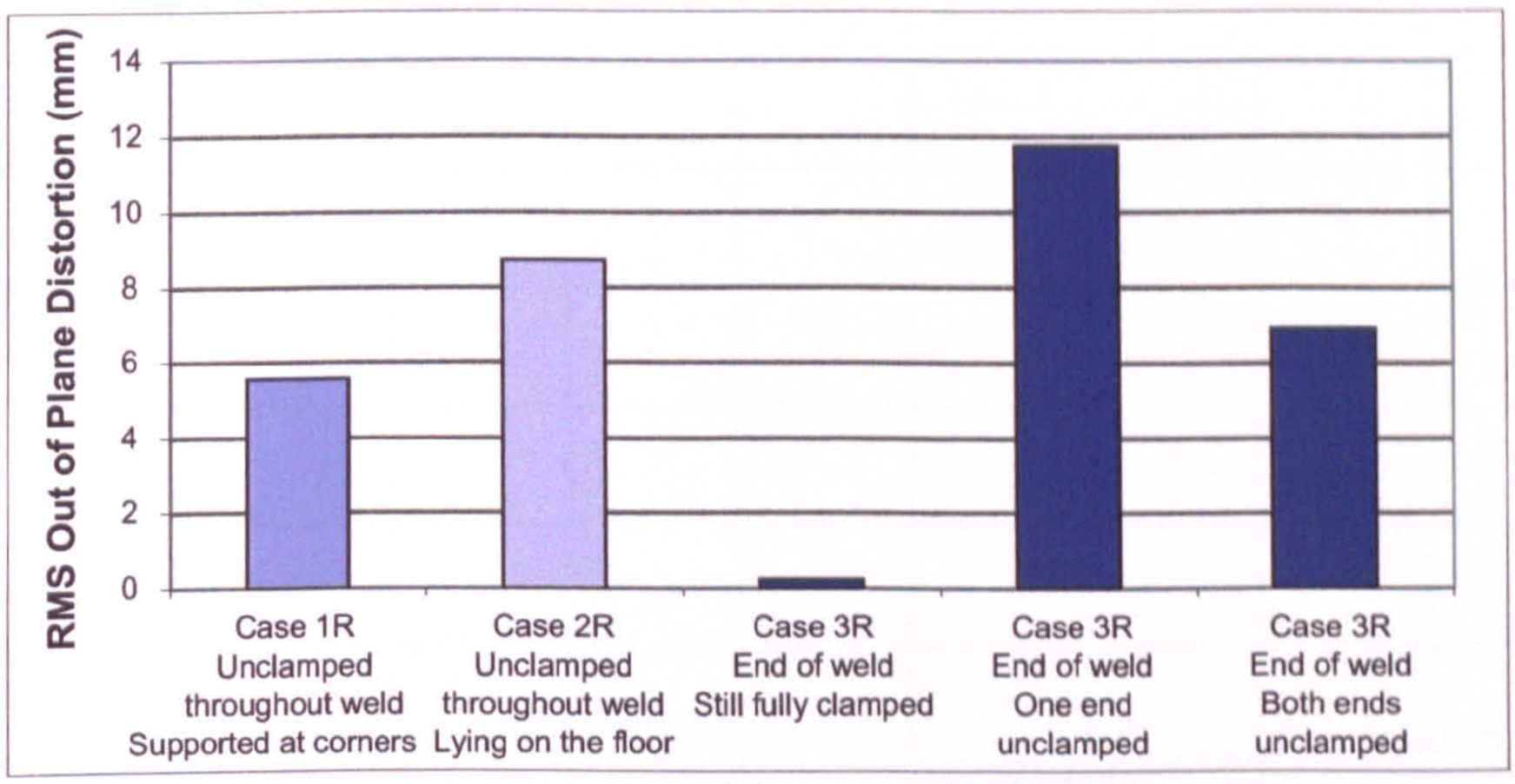

(a)

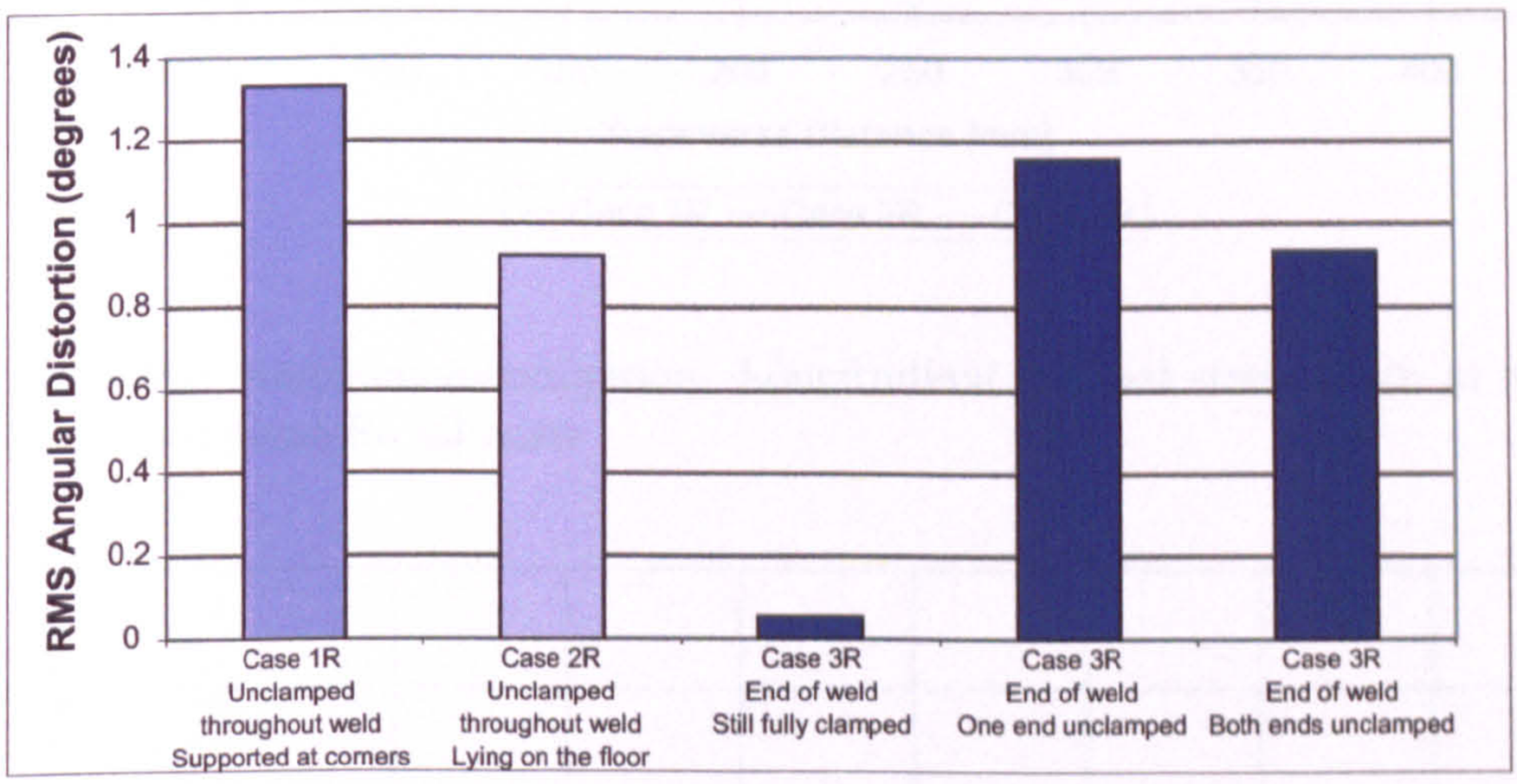

(b)

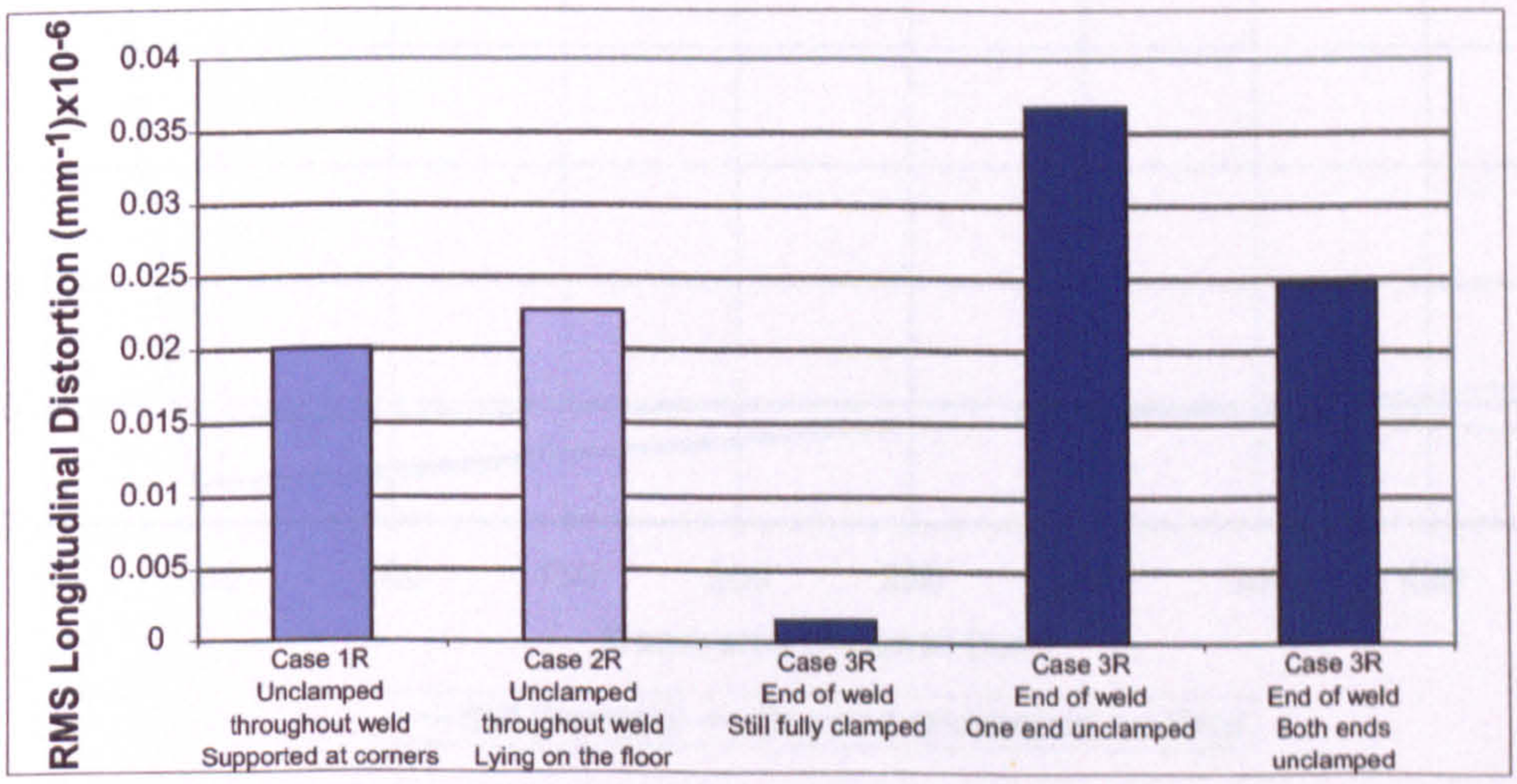

(c)

Figure 6.25: Restraint investigation. RMS values for: (a)out of plane, (b) angular and (c) longitudinal distortion

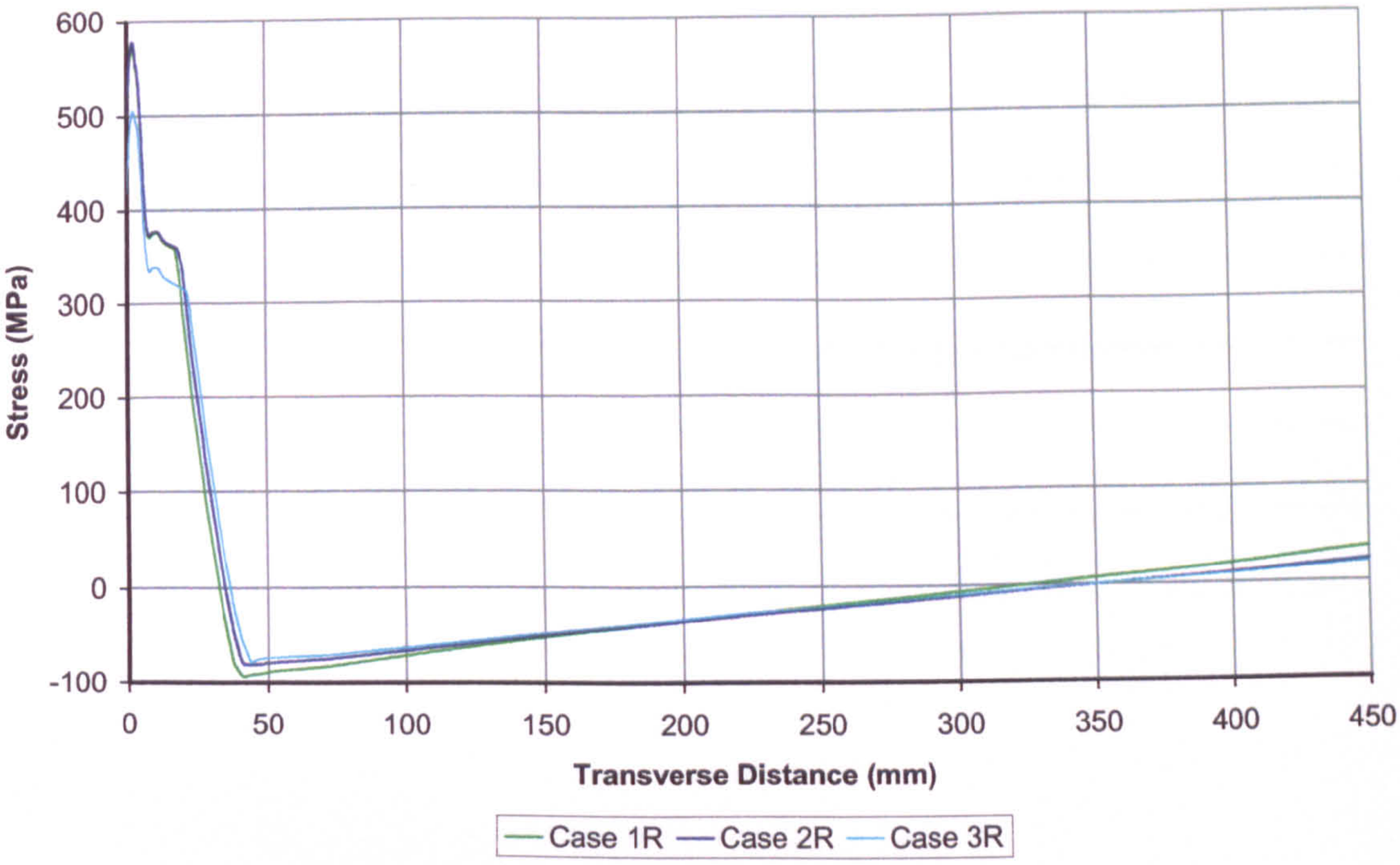

Figure 6.26: Restraint investigation. Longitudinal residual stress taken at mid-thickness mid-plane for all cases

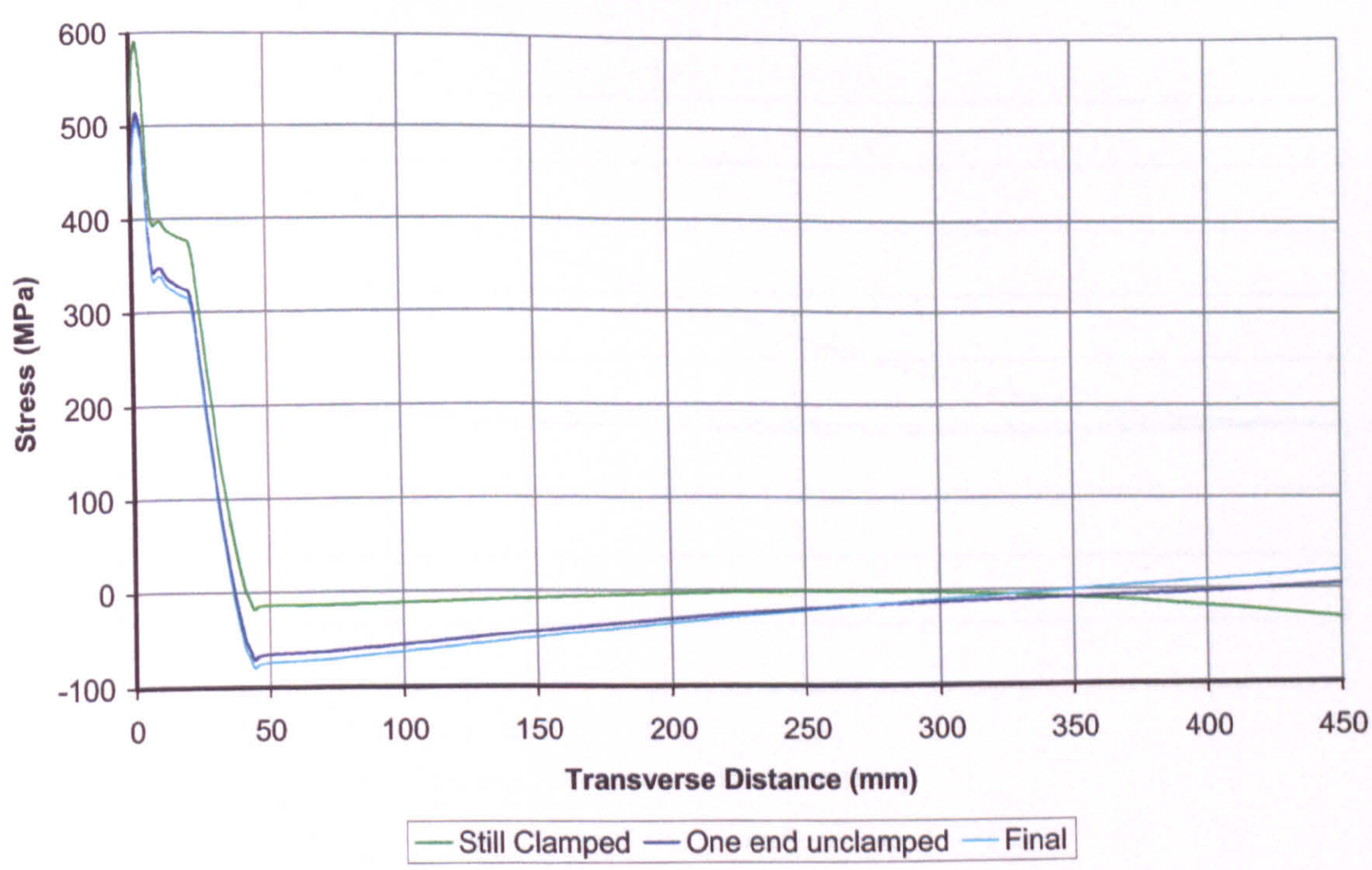

Figure 6.27: Restraint investigation. Longitudinal residual stress taken at mid-thickness mid-plane for three different stages of Case 3R

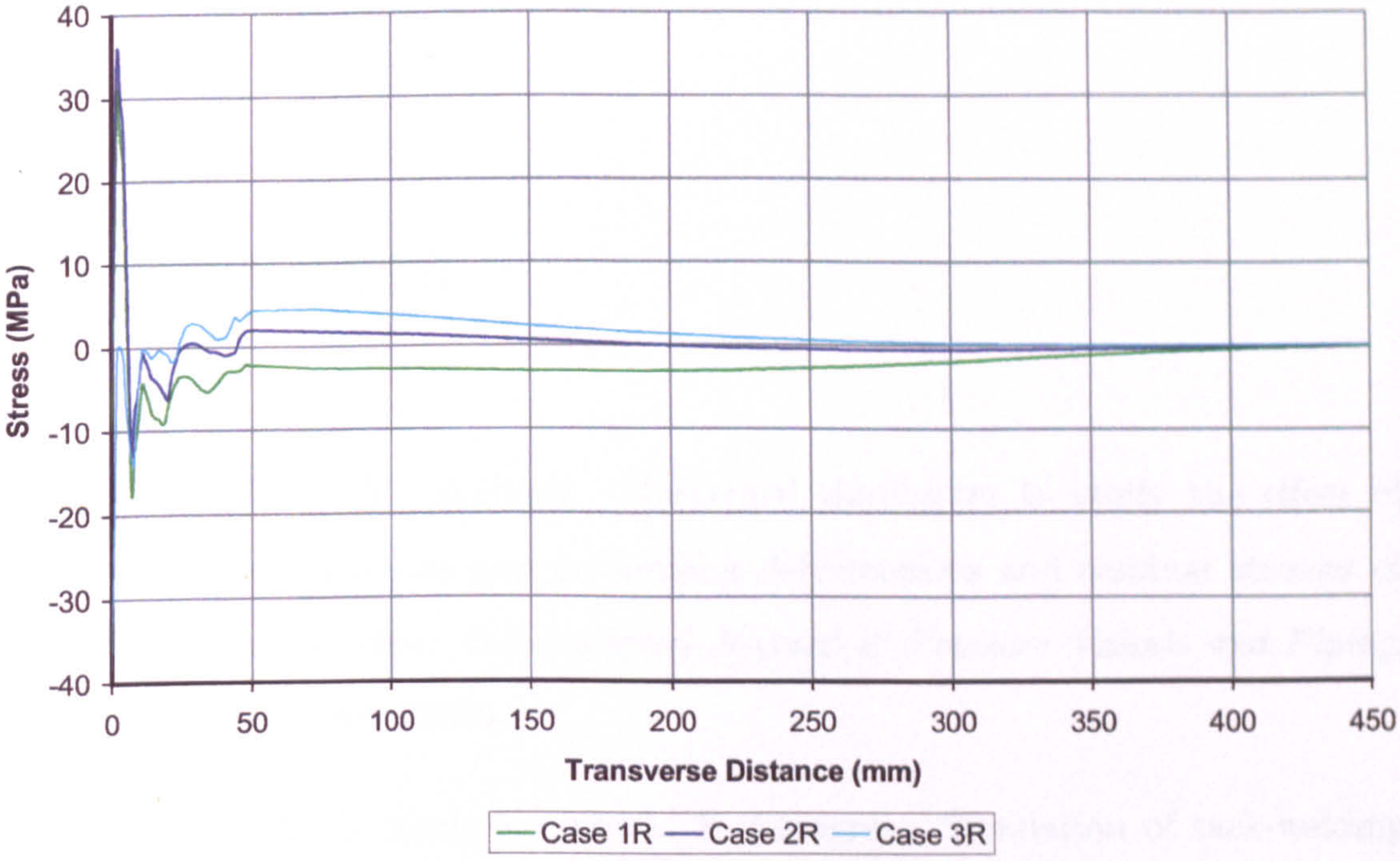

Figure 6.28: Restraint investigation. Transverse residual stress taken at mid-thickness mid-plane for all cases

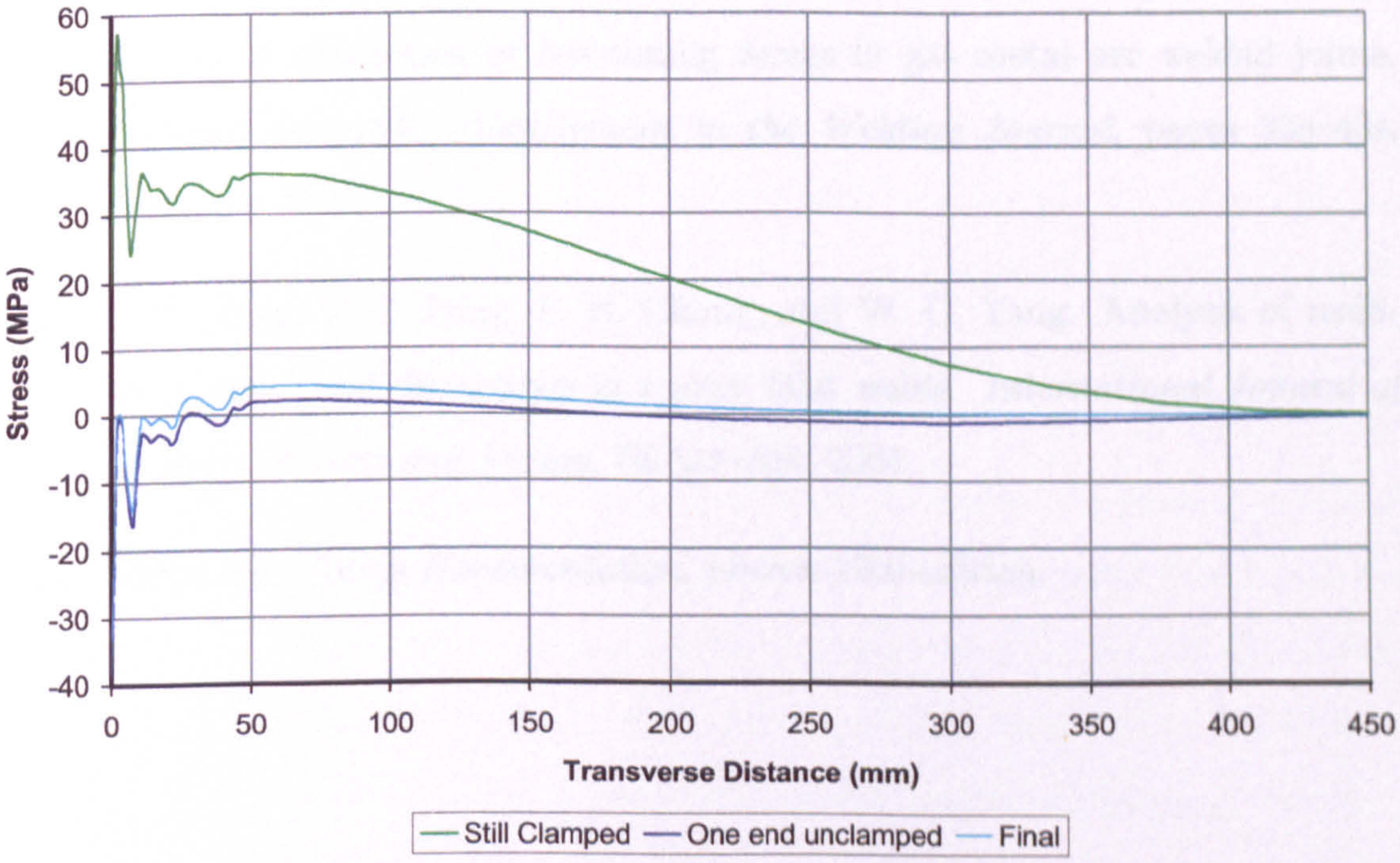

Figure 6.29: Restraint investigation. Transverse residual stress taken at mid-thickness mid-plane for three different stages of Case 3R

References

[6.1] M. Abid and M. Siddique. Numerical simulation to study the effect of tack welds and root gap on welding deformations and residual stresses of a pipe-flange joint. *International Journal of Pressure Vessels and Piping*, 82(11):860 – 871, 2005.

[6.2] M. Jonsson, L. Karlsson, and L. E. Lindgren. Simulation of tack-welding procedures in butt-welding of plates. *Welding Journal, Welding Research Supplement*, 64:296s–301s, October 1985.

[6.3] M.A. Wahab, M.S. Alam, M.J.Painter, and P.E. Stafford. Experimental and numerical simulation of restraining forces in gas metal arc welded joints. *Welding Research - Supplement to the Welding Journal*, pages 35s–43s, February 2006.

[6.4] T. L. Teng, C. P. Fung, P. H. Chang, and W. C. Yang. Analysis of residual stresses and distortions in t joint fillet welds. *International Jounral of Pressure Vessels and Piping*, 78:523–538, 2001.

[6.5] Ansys Inc. *Ansys Documentation*, release 10.0 edition.

Chapter 7

Conclusion

7.1 Summary and Discussion

The present work has set out to develop, validate and apply numerical models for the prediction of welding induced distortions and residual stress. The current literature was reviewed in Chapter 2, identifying areas of welding simulation that are of industrial relevance but still lack particular attention. State of the art in this field offers many different approaches in a wide range of welding applications. These do not always deal with shipbuilding gas metal arc welding (GMAW), but are still essential to understand what the current simulation tools and methods offer. In order to clarify the scope of the review, the literature was divided into groups depending on the specific purpose of the simulation (thermal vs. structural), together with the level of complexity normally encountered. The latter subdivision consisted of: simplified methods aimed at adopting the most computationally efficient approach in order to widen the physical range of application, and complex methods aimed at including advanced aspects in the simulation. Furthermore, other alternative methods (such as the use of artificial neural networks) were identified. Their use is a direct symptom of the difficulties and limitations encountered when using purely numerical techniques such as finite element analysis.

The review provided the basis for identifying a clear scope of work for an original contribution. This consisted in developing numerical models using a

commercial finite element software package and successfully predicting welding induced distortions and residual stresses for cases of industrial relevance. Fabrication procedures of tack welding and restraining were then investigated using the developed models, as these fabrication procedures have previously received little or no attention whilst still having a substantial effect on the induced deformations.

Emphasis was placed on cases relevant to the shipbuilding industry throughout the project. The models proved successful in predicting welding induced distortion and residual stresses for all cases under investigations. Basic theoretical considerations relating to the thermal and structural analysis used were illustrated in Chapter 3, whilst development of the models was illustrated in Chapter 4. Distortion reference data was used to validate the numerical results. Satisfactory correlation was achieved and the best modelling techniques were identified. The different approaches investigated related to the type of spatial analysis (two vs. three dimensional modelling), use of boundary conditions and complexity of the material model.

Two dimensional models proved attractive as they only required a fraction of the computational effort employed by their three dimensional counterpart, but included a degree of uncertainty as regards the adoption of boundary conditions and additional simulation procedures, such as the use of link elements. These were required in order to eliminate any effects that are present in the simulation but were not observed in the experimental reference data. The three dimensional models required less manipulation and hence proved to be a more transparent and clear methodology at the expense of greater computational effort. Nevertheless, both cases of butt and fillet welding configurations were successfully simulated using the developed thermo-elasto-plastic models. Furthermore, a comparison was made with a simplified simulation technique in order to get a better understanding of when it is most suited to use either technique. It was concluded that the transient elasto-plastic method is essential when the following aspects are

significant:

- Material properties which are highly temperature dependant
- Where phase changes are pronounced
- Non-linear response of the material when loaded beyond the yield point
- When the transient aspect is significant due to the boundary conditions
- Constraint exists on angular contraction, either from clamps or 3D action

Following validation of distortion predictions, experimental measurements using the hole drilling method were carried out to compare finite element predictions of induced stresses. The calculations for a constant stress through thickness proved to be the most convenient way of extracting the required results. Longitudinal stresses matched well with results predicted by the finite element models. Transverse residual stress did not match as well, even though these are of much smaller magnitude. Notwithstanding these discrepancies, important consideration could be made from these comparisons:

- The simplifications adopted in the material model nevertheless led to a correct prediction of the the longitudinal stresses, which are the largest and of most interest for this type of application
- Mismatches for the longitudinal stress predictions were found for regions close to the weld, and for all regions in the case of transverse stress. This is probably due to the type of material model adopted, which does not include all phase change related aspects
- Notwithstanding the latter consideration, it was concluded that a satisfactory prediction was achieved in a an efficient and practical manner as it depends only on data from quasi-stationary tensile testing tests, and simple dilatometry measurements

- A more detailed and accurate prediction for the residual stresses would require a much larger data set for the material properties, together which a much more refined mesh in the weld line region, which would seriously compromise the computational efficiency and hence the applicability to cases of industrial relevance

Following the above considerations, the models were used to investigate cases of welding induced distortion and residual stress due to the application of initial tack welds and restraints on the structure. These are operations regularly carried out in the fabrications of large assemblies, to which little attention is usually given due to their perceived insignificance compared to the effects of the final welding process. Their effects are in fact substantial and were investigated by using numerical models together with experimental trials. The main conclusions related to the procedure that must be employed and best practice for minimal distortion, as distortion is the main cause of set-backs in industry. For the tack welding investigation the best sequence for laying the tacks was identified using both numerical models and experimental trials. The experiments proved to be essential in picking up a further mode of deformation, dependent on the initial configurations of the plates, which was not embodied in the finite element simulations. The other mode of deformation was instead predicted by the finite element model, and matched measured distortion data.

The restraint investigation was carried out by means of the thermo-elasto-plastic models. The thermal part was compared to experimental data extracted from runs on a similar weld configuration, in order to keep realistic temperature predictions. Again, different cases representative of the most commonly used restraint conditions were investigated. The case when the plate is completely restrained during welding and then released following cooling to room temperature, proved to be the most problematic to simulate. Nevertheless, the results showed some interesting features, the main conclusions being that the use of clamps did not prove to be beneficial, and led to a reversal of the distortion mode, together

with undesired buckling effects occurring in the transient phase of the welding process.

The overall project demonstrated the development, validation and use of thermo-elasto-plastic models for the prediction of welding-induced distortion and stresses. The experimental measurements were essential in identifying the aspects that are strongly supported by the results of numerical models and those which require more attention computationally. Simulation for welding-induced distortion and residual stress is an application of numerical analysis which finds many different aspects and it is hence natural to identify areas in which the current work can be expanded, in order to improve the numerical models and apply them to a wider range of applications. An attempt to highlight such aspects is made in the following section.

7.2 Scope for Further Work

A methodology for thermo-elasto-plastic analysis of welding induced distortions and residual stresses has been illustrated, together with applications to cases of industrial relevance. The experimental work, apart from serving as a validation tool, helped to identify the deficiencies and limitations of the models. The residual stress aspect seems to be more complex to analyse, and requires careful consideration of the chosen material model. Scope for further work can therefore be found in developing the current models so as to adopt more complex material modelling aspects, such as more detailed phase change considerations, including the effects of the material alloying composition and metallurgical factors, and the inclusion of visco-plastic effects.

This may in turn lead to the development of a more refined thermal analysis. Although the adoption of a welding efficiency and cut off temperature technique proved successful for the scope of the current work, a more detailed structural material model might require a more refined prediction of the temperature distribution close to the weld. The current thermal analysis can therefore

be extended to include simulation of other physical phenomena affecting the arc physics. Multi-physics analysis tools are becoming readily more available, and a general purpose multi-physics analysis software package could be used to develop a more detailed thermal model, in the same way the thermal analysis features of the finite element software package were used in the current work. This could lead to a better understanding of the heat transfer phenomena taking place and would be the basis for another interesting aspect such as the prediction of the welding efficiency, which is still relatively limited in the current literature.

The other aspects that are of interest for further work are related to the investigation of fabrication procedures related to welding induced distortions. With the steady increase in computer power, the current model could be used to investigate cases of larger subassemblies, which would be of more interest from the industrial application point of view. Multiple steps taken during the assembly procedure could be investigated, such as the application of the full weld following the initial application of the tack welds. Multi-pass welding could also be included, as the increase in computational power makes it possible to adopt larger and more refined meshes.

Another interesting aspect, recurring throughout the current project, is the importance of the initial shape of the structure in relation to the induced distortions. The finite element models used here assumed an initial flat shape, the main justification being that the experimental data used for comparison of distortion was extracted by subtracting the initial shape from the final deformations. An investigation could be carried to quantify the effects of initial imperfections, and lay out a methodology for inclusion in the numerical models.